Theses and Dissertations

5-2016

Field Observations and Computer Modeling of Tornado-Terrain Interaction and its Effects on Tornado Damage and Path

Nawfal Shihab Ahmed
University of Arkansas, Fayetteville

Field Observations and Computer Modeling of Tornado-Terrain Interaction and Its Effects on Tornado Damage and Path

A dissertation submitted in partial fulfillment
of the requirements for the degree of
Doctor of Philosophy in Engineering

by

Nawfal Shihab Ahmed
University of Baghdad
Bachelor of Science in Civil Engineering 2000
University of Baghdad
Master of Science in Civil Engineering 2003

May 2016
University of Arkansas

This dissertation is approved for recommendation to the Graduate Council.

_____
Dr. R. Panneer Selvam
Dissertation Director

_____   _____
Dr. Micah Hale   Dr. Rick J. Couvillion
Committee Member   Committee Member

_____
Dr. Ernie Heymsfield
Committee Member

ABSTRACT

Tornado forces on structures have been a research focus for the past decades, and some comparisons have been made to distinguish between straight boundary layer (SBL) wind and tornado wind forces on specific structures. However, very little attention has been paid to terrain effects on tornado damage and path. Available damage investigation data for four tornado locations (Joplin-2011, Tuscaloosa-2011, Parish-2011 and Mayflower-2014) is utilized to explore terrain effects on tornado damage and path. Google Earth, site visits and aerial images are employed to study the influence of terrain on an extent of damage and path variation. Additionally, a three dimensional computer model is developed by employing computational fluid dynamics (CFD) to study terrain (hills) effects on tornado path deviation and tornado forces reduction in the sheltered region.

From the study, it is concluded that there is a significant effect of hills on tornado damage. Much damage is observed on the windward side of a hill comparing to its leeward side. When the tornado crosses the investigated hills, the hills provide sheltered zone on its leeward side. Furthermore, measurements of the sheltered zone on the leeward side of the investigated hills show that the sheltered zone length is about five times the hill height (5H) along tornado travelling path. After that, a modified version of the computer model presented in Selvam and Millet (2002) is utilized to simulate tornado-terrain interaction, and then the model is validated for further investigation of terrain effects on tornado path deviation and forces. The Navier–Stokes equations are approximated by the finite elements method (FEM), and the numerical domain is discretized using a terrain following coordinate system. It is shown that the ratio of tangential velocity to translational velocity (V_θ/V_t) significantly affects the tornado deviation shape when a tornado interacts with the investigated 2D hill. The deviation shape changes from

straight line to double curvature shape as the ratio (V_θ/V_t) increases. The UA numerical results

for tornado path deviation shape are comparable to field data (single and no curvature) for

(V_θ/V_t) < 4. The UA Numerical results for (V_Θ/V_t) >4 are comparable to wind tunnel data (V_θ/V_t

≈45) in which the deviation is double curvature. Therefore, the computer model is considered for

further investigation. Finally, the computer model is utilized to measure tornado forces on a

sheltered dome building. Rounded and triangular hill profiles are considered with varied heights,

and it is concluded that the hills reduce tornado forces and velocities on their leeward side. The

computer model outcome is that tornado forces applied on a structure are reduced by more than

70% when the structure is located within six times the hill height (6H) on the leeward side.

ACKNOWLEDGEMENTS

TABLE OF CONTENTS

LIST OF FIGURES

LIST OF TABLES

NOMENCLATURE

a	the aspect ratio
C_s, C_K	Smagorinsky model constants
h(x,y)	The ground elevation for at point (x,y).
h_1,h_2,h_3	non-dimensional control volume spacing in the x, y, and z directions
H_{Domain}	numerical domain height
h^f	total height of the numerical domain over flat region
h_{hill}	hill height or terrain height
h_i	the height of inflow
h^t	total height of the numerical domain from the highest point of the terrain region
IM,JM&KM	the number of points in the x, y and z direction
k	the turbulent kinetic energy
K	Von Karman empirical constant (0.4)
L*, U*	non-dimensional length, velocity respectively
L_{Domain}	numerical domain length
L_{hill}	hill length or terrain length
P	non-dimensional pressure
R	the distance from the center of the tornado

R_{max}	the tornado radius where the maximum tangential velocity occurs.
r_o	the minimum updraft radius
S	swirl ratio
S_{ij}	strain-rate tensor
t^*	non-dimensional time unit
u^*	frictional velocity at certain height
U, V & W	non-dimensional the velocities in the x, y and z direction
U_i	non-dimensional velocity components in (X,Y&Z)
V_x	velocity in x direction
V_y	velocity in y direction
V_r	the radial velocity
V_θ	the tangential/amgular velocity
W_{Domain}	numerical domain width
W_{hill}	hill width or terrain width
z_0	roughness length of the ground
Z_1^f	ground elevation for the flat region (zero elevation)
Z_f	boundary layer profile
Z_{km}^f	the highest elevation in the numerical domain
Z_K^t	the grid height at the certain required point
α	a rotational constant
ρ	non-dimensional density of the fluid

ν_T the turbulent eddy viscosity

ν the kinematic viscosity

Θ the angle of inflow measured with respect to the radial

Δt non-dimensional the time step

List of Publications

Publications in Journals:

Ahmed, N., & Selvam, R. (2015). Ridge effects on tornado path deviation. *International Journal of Civil and Structural Engineering Research*, *3(1), 273-294.*

Ahmed, N., & Selvam, R. (2015). Tornado Forces on a Sheltered Building. *Journal of Wind Engineering & Industrial Aerodynamics.* (Submitted under review)

Ahmed, N., & Selvam, R. (2015). Hilly Terrain Effects on Tornado Damage and Path. *Structural Safety*. (Submitted under review)

Ahmed, N., & Selvam, R. (2015). Tornado-Hill Interaction: Damage and Sheltering Observations. *International Journal of Applied Earth Observation and Geoinformation strucs*. (Submitted under review)

Shatnawi, A. S., Al-Sadder, S. Z., Abdel-Jaber, M. S., Othman, R. A., & **Ahmed, N. S.** (2010). Method of Characteristics for Dynamic Geometrically Non-Linear Analysis of Beams. *International Journal of Advanced Steel Construction, The Hong Kong Institute of Steel Construction*, *6*(3), 831-852.

Publications in Conferences:

Selvam, R. P., **Ahmed, N. S.**, Yousof ,M.A, Strasser, M, and Ragan, Q. (2015).Study of Tornado-Terrain Interaction from Damage Documentation of April 27, 2014 Mayflower, AR Tornado. Proceeding of the Structures Congress 2015. Portland, Oregon, USA.

Ahmed, N. S., and Selvam, R. P. (2015). Terrain Effects on Tornado Path Deviation. The Arakansas Acadimy of Science 99th Annual Meeting, Arkadelphia, AR

Ahmed, N. S., and Selvam, R. P. (2014). Tornado-terrain Interaction Effects on Tornado Damage Using Google Earth. The Arakansas Acadimy of Science 98th Annual Meeting, Searcy, AR

Selvam, R. P., and **Ahmed, N. S.** (2013). The Effect of Terrain Elevation on Tornado Path. Proceedings of 12th Americas Conference on Wind Engineering. Seattle, WA, USA.

Othman, R. A., and **Ahmed**, N. S. (2003) Dynamic behavior of beams subjected to large_angle bending. Proceedings of 9th Arab Structural Engineering Conference (9ASCE), Nov./Dec. 2003, Abu Dhabi, United Arab Emirates, pp. 251-260.

1. INTRODUCTION

1.1. Introduction

The United States experiences the most number of tornadoes in the world. Every year an average of more than 1200 tornadoes kills up to 60 individuals, injures 1,500 and causes at least $400 million in economic damage in the United States (NWS, 2010). In 2011which was a record year for the United States tornado losses, 1690 tornadoes were reported, and the total damage from the outbreaks exceeded $28 billion. As reported by the Insurance Information Institute (I.I.I.) for 1993-2013, tornadoes losses are ranked as the second highest losses after hurricanes (See Figure 1.1).
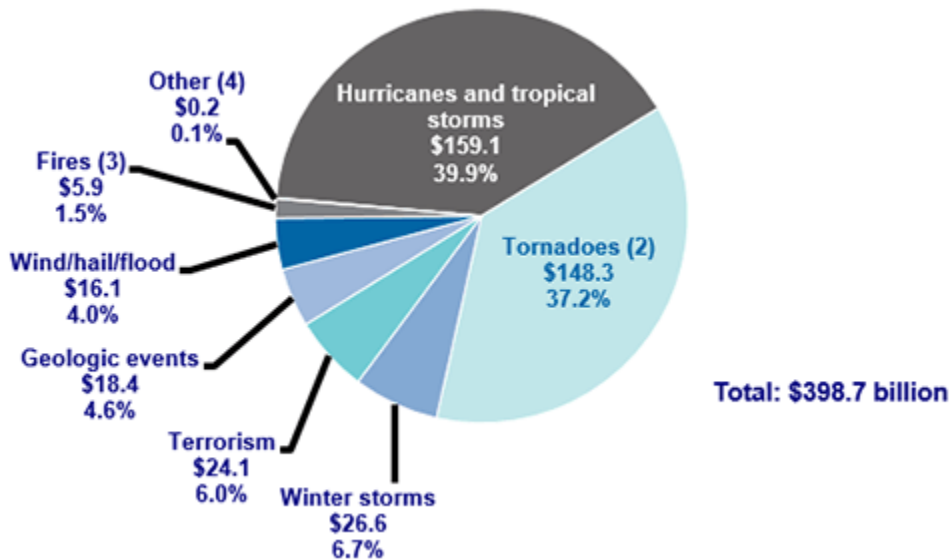
Figure 1.1 The average losses due to severe events taken from Catastrophes: U.S. (2014).

Even though the reported damage and loss of lives due to tornadoes are increasing, this does not necessarily mean tornadoes are becoming more severe. As shown in Figure 1.2, population in United States is growing, and at the same time the amount of developed lands (residential houses, buildings, etc.) is increasing. Therefore, the chances of tornadoes hitting

densely populated areas are more likely. This leads to a conclusion that more research is required to develop our understanding of tornado wind and to improve tornado warning systems. Tornado warning systems improvement can help to provide a better opportunity for reaching a tornado shelter and saving more lives. The development in tornado wind modeling can improve the prediction of tornado maximum forces and the tornado path. Then, the modeling predictions can be implemented for improving design standards (building codes). Also, the modeling outcome can be utilized to select a better location for a building (e.g. shelters) with less probability for direct exposure to a tornado.
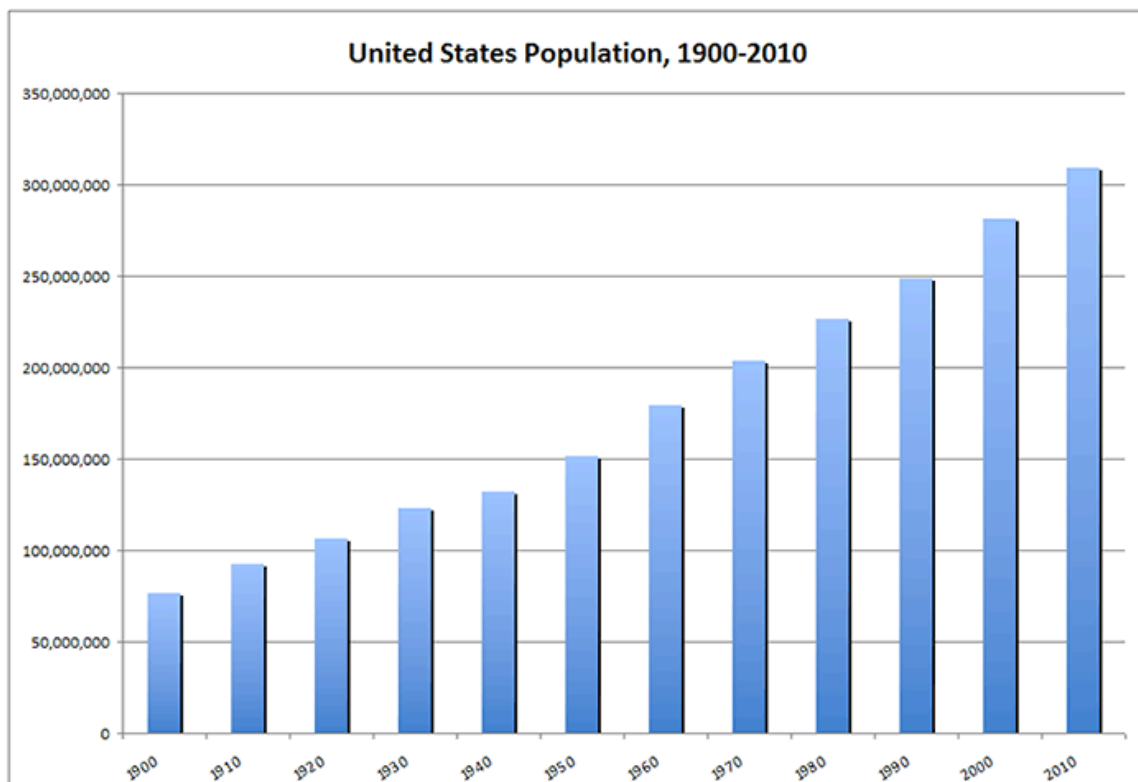
Figure 1.2 The population growth in United States (U.S. Demographic History (2014)).

1.2. Evaluation of Tornado Forces on Structures

The most precise way to evaluate tornadoes forces and identify tornado wind velocity and tornado severity would be measuring an actual tornado wind velocity; however, this is

currently difficult due to the high risk associated with being in the vicinity of an actual tornado and due to the fact that tornado's occurrence time and location are unpredictable. Even though the WSR-88D Doppler Radar network was created to provide velocity profiles for tornadic winds, there are still limitations due to the obstructions for the radar beam waves (Doswell et al., 2009). Also, a radar can only provide velocities at heights more than 100m above the ground level. However, velocities are desired close to the ground. This means that alternative methods should be used for evaluating tornado wind speed, especially near the ground where a tornado interacts with structures and causes the most damage. Several approaches were used to evaluate tornado forces on structures and to develop the knowledge about tornadoes. Some of these approaches are discussed briefly in the following sections.

1.2.1. Post Damage Investigation

Post damage investigation is an approach utilized to estimate tornado wind velocity and severity. The post damage investigation was first started by Fujita et al. (1967). Fujita (F) scale for rating tornado intensity (severity) is based primarily on the damage that tornadoes inflict on buildings. The final version of Fujita scale was published in 1973 and it was used to evaluate the documented tornadoes' damage back to 1950. The F scale is associated with several limitations, and these limitations are a lack of damage identifiers, no awareness for construction quality and no clear link between damage and wind speed. Hence the F-scale over estimates the wind speed. Therefore, an enhanced edition of Fujita (EF) scale was approved in 2007 by the American National Weather Service (NWS) considering some of the good aforementioned damage identifiers (McDonald & Mehta, 2006). Tornado wind is much more complicated than straight wind and consists of translational, tangential and vertical velocities. Also, tornadoes change their

velocity direction and magnitude suddenly. Moreover, buildings strength are not identical and human evaluations are subjective.

Tornado post damage investigation is mainly done by expert engineers who have design experience and damage assessment. Mostly they identify and classify tornado damage to EF scale according to damage severity. Different levels of damage are categorized by the EF scale numbers. For example, some damage to gutters or siding or branches broken off trees can be classified as an EF0 tornado with wind velocity range of 65-85 mph. The EF scale represents the main outcome from current tornado post damage investigations.

The damage ratings reported by National Weather Service (NWS) for the Tuscaloosa-2011 tornado are reported in Figure 1.3, and the terrain elevation profile along the tornado damage line is reported below. By analyzing the elevation and damage ratings, one can see that the damage ratings vary from EF3 to EF4 in flat terrain regions and EF0 to EF2 in hilly terrain regions. Therefore, this observation raises a question for the author, "Are the variation in tornado damage linked to the building location in a hilly region and the shape and height of a hill?" Even though it can be linked to a structures' strength and construction methods, a further step is taken to check a potential link between terrain and tornado damage. Also, the literature does not provide an answer whether there is a connection between terrain and tornado damage. This means that tornado damage evaluation for buildings has never been connected to their position with respect to a natural or artificial obstacle. Also, there is no documentation for tornado tracking over topographical configurations (hills, escarpments, ridges). If there were documented data for this kind of damage, it would have helped in analyzing the effect of terrain on tornado damage. Therefore, it is very important to study terrain effects on tornado damage and start documenting this type of damage now on.
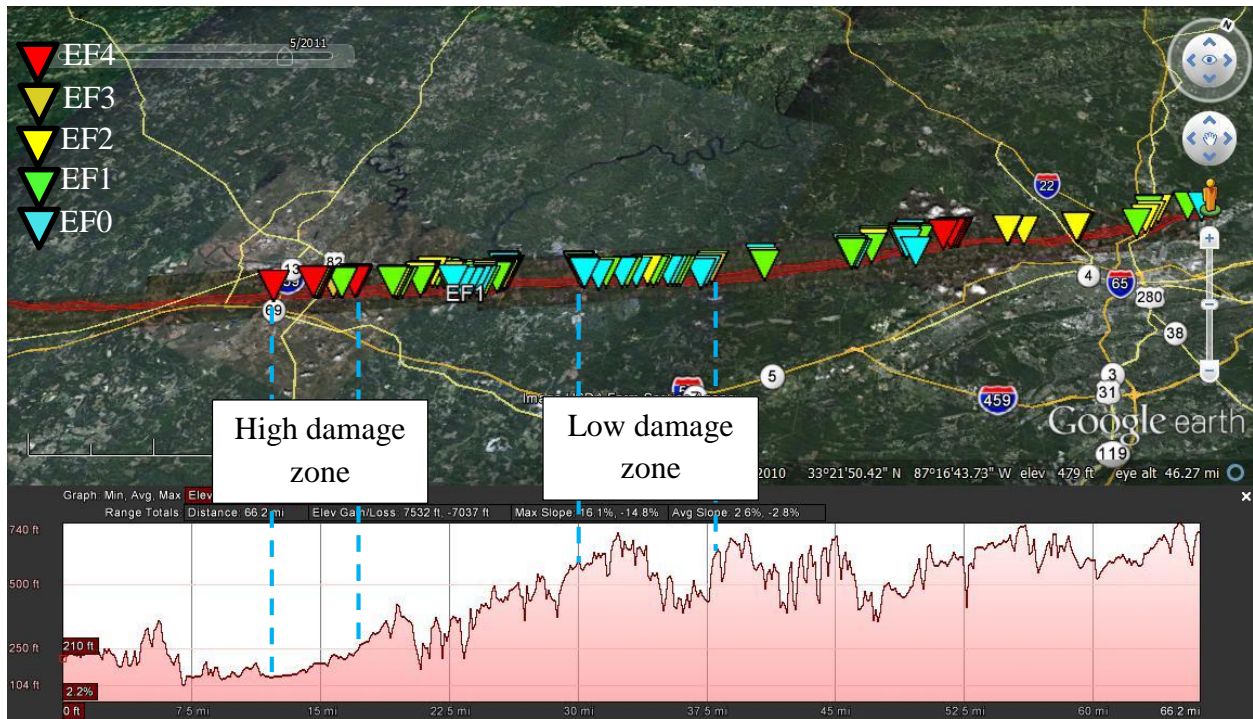
Figure 1.3 Tornado damage ratings for Tuscaloosa-2011 EF4 tornado laid along terrain variations profile.

1.2.2. Numerical Investigation for Tornado Characteristics

In the last three decades, there has been much development in the field of computational wind engineering, and wind flow around buildings and a tornado-like vortex are modeled considering the effects of viscosity and turbulence. Computational fluid dynamics (CFD) has been a great tool which has provided most of the initial development and basic understanding in wind engineering. Selvam et al. (2002) provided the state of the art for tornado forces on structures. The first three dimensional CFD simulation of a translating tornado was conducted by Selvam and Millet (2002). This development is considered a great achievement in developing the tornado knowledge and distinguishing between straight line wind forces and tornado forces on structures. Selvam and Millet confirmed that the tornado flow characteristics differ extremely

5

from that of straight boundary layer (SBL) wind. Therefore, tornado damage should not be represented by straight wind equivalent velocity. Several studies (Selvam and Millet, 2003and Selvam and Millet, 2005) were conducted later at the computational mechanics laboratory at University of Arkansas. They concluded that the translating tornado generated about 200% more force on the roof of a cubic building and about 45% more force on the walls compared to straight boundary layer (SBL) wind loads.

In all previous computational work, the interaction of a tornado on a small cubic building was examined where the building width was one third of the tornado radius. In recent times, tornado interaction with a rectangular building width of up to eight times the tornado radius has been examined by Alrasheedi and Selvam (2011). They found that the forces on the building decreased when the ratio of tornado radius to building width increased. Selvam and Gorecki (2012a) used a similar approach to investigate the effects of increasing tornado radius on a circular cylinder. They confirmed the results from the earlier study (Alrasheedi and Selvam, 2011). However, only the plan area influence was investigated and no attention was paid for the building height.

Gorecki and Selvam (2013) were motivated by Selvam and Ahmed (2013) to study the interaction of tornado with large structures. They assumed a 2D rectangular prism (man-made wall) and their focus was only the flow characteristics on the leeward side of the hill.

In the present work, the CFD program presented by Selvam and Millet (2002 and 2003) is modified using finite elements method (FEM) and a terrain following coordinate system to investigate tornado interaction with real terrain data (i.e. hill dimensions and elevations can be imported to the program form an actual complex terrain site (GIS coordinates)). Tornado-like vortex interaction with a 2D rounded hill and a 2D triangular hill is investigated. University of

Arkansas (UA) numerical tornado simulator is capable of producing a significant amount of information for the whole field velocity and pressure values for each time step. Also, tornado-like vortex characteristics (i.e. radius, translational and angular velocities) can be changed to have different tornado-like vortex structure and strength (intensity). Moreover, configurations of topographical obstacle (surface profile, height, length and width) are also changeable so that it economically provides opportunities to investigate wide variety of cases. On the other side, like most of the numerical simulator, the UA simulator has some limitations and drawbacks. In the UA simulator, Rankin Combined Vortex Model (RCVM) is utilized, and only the tangential velocity profile is represented. Vertical velocity is not included in RCVM. Also, different numerical errors are involved due to numerical rounding up error and truncating error due to the approximation of governing equations. Grid independent result is another limitation that it is difficult to achieve due to the high computational cost and the large required storage.

1.3. Tornado-Terrain Interaction Investigation

The term terrain here refers to any topographical configurations (ridges, knolls, valleys, ridge pairs, hills, etc.) which may affect the tornado's path, damage or any other characteristics of a tornado. Even though tornado occurrence location is never predicted and tornado could happen at any place, it frequently happens in the Tornado Alley. Even though flat terrain is predominant feature in the Tornado Alley, there is a quite good amount of complex terrain (hilly terrain) in this region. Since the tornado-terrain interaction effects have not been explored, several questions are raised by the author seeking for answers. Will tornado cross a hill or move by the side of a hill (along it)? What will happen if a tornado crosses a hill? Does the hill provide any sheltering or shielding? If a tornado crosses a hill, is there going to be any difference in the damage experienced by buildings on the windward side and buildings on the leeward side? If a tornado crosses a valley

(a place surrounded by hills), is the valley going to experience damage? Or not? When a tornado interacts with terrain (hill or hills), does the hill orientation angle affect tornado characteristics and damage amount? Finding answers for all these questions might be helpful in reducing life losses and economic crises. Therefore, finding answers for some of the aforementioned questions is sought through damage investigation using Google Earth and field data. Also, computational fluid dynamic (CFD) is utilized to explore and determine terrain effects on tornado damage and path. By employing the UA numerical tornado simulator, the pressure coefficients are determined on the topography surface along the tornado-like vortex traveling track for different tornado-like vortex intensity. Results for a tornado's path deviation are compared with experimental results and field observations for model validation and further use. Results from field investigation (Google Earth and site visits) for terrain effects on tornado damage and path are presented. Tornado-like vortex interaction with different hill-profiles and heights are explored for terrain effects on tornado forces. Results show reasonable agreement with field observations and experimental results.

1.4. Dissertation Motivation and Objectives

In the past research, great amount of efforts has been paid for tornado forces on specific structures, and comparisons between tornadic wind forces and straight line wind forces applied on the same structure have been made as discussed later in background chapter. However, no attention was paid for the structure location with respect to terrain obstacles and terrain effects on tornado damage and forces exerted on that structure. For civil engineers, near-surface characteristics for tornado-terrain interaction are very important because most of the damage and life losses happen within the first 50 meters above the ground level. Therefore, investigations for the terrain effects on tornado damage and path is sought here. The objectives of this dissertation are built to fill the

literature gaps with the required pieces of information and are divided into the following three objectives:-

<u>Objective 1: Investigate the influence of terrain (e.g. hills) on tornado damage</u>

Three tornadoes, Tuscaloosa, AL (04/27/2011), Parrish, AL (04/27/2011) and Mayflower, AR (04/27/2014) are considered to achieve this task. The software Google Earth is employed to track the tornado damage. This task is divided to three different parts.

- ❖ Investigate the effects of hills on tornado damage on both sides of a hill (i.e. windward and leeward sides of the hill).
- ❖ Evaluate tornado damage for a region surrounded by hills on the tornado path.

<u>Objective 2: Investigation of different terrain effects on tornado damage intensity and path</u>

A tornado hit central area of Arkansas (Mayflower and Vilonia, 04/272014) is investigated. A team from UA has surveyed the hit places few days after the events. There is a wide variety of different terrain configurations, flat, water surface and hilly terrain, in that region. Therefore, it is considered for assessing terrain effect on tornado damage intensity and path.

- ❖ Investigate influence of hilly terrain on tornado ground-level damage intensity.
- ❖ Investigate the influence of gaps in ridgeline on tornado path change.

<u>Objective 3: Simulate tornado-terrain interaction numerically using CFD and validated the model for future investigation of terrain effects on tornado damage and path deviation.</u>

A CFD code presented in Selvam and Millet (2002 and 2003) is modified to model a tornado interaction with real terrain data hills in 3D domain as shown in Figure1.4. Rankine Combined Vortex Model (RCVM) is utilized to represent tornado wind field, and the Navier–

9

Stokes equation is approximated by the finite elements method (FEM) in a terrain following coordinate system. This task is approached by the following phases.

❖ Validate the computer model by a comparison with wind tunnel and field data.

❖ Visualize flow field velocities and pressure for tornado-terrain interaction using various visualization techniques.

❖ Utilize the computer model to examine the following subtasks.

o Measure tornado forces on a building sheltered by different topographical shapes.
o Investigate the sheltering zone on the leeward side of a rounded hill by the computer

model and compare the results to field observations.

o Compare the sheltering efficiency for a rounded hill and a triangular hill (topography

shape effect on sheltering).
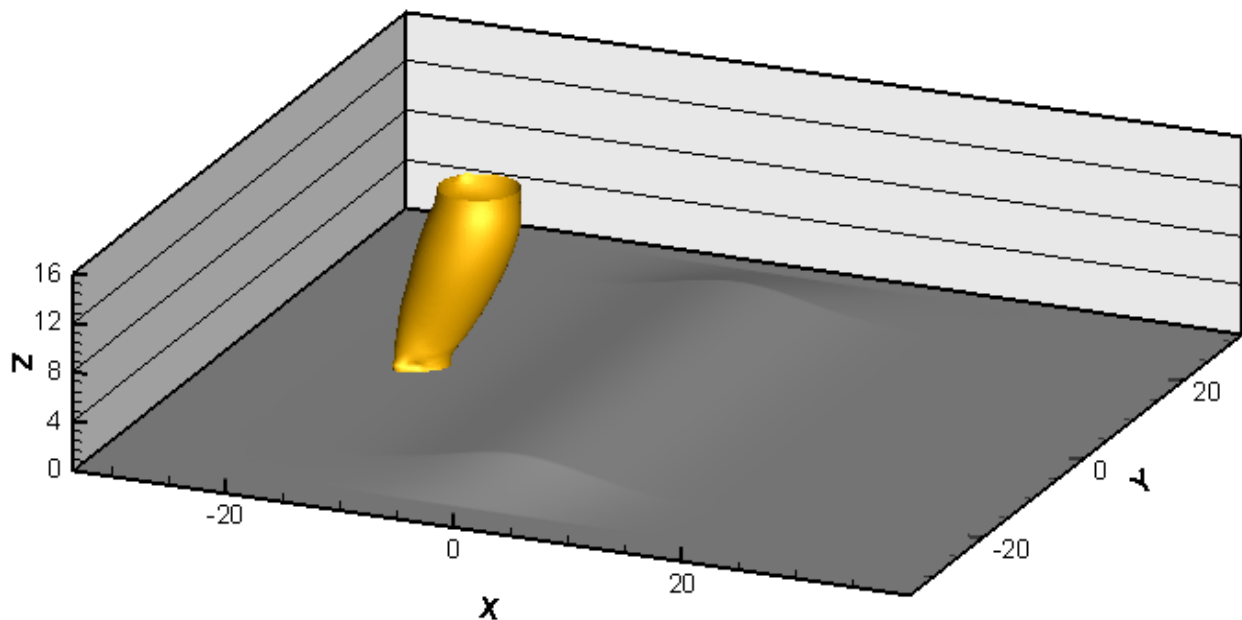
Figure 1.4 A 3D view of tornado-terrain interaction.

2. BACKGROUND

2.1. Introduction

Tornadoes are one of the strongest winds on earth and more likely cause significant damage if they pass through a heavily occupied area.

Although tornadoes occur across the world, the US experiences the most number of tornadoes in the world every year. Tornadoes in the US are annual events. Every year, an average of more than 1,200 tornadoes kills at least 60 people, injures an average of 1,500 and causes over $400 million in economic damage (NWS, 2010). This means that tornadoes are the most significant US severe weather threat in two phases: life losses and properties losses. In 2011, there was an infrequent deadly activity for tornadoes in the United States with more than 1,600 tornadoes documented across the country, and this is more than any other documented year except 2004 (NOAA, 2011). 2011 was an exceptional year in terms of the greatest daily tornadoes occurrence (2011, 27 April) NOAA (2011). The documented damage costs from seven individual tornadoes on that day were high and exceeded $1billion. Total damage cost from tornadoes and severe weather outbreaks is estimated to have been more than $28billion in 2011 (Tornadoes, 2011). This number has not been greater in terms of property damage from tornadoes in a single year since tornadoes damage documenting was started. The economic damage costs from the two 2011 events (Joplin, MO and Tuscaloosa, AL tornadoes) are ranked as the top ten natural disaster losses for the US (Tornadoes, 2011).

Due to tornadoes huge losses, frequency and devastation, the year of 2011 attracts many scientists and researchers to develop a better understanding for tornadoes.

The main objective of this chapter is to discuss the available tornado knowledge in general and provide the state of the art for tornado-terrain interaction. The tornado phenomenon has been investigated by three main approaches: Numerical simulations, experimental simulations and field investigations. In this review, all these approaches are reviewed, but more focus is paid to numerical simulations and field (post damage) investigations.

2.1.1. Layout of the Chapter

First, the nature of tornado and tornado formation are discussed. Then, research work concerning tornado damage investigations is presented. Next, development in computer models for tornado simulation is discussed. Then, some important and recent experimental works are mentioned. Finally, summarized analysis emphasizing what the literature is lacking is presented in the end of the chapter.

2.2. The Nature of Tornadoes

Tornadoes are one of the fiercest storms in the globe. A basic description for tornado is that tornado is a narrow vortex of air that extends from the base of a thunderstorm to the earth surface. Tornadoes cannot be seen due to the fact that air is invisible, unless moisture is carried by the wind to form a dark. When the pressure inside the vortex drops, the moisture condenses out of moist air due to drop of the temperature. The vortex must be in touch with both the ground surface and the parent cloud base to be classified as a tornado (NOAA, 2010a).

Tornadoes change velocity directions and magnitudes frequently, and the tornado's size does not necessarily represents the tornado's strength. Huge size tornadoes might be weak, and some of the least size tornadoes might be the most destructive ones. Usually tornadoes move from southwest toward northeast; however, tornadoes can travel in any direction and change

their direction unexpectedly. Even though there is no limitation for tornado radius size, the average observed or recorded size for tornado diameter is about 300 ft (90 meters) (DOE-US, 2002). Also, tornado trace path length average is just about a few miles/ kilometers, however; the longest observed tornado path is more than 200 miles (322 km). Although tornado translational velocity may vary from zero up to 130 mph (209 km/h), the average recorded translational velocity is about 55 mph (88 km/h). The maximum tangential velocity of a tornado is assessed to surpass 550 mph (885 km/h) relying on radars observation for a few events, and this is considered as the highest speed of all windstorm phenomena NOAA (2010a).

2.3. Tornado Formation

Even though tornadoes occurrence is unpredicted, tornadoes are usually associated with the thunderstorms occurrence. Also, tornadoes can be associated with tropical storms and hurricanes when moving over land. When the vortex is formed over the water, it is identified as waterspout. If the waterspout reached shore areas, it can cause an extensive damage (NWS, 2010).

Generally, the often time at which tornadoes may occur is during the spring and summer in the central latitudes of northern and southern hemispheres as reported in Snow (2014). Figure 2.1 shows the Tornado Alley and illustrates the conditions under which tornado more likely might be formed. The first stage of tornado forming is horizontal spinning wind which is then forced by updraft wind to form the vertical rotating wind, a tornado, as shown in Figure 2.2. Even though the aforementioned information states certain conditions for a tornado formation, there is still huge unknown facts regarding the tornadoes generation. Identifying the proper environment which can lead to produce thunderstorms and severe weather is not easy, and

tornado can only be developed by the existing of a specific combination of conditions (temperature, moisture, etc.) which are very difficult to be predicted and identified (Brooks and Dotzek, 2008). Even though thunderstorms might lead to tornado generation sometimes, statistics show that only about 5% of thunderstorms become severe and only about 1% produce tornadoes (NOAA, 2010b).

Tornadoes are formed when there are very violent storms, and the moisture level is at its highest level in these storms. These conditions usually happen when cold and warm fronts coincide, and then the warm air is enforced up toward higher layers quickly causing strong updrafts of air. The strong updrafts create a low pressure region in the lower level of the cloud, and that leads to suck in warmer air from below to replace the updraft. The updrafts is strengthened by the warm air which rushes up, and that adds more rotation energy to the soaring air into a rotating spiral as mentioned in Doswell III (2011).

Thunderstorms are identified as the major cause for tornado (NWS, 2011a), however; it is important to recognize that not all the spinning thunderstorms will lead to tornadoes formation. As aforementioned, there are certain environment conditions necessary to form the tornado, and if these conditions do not coincide the thunderstorms, then no tornado is formed. Therefore, understanding tornado formation has been a challenge for researchers and scientists.
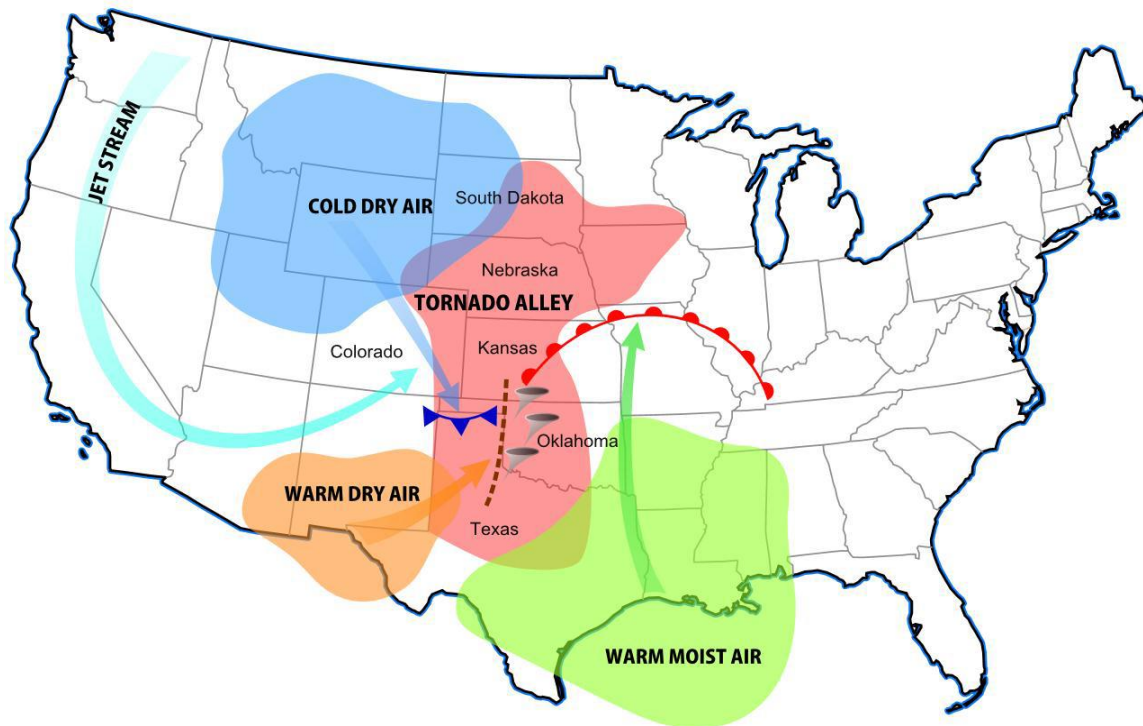
Figure 2.1 Tornado Formation in Tornado Alley taken from Tornadoes (2012).

Prior to thunderstorms formation, winds velocity changes with height. This leads to an invisible, horizontal spinning air in the lower atmosphere.
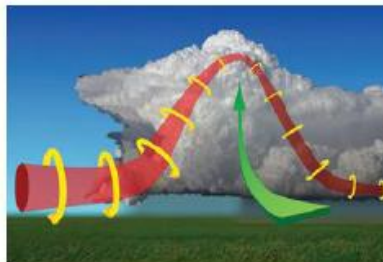
Thunderstorm updraft angles the horizontal rotating air to vertical.

A rotation area of 2-6 miles wide ranges over most of the storm and then guides tornado.

Figure 2.2 Tornado formation taken from NWS (2010).

2.4. Tornado Damage Investigation

Tornado damage investigation is a method which has been developed to estimate tornadoes intensity and evaluate tornado damage levels. Different approaches have been used to

achieve the purpose of this method. First, an airplane and a good quality camera are used to follow the tornado damage. Then, tornado damage is evaluated based on a comparison with damage indicators and linked with a straight line wind gust velocity to evaluate the tornado intensity. Also, a ground survey is used to document structures damage due to tornado and then the damage is evaluated, and the tornado damage is rated as aforementioned.

The basic elements in this investigation are the images and photographs. Therefore, quality and multidimensionality of the images are very important to have better interpretation for tornado behavior and damage estimation. However, this has been very limited due to high cost associated with conduction the field investigation and due to difficulties to integrate the data (images and photos). Data integration issues are the scale, angle and direction of the image. However, in recent days, the development of satellites and images processing have led to have software, i.e. Google Earth, that provide two and three dimensional images from any angle at different time. Therefore, the limitation is almost eliminated.

Fujita and his group (Fujita et al. 1967) were the first group who started this idea (tornado post damage investigation). They recommended using and gathering aerial photographs in order to provide a tornado damage database. Several other works (Fujita et al. 1970, 1976; Fujita 1981, 1989) were conducted similarly utilizing the same technique to evaluate tornado damage. Fujita and his group employed such photographs to evaluate tornado damage, compose damage paths, and relate tornado trace patterns to tornado near-surface dynamics. Aerial oblique photographs were critical in identifying cyclical marks (vortex rotating signature on the ground), or lines trace of debris deposition for many damage paths of tornadoes. These marks are utilized by Fujita to conclude that there were multiple vortices which are linked to the parent tornadic circulation. Aerial vertical photographs, stereo image pairs as well as oblique aerial photographs were all

used by Fujita (1989) to document an uncommon (F4) tornado happened on 21 July 1987 in Wyoming. This Wyoming tornado traveled over a complex terrain at elevations that ranged from approximately 2380 to 3270 m above sea level. Fujita was able to locate the tornado's starting point and ending point as well as calculate the length and spatially varying width for that tornado. Identifying this data would have been very difficult, if not impossible, without the utilizing of aerial photographs as reported by Fujita (1989).

Metha et al. (2008) utilized remote-sensing to assess windstorm damage and to follow up the recovering process. Karstens et al. (2013) used freely available photos by National Weather Service (NWS) to determine tornado effects in both Tuscaloosa- Birmingham and Joplin on directions of tree falling. They compared aerial photo observations with analytical models and concluded that there is strong near surface tornado radial wind causing the tree falling. Karstens recommended doing further research to distinguish between tornado and rear-flank downdraft effects on trees falling.

Selvam and Ahmed (2013) have investigated the tornado-terrain interaction effects on tornado damage by considering two deadly tornadoes in Tuscaloosa (04/27/2011) and Joplin (05/22/2011). Google Earth is employed to track the tornado damage and terrain effects on tornado's path and damage level. They observed that tornadoes caused much damage when they traveled uphill, and less damage was noticed downhill. Also, they found that hills show sheltering capabilities. Here sheltering means, the ability of the structure to reduce wind velocity on its leeward side, as illustrated in details in chapter four.

Although the utilization of aerial photographs has richened our knowledge about tornado, there are still many limitations and complexities associated with this work. This work requires a

lot of efforts for photo integration and scaling as well as time and money. Also, the photos need to be taken from close to vertical view for better interpretation. In addition to the limitations, no clear connection has been made between tornado damage and terrain influence on tornado damage in the literature. The development in technology eliminates some of these limitations, and software like Google Earth nowadays are capable of providing multidimensional images at different times so that tornado tracking is easier and more economic than the past days.

2.5. Tornado Wind Field Models

Tornado wind field model is a mathematical model that governs the wind velocities in the numerical domain to approximately represent a real life tornado, and also this model needs to satisfy the Navier-Stokes equations. In the literature, there are quite a good number of numerical models which can be consider to represent tornadoes. However, there are few of these models do satisfy the Navier-Stokes equations. Some of these models are the Rankine Combined Vortex Model (RCVM), Burgers-Rott Vortex (BRV) and Sullivan Vortex (SV). Each of these models has advantages and drawbacks. A detailed comparison is provided by Millet (2003) and Alrasheedi (2012).

Rankine Combined Vortex Model (RCVM) (Rankine, 1882) is utilized in our numerical simulator. This model comprises of two different flow fields as shown in Figure 2.3. The forced vortex region (inner flow field), the tangential velocity increases linearly from the center of the rotation to the maximum inner core radius (R_{max}). The free vortex region (outer flow fields), outside the range of the maximum inner core radius (R_{max}) the tangential velocity diminishes inversely with the increasing of the distance (R) from the center of rotation. Equations represented the two field are shown below.

$$V_\theta = \alpha.R \quad if \ R \leq R_{max} \tag{2.1}$$

$$V_\theta = \frac{\alpha.R_{max}^2}{R} \quad if \ R > R_{max}$$

(2.2)

Where V_θ is the tangential velocity, α is a rotational constant, r is the distance from the center of

the tornado and R_{max} is the tornado radius where the maximum tangential velocity occurs.
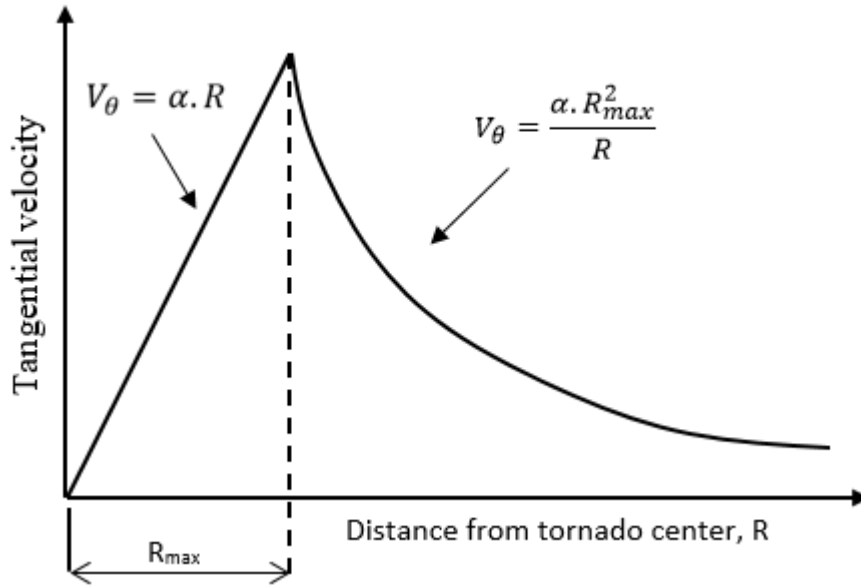
Figure 2.3 Rankine combined vortex model.

This model has been first introduced for tornado 2D simulation program by McDonald

and Selvam (1985) and then Selvam and Millet (2003) have developed this program to simulate

tornado in 3D.

2.6. Tornado-Structure Interaction Using Computer Model

Computer models have been developed to study tornado genesis and tornado-structure

interaction in the last three decades due to great advancement in computer software and

hardware. Computer models are utilized for different interests (e.g. meteorological and

engineering researches). Tornado has been modeled as a stationary vortex as well as non-

stationary vortex without any interaction with structures for the purpose of studying tornado

19

outbreak and tornado characteristics. However, the focus of this section is the interaction of a non-stationary tornado with structures.

Even though several researchers have modeled tornado numerically, Selvam and his research group at University of Arkansas have the major contribution in developing tornado-structure interaction models. Selvam et al. (2002) provided a review for tornado-structure interaction models until 2002. Tornadoes simulations have been done mainly in 2D with circular cylinder and 3D with cubical buildings as illustrated in the next subsections.

2.6.1. Tornado-Structure Interaction (2D)

Vortex interaction with a circular cylinder in 2D has been conducted by Selvam et al. (2002). They concluded that tornado forces are about 5 times less than forces found in (Wen, 1975). In Selvam et al. (2002), direct simulation method is applied to model the turbulence in the CFD simulation. The model was validated by comparing forces coefficients when the tornado was far away from the circular cylinder. At this time only the straight-line wind was acting and the force coefficients were similar to those found in the literature. Recently, Selvam and Gorecki (2012a) studied the influence of the different ratios of tornado radius to circular cylinder radius on the tornado forces. They found that the tornado forces depend on the size of the building. When the building size is decreasing, comparing to the tornado size, the forces are increasing. The study was conducted up to ratio of an 8:1. Ragan et al. (2012) have done similar study to Selvam and Gorecki (2012a), but the study was up to ratio of 30:1. They concluded that the tornado forces tend to be constant when tornado to cylinder ratio is more than 18:1. Strasser and Selvam (2015) studied the effect of a 2D vortex impinging time on force coefficients applied on a circular cylinder. They concluded that there is under estimation in maximum loading when the

vortex and cylinder size are similar. The maximum load under estimation is negligible when the vortex size is greater than three times the cylinder size. Although the aforementioned studies are vortex-structure interaction in 2D, they reveal that there is an effect of the structure size on tornado forces. Therefore, terrain effects on tornado path and damage in 3D simulations need to be investigated.

2.6.2. Tornado-Structure Interaction (3D)

Selvam (2002) and Selvam and Millett (2002, 2003 and 2005) used large eddy simulation (LES) turbulence model by filtering the NSEs in space. Selvam (2002) used 0.1D grid spacing close to the building and found that the force coefficients in the x and y-directions were less than the SL wind loads whereas the updraft force coefficient in the z-direction was higher than the SL wind loads. Selvam and Millett (2002) used a fine grid spacing 0.072H and found that the force coefficients in the x and y direction were less than the straight boundary layer (SBL) wind loads which is in line with Selvam (2002). However, the force coefficient in the z-direction was almost twice the SBL wind loads. Selvam and Millett (2003 and 2005) used a refined grid 0.0055H normal to the building and the tornado approached the building with 0° and 45° degrees. They concluded that the translating tornado generated about 200% force on the roof and about 45% more on the walls compared to SBL wind loads. Sengupta et al. (2008) conducted both CFD simulations and laboratory experiments of different tornadoes interacting with a cubic building. Their tornado horizontal force coefficients were in good comparison with those obtained by Selvam and Millet (2005). The tornado vertical forces were found to be even greater than that found by (Selvam and Millet, 2005), and this difference in the force values was related to the use of different tornado updraft models. Sengupta et al. (2008) also noticed that the slower tornadoes produce greater forces on a building than the faster one. They compared their results with wind

load standards (ASCE 7-05) and noticed that force coefficients provided in wind load provisions are more than 1.5 times less than tornado force coefficients resulted from their work.

Recently, Alrasheedi and Selvam (2011) conducted a computer study of the tornado impact on buildings of different plan area sizes. They reported that buildings which have planer area much wider than the tornado radius, the tornado force coefficients are similar to the straight boundary layer wind force coefficients. Selvam and Gorecki (2012b) provided more detailed study for the interaction between tornado and a longitudinal rectangular hill .They found that the hill creates a sheltering region on its leeward side.

Even though tornado interaction with large structure is studied in Selvam and Gorecki (2012b), their focus was only velocity reduction on the leeward side and the difference in forces on windward and leeward sides is never discussed.

2.7. Tornado Experimental (Wind Tunnel) Models

In this section, a review for the existed wind tunnel work is presented and discussed to demonstrate the lack of knowledge for studying terrain effects on tornado damage and forces as well as the lack of providing clear comparison with real life tornado observation.

Several tornado simulators have been built in the last 50 years. In all these simulators, two main flow components were generated to produce a tornado. The first one is an updraft flow, and the second one is an angular flow. Different ways have been used to produce each one of these flows which will be discussed in the next subsections. Also, different flow rates and ratios

between angular and vertical flow have been implemented to produce various strength and shape of vortices. Although different terms have been used to define the swirl ratio mathematically, a general definition is the ratio of maximum tangential velocity at the circulation edge to mean updraft (vertical) velocity as stated by David Jones (1973).

Basically, the tornado simulators can be divided into two types of apparatus: close chamber (stationary simulator) and open chamber (translational simulator). Then, under each category, four or more different approaches are used to generate the tornado as discussed next.

2.7.1. Close Chamber Simulators

Ying and Chang (1970) were the pioneers who built the first tornado simulator which is shown in Figure 2.4. In this model, the circulation is produced by a rotating cylindrical screen and the updraft is generated by a separate exhaust fan at the center axis of the top hood opening. The circulation flow is controlled using three different rotating velocities for the screen, and the exhaust fan located far above the hood opening to reduce the fan turbulence effect on the vortex in the circulation domain. The vortex is visualized by using the kerosene smoke, and that shows that the model is working successfully. They concluded that the measured pressure is almost constant in the boundary layer except near the center of the vortex and that the angular velocity is proportional with the distance from the center of the model. The main purpose of this research was studying tornado near surface flow. In Ying and Chang model, the inward flow height, diameter of the hood opening and exhaust fan speed were all fixed, however, only the rotating screen speed was changeable. Even though the model is capable to produce the vortex, there were limitations to examine tornadoes in details because of the fixed parameters.

Ward (1972) built tornado simulator similar to that built by Ying and Chang (1970), but in Ward model the inward flow height, exhaust fan speed and the diameter of the raising air column in the model are all changeable. Also, at the top opening of the chamber, Ward introduced new technique to represent the atmosphere condition. He used honeycomb mesh to straighten the air flow and prevent the effect of secondary turbulence flow of the exhaust fan. Ward model is shown in Figure 2.5, and this model becomes the standard referable model by almost all the other new models. Ward produced successfully single and multi-vortex in his model by applying different configuration ratio (diameter of updraft flow to height of inward flow). Ward concluded that a large influx of radial momentum is essential for vortex production, and that multi-vortex can be produced in single convergence system when the configuration ratio is greater than one. He also recommended further investigation to examine the effects of configuration ratio on pressure and velocity measurements.

Davis-Jones (1973) re-analyzed the Ward's output and concluded that it is not important to have huge radial inflow momentum to produce the vortex; however, it is necessary to have high volume flow rate for certain swirl ratio. Davis-Jones defines swirl ratio as stated in Equation (2.3).

$$S \equiv \frac{tan\theta}{2a} \tag{2.3}$$

Where: θ is the angle of inflow measured with respect to the radial axis, and a is the aspect ratio.

$$a = \frac{h_i}{r_o} \tag{2.4}$$

Where: h_i is the height of inflow and r_o is the minimum updraft radius.

Jischke and Parang (1974) indicated that the swirl ratio controls the vortex production in Ward-type simulators. Also, they stated that increasing swirl ratio beyond critical number causes the usual single-celled vortex to undergo a transition to a two-celled vortex configuration.

Church et al. (1977) at Purdue University used Ward model with modifications which are represented by all critical variables: depth of the inflow, the radius of updraft opening, updraft flow rate and the tangential velocity. They confirmed that swirl ratio control the single and multi-vortex formation. They also defined swirl ratio as shown below in equation (2.5). Their model is shown in Figure 2.6. This model demonstrates successfully the single vortex multi-vortex formation.

$$S \equiv \frac{V_\theta}{2V_r a} \tag{2.5}$$

Where: V_θ & V_r are the angular and radial velocities of inflow respectively.
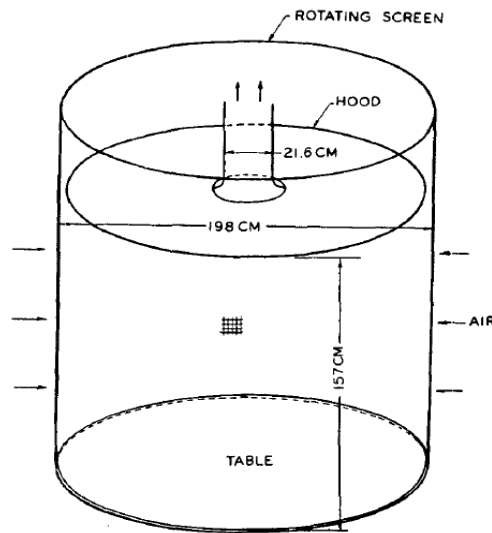
Figure 2.4 Schematic illustrations for Ying and Chang apparatus
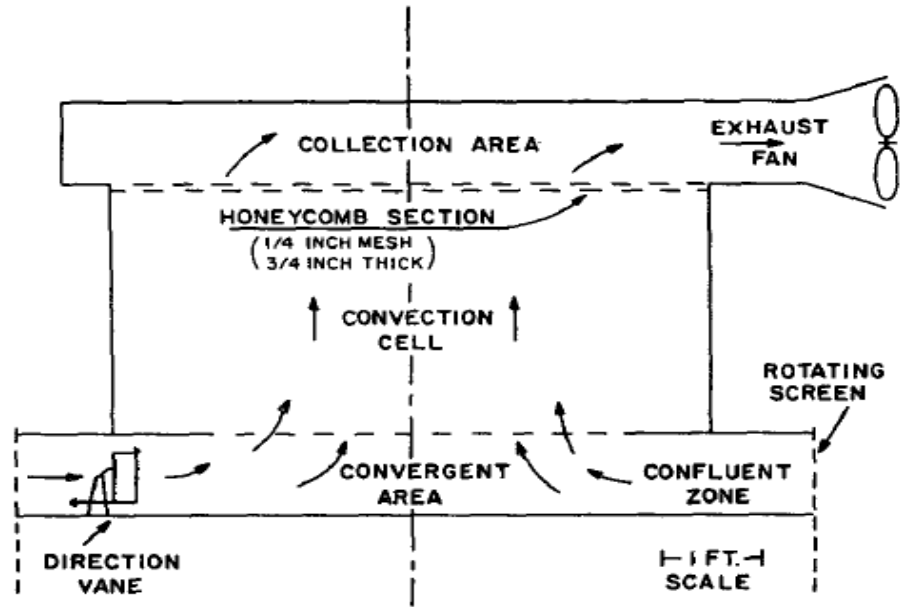
Figure 2.5 Vertical section of ward model
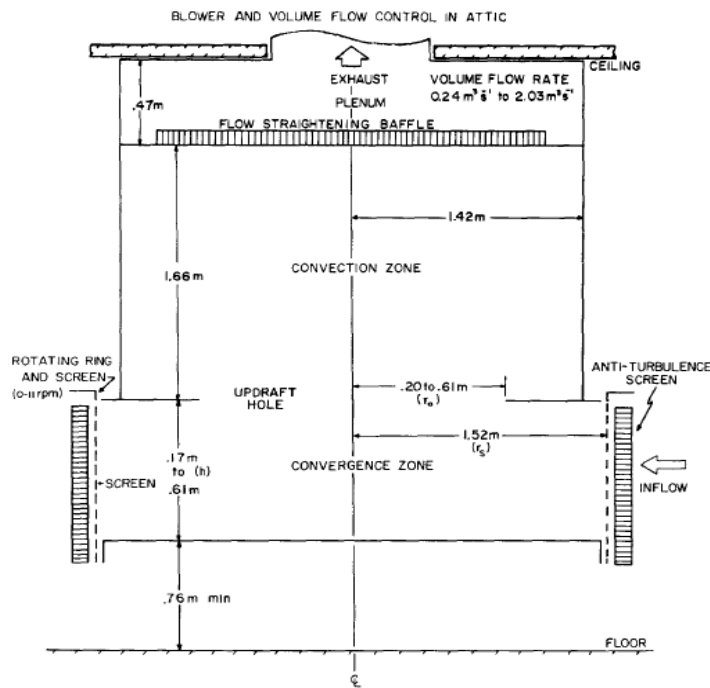
Figure 2.6 Church et al. simulators schematic section

Mitsuta and Monji (1984) introduced a new approach to produce circulation. In this

model the circulation was generated by using four small fans as shown in Figure 2.7. They

defined the swirl ratio as shown in Equation (3). They concluded that the radius of the vortex depends on the swirl ratio and it does not get affected by Reynolds number. The transition from single vortex to multi-vortex happened at unknown swirl ratio value. The flow was turbulent for both single and multi-vortex and this could be because of the turbulence of the inflow.

Mishra et al. (2008a & 2008b) have built another version of Ward simulator at Texas Tech University; however, they used blower which is connected to the top of the chamber through a long duct. Also, the circulation has been provided using slotted jets. The apparatus is illustrated in Figure 2.8. The data for tangential velocity were in good agreement with both RCV model and full-scale data from actual tornadoes. Also, the redial velocity data were comparable with the available date Spencer tornado of 1998. They also used another approach to validate their model by comparing pressure data from the ground of the simulator with the full scaled data.
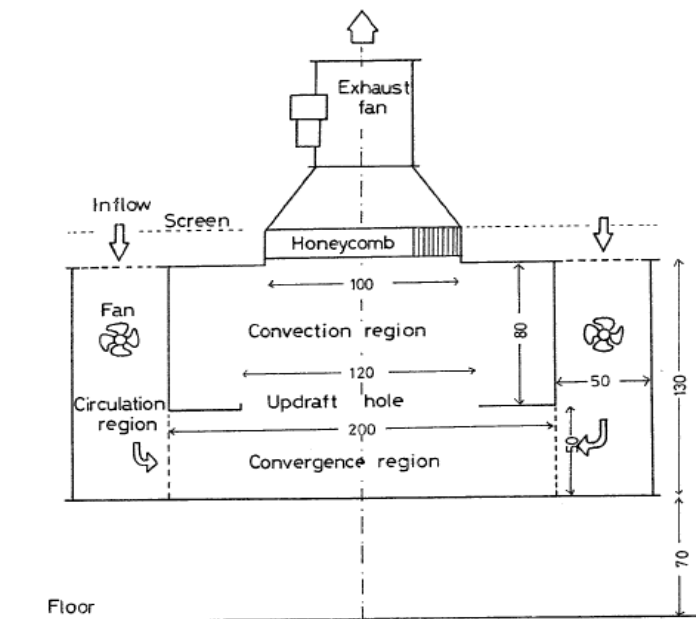
Figure 2.7 Mitsuta and Monji apparatus
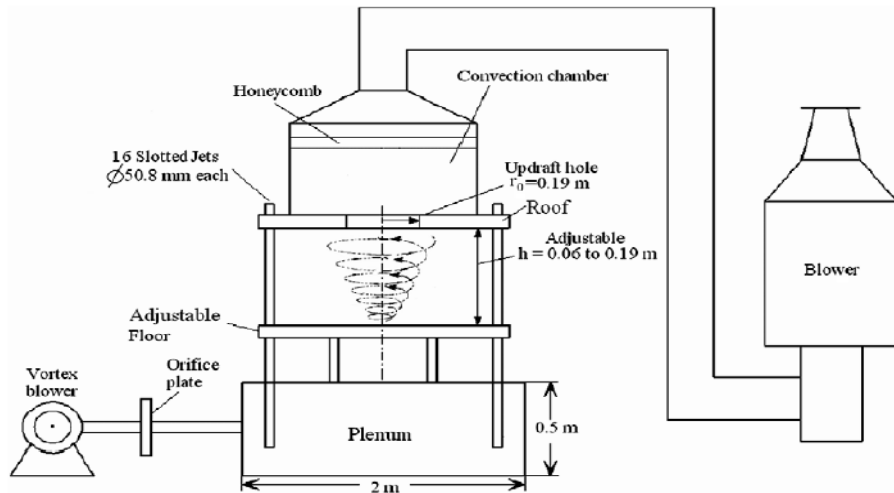
Figure 2.8 Texas Tech University Simulator

2.7.2. Open Chamber Simulators

The first translating tornado simulator was built by Iowa State University (ISU) research group (e.g. Sarkar et al. 2006, Hann et al. 2008 and Yang et al., 2011) as shown in Figure 2.9. In this tornado simulator, the updraft flow is generated using a huge direct drive fan. Then, the outflow is imparted by directed vanes through a circular duct to provide the required angular flow. The simulator successfully produced one-cell and two-cell vortices for a swirl ratio ranging from 0.08-1.14. Their experiment illustrates that the tornado simulator can be used in capturing the characteristics of a real tornado, and it could be a useful tool to study tornado forces on structures.
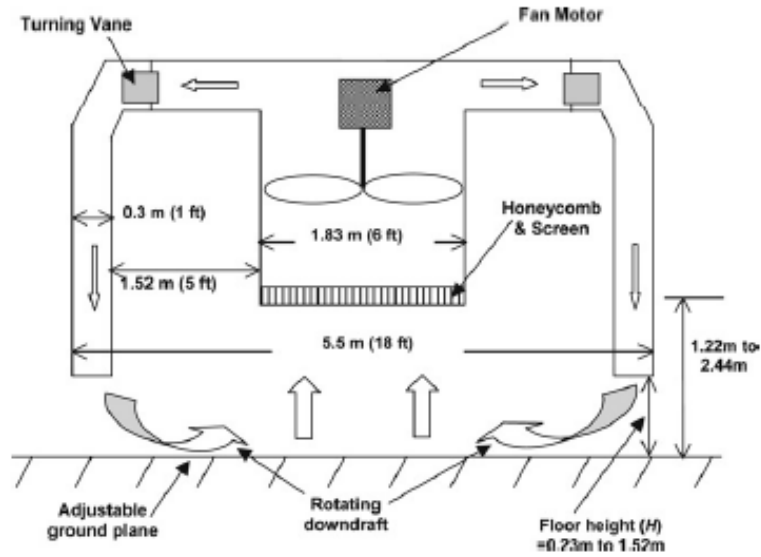
Figure 2.9 Iowa State University tornado simulator

In these entire tornado simulators, the main focus was tornado itself. Therefore, different geometrical parameters (e.g. aspect ratio, inward height, flow rate, rotation velocity, etc.) have been studied to determine the geometrical effects on the generated vortex. The most significant dimensionless parameter affecting the tornado outbreak and tornado structure is the swirl ratio which is defined in equations 2.3 to 2.5. Even though different types and dimensions of tornado simulators have been built, the effects of changing the updraft opening diameter and the height between updraft opening and inward upper edge have not been studied. It is expected that changing the updraft opening diameter may produce vortex of different sizes. Also, the adjustable height between the updraft opening and the inward upper edge may produce higher pressure on the ground surface. In the aforementioned wind tunnel studies, the influence of changing the tornado size and tornado updraft pressure on tornado forces applied on structures has not been investigated. In addition, the tornado-terrain interaction has not identified clearly.

2.8. Tornado-Terrain Interaction

As aforementioned, tornado may strike any location. Also, it has been seen that tornado has been tracked in a mountain and hilly regions by Fujita and his group through post damage investigations. However, no attention has been paid to terrain influence on tornado characteristics and damage.

Lewellen (2012) employed immerse boundary method and a modified LES model presented by Lewellen et al. (2008) to simulate tornado interaction with different topography. Figure 2.10 shows a sample simulation conducted by Lewellen (2012). He has conducted more than 250 simulations with different tornado characteristics (tornado swirl ratio, size, and translation velocity) and different topographical shape (ridges, knolls, valleys, ridge pairs, ridges with gaps, etc.). They stated that topography has effects on tornado near-surface flow, and they mainly noticed that tornado path deviates due to the presence of topographical objects. Even though a lot of simulations have been conducted, no clear conclusion is provided regarding tornado damage difference between windward side and leeward side. Also, they did not provide any information for the tornado characteristics, topography dimensions and tornado deviation details.
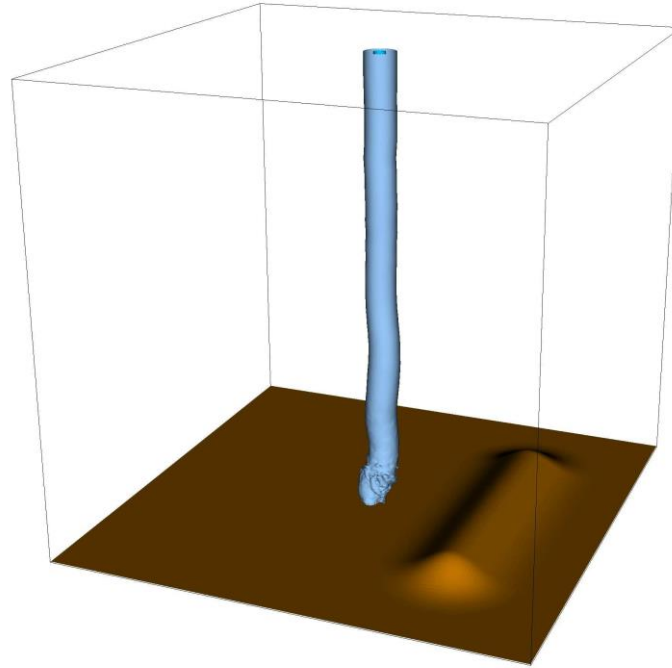
Figure 2.10 Sample simulation for tornado-terrain interaction (taken from Lewellen 2012)

Karsten et al. (2012) utilized the ISU simulator to investigate the topography effects on tornado characteristics. They transport the vortex over idealized two-dimensional models of a ridge and an escarpment. Figure 2.11 shows the minimum negative pressure on the surface of the 2D ridge investigated by Karsten et al. (2012). They observe that the tornado deviates from the center line to the left while climbing up the ridge and to the right when it moves down ridge. However, an explanation for why the deviation is happening has not been provided.
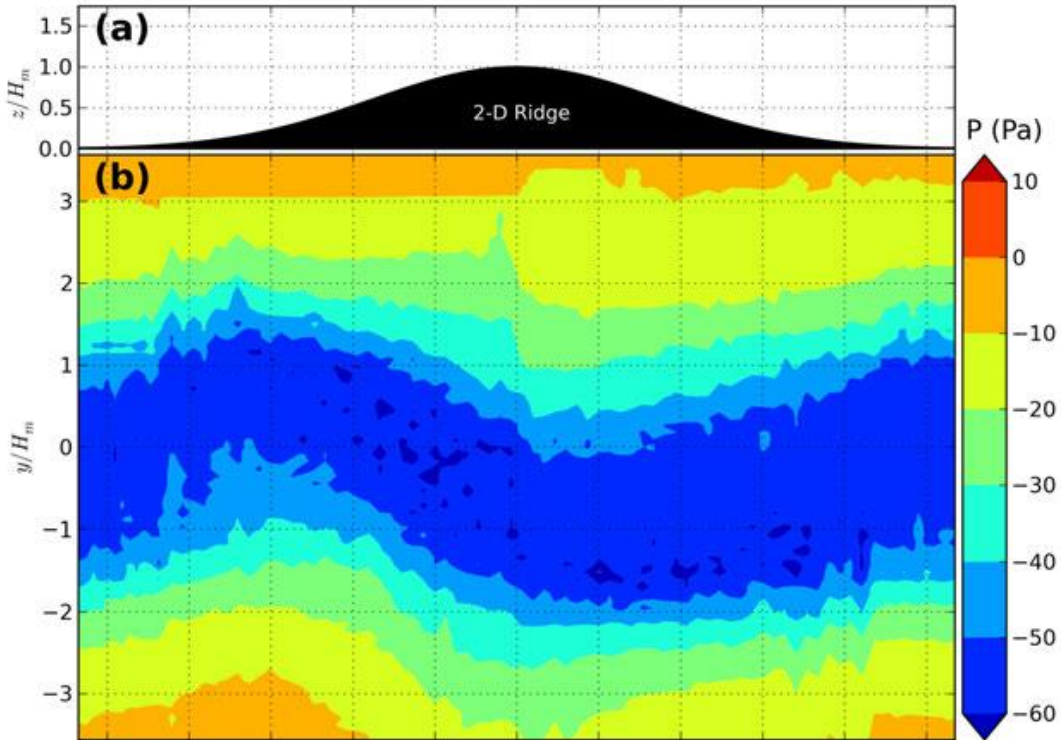
Figure 2.11 a) Cross section of the idealized 2-D ridge, b) minimum negative pressure on the model surface. Vortex translation is from left to right. (Taken from Karsten et al. (2012).)

2.9. Summary of the Reviewed Works

Tornado has been a focus for different research disciplines in the last five decades. Tornado damage is assessed and rated by a comparison to damage indicators. Then, tornado severity is defined using the F and EF scales. Also, tornado is simulated extensively by wind tunnel simulators to understand tornado outbreak and tornado forces on structures. In addition, CFD is employed to simulate tornado numerically and to determine tornado forces on buildings. However, terrain effect on tornado has not been investigated or identify clearly. According to the author knowledge, there is no field survey is done to explore topography effects on a real tornado. In addition, terrain (ridges and hills) influence on tornado wind and forces has not even been touched. Therefore, tornado-terrain interaction studies are initiated to richen the knowledge.

In this work, field investigation using Google Earth and field survey conducted by University of Arkansas (UA) investigation team are utilized to determine terrain influence on tornado damage. Also, a computer model using CFD is developed to simulate tornado interaction with terrain and study this interaction in details.

3. COMPUTER MODELING

3.1. Introduction

Tornadoes are one of the most violent phenomena in the universe. Best way to have better understanding for tornadoes is to study real tornadoes and collect tornado velocities and pressure during tornado life. Also, it is much better to determine the effects of terrain and structures on tornado characteristics in reality. However, these tasks are impossible right now and associated with high risk. The best alternatives are computer and experimental modeling. In this chapter, the computer modeling is discussed. Tornado-terrain interaction is a complex phenomenon. However, due to huge development in Computational Fluid Dynamic (CFD) in recent years, several attempts have been conducted to clarify and understand this phenomenon. CFD promises huge advantage over experimental work due to easiness and economic cost. CFD provides full access to wind field (details of pressure and velocities) as well as allowing a control of important simulation parameters. The CFD program for tornado simulation is first developed by McDonald and Selvam (1985) to calculate tornado forces on a building in 2D, but the main development to this program is done when Selvam and Millet (2003) introduced the first 3D translating tornado. The program simulates tornado interaction with cubic structures. The Navier-Stokes equations for incompressible flow were approximated by control volume method, which was found to be more efficient than FEM for orthogonal grid system. The turbulence was considered by LES. In this work the the program is modified to simulate tornado interaction with real terrain data or smooth shape hills and structures using finite element method which provides better discretization for the terrain problem as well as faster convergence with less grid size.

3.2. Tornado Numerical Model

CFD is utilized to study tornado terrain interaction. Tornado wind field model is considered by implementing Rankine Combined Vortex Model (RCVM) which is the simplest model that satisfies Navier Stokes equations (NSEs) as reported by Lewellen (1976). More details for RCVM can be found in Selvam (1993). Details for boundary conditions and implementation of RCVM can be found in Selvam and Millett (2003 & 2005). The turbulence is modeled utilizing Large Eddy Simulation (LES). Finite Elements Method (FEM) is used to approximate the NSEs. Then the approximated equations are solved using a semi-implicit method as explained in the following section.

3.3. NS Equations Solution procedure

The three-dimensional equations for an incompressible fluid using the LES turbulence model in general tensor notation are as follows:

Continuity Equation: $U_{i,i} = 0$ (3.1)

Momentum Equation: $U_{i,t} + U_j U_{i,j} = -(p/\rho + 2k/3)_{,i} + [(\nu + \nu_T)(U_{i,j} + U_{j,i})]_{,j}$ (3.2)

where : $\nu_t = (C_s h)^2 (S_{ij}^2/2)^{0.5}$, $S_{ij} = U_{i,j} + U_{j,i}$, $h = (h_1 h_2 h_3)^{0.333}$, and $k = (\nu_T/(C_k h))^2$. Empirical Constants: Cs=0.1, and C_k=0.094

Where U_i, and p are the mean velocity and pressure respectively. k is the turbulent kinetic energy, ν_T is the turbulent eddy viscosity, h1, h2, and h3 are control volume spacing in the x, y, and z directions, respectively, and ρ is the fluid density. Here the area or volume of the element is used for the computation of h. A comma represents differentiation, t represents time, and i =1,

2 and 3 refers to variables in the x, y and z directions. For further details, one can refer to Selvam (1997)

The incompressible momentum and continuity equations are solved using sequential solution procedures. In this work the following sequential procedure is used to solve the unsteady NS equations:

1. Solve velocities using the momentum equations.

2. Solve the pressure using the new velocities:

$$\Delta P = [\partial U / \partial x + \partial V / \partial y + \partial W / \partial z] / \Delta t - [\partial(U\partial U / \partial x + V\partial U / \partial y + W\partial U / \partial z) / \partial x$$
$$+ \partial(U\partial V / \partial x + V\partial V / \partial y + W\partial V / \partial z) / \partial y + \partial(U\partial W / \partial x + V\partial W / \partial y + W\partial W / \partial z) / \partial z]$$

(3.3)

Here U, V and W are the velocities in the x, y and z direction, P is the pressure over density and Δt is the time step. At each time step the variables are solved sequentially in an implicit manner. The absolute sum of the residue error for each variable is reduced to certain convergence value say IM*JM*KM*10^{-5} where IM, JM and KM are the number of points in the x, y and z direction respectively. At the same time the iteration is repeated until the beginning residue of all the variables reduces to certain converged value. The sub-iteration makes sure that a converged solution is obtained. In the beginning of the computation the velocities are assumed as undisturbed values and hence the sub-iteration will be very high to reduce the error. After a while the number of sub-iteration could be around 5.The above sequential procedure is a general version of the one used by de Sampio et al. (1993) using least square FEM. The procedure is also similar to Selvam and Paterson (1993) and Tamura (1995 & 1999) using FDM. The pressure equation is arrived by differentiating the momentum equation with respect to x, y and z and adding them. In the equation, higher order terms as well as the continuity equation for the current

time step are dropped. This eliminates the pressure correction step suggested in Selvam (1997 & 1998) and hence is computationally efficient and also conducive for higher order elements. This procedure is also much stable and useful for adaptive and other techniques. When solving the equations by FDM or CVM using cell centered grids, the pressure values are solved in the fluid cell center and then the pressure is extrapolated on solid. Rather than this approach, if the pressure is solved over the solid body the accuracy is much better as discussed by Selvam and Peng (1998). The above equations are solved by FEM. Even though FEM takes more computer time the transport accuracy of the vortices are very high as reported in Selvam (1998) and hence it is preferred in this work. Because of the large computing time, the model is parallelized by making subdomain in the vertical direction. The data from one processor to another is communicated using MPI. The detail of the parallel computing is reported in Sarkar and Selvam (2009). The equations are solved by preconditioned conjugate gradient (PCG). The initial time step used is 0.01 time unites (0.01 sec), and the computer model is ran for 90 time units and this takes 720hrs (30days) when serial computing (one processor) is used. However, this time is reduced ten times to 72hrs (3 days) when the distributed parallel computing (24 processor, MPI) is utilized. The processors used are dual hex-core Xeon X5670.

3.4. Computational Domain and Grid Generation

A terrain following grid system shown in Figure 3.1 is used here. Different terrain following coordinate systems are discussed in Pielke (1984) and Selvam and Rao (1996). To reduce the time in grid generation, equal spacing is used in the x and y directions and almost the same spacing in the z-direction. The top boundary in the z-direction is kept far away from the ground and having the same elevation from the flat ground. The equal spacing in the horizontal directions (X&Y) helps to use the program to directly consider the coordinates from the GIS

system for an actual complex terrain site. The ground elevation for each x and y point is provided as h(x,y). The desired grid spacing in the z-direction far away from the ridge is provided at one (x,y) point. In this study the z-spacing is kept constant. When the distance between the ground and the top boundary changes because of ground elevation then a proportional spacing to that of the flat ground spacing is used from the following relationship:

$$Z_K^t = h(x, y) + (h^t / h^f)(Z_K^f - Z_1^f) \qquad (3.4)$$

Where $h^f = Z_{km}{}^f - Z_1{}^f$ and $h_t = Z_{km}{}^f - h(x,y)$. Here the superscripts f and t refer to the reference height at the inflow and a height at any point in the domain respectively.
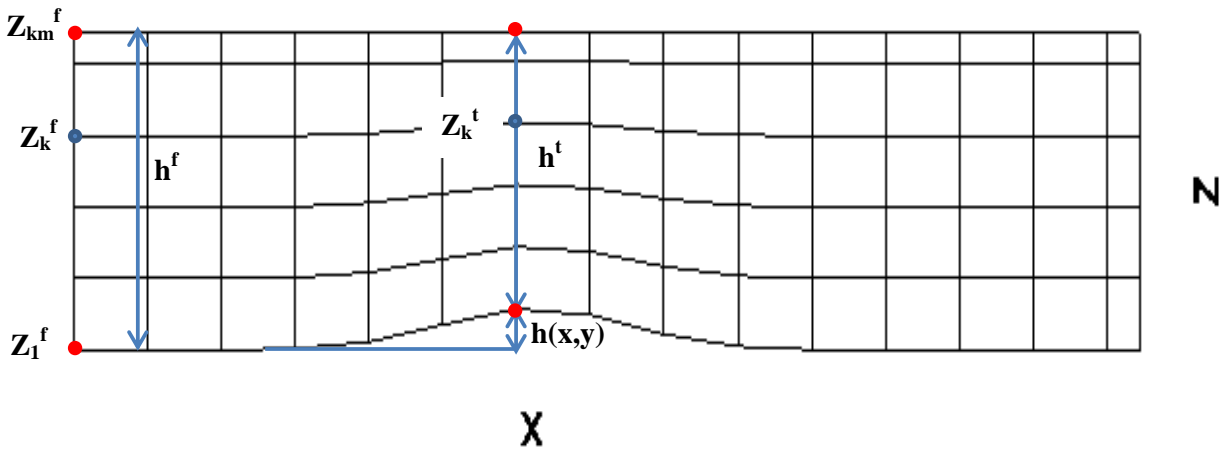
Figure 3.1 Notations for terrain following grid system.

3.5. Problem Geometry

The CFD tornado model at the University of Arkansas is developed to simulate tornado interaction with a smooth hill or even real terrain data hill. Figure 3.2 illustrates basic parameters for the computational fluid domain.
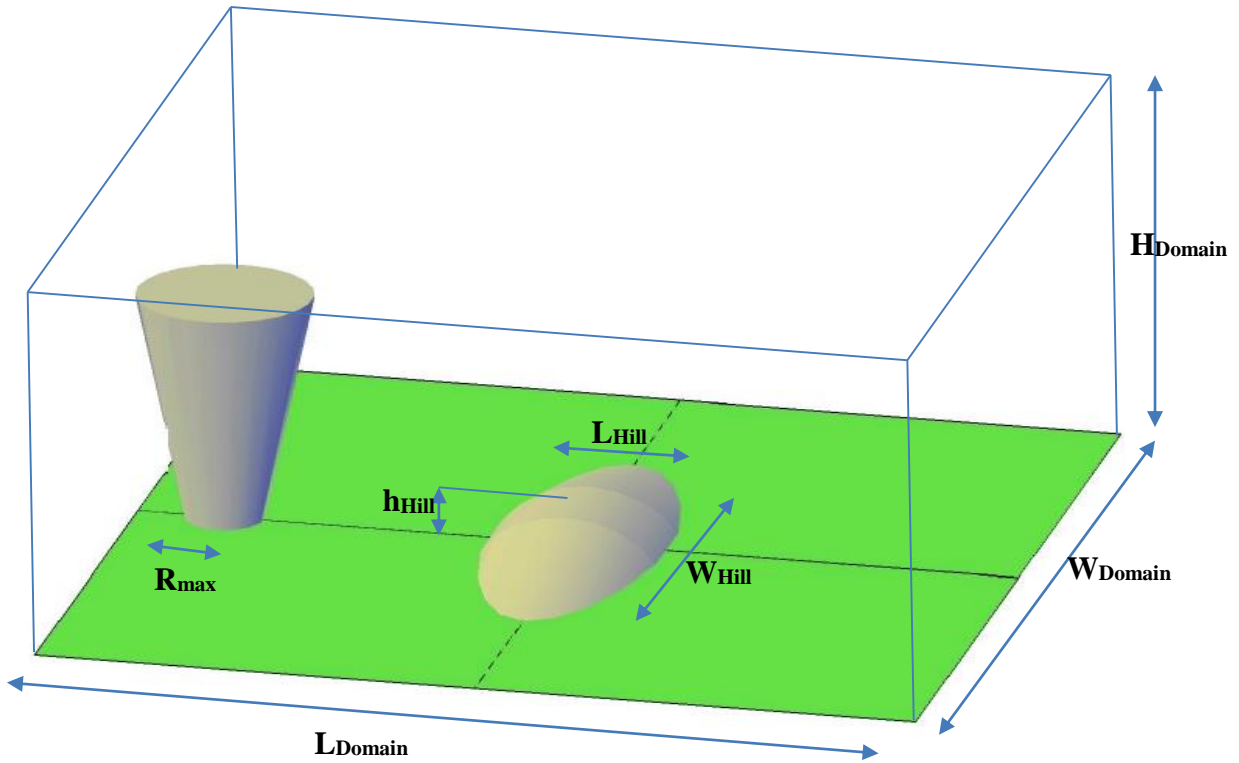
Figure 3.2 Basic parameters for computational fluid domain.

Where R_{max} is the tornado radius, and h_{hill}, L_{hill} and W_{hill} are the height, length and width of the hill respectively. H_{Domain}, L_{Domain} and W_{Domain} are the height, length and width of the domain respectively. The hill center is located at the origin. The tornado coincides with center of the hill after time equals to time lag as illustrated in Figure 3.3.
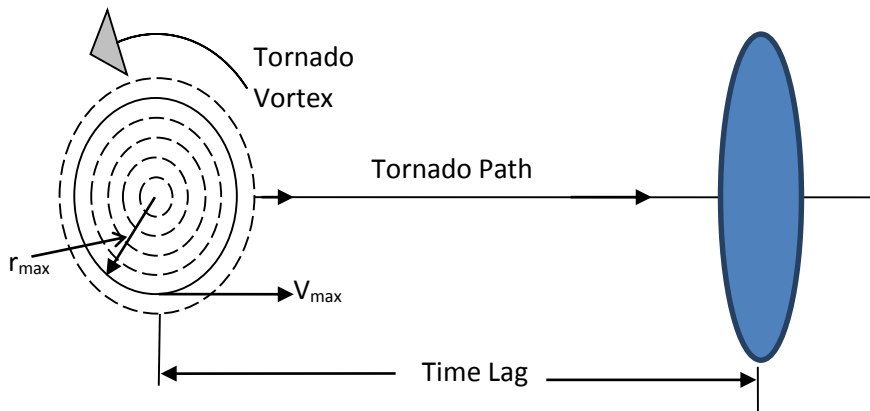
Figure 3.3 Simulation parameters and geometry.
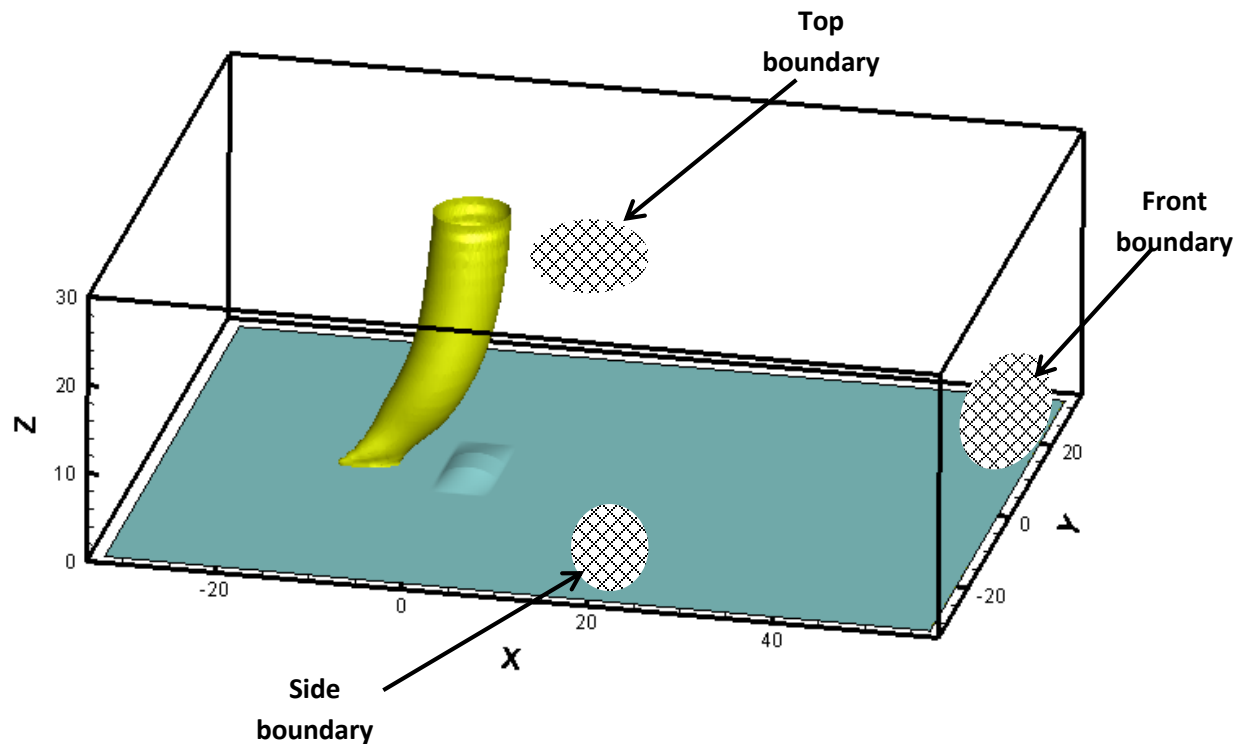
Figure 3.4 Boundaries for the computational domain.

Computational domain size has great influence on tornado simulation. This means that the boundaries of the computational domain should be located at a distance so that there is no influence of the boundary conditions on the numerical solution. By choosing an optimal computational domain size, convergence can be achieved faster as well as computational can be reduced (Gorecki, 2015). Also, better choice for the domain size can lead to less number of grid points and less memory storage. In the same time the boundaries of the domain should be kept at a reasonable distance away from the hill to avoid influencing the tornado flow. Figure 3.4 shows the front boundary, top boundary and side boundary for the computational domain. A detailed study for the grid size and domain size is investigated in chapter five. All parameters used in the

model are non-dimensional. The dimensionless length, velocity and time (respectively: L*, U*, t*) are calculated as follows:

$$L* = L/Lref, \ U* = U/V, \ t* = t.V/Lref$$

Where: L, U and t are length, velocity and time; Lref – referenced length equal to the height of the hill; V – referenced velocity, equal to the translational velocity.

3.6. Boundary Conditions

For the University of Arkansas tornado simulator, boundary conditions considered to be one of the most important factors in generating the translating vortex. Every grid point on the boundary is assigned a specific velocity component so that the tornado is created. Since the vortex is assigned to move along the X-axis where X=0, these velocities are calculated depending on the tangential velocity profile of RCVM. The computational domain used for tornado simulation is shown in Figure 3.5. The velocities are specified for all six surfaces. The no-slip condition is implemented for the ground of the domain. For all the vertical surfaces, the vertical velocity component V_z is assumed to be zero. V_x and V_y are calculated using RCVM as presented in the equations below.

$$V_x = \left[V_{tx} + \left(V_{ty}t - y\right).\alpha\right].Z_f \ \ for \ r \le r_{max} \tag{3.5}$$

$$V_x = \left[V_{tx} + \left(V_{ty}t - y\right).C\right].Z_f \ \ for \ r > r_{max} \tag{3.6}$$

$$V_y = \left[V_{ty} + (x - V_{tx}t).\alpha\right].Z_f \ \ for \ r \le r_{max} \tag{3.7}$$

$$V_y = \left[V_{ty} + (x - V_{tx}t).\alpha\right].C.Z_f \ \ for \ r \le r_{max} \tag{3.8}$$

Where: V_{tx} - x-component of V_t, V_{ty} - y-component of V_t, $C= \alpha r^2_{max}/r^2$, $r^2= (x\text{-}V_t.t)^2+y^2$, $Z_f= u^*{\cdot}ln((z+z_0)/z_0)/\kappa$, z_0 – roughness length of the ground (equal to 0.00375), u^* – frictional velocity at certain height, determined from known velocities, κ - constant, equal to 0.4, z – height from the ground. The details of the formulation of these equations are presented in (McDonald and Selvam, 1985) without the boundary layer effect. The boundary layer effect is introduced in Selvam (1993).
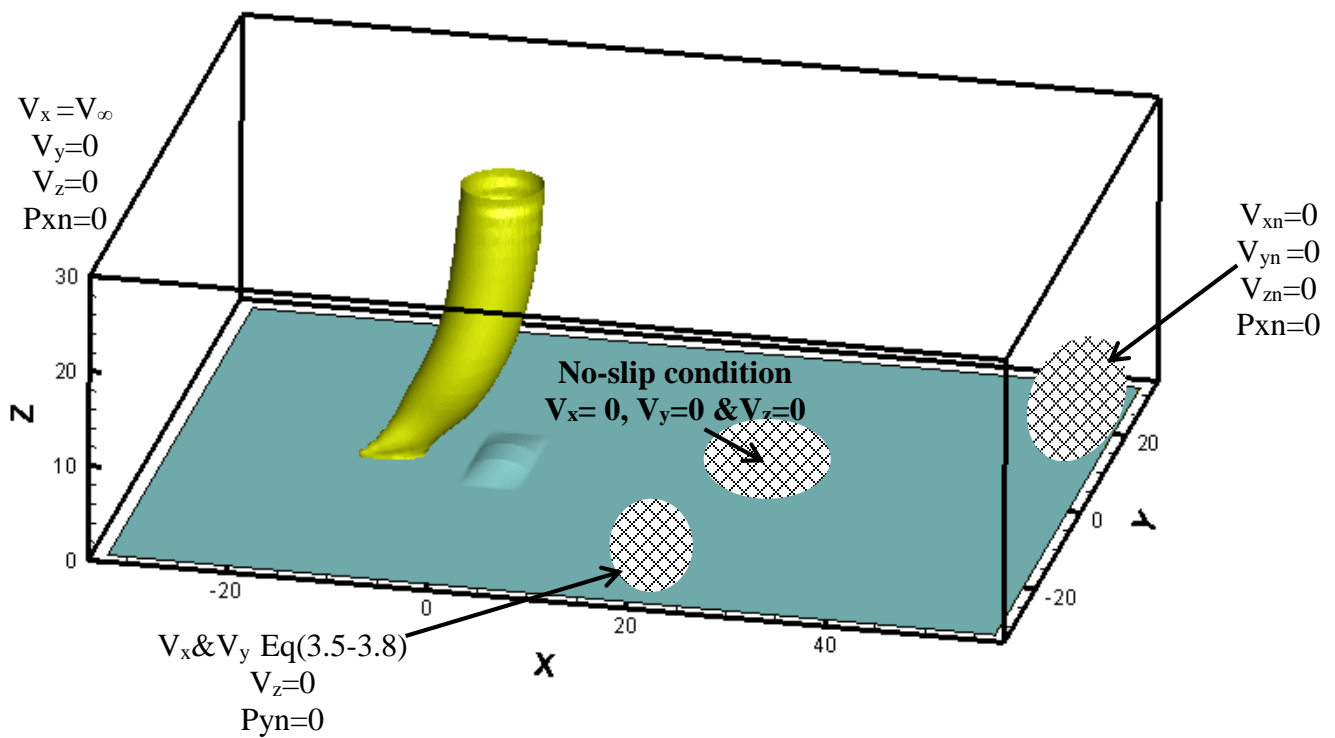
Figure 3.5 Boundary conditions for the computational domain.

3.7. Parallel Computing

3.7.1. Why Parallel?

There has been a huge advancement in computer hardware technology, and computer processers speed have increased about 5000 times since 1970. However, in a sense of serial computing, there is still huge limitation since one operation is done at a time in serial computing process (see Figure 3.6 a). Therefore, to run a problem of tornado simulation over a complex terrain with reasonable accuracy (about 8 million points with equal spacing) using serial computing takes 720 hrs. This is a whole month to have only one set of data without any post processing or visualization. Therefore, the distributed parallel computing is utilized to solve the problem and check the performance. A schematic illustration for how the parallel computing is done is presented in Figure 3.6 b. A problem of (290x290x90) 7.569 million points is run using single- and multi-processor to find the optimum number of processors which provide the minimum run time. The results are presented in Table 3.1. It is concluded that for this specific problem the optimum number of processors is 24. The parallel computing is done by solving the pressure equation which usually takes most of the computation time. This is done by assigning certain number of z-plane for each processor as shown in Figure 3.7, and it is known as domain decomposition. The node information at edge of neighboring domain needs to be transferred often, and it is called boundary swapping. General data swapping between processors is illustrated in Figure 3.8.
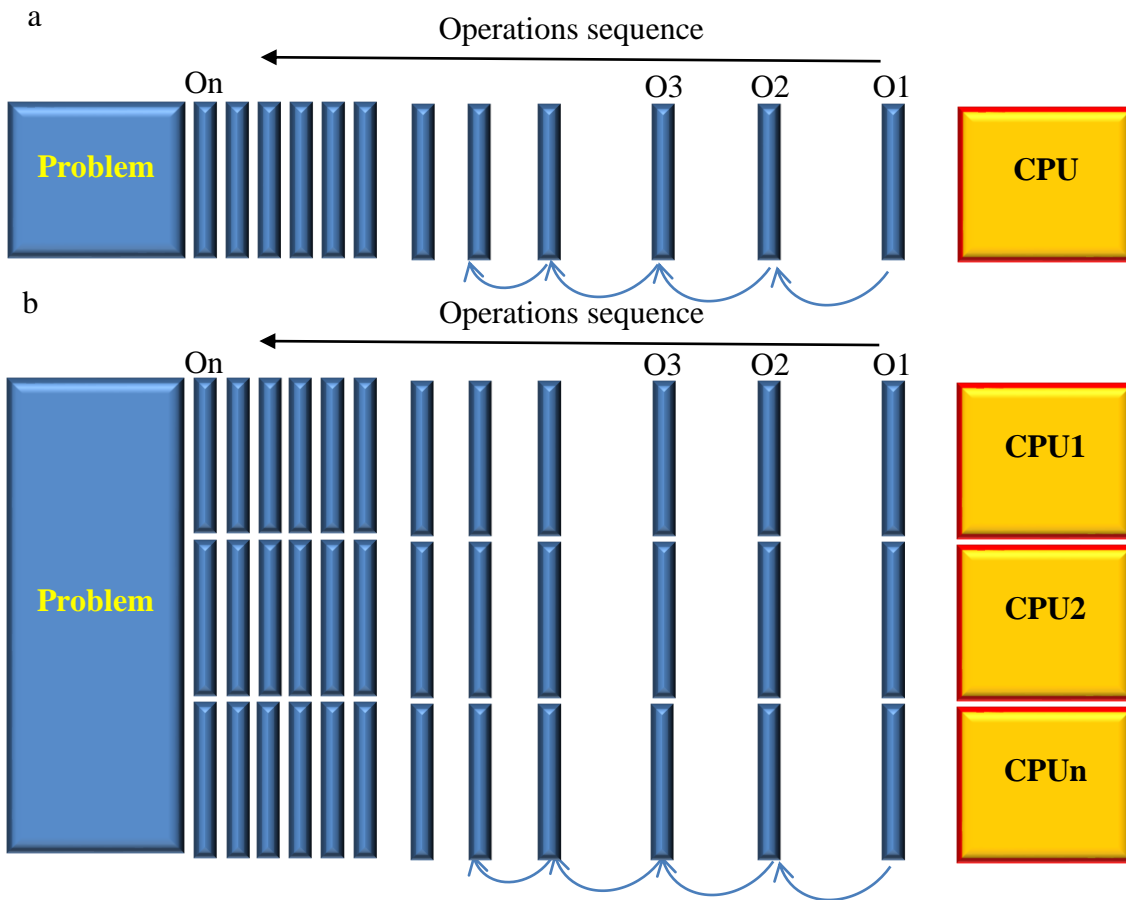
Figure 3.6 a) serial computing b) parallel computing.

Table 3.1 Optimum CPU time for single- and multi-processor.

Number of Processors	CPU time (hrs)	Speed-up Factor
1	720	1
2	379.8	1.81
4	225	3.2
6	166.67	4.32
8	160	4.5
24	72	10
36	90	8
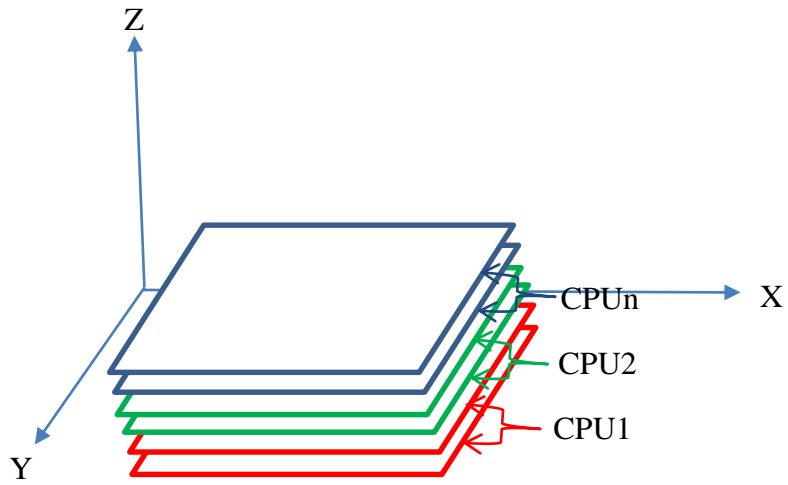
Figure 3.7 Tasks distribution in parallel computing.
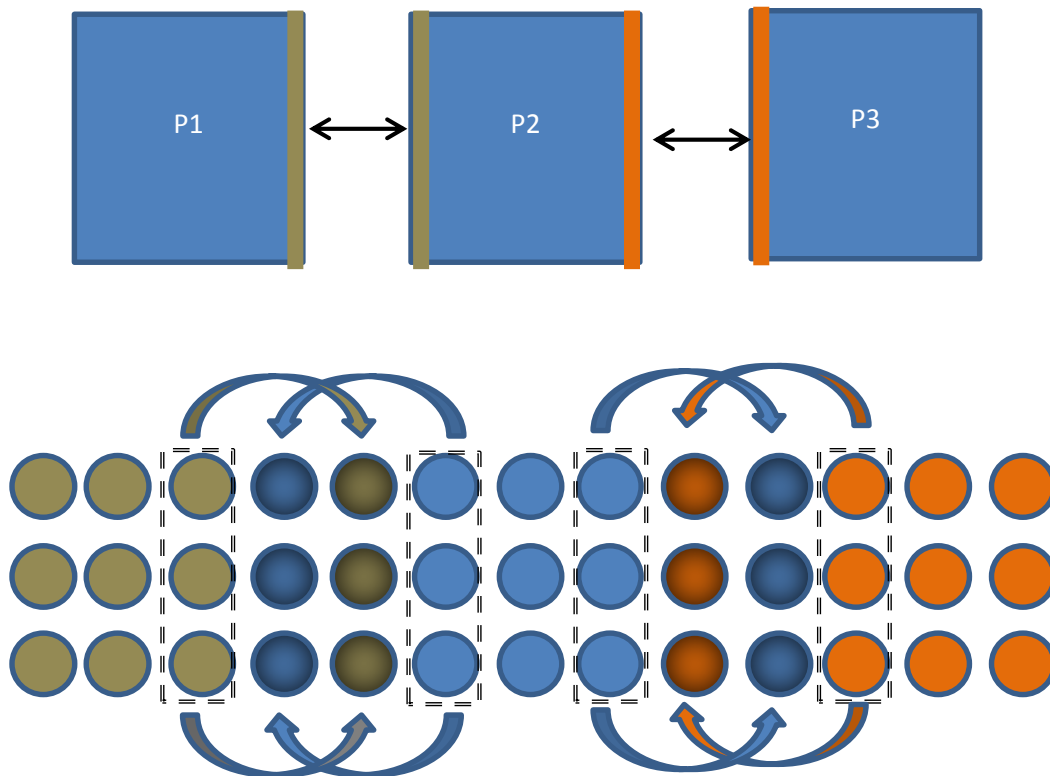
Figure 3.8 Data Transfer in 1D domain decomposition. Shaded circles are the ghost points and the circles encircled by the dashed lines are points to be moved.

3.7.2. Speed Up and Efficiency Study for Parallel Computing

Two common parameters to monitor the parallel computing performance are "speed up and efficiency". The speed up is defined as ratio of single processor time to the time of a certain number of processors (serial time/parallel time) for a specific problem. On the other hand, efficiency is the percentage of the speed up to the number of processors (Sarkar and Selvam, 2009). When algorithms are designed originally for traditional serial computing may not perform efficiently on parallel computers. Therefore, a better approach to perform parallelism is to subdivide the solution domain into sub-domains and assign each sub-domain to one processor. This is called domain decomposition (DD) which can be done in 1D, 2D and 3D to achieve a better efficiency as discussed in Gropp et al. (1994). In this case, the same code is used on all processors. Since each processor needs data available in the neighboring sub-domains, exchange of data between processors is necessary. This is called communication overhead. In this work, 1D domain decomposition is used in the Z direction as illustrated in Figure 3.7. Figure 3.9 a and b show the speed up and the efficiency performance of parallel computing for different number of processors. From Figure 3.9 a, one can see that there is slow down after the number of processors is more than 24 processors. As show in Table 3.2, the minimum number of planes assigned for each processor is 3 which requires communication with the two neighboring top and bottom domain for solution compilation. Three is the optimal number of planes that can provide better computation performance over the processors communication time. When the number of planes is two, then the processors communication time will govern the computation time.
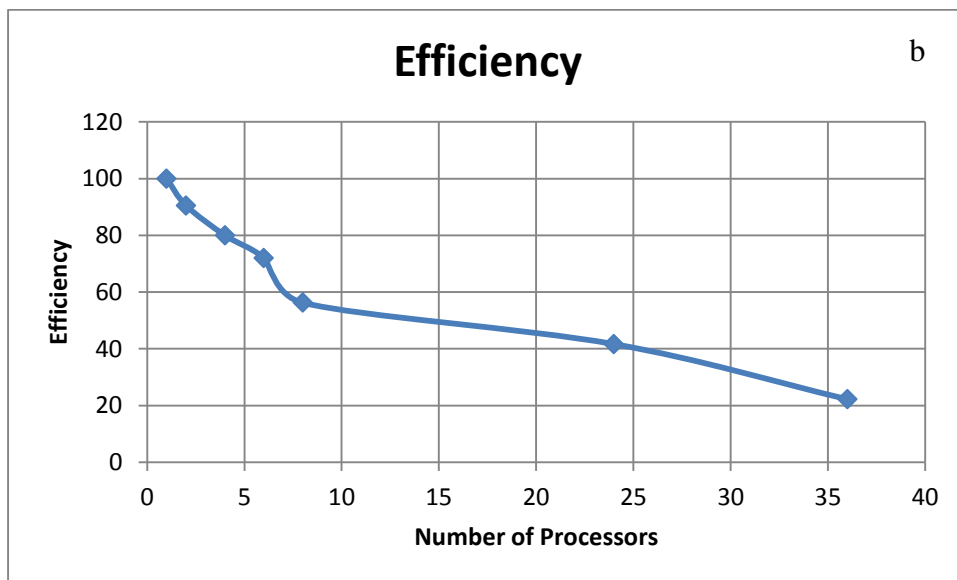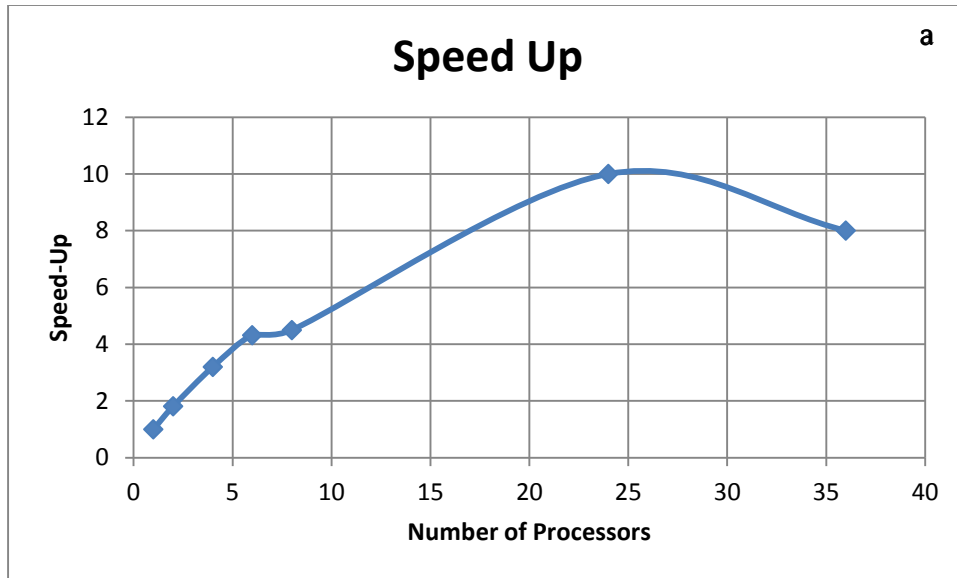
Figure 3.9 a) Speed up b) efficiency of parallel computing

Table 3.2 Domain decomposition in 1D (Z axis) for parallel computing using 24 processors.

Processor ID	Start plane index	End plane Index	Plane for a Processor
0	1	4	4
1	5	8	4
2	9	12	4
3	13	16	4
4	17	20	4
5	21	24	4
6	25	28	4
7	29	32	4
8	33	36	4
9	37	40	4
10	41	44	4
11	45	48	4
12	49	52	4
13	53	56	4
14	57	60	4
15	61	64	4
16	65	68	4
17	69	72	4
18	73	75	3
19	76	78	3
20	79	81	3
21	82	84	3
22	85	87	3
23	88	90	3
Total Number of Planes			90

4. TORNADO-HILL INTERACTION: DAMAGE AND SHELTERING OBSERVATIONS

4.1. Introduction

Tornadoes occurrence is not restricted by a place or time. However, tornadoes happen frequently in a regain called Tornado Alley which is often not associated with a complex terrain – a terrain of several successive topographical configurations (hills, ridges, escarpments and knolls, etc.). Therefore, it is reasonable that very less attention is paid for topography effects on tornado damage. However, tornado can hit a hilly terrain or even a mountain area. Tuscaloosa-2011which is one of the deadliest tornadoes in the last fifty years grasps researchers' attention to investigate the effects of a complex terrain on tornado damage.

In this chapter, three tornadoes (Parrish-2011, Tuscaloosa-2011 and Mayflower-2014) are considered to investigate the effects of topography (hills) on tornadoes damage. The analyzed data comprises Google Earth views, aerial images provided by Civil Air Patrol (CAP) and ground photos taken by University of Arkansas (UA) team. Tornado damage is investigated on windward and leeward sides of several hills to evaluate hills sheltering. Also, tornado damage is explored when a place is surrounded by hills. Damage of houses around a hill is analyzed and rated using EF scale to illustrate the difference between damage uphill and downhill. It is found that there is significant influence of hills on tornado damage, and much damage is observed on windward side of a hill comparing to its leeward side. Also, when a tornado crosses a hill, the hill provides sheltered zone on its leeward side. For the investigated hills, measurements for the sheltered zone on the leeward side of the hills show that the sheltered zone length is about five times the hill height (5h).When the tornado hits a place surrounded by hills and the distance

between the hills along the tornado path is almost equal to the tornado radius, the damage is noticed only on the top of the surrounding hills. The place which is surrounded by the hills is completely protected. When tornado damage is investigated around a hill, the tornado damage observed uphill is higher than the damage observed downhill for the same region hit by the tornado. More investigations to examine the effects of changing hill dimensions and shapes on the sheltered zone length need to be done employing computer models or experimental simulations.

4.2. Background

Recently, a few studies have been made to investigate effects of terrain on tornado path and behavior after the Tuscaloosa-2011 tornado. Lewellen (2012) implemented the immersed boundary method and large eddy simulation (LES) to simulate tornado in 3D domain and study the effects of topographical shapes (ridges, knolls, valleys, ridge pairs, ridges with gaps, etc.) on tornado near-surface wind. For different topographical shapes, different tornado behaviors (e.g. path deviation and pressure values) are observed. Karstens et al. (2012) utilized the Iowa State University (ISU) tornado simulator to determine the effects of idealized topography (ridges and escarpments) on tornado path deviation. They noticed that tornadoes experience deviation from the center line while climbing up and down the topographical profiles. However, the mechanism causing this behavior is not clear. Gorecki and Selvam (2013, 2014 & 2015) studied sheltering efficiency of rectangular man-made walls (rectangular prism). For a wall height equal to the tornado radius, they reported that the sheltering efficiency, the ability of the structure to reduce wind velocity on its leeward side, is almost 40%. Selvam and Ahmed (2013) employed Google Earth to explore terrain effects on tornado damage. Their focus was tornado damage uphill and

downhill as well as sheltering on the leeward sides of hills. They reported that there is no damage in a region surrounded by hills located on the tornado path.

In this work, Field data for Tuscaloosa-2011, Parrish-2011 and Mayflower-2014 tornadoes is considered to examine effects of topography on tornado damage and sheltering. Google Earth is considered for vitalizing available aerial images for Tuscaloosa-2011and Parrish-2011 tornadoes. For Mayflower-2014, ground images arrived by University of Arkansas (UA) team and aerial images provided by Civil Air Patrol (CAP, 2014) are utilized to examine the topography effects on tornado damage and sheltering.

The objectives of this chapter are to examine the topography configurations (e.g. hills) ability on providing hill sheltering (the difference in tornado damage between the windward and the leeward sides) against tornado wind and to determine the difference in tornado damage uphill and downhill. First, the effects of a hill on tornado damage is investigated, and the damage difference on the windward and leeward sides of a hill is examined. Then, the sheltered zone on the leeward side of a hill is measured and evaluated. After that tornado damage for a region surrounded by hills on the tornado path is assessed. Finally, the Enhanced Fujita (EF) scale is utilized to evaluate tornado damage up and downhill by analyzing field data for damage around a hill.

4.3. Tornado Damage on 2D-Type Hill Sides (Parrish-2011)

Parrish-2011 is a short life tornado; however, it has intensity of EF3. The tornado touched down six miles southwest Parrish, AL, and it lifted two miles southwest Bangor, AL. The total travelling path is almost 31 km (19 miles) in 18 minutes (approximate travelling velocity is 103 kmh^{-1}(64 mph)), and the maximum damaged width 0.34 km (0.2 miles) as reported by National

Weather Service Weather (NWS, 2011b). The tornado track (bright color between dashed

Yellow lines) is shown in Figure 4.1 where tornado traveled from southwest to northeast. The

terrain is rich with many hills, so it provides great environment to study terrain effects on

tornado damage. Four sites are selected in this tornado location to examine hills sheltering

efficiency against tornado damage. These sites are four hills labeled by notations (H1 to H4).

Vegetation damage or houses damage are considered to show the hills sheltering. For vegetation

damage monitoring, the undamaged or less damaged area has dark green color, and the damaged

area is distinguished by its faded brown or gray color. The damage percentage based on ground

observation of vegetation damage may differ from damage observed for structures. For each site,

a close up view and the hill elevation profile are illustrated for clear discussion. In Figures

provided in this section, tornado travels from southwest (down left corner) to northeast (upright

corner) unless otherwise mentioned. Tornado struck Parrish, AL on Apr, 27 2011, and the

images were available in Google Earth right the next day (Apr, 28 2011).

A close-up view for the site H1 is shown in Figure 4.2. From Figure 4.2, one can see that

tornado crossed the Hill (H1) causing much damage (enclosed by the dashed yellow line) on the

windward side of the hill (H1), while the leeward side (blue line) is almost completely protected.

This means that the aforementioned hill has provided sheltering on its leeward side. The

approach used in this work to identify the sheltering efficiency for the hills is by measuring the

length of the sheltered zone on the leeward side for each hill. The height of the hill (H1) is about

61 m (200 ft), and the elevation profile for hill (H1) is shown in Figure 4.3. The hill height is

measured as the hill prominent height from the surrounding ground. Slope on both sides of the

hill is very similar. This hill (H1) provided sheltered zone length of almost 305 m (1000 ft)

measured from the yellow diamond (a point where damage is noticed to be reduced or

discontinued) to the end of the sheltered region where the damage is noticed again the leeward

side of hill (H1) as shown in Figure 4.3. Beyond the sheltered region, tornado damage increases

gradually. The sheltered zone length is measured along the tornado traveling line where the

damage is at its maximum level. The sheltered length may vary moving toward the hill side far

from the tornado travelling path.
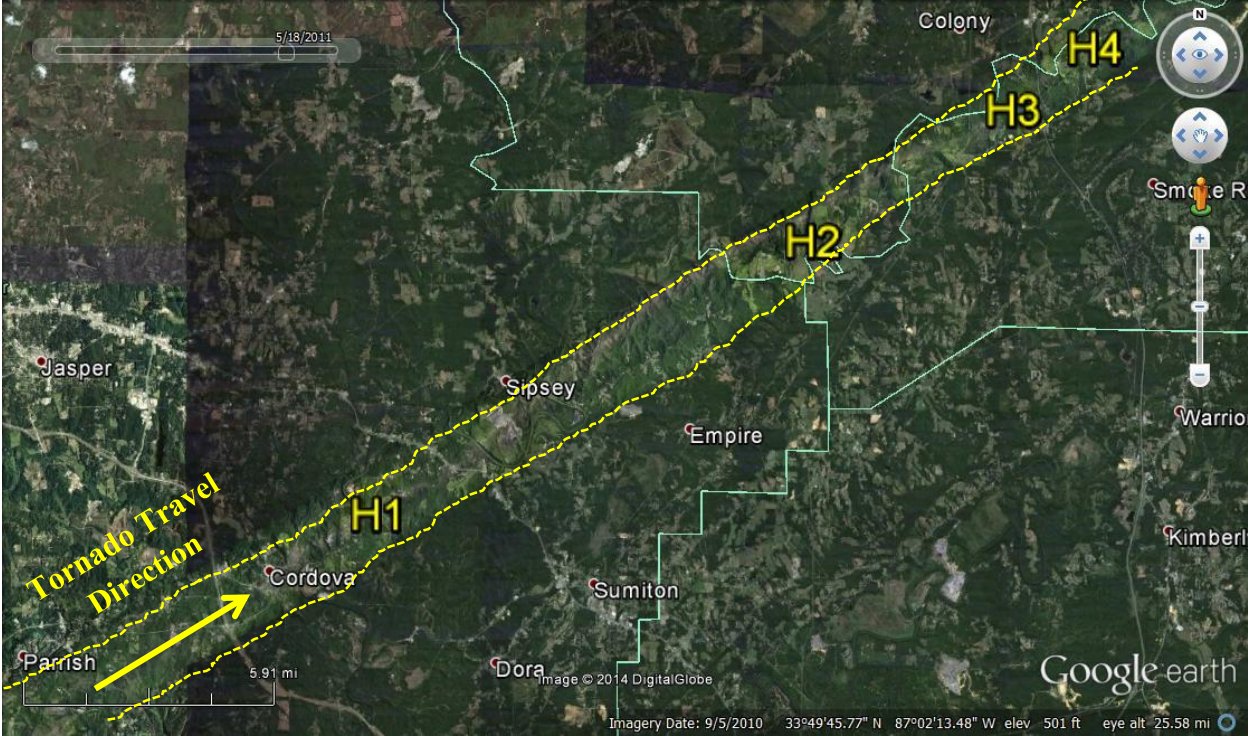
Figure 4.1 The tornado path of Parrish-2011 tornado show the four investigated sites (the bright
color area is the damaged area path).
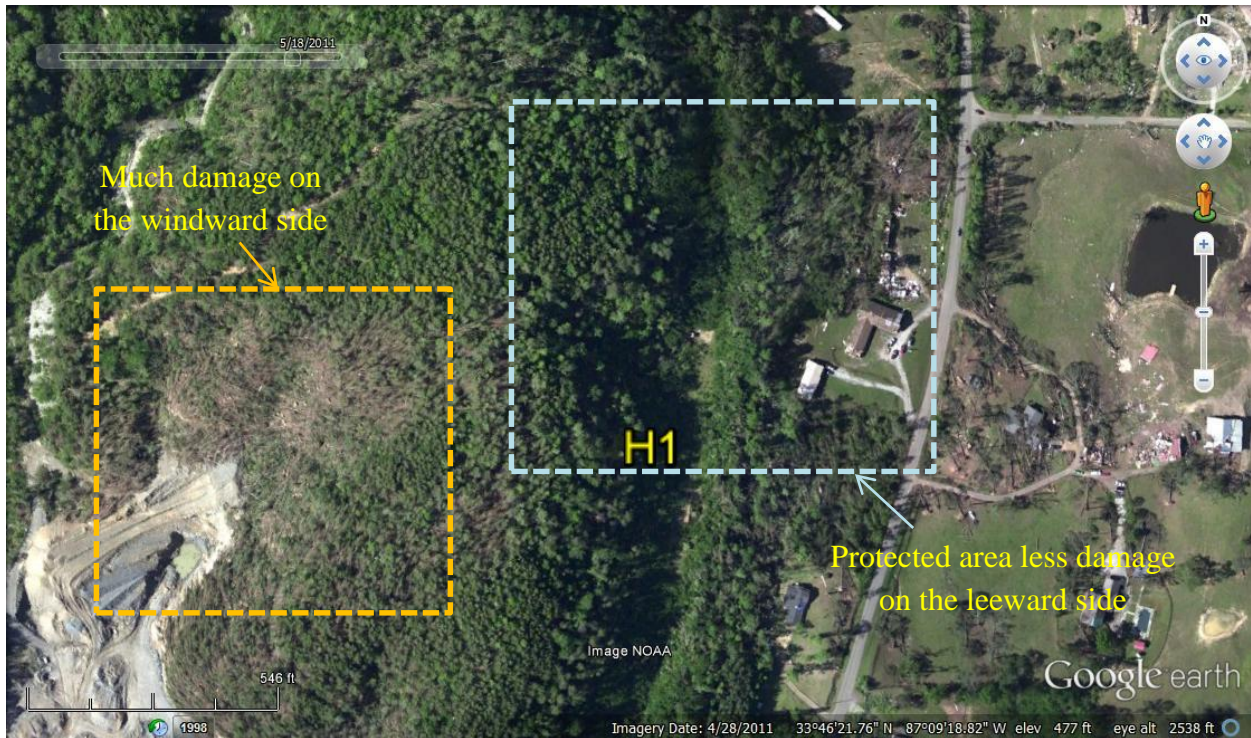
Figure 4.2 Close-up view for hill (H1), much damage on wind ward (the faded brown area, yellow line) and the protected area on the leeward (dark green, blue line).
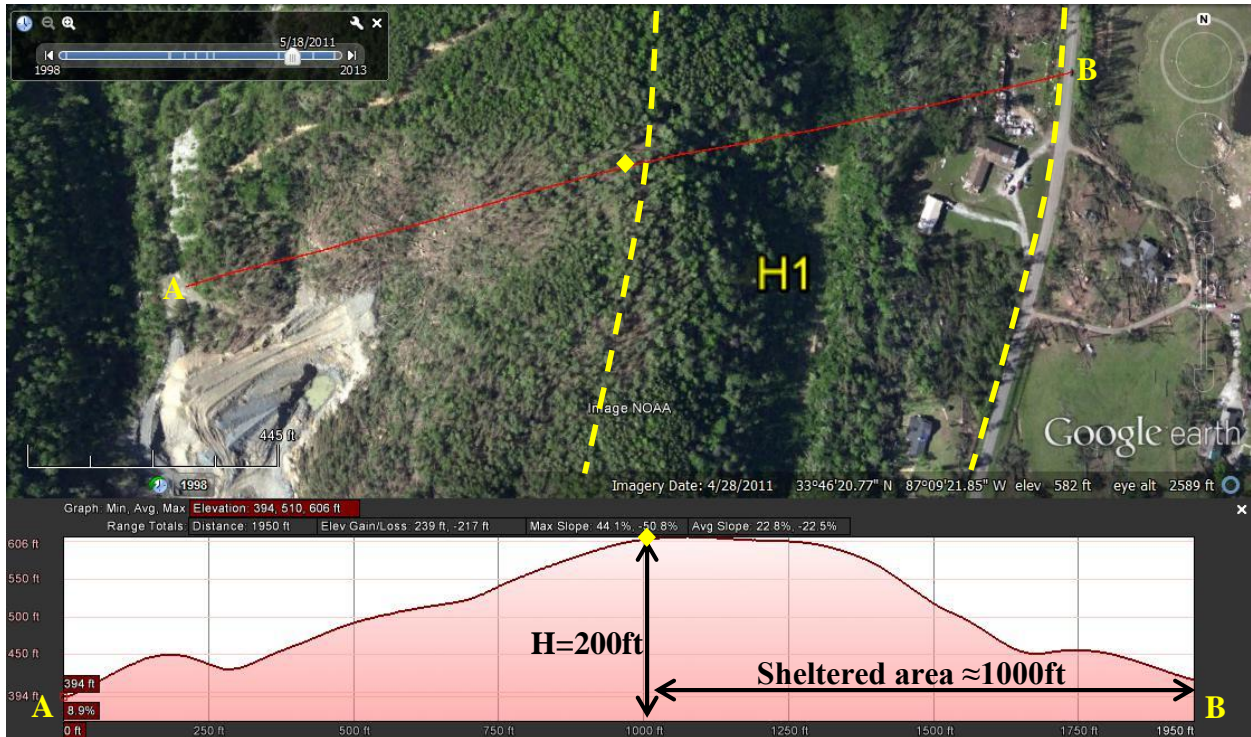
Figure 4.3 Elevation profile along the hill (H1), the protected zone is 5H.

The same analysis is used for the other three sites (H2, H3 and H4) to quantify the outcome. Figure 4.4 is a close-up view for the site H2 showing the damaged and the protected areas on windward and leeward sides respectively. Height of H2 which is detected from the elevation profile shown in Figure 4.5 is about 61 m (200 ft). The sheltered zone length is about 259 m (850 ft) on the leeward side. Even though the heights of the hills (H1 and H2) are the same and they both were hit by the same tornado, their sheltered zone lengths are different. This could be because of difference in slope between these hills, or it could be due to little variation in tornado translational velocity while interacting with terrain and structures causing damage. From Figures 4.6 and 4.7, one can measure the height of hill (H3) and the sheltered zone length on its leeward side. The height of H3 is about 30.5 m (100 ft), and the undamaged zone length is 168 m (550 ft). The site H4 is close to the end of the tornado track and one can see that tornado intensity is lessened from the amount of damage (bordered by dashed yellow line) observed on the windward side as illustrate in Figure 4.8. Like the aforementioned hills, this hill provides highly protected area on it leeward side. In the this site, the hill height is almost (27.5 m) 90 ft and the protected zone is about 152.5 m (500 ft). When the protected zone length is normalized to its hill height, the following outcome is arrived. For H1, the protected zone length is 5.0H where h is the hill height. Similarly, the protected zones for H2, H3 and H4 are 4.25H, 5.5H and 5.0H respectively. Table 4.1 shows the slope on both sides of the studied hills as well as the length of the normalized sheltered zone. From table 4.1, one can see that there are different sheltered zone lengths for the same hill height when the slope varies. This means the slope of the hill also affects the sheltered zone length, and its effects can't be investigated easily through field investigation. For the investigated sites, it observed that when the tornado crosses a hill of height H, the hill most probably provides protected zone of length about 5.0H on its leeward side and

some differences are observed due to different slopes of the investigated hills. Also, the sheltered length is normalized with respect to the highest hill elevation, and different length may be observed on the lateral sides of the hill (away from the tornado path center). The tornado core radius is evaluated by measuring the track width to be in range of 25 m to 45 m (82 ft to 148 ft). Also, the hill width average is about 1 km (0.6 miles) which is almost 29 times the tornado core radius. Therefore, it is hypothesized here that the hill height is greater than or equal the tornado core radius and that the hill shape is close to be a 2D hill. For a rectangular wall (a man-made hill), Gorecki and Selvam (2013, 2014 & 2015) found that the partially protected zone distance beyond the hill is six times the hill height.

Table 4.1 Sheltered zone length and slope of windward and leeward side of the studied hills.

Hill ID	Windward Slope	Leeward Slope	Sheltered Zone Length
H1	23%	23%	5H
H2	28%	19%	4.25H
H3	12%	12%	5.5H
H4	19%	15%	5H
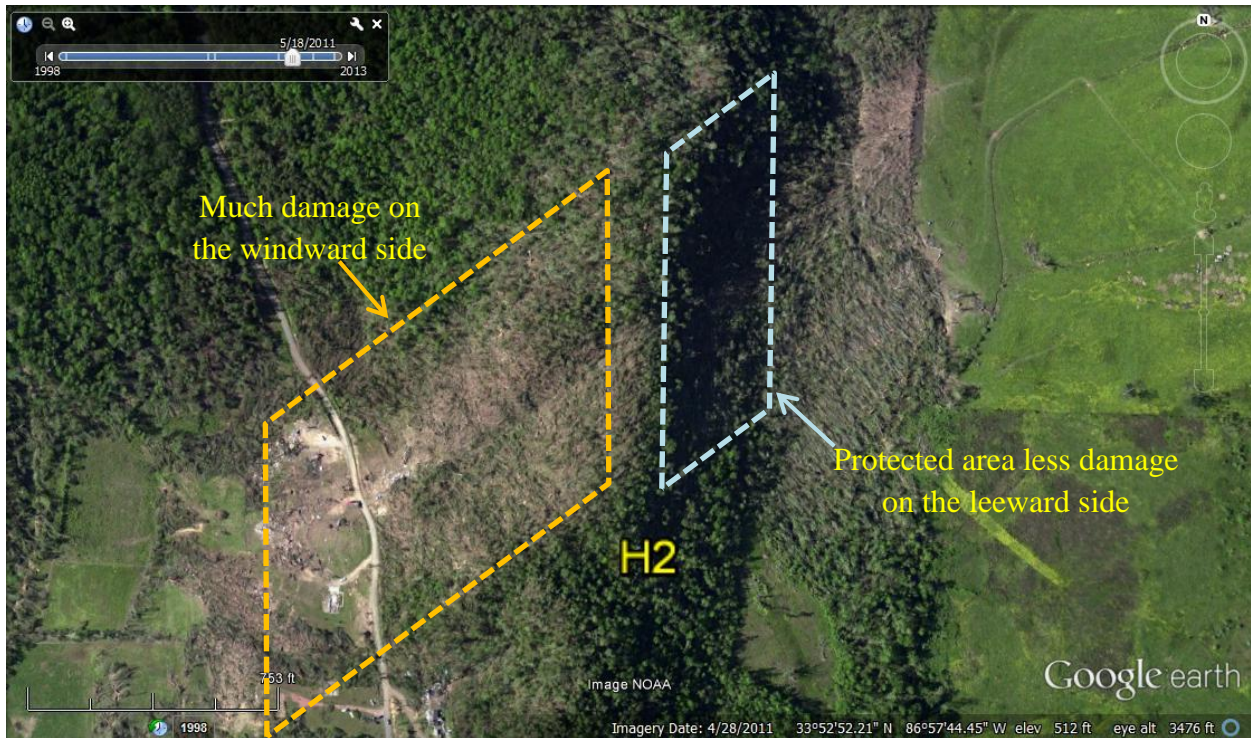
Figure 4.4 Close-up view for hill (H2), much damage on wind ward (the faded brown area, yellow line) and the protected area on the leeward (dark green, blue line).
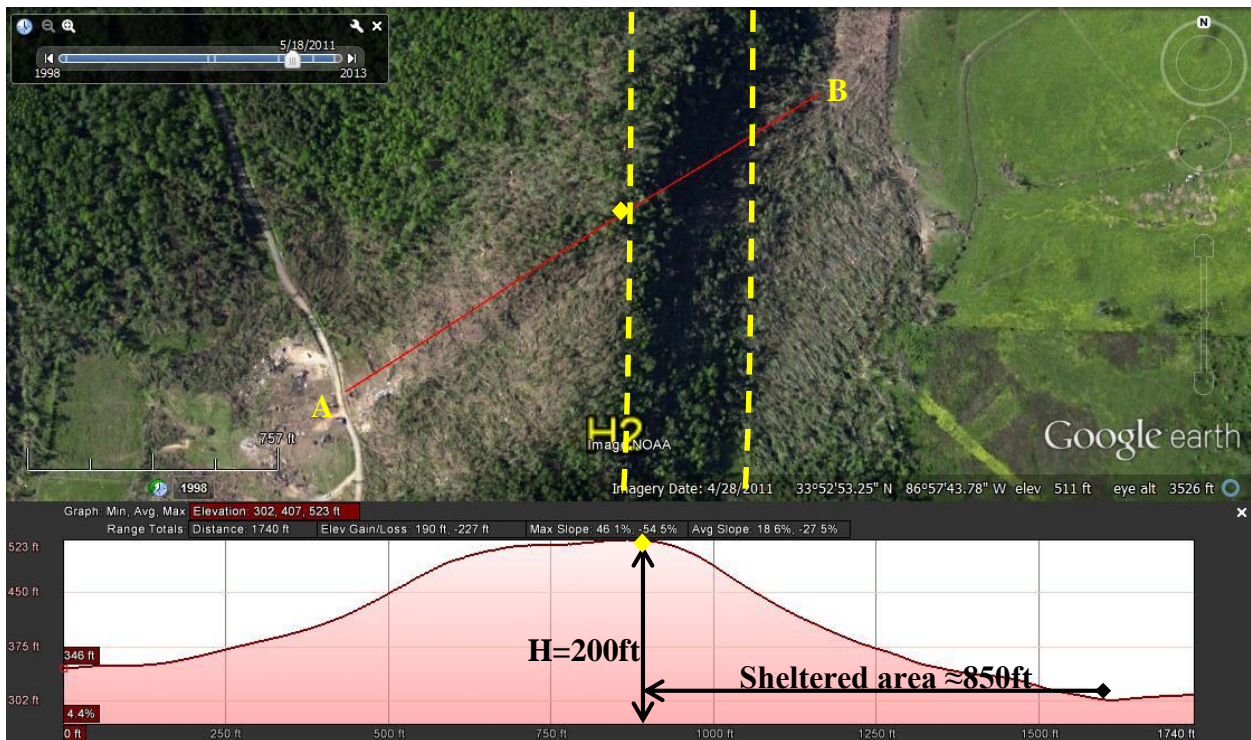
Figure 4.5 Elevation profile along the hill (H2), the protected zone is 4.25H.
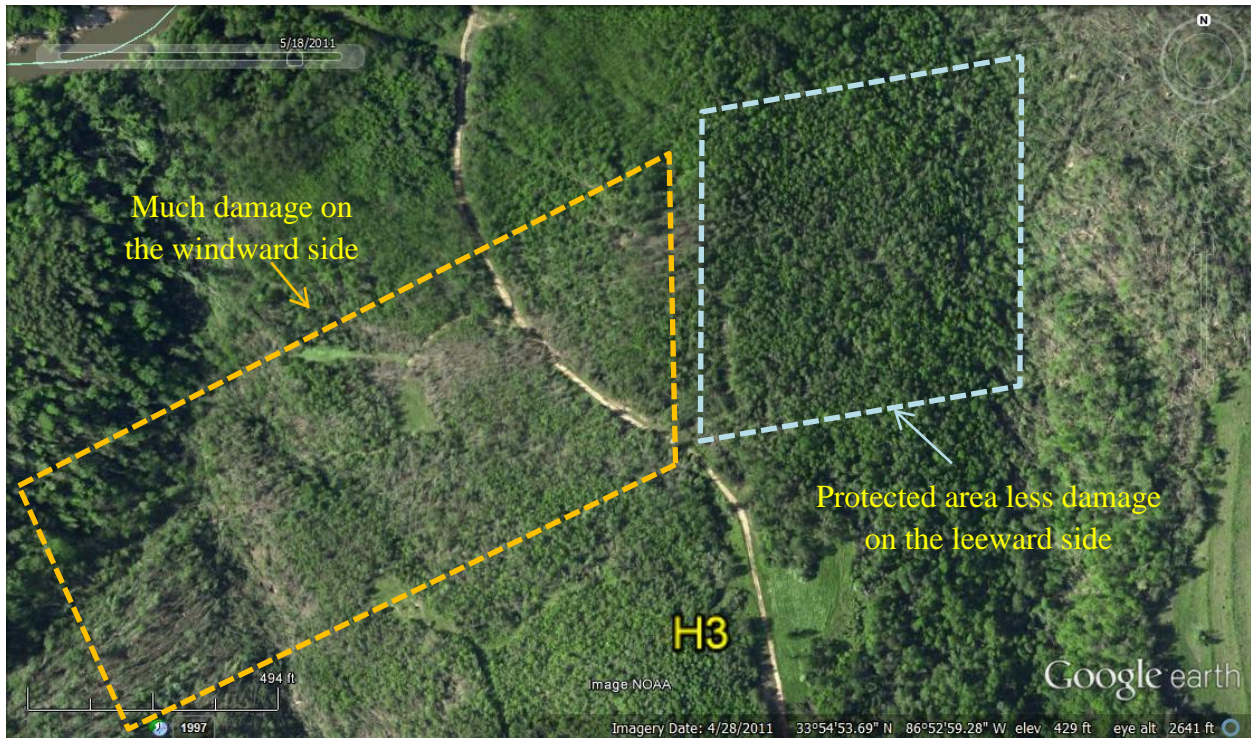
Figure 4.6 Close-up view for hill (H3), much damage on wind ward (the faded brown area, yellow line) and the protected area on the leeward (dark green, blue line).
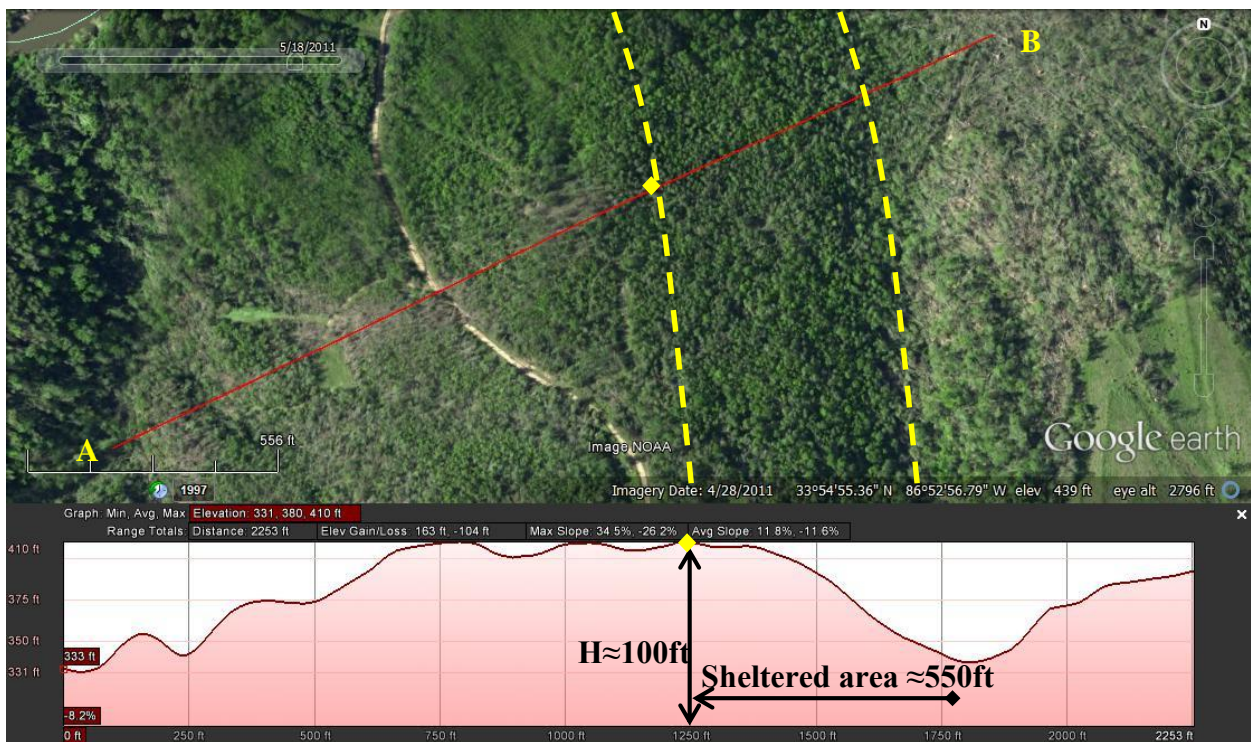
Figure 4.7 Elevation profile along the hill (H3), the protected zone is 5.5H.

Figure 4.8 Close-up view for hill (H4), much damage on wind ward (the faded brown area, yellow line) and the protected area on the leeward (dark green, blue line).
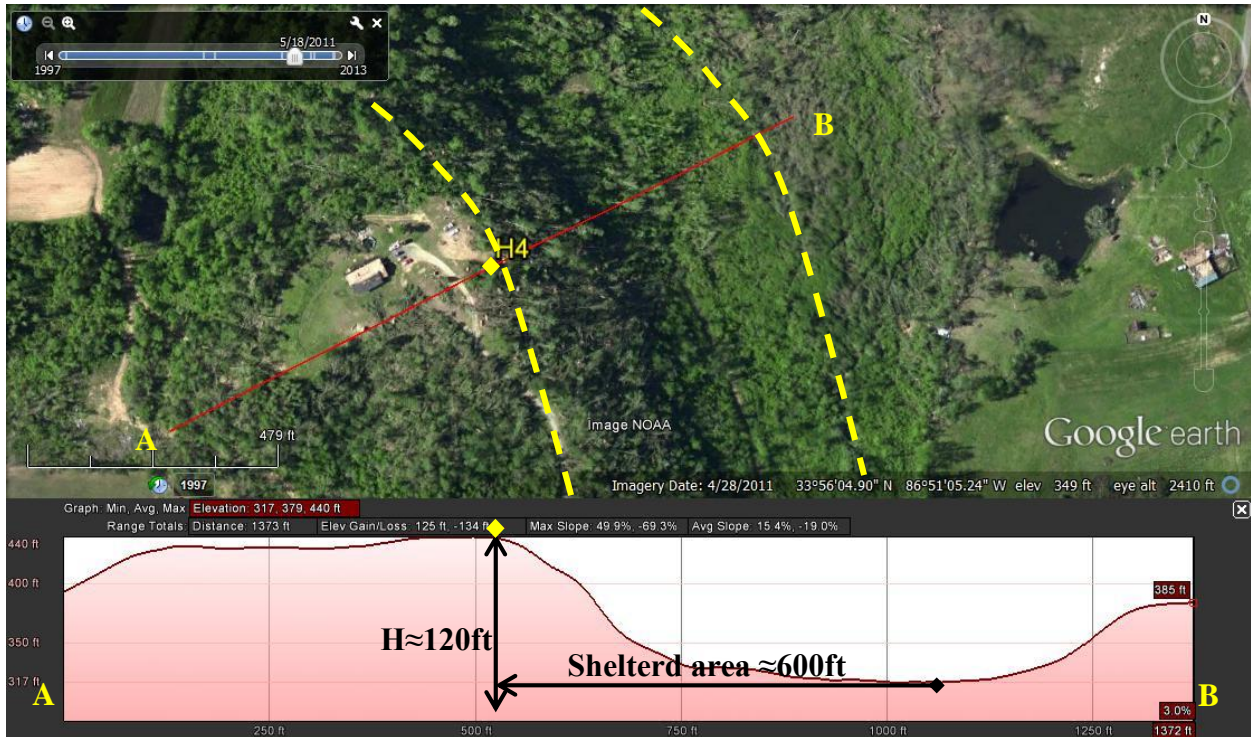
Figure 4.9 Elevation profile along the hill (H4), the protected zone is 5.0H.

4.4. A Place Surrounded by Hills (Tuscaloosa-2011)

Tuscaloosa-2011 is one of the deadliest tornado hit the United States in the last five decades. This tornado is rated as EF4 and results in 65 fatalities and 1500 injuries. The total traveling path is about 130 km (81 miles) and the maximum reported damage width is 2.4 km (1.5 miles) as informed by NWS (2011c). The average traveling velocity for this tornado is 86 kmh^{-1} (53.4 mph) (detected from NWS, 2011c). Tuscaloosa-2011 touched down few miles southwest Fosters and hit Tuscaloosa, and then it lifted near the downtown of Birmingham. The tornado damage path is shown in Figure 4.10 (bright color between dashed Yellow lines).

The site S1 is selected along the tornado path as shown in Figure 4.10. S1 is a valley, an area of irregular shape surrounded by hills and located right on the tornado path. The projected dimensions of the hills surrounding S1 are presented in Figure 4.11. The summit of the hill all around is about 161.6 m (530 ft) above sea level, and elevation of center of the valley is about 144.8 (475 ft) above sea level. The elevation profile of line ABC (a section in the valley and the surroundings hills) is illustrated in Figure 4.12. From Figure 4.12, one can see that the valley region is surrounded by almost 16.8 m (55 ft) height hills. From both Figures 4.11 and 4.12, one can see that there is no damage (shiny green color) in the valley, a region surrounded by hills, whereas there is much damage (faded brown color) on the surrounding hills. The maximum distance between hills along the tornado path is about 0.16 km (0.1 miles). The tornado core diameter is estimated from the tornado trace on the ground to be about 0.201 km (0.125 miles). Therefore, for these measured dimensions and elevations, it is observed that the tornado tends to skip the valley, and the damage is noticed only on the tops of surrounding hills. It is interpreted that this place is protected because the tornado diameter is greater than or equal the maximum width of the valley along the tornado path. Computer model can be utilized to explore the effect of changing the hills

and valley dimensions on the damage distribution. This observation could be used as an advantage in selecting a location for critical buildings such as hospitals and shelters to provide better lives saving.
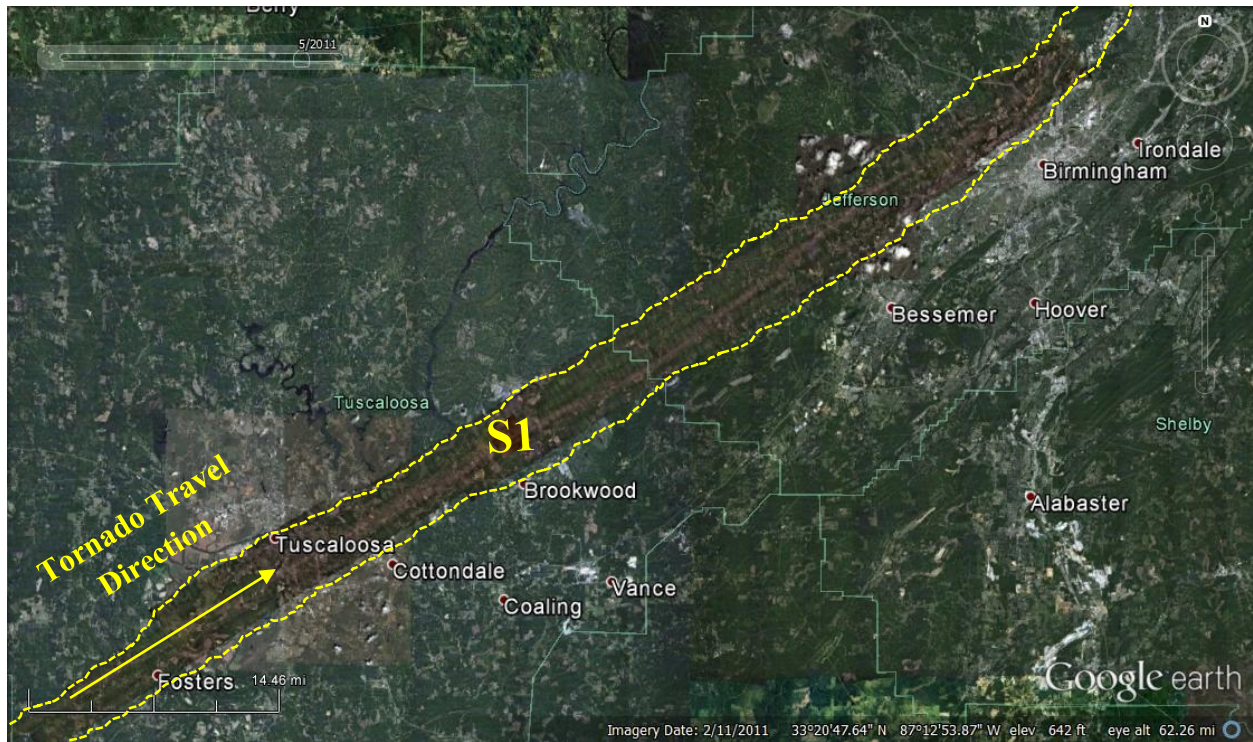
Figure 4.10 The tornado path of Tuscaloosa-2011 tornado show the investigated site (the bright color area is the damaged area path).

Figure 4.11 Close-up view for site (S1) on Tuscaloosa tornado's path with detailed dimensions for the surrounding hills.

Figure 4.12 An elevation profile for line ABC, at center of hills and valley.

4.5. Tornado Damage Uphill and Downhill (Mayflower-2014)

The Mayflower-2014 tornado is rated as EF4. The length of the tornado path is about 66 km (41 miles) as reported by NWS (2014a) and the University of Arkansas damage team (Selvam et al.. 2014 and 2015). The number of fatalities results from this tornado is 16. This tornado touchdown southwest of Lake Maumelle and passed over Mayflower and Vilonia, then it lifted near El Paso, AR. The damage path is shown in Figure 4.13 (NASA, 2014).

One site is selected for detailed analysis of damage around a hill in this tornado location, and it is circled by yellow color (See Figure 4.14). The tornado passed over a water surface before it hit the selected site, so it had a considerable intensity. The Enhanced Fujita scale with examples of damage level for different houses illustrated in Figure 4.15 is utilized to evaluate the damage level for the houses in the selected hill D1. Google Earth is used to provide images and elevations for the selected site D1 before and after the tornado occurrence. Figure 4.16 shows four houses on the investigated hill D1, and they are identified as H1-H4. The elevation profile for the hill along the tornado traveling path represented by line AB is shown in lower part of Figure 4.16. Figure 4.17 shows the elevation profile for line CD which is almost normal to the tornado traveling path (along the line of the houses). From elevation profiles in Figures 4.16 and 4.17, one can see that the house (H1) is located at the point of the highest elevation of 92 m (302 ft) above the see level. The elevations for houses (H2, H3 and H4) are 87.8 m (288 ft), 86 m (282 ft) and 83.8 m (275 ft) above the see level respectively. By refereeing to the EF scale in Figure 4.15, the house H1 on the top hill is damaged the most and its damage is estimated to be EF3 as shown in Figure 4.18. For the house H1, one can see that the roof has been detached from the majority of the house, and walls from the near side of the house have been destroyed and transported to the far side of the house. However, H2-H4 show only minimal roof damage and

loss of shingles as shown in Figure 4.19. An aerial view taken from east side shown in Figure 4.19 a, shows the difference in damage between house (H1, much damage) uphill and house (H2-H4, less damage) downhill. Figure 4.19 b is a close-up aerial view taken from the west side for the houses (H2-H4) which have low elevation on the leeward side and experienced less damage (EF1). Figure 4.20 is an aerial view for the investigated hill D1after the tornado occurrence. Even though this image does not have a great quality, it can still illustrate the elevation difference between the houses as well as the damage difference.

It is evident that the houses on leeward side of the hill with lower elevation experienced less damage as shown in Figures 4.19-4.22. The damage in houses (H2, H3 and H4) is minor roof damage and it is evaluated as EF1. It can be interpreted that the house H1 on top of the hill faced much higher wind speed, and therefore higher damage. Therefore, it is shown that houses in the same region experience different level of damage. Conversely, the other houses H2-H4 are located at lower elevation and has faced wind of less velocity and experienced less damage. As a result, the uphill house experienced more damage than those of downhill. This also can be interpreted as that the hill provided sheltering for the houses located on the side of the hill. Wind tunnel or computer model is important to examine these theories for different cases and utilizes the outcome for improving building design standers.
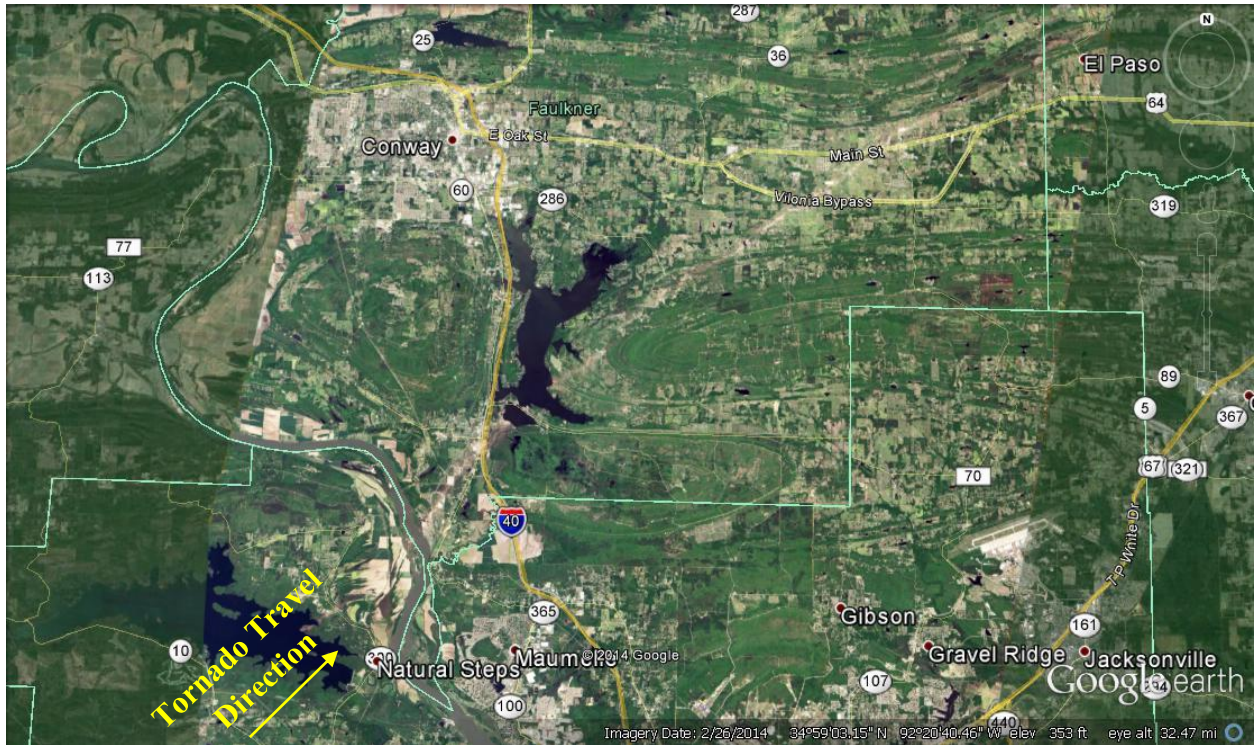
Figure 4.13 Tornado damage path from satellite photograph (NASA, 2014).

Figure 4.14 Close up view for the studied site near Lake Conway (NASA, 2014).

EF5 — **Incredible:** Strong frame houses are lifted from foundations, reinforced concrete structures are damaged, automobile-sized missiles become airborne, trees are completely debarked.

EF4 — **Devastating:** Well-constructed houses are destroyed, some structures are lifted from foundations and blown some distance, cars are blown some distance, large debris becomes airborne.

EF3 — **Severe:** Roofs and some walls are torn from structures, some small buildings are destroyed, non-reinforced masonry buildings are destroyed, most trees in forest are uprooted.

EF2 — **Considerable:** Roof structures are damaged, mobile homes are destroyed, debris becomes airborne (missiles are generated), large trees are snapped or uprooted.

EF1 — **Moderate:** Roof surfaces are peeled off, windows are broken, some tree trunks are snapped, unanchored mobile homes are overturned, attached garages may be destroyed.

EF0 — **Light:** Chimneys are damaged, tree branches are broken, shallow-rooted trees are toppled.

Figure 4.15 The Enhanced Fujita (EF) scale damage examples (Taken from Safeguard, 2009).
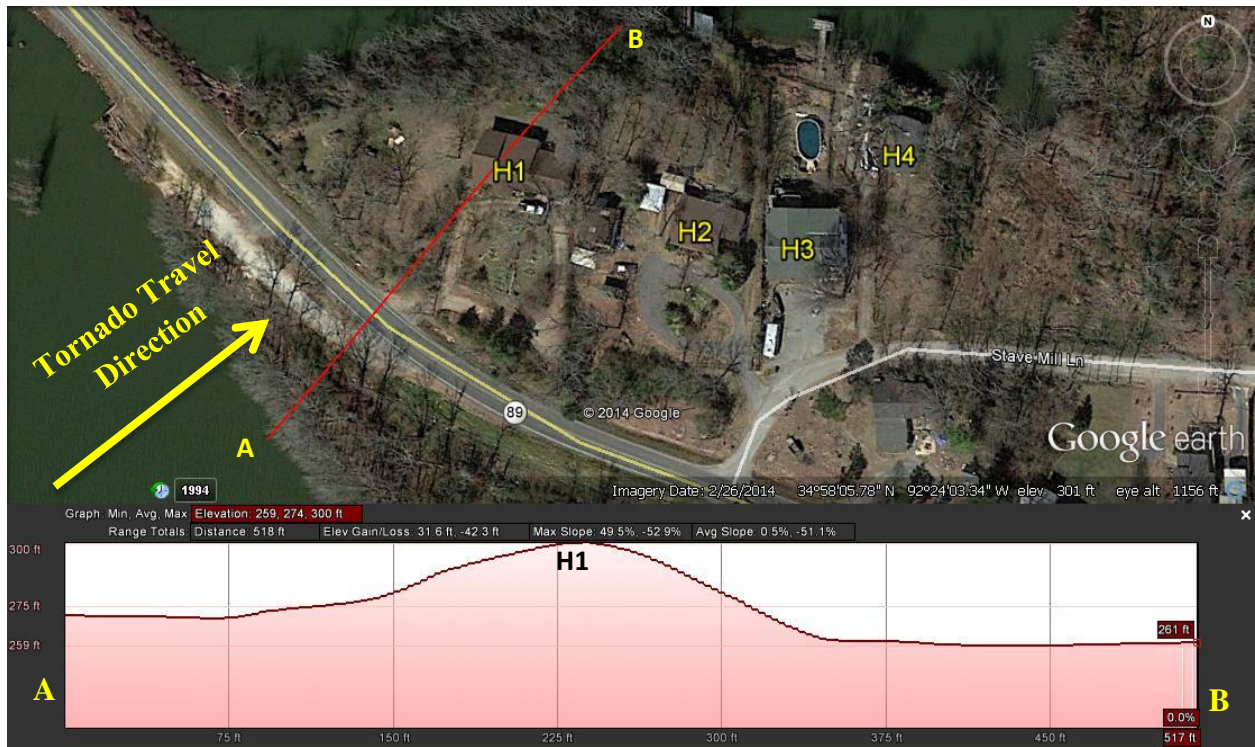
Figure 4.16 Elevation profile for the hill along tornado travel direction.
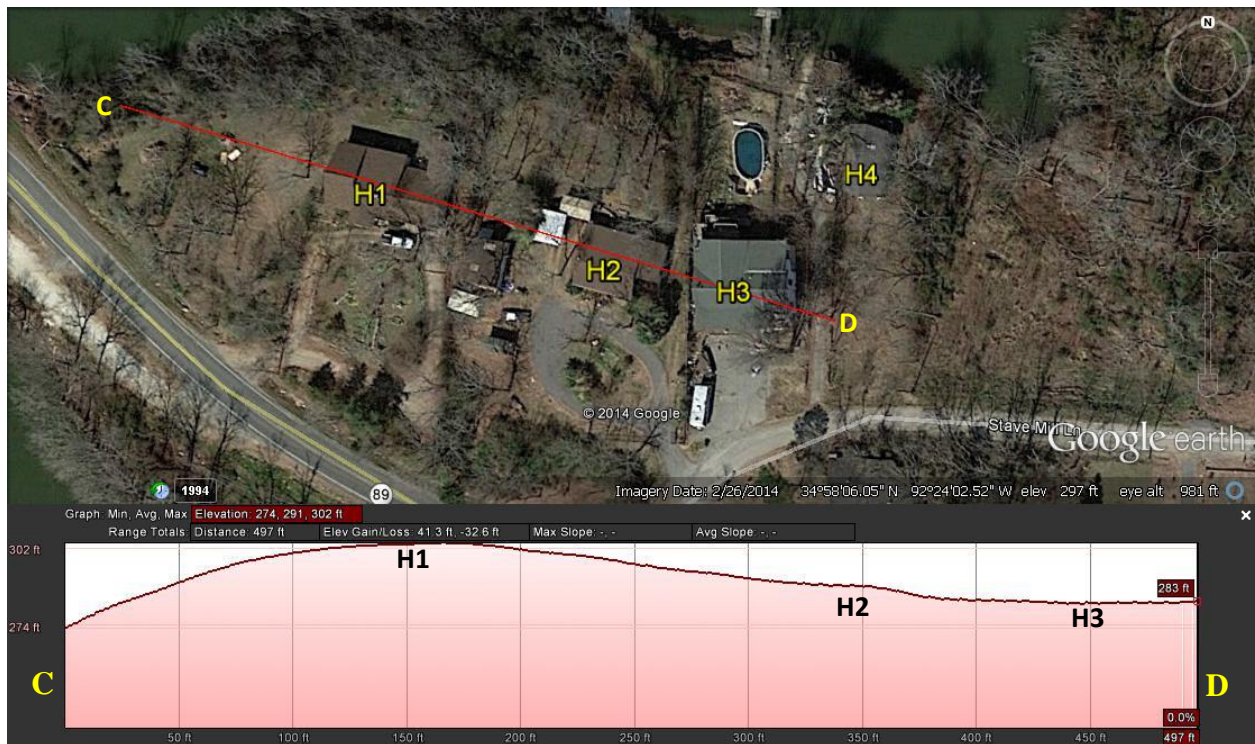
Figure 4.17 Elevation variations along line CD normal to tornado travel direction.

Figure 4.18 Arial image for a severe damage for house (H1) uphill (Source CAP, 2014).

Figure 4.19 a) Aerial view taken from the east side for house (H1-H4) taken from CAP (2014).

Figure 4.20 b) Aerial view taken from the west side for house (H2-H4) on the leeward side (low elevation, less damage EF1) taken from CAP (2014).

Figure 4.21 Google Earth aerial view for the hill D1 after the tornado occurrence.

Figure 4.22 Minor damage (EF1) for the house (H3) on the leeward side (low elevation) (UA team photo).

Figure 4.23 Minor roof damage (EF1) for the house (H4) on the leeward side (low elevation 83.8 m (275 ft)). (UA team photo).

4.6. Conclusions

Three tornado events (Parrish-2011, Tuscaloosa-2011 and Mayflower-2014) are investigated using Google Earth, aerial images provided by CAP (2014) and ground investigations photos taken by UA team (Selvam et al. 2014 and 2015). Tornado damage is investigated on windward and leeward sides of several hills to evaluate hills' sheltering. Also, the damage is inspected for a place surrounded by hills on the tornado path. Finally, damaged houses around a hill are analyzed and rated using EF scale to illustrate the difference between damage uphill and downhill. The following conclusions are drawn.

- There is a significant effect of hills on tornado damage, and much damage is observed on windward side of a hill comparing to its leeward side.

- When a tornado crosses a hill, the hill provides sheltered zone on its leeward side

- Observations for the investigated hills show that the sheltered zone length on the leeward side of the hills is about five times the hill height (5h).

- When the tornado hits a place surrounded by hills and the distance between the hills along the tornado path is less than or equal the tornado diameter, the damage is noticed only on the top of the surrounding hills. The surrounded place is completely protected.

- The tornado damage observed uphill is higher than the damage observed downhill for the same region hit by a tornado.

More investigations for the effects of changing hill dimensions and shapes on the sheltered zone distance on the leeward side need to be done utilizing computer models or experimental simulations. Also, the effect of changing the distance between hills surrounding a protected area needs to be investigated to determine if the protected area is maintained or lost.

5. TERRAIN EFFECT ON TORNADO GROUND INTENSITY AND PATH

5.1. Introduction

More than 1200 tornadoes happen every year in the United States, and they are associated with huge life and financial losses (NWS, 2010). Therefore, a better understanding for tornado wind near ground is significant to lessen life and financial losses. One of the critical ways to build up our tornado understanding is by documenting tornado interaction with structures and terrain from tornado post damage investigation. Also, it is crucial to analyze these documentations for any potential hypothesis.

Usually tornado post damage investigations focus only on structures damage, with minor attention paid to the topography effects on tornado damage (Fujita et al. 1970, 1976; Fujita 1981, 1989). Basically, local damage to structures, vegetation, etc. is observed and used to estimate the tornado maximum wind speed and the corresponding EF rating.

Previous investigations performed within our research group have led to a conclusion that hilly terrain may significantly influence the tornado damage and path. Investigation of tornado damage over hilly and forested regions by Selvam & Ahmed (2013) reported that when a tornado crosses a hill, there is much damage observed uphill comparing to that on leeward side downhill. 3D CFD modelling reported in Gorecki & Selvam (2014 and 2015) show that a translating vortex will attempt to divert around the side of a short rectangular hill located perpendicular to the travel direction of vortex. For longer hills, the vortex is unable to divert around the side and must pass over the top of the hill. However, the hill distorts the vortex, which does not recover until it passes well beyond the hill. This produces a "sheltered" region on the downstream side of the hill, where the velocity magnitude reduced by 30% to 40% depending upon the location from the hill and the height from the hill top. Selvam et al. (2014 and 2015) performed site

investigations for the Mayflower tornado in 2014. Their focus was terrain effects on tornado damage. However, a detailed analysis for hilly terrain effects on tornado damage is not reported.

The main challenges for tornado post damage investigations are: unreachability for hilly regions, detailed evaluation of terrain elevation, coordination of damage pictures with its exact location and elevation, trace the tornado damaged path, proper visualization of damaged area and requirement for a lot of technical, laboring and financial resources. However, thanks to the technology development which has made these investigations much affordable and reachable using different computer software. Using a camera has a GPS feature, like IPhone, the picture is connected to the place where the picture was captured. Then, using a computer software, Google Earth, the damaged location is visualized in 2D and 3D views as well as in different times before and after the tornado occurrence. The objectives of this chapter are exploring the terrain influence on tornado damage, and evaluating hilly terrain effects on tornado damage ratings (ground level intensity). Also, terrain influence on the tornado path change is examined.

5.2. Tools Used for the Study

The data analyzed in this study is mainly provided from two sources: ground images by University of Arkansas (UA) investigation team (Selvam et al., 2014) and Civil Air Patrol (CAP) images (CAP, 2014). The photos are mainly taken by an iPhone, NIKON D200 and SONY SLT-A55V cameras which have GPS feature. Then, the photo GPS coordinates are synchronized to the computer using the software Google Picasa 3. The data is analyzed and interpreted using the software Google Earth and Google Maps.

In this work, tornado damage ratings provided by NWS (2014b) for the Mayflower-2014 tornado are taken and imposed on terrain map to reveal terrain effects on tornado damage.

Observations are supported by photos and aerial images associated with the specific damage location. Also, terrain effects on tornado path is investigated.

5.3. Tornado Facts and Details

On April 27-2014, at 7:06 the region of central Arkansas (Mayflower and Vilonia) was struck by a tornado ranking EF4 on the Enhanced Fujita (EF) intensity scale. The tornado started about nine miles southwest Lake Maumelle, and traveled toward northeast over Mayflower and Vilonia communities. Then, it loft near El Paso.

The tornado damage path is shown in Figure 5.1. Radar data indicates that the tornado formed at location "2" at 7:06 PM and travelled north-west, finally dissipating around location "26" at 8:02pm. The tornado resulted in sixteen fatalities (ArkansasOnline, 2014). Figure 5.1 shows the locations and number of fatalities occurred in Mayflower-2014 tornado (Selvam et al, 2015). More tornado information is reported in Table 5.1.

There is very little documentation of tornado damage in hilly terrain, and that is due to the fact that hilly regions are hard to access as well as less occupied. The terrain of the tornado path is a mix of hilly terrain, flat terrain and water surfaces. From Figure 5.2, one can see that the EF ratings change along the tornado's path as the terrain varies. The EF ratings are reported by NWS. Even though variation in tornado damage ratings can be liked to structure's strength, a further step has been taken to investigate potential like between terrain and tornado damage. Therefore, the Mayflower tornado provides the best environment to explore hilly terrain effects on tornado damage and path (Selvam et al., 2015).

Table 5.1 Basic information of Mayflower-2014 tornado.

Parameter	Value	Source
Length of Damage Tract	66 km (41 miles)	(NWS, 2014a)
Max. Tornado Diameter	0.80 km (0.5 miles)	(NWS, 2014b)
Max. Damage Rating	EF4	(NWS, 2014b)
Max. Wind Speed	267-322 km/hr (166-200 mph)	(NWS, 2014b)
Avg. Translation Speed	66 km/hr (41 mph)	(ARCgis, 2014)
Fatalities	16	(ArkansasOnline, 2014)
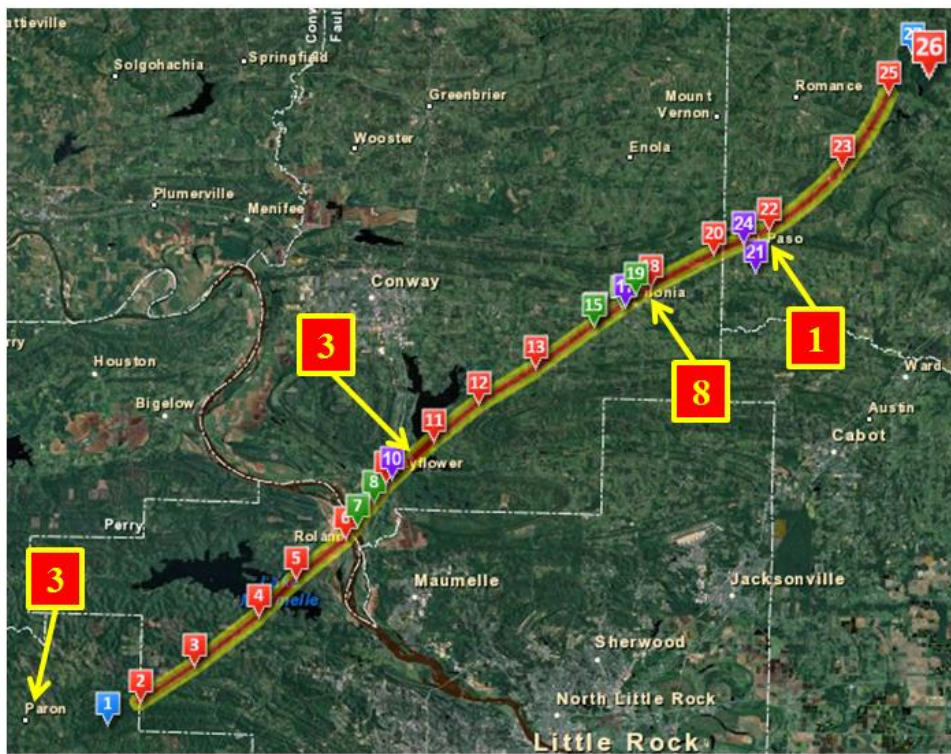
Figure 5.1 Mayflower-2014 tornado damage path showing the reported deaths (NWS, 2014a).
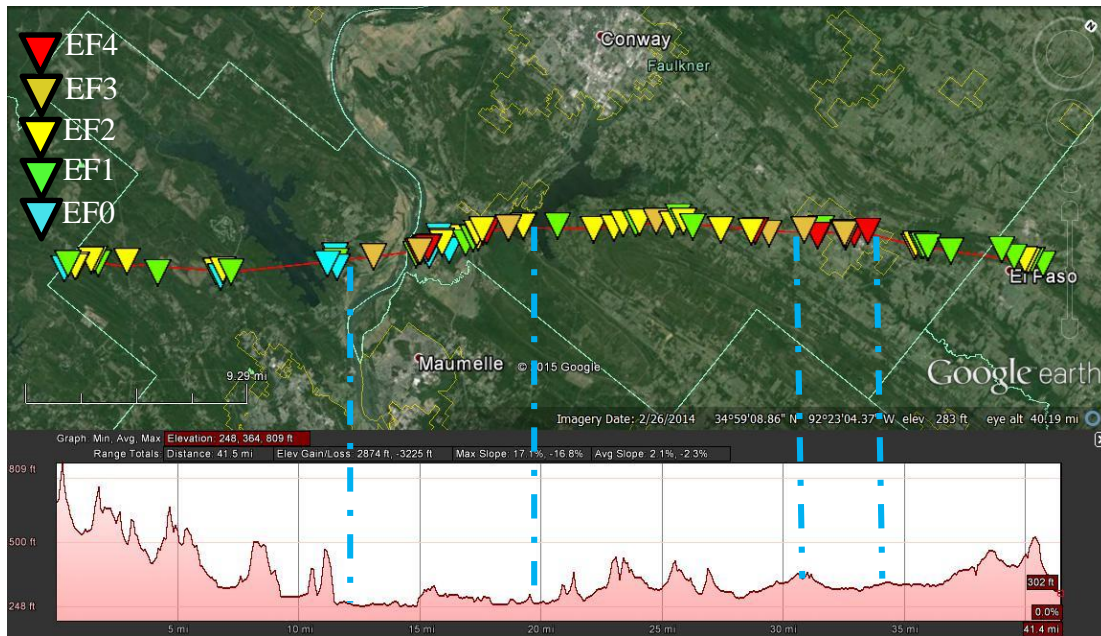
Figure 5.2 Tornado damage track with local EF rating indicated by gradient icons, the regions confined between the dashed lines have less differential elevation and higher damage.

5.4. Significant Reduction of Tornado EF Ratings due to Interaction with Hilly Terrain.

Mayflower tornado path reported by (NWS, 2014b) is shown in Figure 5.2. The tornado moved from southwest toward northeast. In Figure 5.2, the tornado path and the damage ratings assigned to shown locations on the path are rotated to be aligned to the elevation profile of the tornado travel path as shown in the bottom of Figure 5.2. The local EF ratings assigned by the NWS are indicated by gradients. These gradients are imposed on the terrain map as shown in Figure 5.3. From Figure 5.3, one can see that terrain map complies with the elevation profile in Figure 5.2 and shows great diversity in the terrain along the tornado traveling path. Four regions (R1-R4) are selected and zoomed for better clarity and better visualization of the association of EF ratings with terrain. The EF ratings legend is shown also on the side of the presented Figures. From Figure 5.2 and Figure 5.3, one can see that the terrain and the tornado EF ratings vary a lot along the tornado path. Also, it is noted that wherever there is hilly terrain the damage ratings are

76

reduced (EF1 to EF2) comparing to flat region areas (EF3 to EF4). A connection between the

tornado intensity (EF rating) and the terrain is observed, and a detailed discussion for each region

is provided in the following subsections.

5.4.1. Region (R1)-Hilly Terrain

Region (R1) shown in Figure 5.4 starts about 10 miles southeast of Lake Maumelle

(34°46'31.9"N, 92°39'11.3"W) and ends right at Lake Maumelle (34°51'34.4"N, 92°31'18.9"W).

The terrain in Region (R1) is very hilly (several successive hills close to each other). When the

tornado went over this hilly terrain, one can see that the average of the EF ratings is about EF1-

EF2. Only one place is reported with EF3 rating when the tornado first touched down and went

over low elevation between two hills. It is reported that the home of EF3 damage ratings was

swept clear of foundations. This home had anchor bolts in place; however, these bolts were not

secured with any nuts and washers as reported by NWS (2014a).

Several locations are selected to show the damage ratings in this region. A notation is

given as R1L1 (Region number, Location number), and a photo and a position are reported for

each location. The location R1L1 is a residential house as shown in Figure 5.5. From Figure 5.5,

one can see that only a shade attached to the house is collapsed, and there is no damage observed

for the main structure of the house. R1L1 is located about a half mile to the north from the wide

hill as shown in Figure 5.6. Also, another location, R1L2, which is a one story residential house

experienced minor damage to the roof and windows glass breaking as shown in Figure 5.7. This

house is surrounded by small hill and experienced very less damage due to the local protection of

the hills. The location of R1L2 on the terrain map is shown in Figure 5.8. On an average, the

damage in region R1 is rated as (EF1-EF2) and it is about 50% less than the maximum damage

(EF4) caused by this tornado. It is interpreted that the hilly terrain functions like wave breaking wall and lessens the tornado strength.
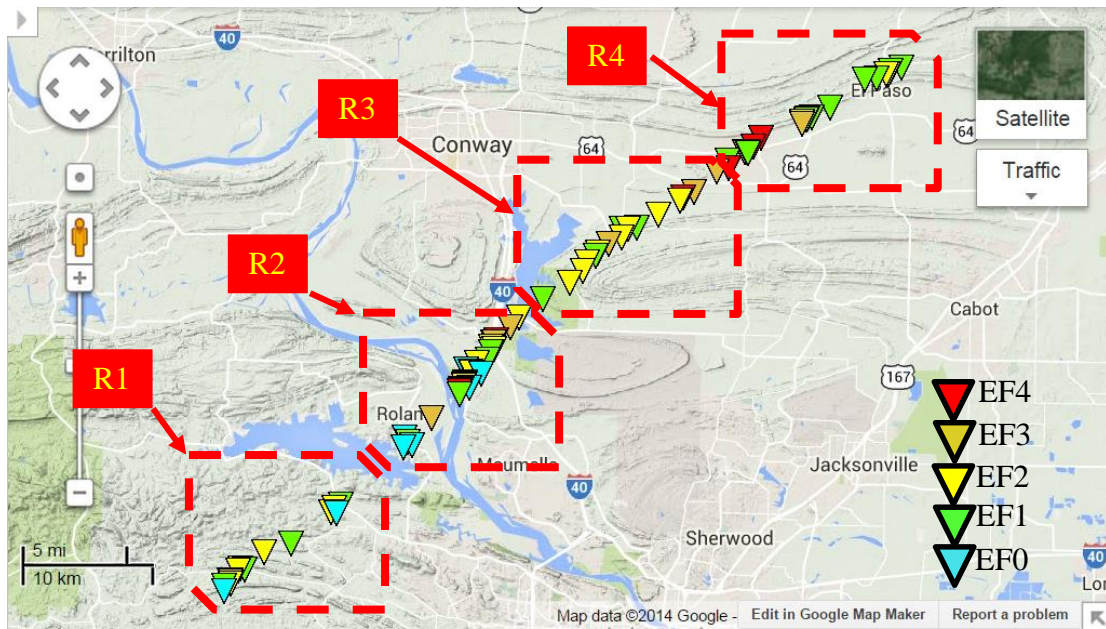
Figure 5.3 Mayflower tornado ratings imposed on terrain map along the tornado path.
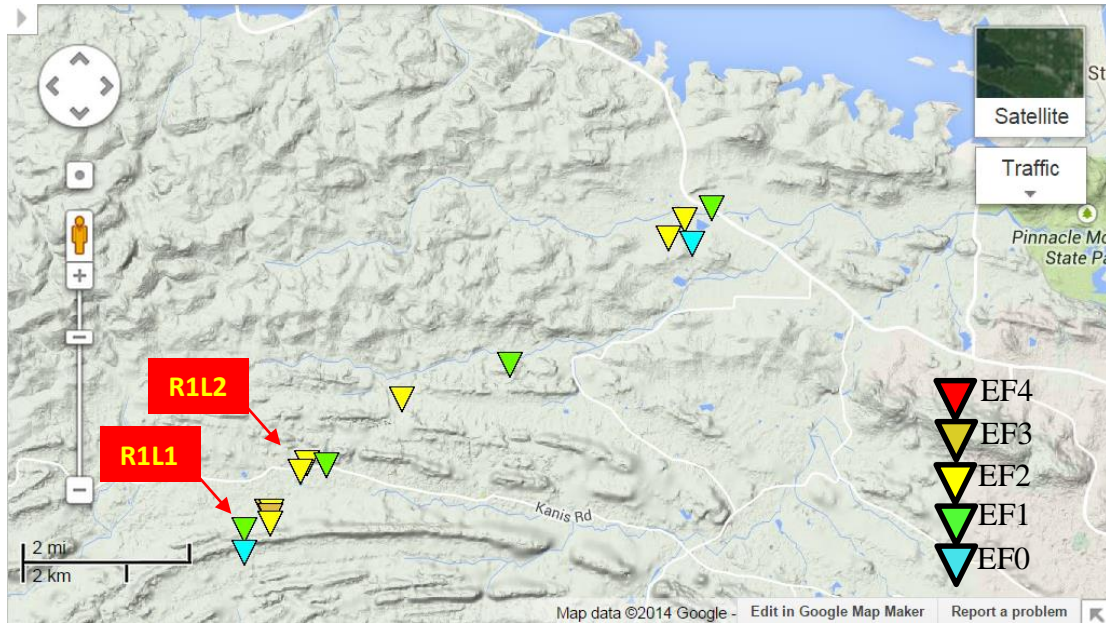
Figure 5.4 Region (R1) law EF rating associated with hilly terrain at the tornado start point, the damage average ratings is (EF1-EF2).

Figure 5.5 A house in location (R1L1) with a damage rating as EF1, only the shade attached to the house is collapse, taken by UA team.
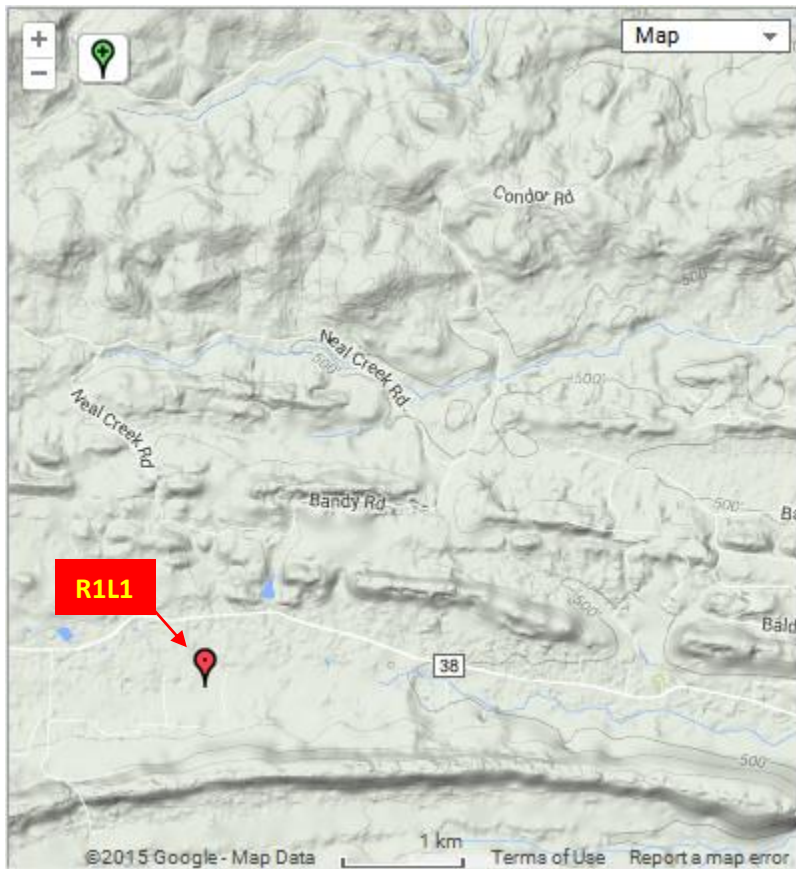
Figure 5.6 the position of selected location R1L1 at coordinates (34 47 10.1 N, 92 38 22.5 W).

Figure 5.7 A house in location (R1L2) with a little damage to the roof rated as EF1, taken by UA team.
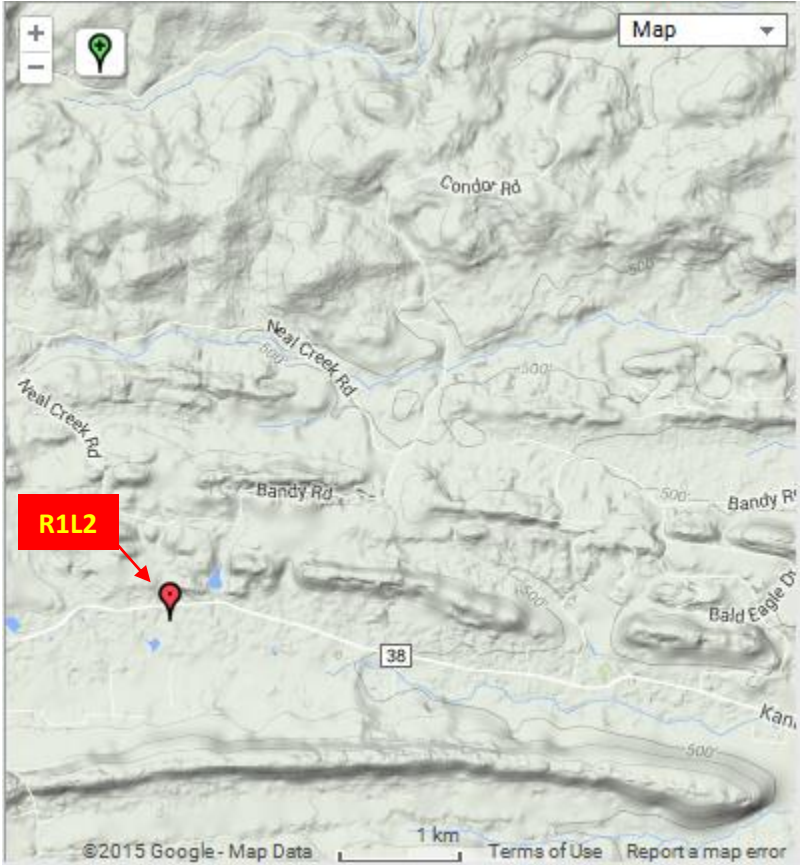
Figure 5.8 The position of selected location R1L2 at coordinates (34 47 34.2 N, 92 38 17.8 W).

5.4.2. Region (R2)-Flat Terrain and Water Surfaces

In region (R2) which starts at Lake Maumelle and ends right before Lake Conway as shown in Figure 5.9, the tornado travelled mainly over water surfaces and relatively flat terrain. Therefore, much higher damage is observed in this region, and the damage path is much wider. In this region, the damage ratings in the core part of the tornado path are EF3 to EF4 and on the edges, far away from the path center, are EF2 to EF1 as shown in Figure 5.9. As one can see, there is severe destruction caused by the tornado when it just crossed the Arkansas River in location R2L1 as shown in Figure 5.10. In this location, R2L1, the tornado caused very severe damage, and a community of several residential houses was completely destroyed. The position of R2L1 is reported in Figure 5.11.

The second location selected in this region is R2L2 about a half mile northeast R2L1. Like R2L1, the damage in R2L2 is also EF4, and also a neighborhood of several residential houses was tremendously damaged and grounded as shown in Figure 5.12. The location of R2L2 in the terrain map is illustrated in Figure 5.13. The average damage rating in this region is about (EF3-EF4) on the centerline of the damaged path. Some EF2 and EF1 ratings are reported on the far side of the damaged path centerline. Before the tornado crossed I40, it hit an industrial community and severely destroyed it as shown in location R2L3 (see Figure 5.14-16). Since the terrain in this region is mostly flat terrain and water surfaces, it is hypothesized that the disturbance experienced by the tornado was at its minimal level. Therefore, the tornado caused much severe damage.
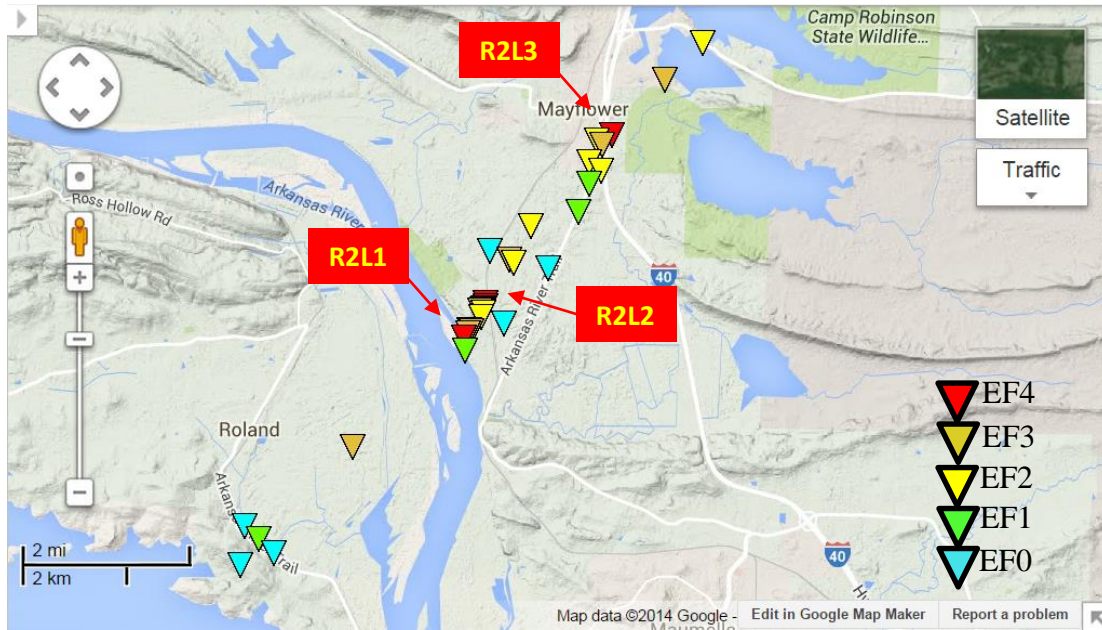
Figure 5.9 Region (R2) tornado went over flat terrain and water surfaces causing extreme destruction, the damage average ratings is (EF3-EF4).

Figure 5.10 Severe damage in a neighborhood at location (R2L1) rated as EF4, taken by CAP (2014).
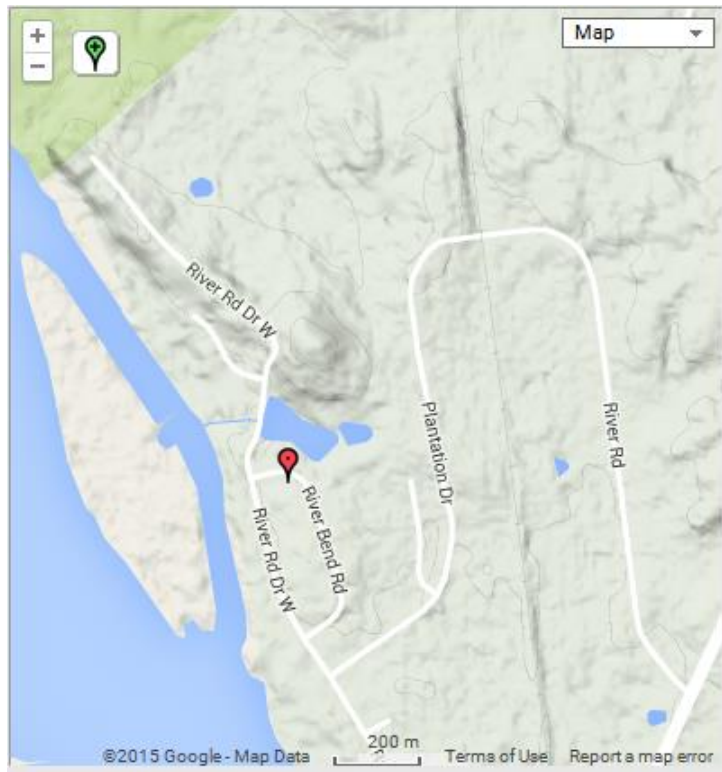
Figure 5.11 The position of selected location R1L2 at coordinates (34°55'5.54"N, 92°27'9.68"W).

Figure 5.12 Severe damage in a community at location (R2L2) rated as EF4, taken by CAP (2014).
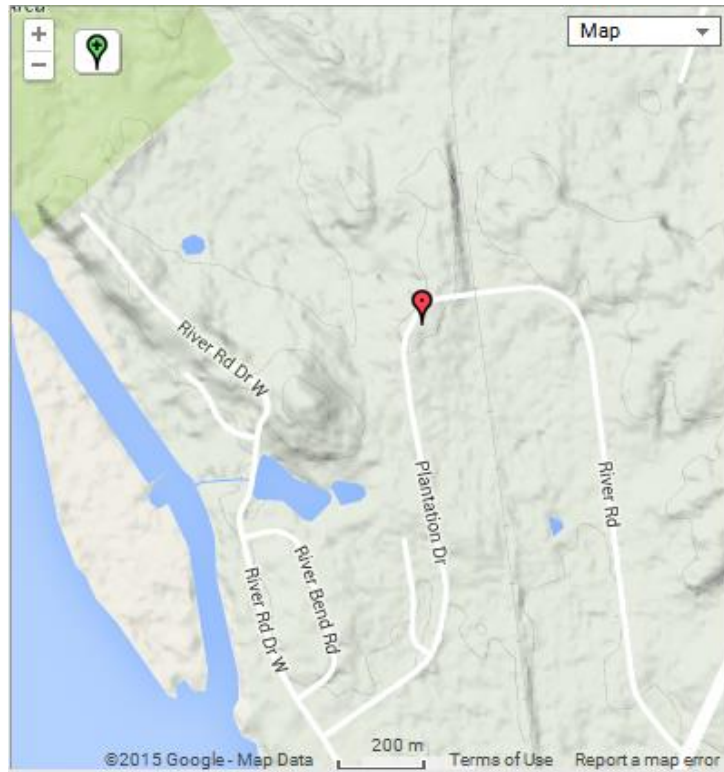
Figure 5.13 The position of selected location R2L2 at coordinates (34°55'22.77"N, 92°26'54.35"W).

Figure 5.14 An aerial image for a metal building severely destroyed and rated as EF4 at location (R2L3), Taken by CAP (2014).

Figure 5.15 A ground photo fora metal building severely destroyed and rated as EF4 at location (R2L3), Taken by UA team.

Figure 5.16 A metal at location (R2L3) harshly damaged, almost all the sheets are detached and many columns and beams are bent, Taken by UA team.
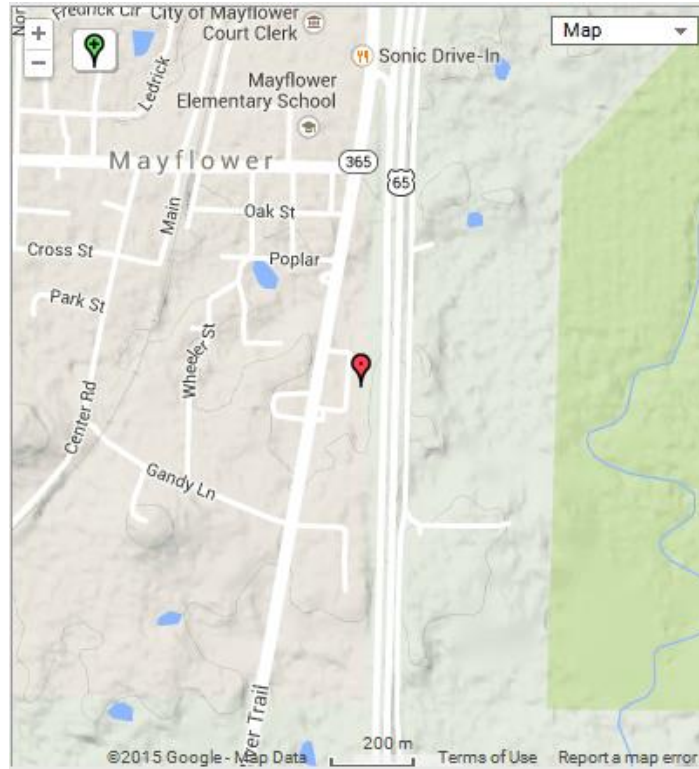
Figure 5.17 The position of selected location R2L3 at coordinates (34°57'5.01"N, 92°25'27.03"W).

5.4.3. Region (R3) a Mix of Hilly Terrain and Flat Terrain

The terrain in region R3 is a combination of both hilly terrain region and relatively flat terrain region. So it provides much better opportunity to evaluate the terrain effects on tornado damage. This region starts at Lake Conway and ends two miles beyond Vilonia bypass. First the tornado traveled over hilly terrain, and the damage rated in this region as EF1-EF2 as shown in Figure 5.18. Then it moved over flat terrain, and one can see that the reported damage is directly increased to EF3-EF4 (see Figure 5.18). The location R3L1 is selected in the hilly region. Three different houses are illustrated in Figures 5.19-21 showing minor damage to the roof rated as EF1-EF2. The position of R3L1 is shown in Figure 5.22. In the selected location R3L2, one can see that the damage sharply increased to have a complete community grounded when the tornado

traveled over the flat terrain as shown in Figures 5.23-24. The position for the selected location

R3L2 is demonstrated in Figure 5.25.
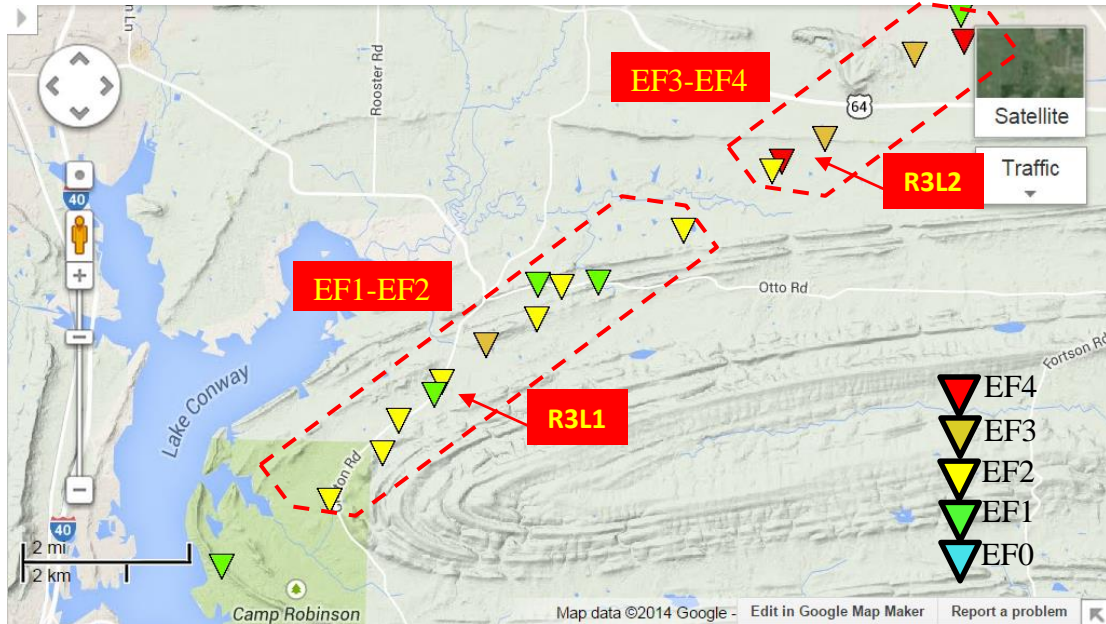
Figure 5.18 Region (R3) low EF rating over the hilly terrain and high EF rating associated with flat terrain, the damage average ratings is (EF1-EF2) for the hilly zone and (EF3-EF4) for the relatively flat zone.

Figure 5.19 Damage in residential house rated as EF2, R3L1 taken by CAP (2014).

Figure 5.20 Minor damage to the residential house roof rated as EF1, R3L1 taken by CAP (2014).

Minor roof damage

Figure 5.21 Minor roof damage rated as EF1, R3L1 taken by CAP (2014).
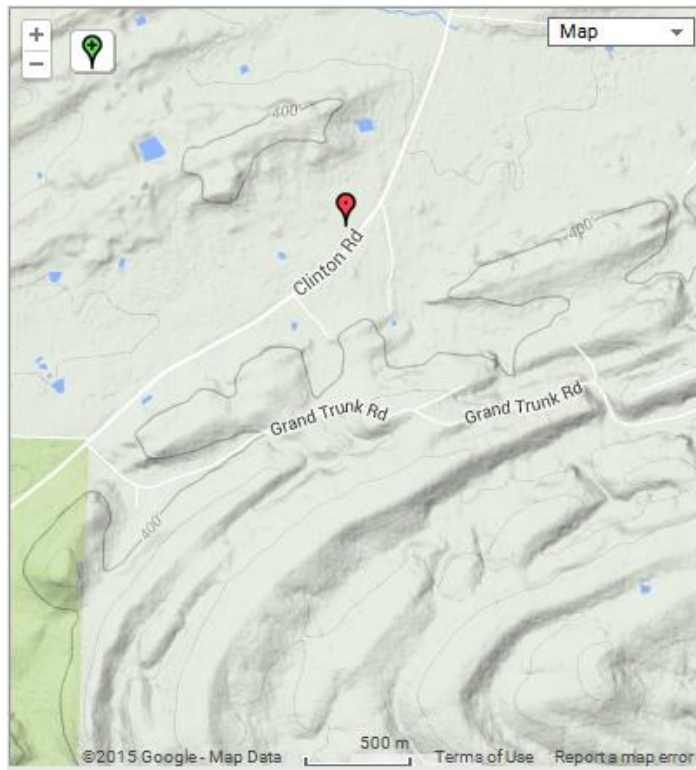
Figure 5.22 the position of selected location R2L3 at coordinates.

Figure 5.23 A whole community destroyed due to tornado right before Vilonia bypass at R3L2.

Figure 5.24 Several communities destroyed due to tornado right before Vilonia bypass at R3L2.
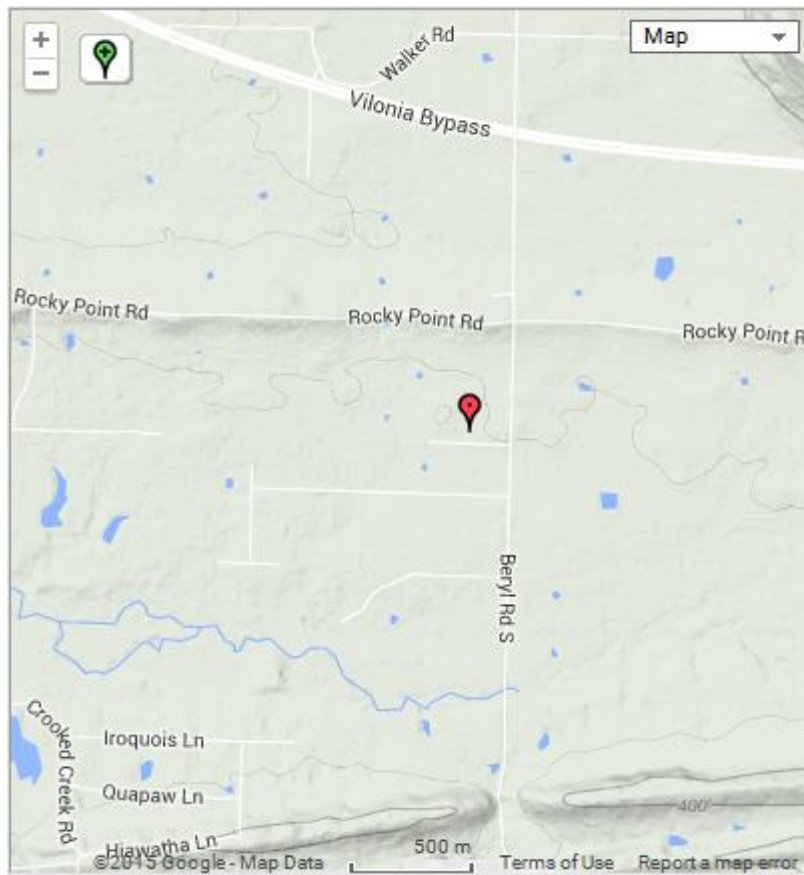
Figure 5.25 The Position of location R3L2.

5.4.4. Region (R3) a Mix of Hilly Terrain and Flat Terrain

Region R4 starts beyond Vilonia bypass and ends near El Paso. In this region, the tornado first travelled over flat terrain (Vilonia) and created massive destruction. Then it interacted consecutive hills to have the damage immediately decreased as shown in Figure 5.26. A new constructed school at location R4L1 heavily damaged and rated EF4 as shown in Figure 5.27. The location R4L1 is positioned over the flat terrain as shown in Figure 5.28. Another EF4 location is R4L2 where almost a complete huge neighborhood is massively destroyed as shown in Figure 5.29. The position of location R4L2 is illustrated in Figure 5.30. Then beyond the hilly region in R4 (R4L3) the damage level decrease to EF1 as shown in Figure 5.31, and the position of this site is demonstrated in Figure 5.32. Therefore, it can be concluded from the provided observation that there is great influence of the hilly terrain on the tornado damage level. When the tornado interacts with a hilly terrain, there is great disturbance experienced by the tornado and the damage level is decreased. On the other hand, when the tornado moves over relatively flat terrain or water surface, it maintains high destructive energy and the damage level is increased.
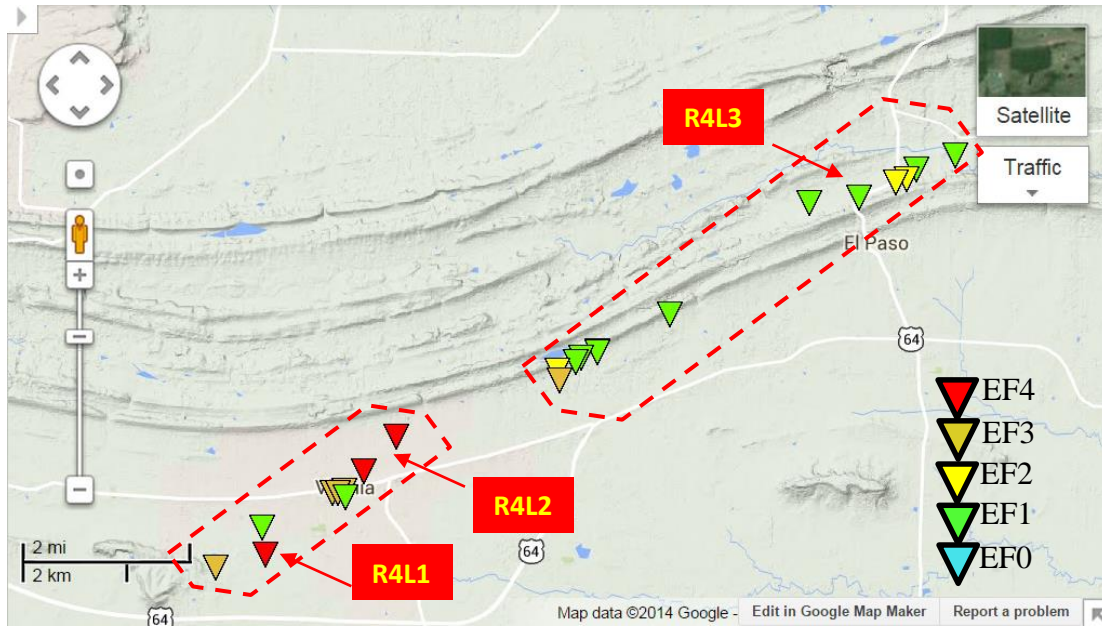
Figure 5.26 Region (R4) tornado EF ratings decreased after tornado interacted with hilly terrain, the damage average ratings is (EF4) for the relatively flat zone and (EF1) for the hilly zone.

Figure 5.27 A new constructed school at location R4L1 heavily damaged and rated EF4, taken by CAP (2014).
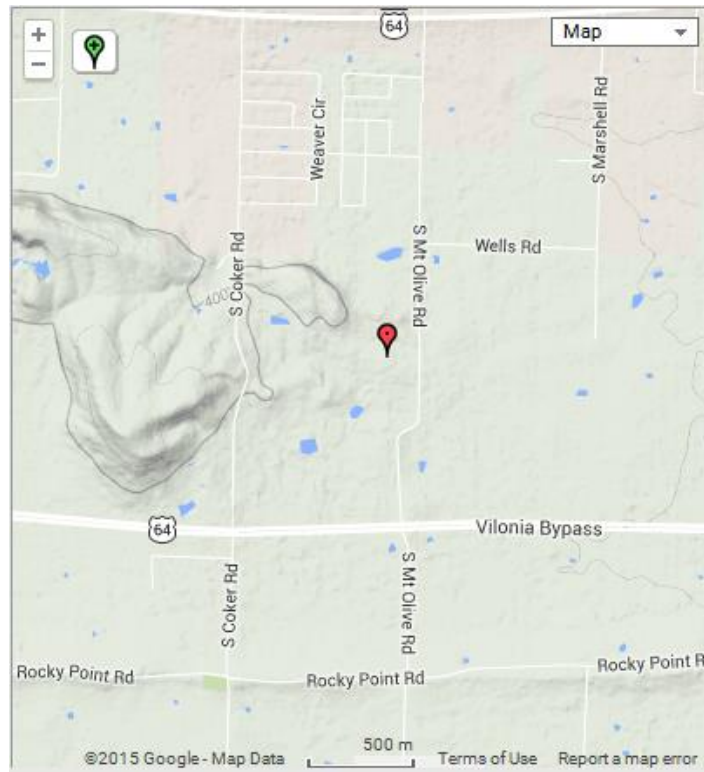
Figure 5.28 the position of the destroyed school (R4L1).

Figure 5.29 A neighborhood in Vilonia (R4L2) almost completely grounded, Taken by CAP (2014).
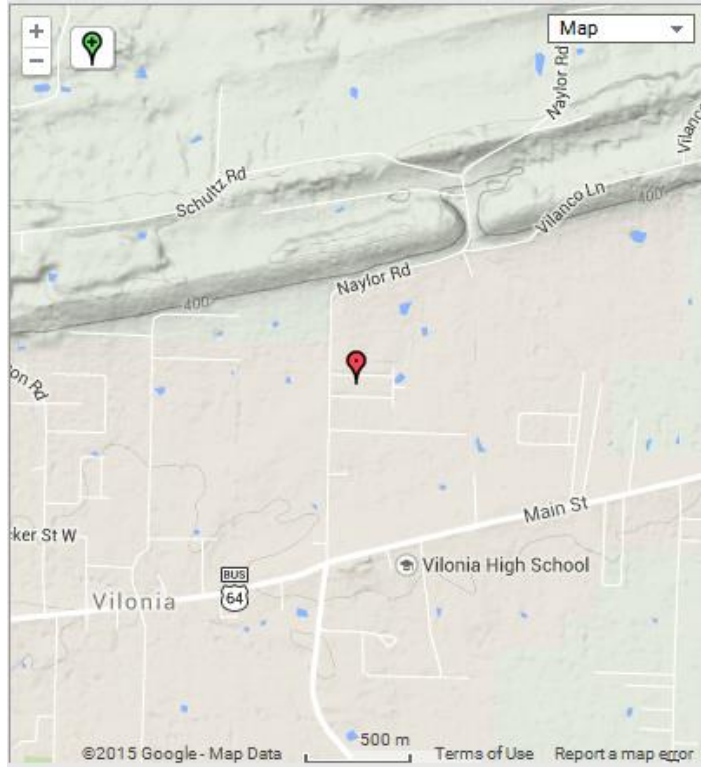
Figure 5.30 the position of the destroyed community (R4L2).

Figure 5.31 Minor damage observed at the house in location R4L3, taken by UA team.

Figure 5.32 the position of location R4L3.

5.5. Tornado Crosses the Hill Where Lower Elevation Available

Tornado occurrence in a hilly area provided a rich environment to study tornado behavior (e.g. path changing) and effects of hill on tornado path and damage. After tornado crossed Vilonia moving toward El Paso, it underwent over several hills. The damage path between Vilonia and El Paso is shown in Figure 5.33 as a yellow line. Two points of interest (POI) are selected and analyzed for tornado path changing. These points are red circled in Figure 5.33, and notations are given as P1 and P2. These two points are imposed on the terrain map as illustrated in Figure 5.34. The tornado approached the hill at an angle of about 20° (see Figure 5.33), and it traveled about 1.25 miles along the hill and after that it changed the traveling direction at point (P1). Then, it traveled for almost three miles between the two parallel hills untill it changed direction for the second time at Point (P2). The cross section of the two parallel hills at two

different locations is illustrated in Figure 5.35. From the Figure 5.35, it can be seen that the

distance between the top of the hills is about 0.3 miles. Also, the hill on the north side has higher

elevation of 525 ft than the hill on the south side (450-490 ft). From the analysis of the tornado

path, it is observed that the tornado moved along the side of the hill and it changed travelling

direction toward northeast whenever a low elevation is available. From Figure 5.34, one can see

that there is discontinuity in the ridgeline in the location of both selected points (P1 & P2). This

provided low elevation and preferred passage for the tornado to move through. The changes in

elevation in the both points (P1 & P2) are shown in Figure 5.36 a and b respectively. Also, aerial

image for tornado damage and path change over the low elevation is shown in Figure 5.37. Four

other sites where the tornado change traveling direction are identified. Two of these are close to

the tornado start point, southwest of Lake Maumelle. The other two sites are in the hilly region

between Mayflower and Vilonia. Therefore, it can be concluded that tornado often moves toward

north east and it follows the least resistance path whenever is possible through a gap in a

ridgeline or low elevation spots. Also, one can conclude from the provided field observations

that tornado changes travelling direction while moving along the side of a hill if a gap

(discontinuity in the hill) is available. Furthermore, it is observed that tornado moves along the

side of the hill of certain orientation, and that the tornado angle of attack affects the way it

crosses the hill. In a different site in region R1, it is noticed that the tornado moved along the

side of the hill when its angle of attack was about 26º. Ahmed and Selvam (2015a) reported that

the tornado crosses a hill of relatively small width when the angle of attack is almost 90º. More

investigations are required either by computer models or wind tunnel to have better

understanding of the field observations.
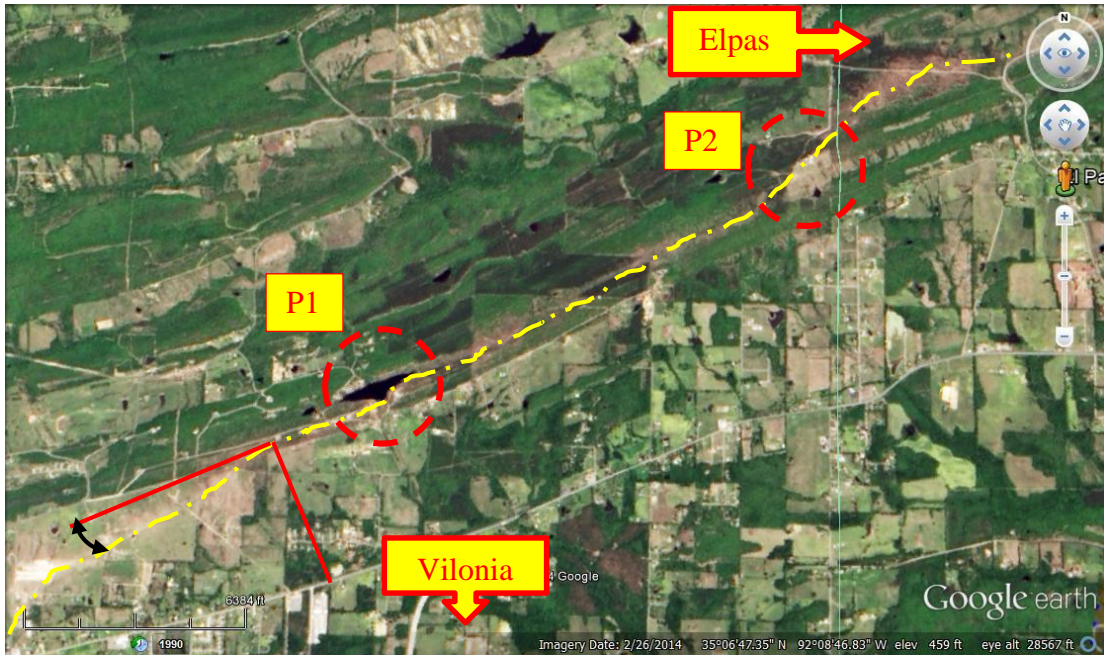
Figure 5.33 Tornado damage path between Vilonia and Elpaso (NASA, 2014).
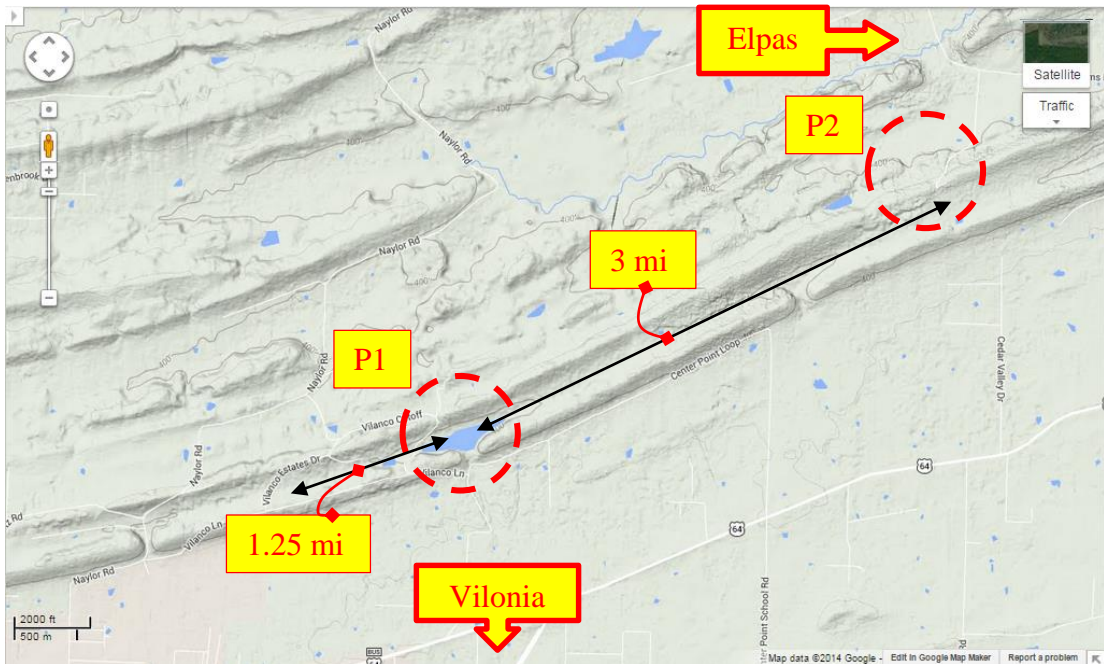
Figure 5.34 Terrain map showing points where tornado change direction.
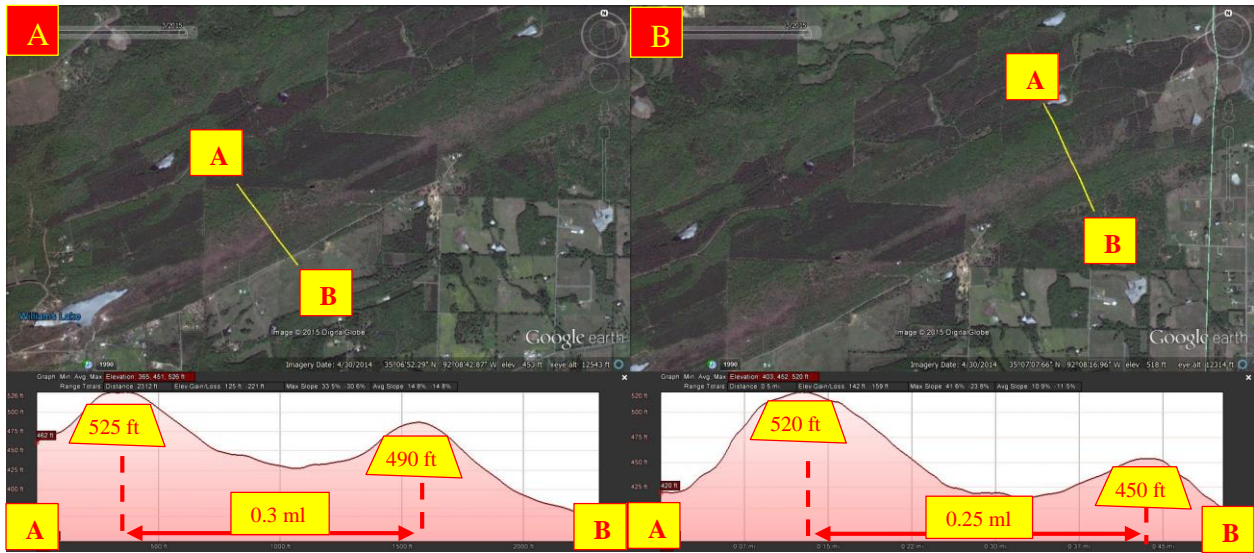
Figure 5.35 Cross section of the two parallel hills a) close to P1 b) close to P2.
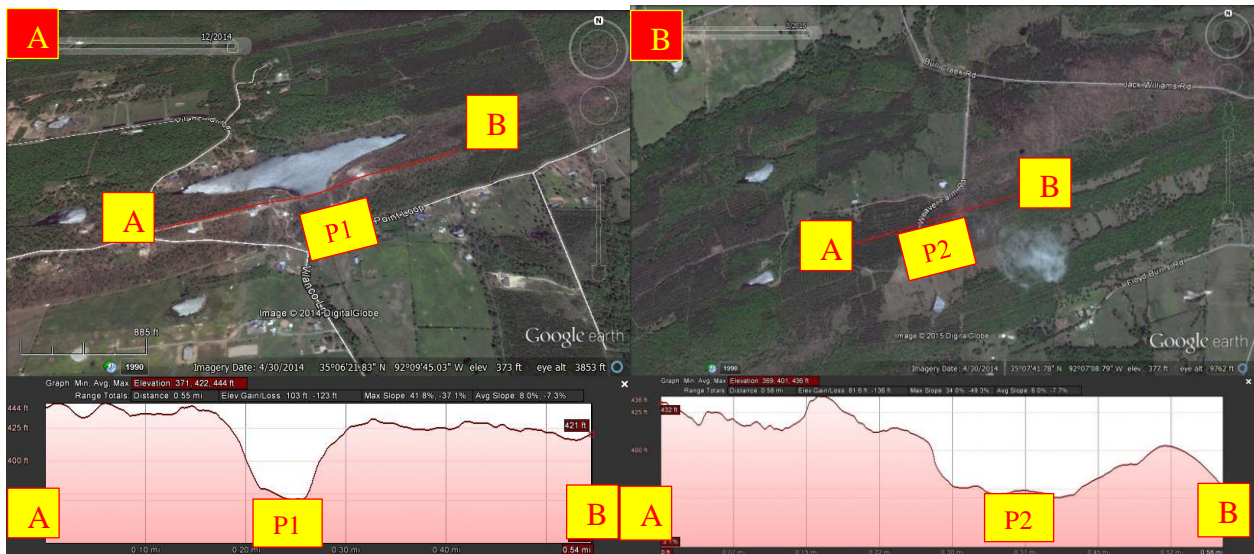
Figure 5.36 Elevation profile along lone AB a) point (P1) b) point (P2).

Figure 5.37 Aerial image for tornado damage and path change over the low elevation at point (P2) taken by (CAP, 2014).

5.6. Conclusions

Damage investigation of the tornado in Mayflower, AR in April 2014, is conducted. Ground and aerial investigation data is gathered and analyzed using Google Earth, Google Terrain Maps and Google Picasa. These computer software are utilized for data synchronization and visualization, and the following conclusions are arrived:

- The Damage intensity is observed to be less when the vortex travels over hilly terrain. The average damage rating over a hilly terrain is estimated less than EF2, while it is almost EF4 where the terrain is flat.

- The presence of several successive hills functions like protection beerier and reduce the tornado damage. This is clearly observed in region (R1) and parts of regions (R3 &R4) where the terrain is hilly.

- When tornado travels over flat terrain or water surfaces, it maintains high devastating power and produces huge ruin (EF4).

- Tornado traveling path is greatly affected by the presence of the hilly terrain, and it leads to alter the tornado path in certain circumstances.

- It is detected from the observations that when tornado approaches a hill with angle of attack much less than a right angle, it is more likely that the tornado travels on the side of the hill, along the hill, rather than crossing it.

- When travelling over hilly terrain, Tornadoes tend to find a gap and travel through it following the least resistance path. Six locations are identified in this tornado site.

6. TOPOGRAPHY EFFECTS ON TORNADO PATH DEVIATION

6.1. Introduction

Tornadoes are considered a major risk for lives and the economy. Researchers have investigated tornadoes in many avenues: tornado geneses, tornado forces, tornado damage, tornado path and direction, and tornado interaction with structures, etc. Recently few researchers reported from wind tunnel and computer model that when a tornado goes over a hill the path of the tornado deviates. In this work further detailed study of the extent of path deviation for various ratios of tangential velocity to translational velocity are investigated. Wind tunnel, field and computer model data are investigated to examine the effects of topography on tornado path deviation (i.e. turns in tornado path while interacting with topography). Field data from both Tuscaloosa (2011) and Mayflower (2014) tornadoes is considered in this study to examine effects of topography on tornado path deviation. Computer model is utilized to run six different ratios of maximum angular velocity to translational velocity (V_Θ/V_t) (i.e.1-4, 6, 8) and study the effects of changing this ratio on tornado path deviation. The hill height and slope and vortex parameters other than (V_Θ/V_t) are kept constant. The topography shape considered in this work is a ridge. Results show that (V_Θ/V_t) ratio has significant influence on a tornado path deviation. As the ratio increases, the deviation shape changes from a straight line to single curvature then to double curvature. For ratio (V_Θ/V_t) =1, the deviation shape is almost a straight line. For $2\leq$ (V_Θ/V_t) <4, the deviation shape becomes a single curvature shape. When the ratio (V_Θ/V_t) $\geq$4, the deviation shape changes to double curvature. Numerical results for (V_Θ/V_t) $\geq$4 is qualitatively comparable to wind tunnel data. Therefore the computer model can be considered with some confidence for further application. The University of Arkansas (UA) computer model results for tornado path deviation shape are comparable to both experimental and field data.

6.2. Background

In the literature, Early attempts have been conducted experimentally (i.e. wind tunnel) to understand tornado outbreak and what factors affect the tornado generation (e.g. Ward, 1972; Davis-Jones, 1973). A common finding is that the non-dimensional factor, swirl ratio, controls the tornado outbreak. Swirl ratio governs the vortex configuration (e.g. low swirl ratio associates with single-vortex, and high swirl ratio leads to two-cell vortex). Furthermore, experimental tornado simulators are employed to measure tornado force coefficients on structures (e.g. Jischke & Light, 1983).

In the numerical endeavors, Selvam and his group (e.g. Selvam, 1993; Selvam and Millett, 2003) have simulated tornado-structure interaction numerically. They reported tornado forces on different types of structures (e.g. circular cylinder and cubic building).

However, very little research in engineering and meteorology has been conducted to understand tornado interaction with terrain (e.g. hills, escarpment, knolls, valleys, mountains, etc.). Recently, a few studies have been made to investigate effects of terrain on tornado path and behavior, especially after the outbreak of the Tuscaloosa tornado in 2011. Gorecki and Selvam (2013) studied sheltering efficiency of rectangular man-made walls (rectangular hills). For a wall height equal to the tornado radius, they reported that the sheltering efficiency, the ability of the structure to reduce wind velocity on its leeward side, is almost 40%. Selvam and Ahmed (2013) employed Google Earth for damage investigation of terrain effects on tornado damage. Their focus was tornado damage uphill and downhill as well as sheltering on the leeward sides of hills. They reported that there is no damage in a region surrounded by hills located on the tornado path. In these studies, no attention was paid to terrain effects on tornado path deviation, instead only damage is monitored.

Lewellen (2012) implemented the immersed boundary method and large eddy simulation (LES) to simulate tornado in 3D domain and study the effects of topographical shapes (ridges, knolls, valleys, ridge pairs, ridges with gaps, etc.) on tornado near-surface wind. Lewellen only visualized tornado path deviation due to the interaction with various topography shape, and no topography height effect was considered. For different topographical shapes, different path deviations and pressure values are observed. However, tornado radius and velocities and topography dimensions are not reported in Lewellen (2012). Therefore, it is not considered in this work for quantitative comparison. Karstens et al. (2012) utilized the Iowa State University (ISU) tornado simulator to determine the effects of idealized topography (ridges and escarpments) on tornado characteristics. They noticed that tornadoes experience deviation from the center line while climbing up and down the topographical shapes. However, the mechanism causing this behavior is not clear yet. Many parameters are involved in the tornado-terrain interaction, and much more research still need to be done for better understanding of terrain effects on tornado damage and path deviation.

In this work, topography effect on tornado path deviation is further investigated. First, wind tunnel data presented by Karstens (2012) and Karstens et al. (2012) is analyzed. Then, data collected from Google Earth for the Tuscaloosa-2011 tornado and from field investigation for the Mayflower-2014 tornado are studied to determine topography effects on tornado path deviation. A connection between the ratio of angular velocity and translational velocity (V_Θ/V_t) and the path deviation shape is noticed. Since the ratio of (V_Θ/V_t) is not directly provided for both wind tunnel and field data, the UA computer model is utilized to determine the effect of changing (V_Θ/V_t) on tornado path deviation as well as to validate the computer model by a comparison with the wind tunnel and field data. In addition, the model is used to explain the flow behavior

up and down the hill using visualization. Knowing the factors that affect tornado path and the possible path that tornado may follow could lead to better measurements of tornado velocities near the ground and better ways to track tornadoes damage. The objective of this chapter is to determine the topography effects on tornado path deviation. Thereof, tornado path deviation due to interaction with topography (ridges) using experimental and field data is analyzed. Then, a computer model to study the effect of changing the ratio (V_Θ/V_t) on tornado deviation shape is utilized. Also, the numerical results are compared with experimental data to validate the numerical model for further applications. Then, the computer model is utilized for visualizing the tornado ridge interaction and explain the reason for the deviation. The tornado path deviation is affected by various properties of the hill and tornado. In this work, only the velocities ratio (V_Θ/V_t) is varied, and the rest are kept constant.

6.3. Wind Tunnel Observations for Tornado Path Deviation (Tornado-Ridge Interaction)

Karstens et al. (2012) utilizes the Iowa State University (ISU) tornado simulator to study tornado interaction with different topographical configurations (e.g. ridges and escarpments see Figure 6.1). The simulator is a huge transferrable chamber with a fan and vanes to generate the tornado. Details of the simulator are reported in Haan et al. (2008). The wind tunnel experiment setup for tornado interaction with topography is presented in details in Karstens (2012). The ridge height is held fixed equal to 0.285 m. the tornado radius used is in range (0.23-0.56) m, so the simulated tornado average radius is assumed to be equal to the ridge height. The ridge profile is shown in Figure 6.2 a which is adopted from Karstens (2012). The maximum slope for the ridge is 20%. Details for the simulated angular velocity values are not reported, however, Haan et al. (2008) is referred to for these details. Karstens reported that translational velocity used is 0.2 ms^{-1}. Based on his setup for the simulator, angular velocity average is estimated to be 9 ms^{-1}.

Therefore, the ratio (V_Θ/V_t) used in their simulation is almost equal to 45. The minimum pressure on the ridge surface is acquired while the simulated tornado interacts with the ridge. The minimum pressure on the ridge surface due to tornado crossing the ridge is shown in Figure 6.2 b. From Figure 6.2 b, one can see that the tornado experiences deviation in its path while climbing up and down the ridge. This deviation is defined as a double curvature deviation with two maximum eccentricities on both sides. The first eccentricity is almost at one third of the way up ridge, and the second one is at 20% of the way down ridge. Karstens reported that translational velocity could not be maintained constantly, and that might also affect the outcome. Also, the energy is provided continuously for angular momentum, while a real life tornado experiences energy loss due to either interaction with structure or topography causing distraction. The real life tornado is much more complicated including climate effects on tornado behavior. This might make their results differ slightly from real tornado behavior. Therefore, the topography effect on tornado path deviation is investigated for two real life tornadoes as discussed in the next section.
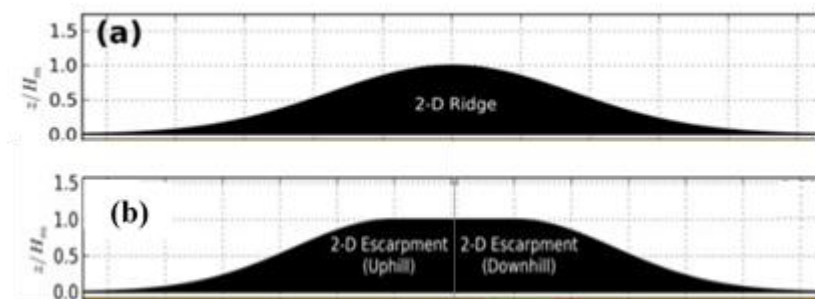
Figure 6.1 Topograghy shapes used by Karstens a) 2D ridge b) 2D escarpment, (taken from Karstens, 2012).
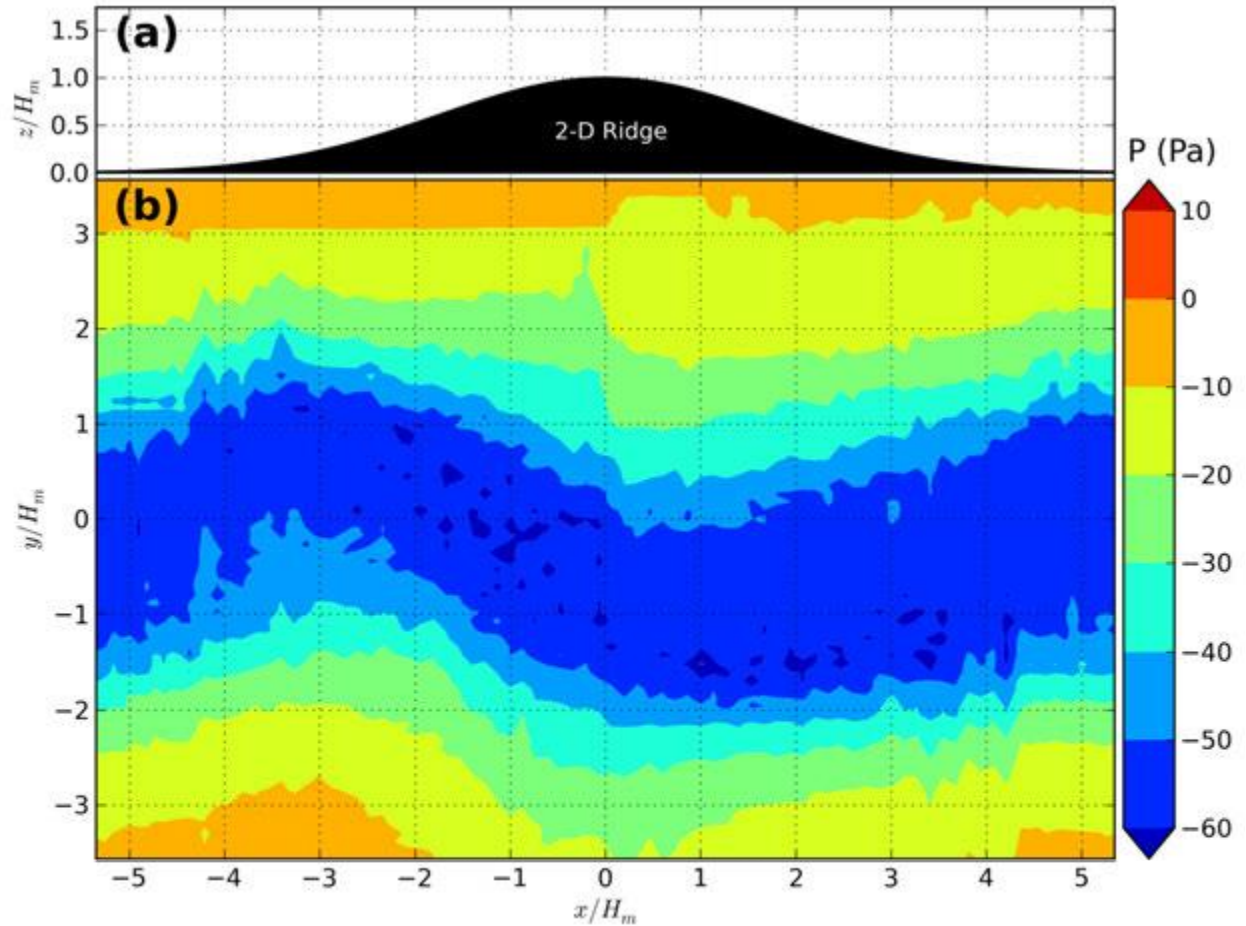
Figure 6.2 a) Ridge profile b) minimum pressure on ridge surface ($V_\Theta/V_t \approx 45$), (taken from Karstens, 2012).

6.4. Field Observations for Tornado Path Deviation (Tornado-Hill Interaction)

In this section, the Google Earth damage path of Tuscaloosa-2011 tornado (Selvam and Ahmed, 2013), and the field data of Mayflower-2014tornado (Selvam et al., 2015) are considered for tornado path deviation study. In both of these tornado sites, the tornadoes interacted with hilly terrain (a terrain which has several consequent hills or any other topographical configurations in certain regions).

6.4.1. Tuscaloosa-2011 Tornado

Tuscaloosa-2011 is considered as one of the deadliest tornadoes in the last five decades. The whole path of approximately 142 km (88 miles) is shown in Figure 6.3. The tornado travels from southwest to northeast as indicated by the yellow arrow in Figure 6.3. About 29km (18 miles) northeast of Tuscaloosa on the tornado path, a close up view is shown in Figure 6.4. Figure 6.4 illustrates the tornado signature over the hilly terrain as a light brown color. Two sites are selected with zoomed views and elevation profiles in this hilly area. For both locations, notations are given as H1 (Hill1) and H2 (Hill2) respectively. The average radius of the tornado core is estimated about 75m (246 ft) from the damaged path using Google Earth measuring tools (maximum reported damaged width is about 2.4km (1.5 miles)). The tornado maximum intensity for Tuscaloosa-2011 is EF4 with maximum velocity of 306kmh^{-1} (190 mph) as reported in National Weather Service report (NWS, 2011c). This velocity range can be on the higher side because it comes from straight line wind damage estimation. The ratio of angular velocity to translational velocity (V_Θ/V_t) is almost (3) as detected from (NWS, 2011c). However, due to interaction with the hilly terrain, tornado loses energy and its intensity changes as shown in Figure 6.5. Figure 6.5 demonstrates tornado damage path and intensities for the same region of H1 and H2 mentioned above. Therefore, the ratio (V_Θ/V_t) for this specific location is estimated to be less than two depending on the reported intensity and average traveling speed for the tornado. The height of H1 is almost 21m (70 ft) as illustrated in the elevation profile in Figure 6.6, and the maximum slope is 32%. The other hill (H2), also located on the tornado path has maximum height of 18m (60 ft) (See Figure 6.7).

The damaged path in Figures 6.6and 6.7 is margined by dashed yellow arrows. From the close-up view for H1shown in Figure 6.6, one can see that the tornado crosses the hill with no

curvature in its path. Also, the tornado with aforementioned intensity passes over the H2 with no curvature in its path as shown in Figure 6.7. In other words, there is no deviation from the original path as one can see from the provided data. Furthermore, Figure 6.5 confirms that tornado damage path (red area) is almost straight (No curvature) even though the terrain is hilly. In this case, the (V_{Θ}/V_t) ratio is estimated to be less than two, and it is interpreted to be connected with no curvature in the tornado path. It is also important to note that hills are very close to each other and with height less than 50% of tornado radius. However, no height effect is studied in this work.
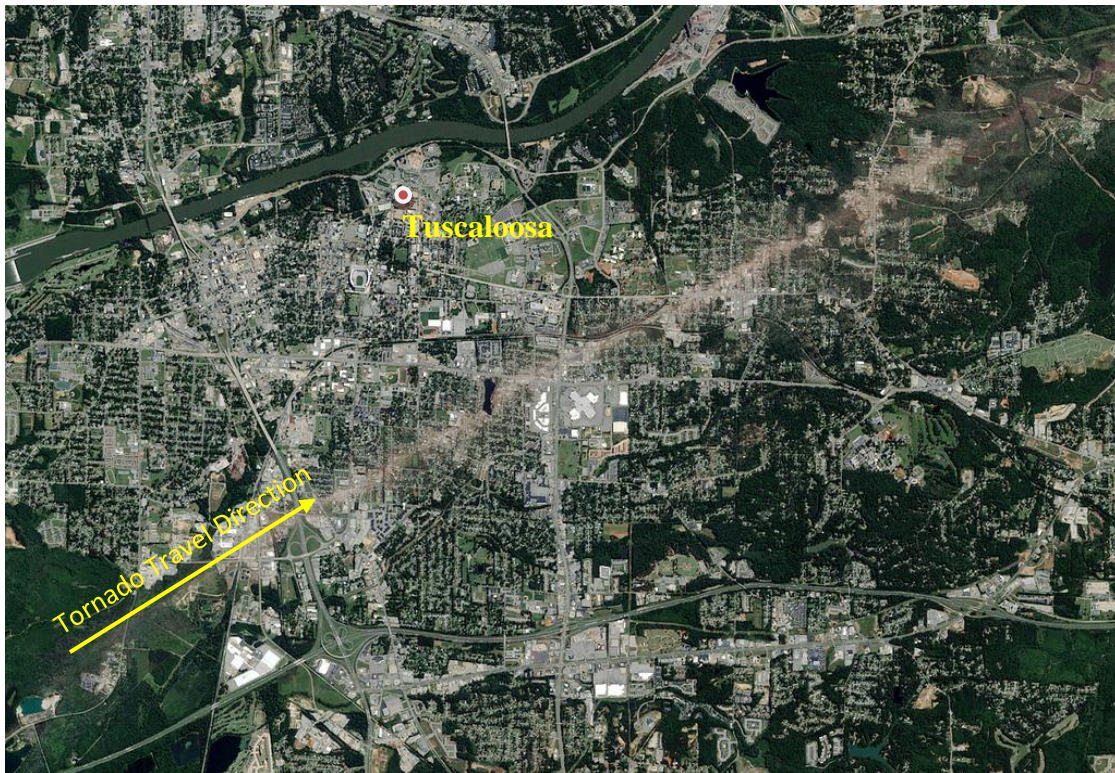
Figure 6.3 Damage path for Tuscaloosa tornado 2011 adopted from NOAA 2011.

Figure 6.4 Close-up view for a hilly terrain region 18 miles NE Tuscaloosa.
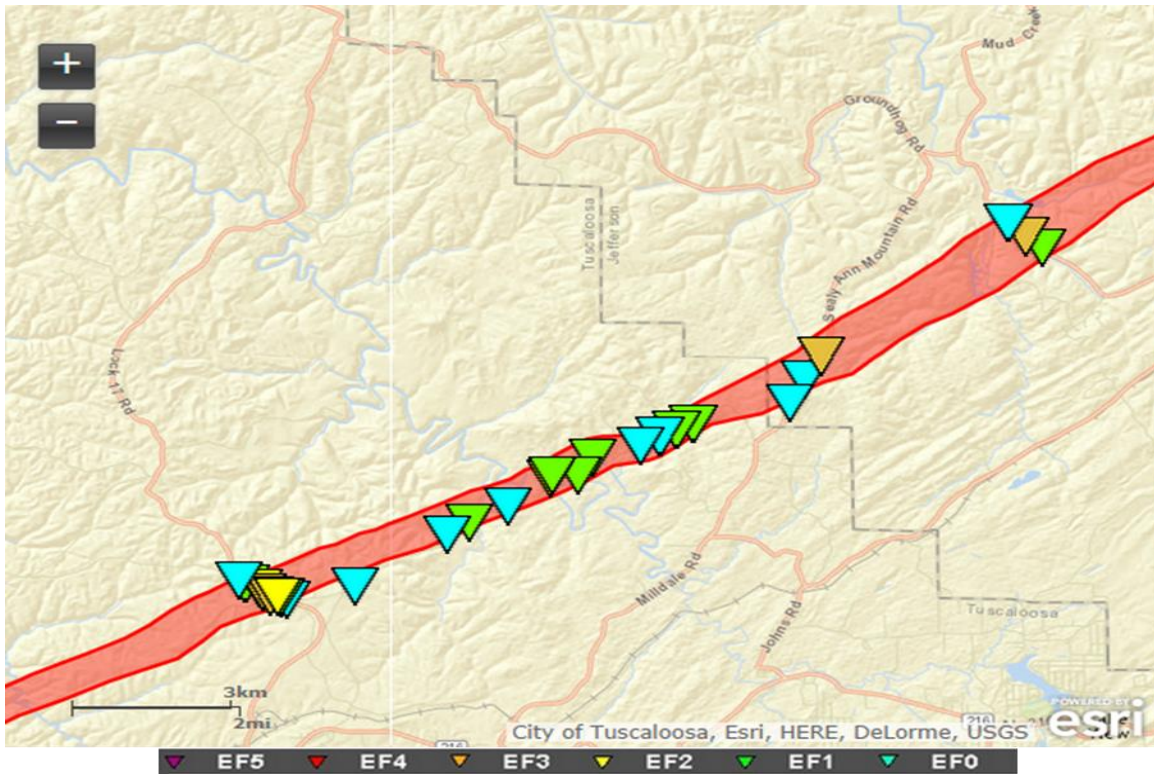
Figure 6.5 Tornado intensities and damaged path for the region of H1 and H2, (NWS, 2011c).
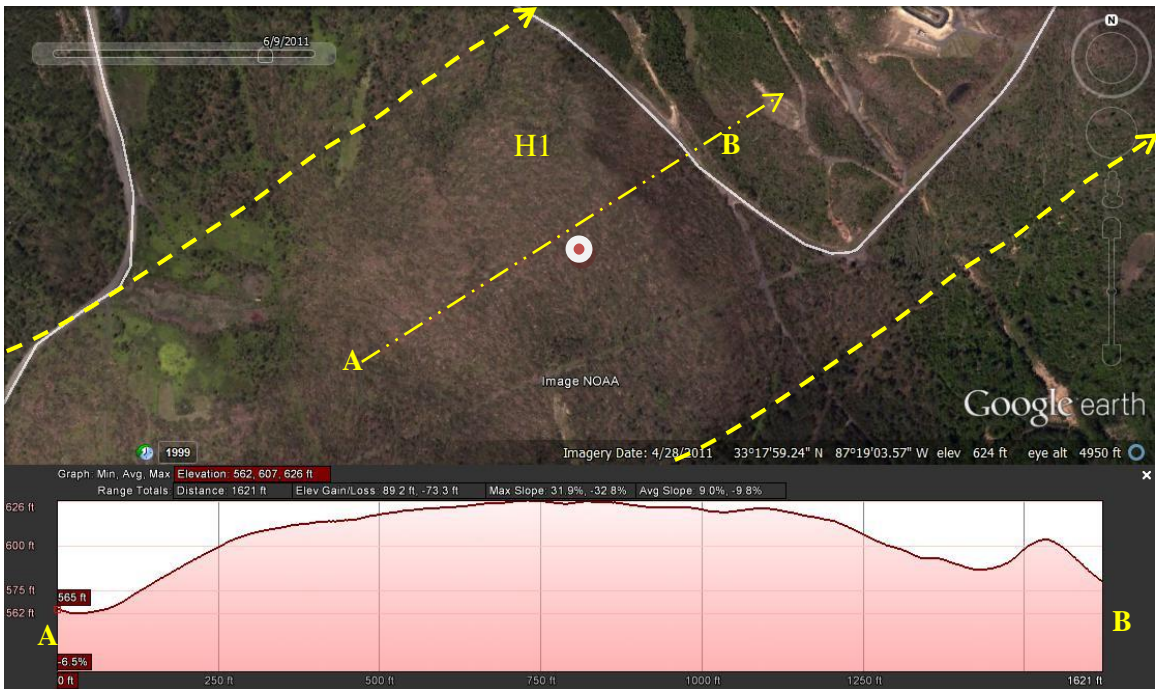
Figure 6.6 Close-up view and elevation profile for the hill in location H1, ($V_\Theta/V_t \approx (1\text{-}2)$). Not much deviation noticed.
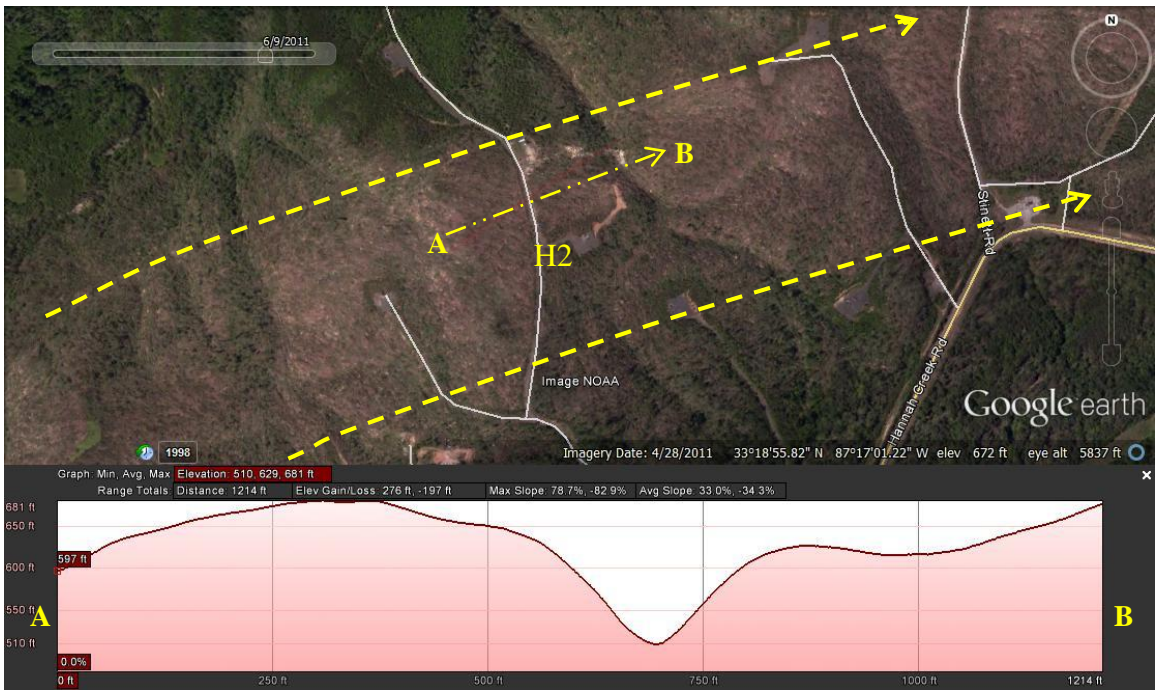
Figure 6.7 Close-up view and elevation profile for the hill in location H2, ($V_\Theta/V_t \approx (1\text{-}2)$). Not much deviation.

6.4.2. Mayflower-2014 Tornado

Another tornado outbreak, Mayflower-2014, is selected for this study as shown in Figure 6.8, an image reported by the National Aeronautics and Space Administration (NASA, 2014). The terrain in this area is also hilly, but data availability and quality are very limited. One location close to Lake Conway is studied in this site. As reported by NWS (2014a), the tornado intensity varies greatly in this location between EF0 to EF2. However, there are few places with intensity of EF3 and EF4 as reported by NWS (2014a). The point here is that tornado intensity changes as it interacts with terrain. Rough terrain weakens tornadoes, while smooth terrain strengthens tornadoes (Selvam et al., 2014). Therefore, the ratio (V_Θ/V_t) may change slightly depending on the terrain nature. The maximum ratio of (angular/ average translational velocity) for this site is estimated to be about (5). The tornado traveled about 64km (40 miles) in one hour as reported by NWS (2104a), so V_t is estimated to be 64kmh^{-1} (40mph).

In the selected location, H3, the tornado passes over a water surface, Lake Conway, before it interacts with H3. Because water is considered a smooth surface, it is assumed that tornado has a high intensity. Figure 6.9 shows a close-up view of the damaged path around location H3. After passing the lake, the tornado interacts immediately with a two-dimensional hill, and then hits H3 as shown in the topographical terrain image Figure 6.10. Therefore, it gets weakened and the ratio (V_Θ/V_t) decreases slightly. The two-dimensional hill height is about 37m (120 ft) and it is located about 0.8 km (a half mile) prior to H3. There is not enough information about the tornado core radius. However, estimation from the damaged path using Google Earth measuring tools shows that the radius is about 61m (200 ft). The NASA image is imposed on Google Earth, and then the tornado core radius is measured. Therefore, a tornado with estimated (V_Θ/V_t) ratio about (4) moves over H3. The height H3 is about 100ft as shown in the elevation profile in Figure 6.11.

From Figure 6.11, one can see that there is a single curvature deviation from the path center. The tornado starts deviating to the right while climbing uphill to reach its maximum deviation at the hilltop. Then, it starts back deviating to the left while climbing down.

These two sites, Tuscaloosa-2011 tornado and Mayflower-2014 tornado, show two completely different cases for tornadoes crossing a hill. In each case the tornado behaves differently and has different deviation configuration for different estimated (V_Θ/V_t) ratios. Therefore, computer model is utilized to verify the theory that ratio (V_Θ/V_t) affects the tornado path deviation while interacting with topography (a ridge). Also, it is used to compare the computer results for tornado path deviation with experimental results for validation and further applications of the computer model.
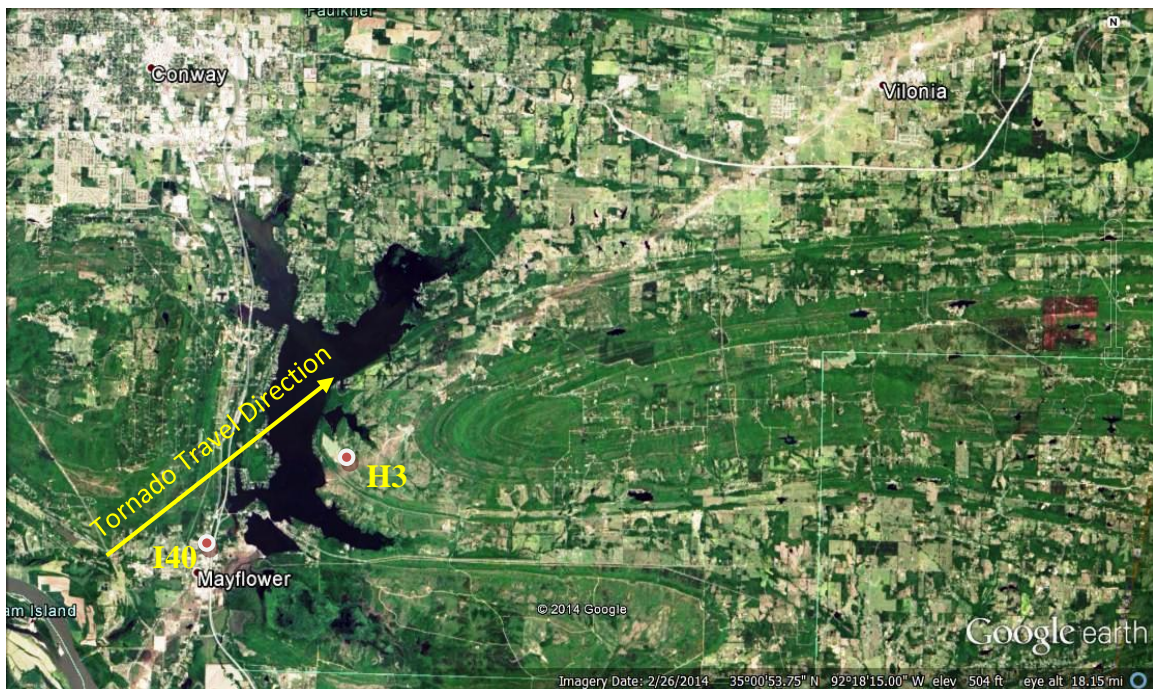
Figure 6.8 NASA image for the tornado path in Mayflower 2014.

Figure 6.9 A close-up view for location close to Lake Conway (Mayflower, 2014).

Figure 6.10 The terrain topography around the selected location in H3 (Mayflower, AR).

Figure 6.11 Elevation profile for the hill in location H3, ($V_\Theta/V_t \approx 4$, single curvature).

6.5. Vortex Transportation on a Flat Terrain

The goal here is to transport the vortex along the X axis, and monitor the minimum pressure on the ground to study the tornado path deviation. No topography is considered for this purpose, and three sets of grid are considered. The grid spacing in X and Y directions are held fixed and equal (0.1H) for all the grids. However, spacing in the Z direction (Vertical direction) is varied. For grid A, equal spacing of (0.085h) is used. For the other two grids (B & C), a logarithmic growth factor is used with minimum grid spacing close to the ground of 0.025h and 0.0025h respectively. The vortex is transported completely along the X axis of the domain as shown in Figure 6.12 a-c. Grid B shows the best vortex transportation with dissipation of 24%; however, it takes double the CPU time comparing to grid A, and the difference in vortex dissipation is only 6%. Dissipation is evaluated by measuring the vortex minimum pressure

114

width near the outlet and compare it with the one near the inlet of the domain. Even though the

minimum grid spacing in grid C is the smallest, it is associated with the biggest numerical error.

Since the main purpose here is monitoring the pressure on the ground and validated with the

wind tunnel data, the grid A is considered for the rest of this study for a good accuracy and

computational cost balance. Also, when topography is presented in the numerical domain, the

iteration time required to achieve the convergence criteria is about five times that required when

there is no topography. Even though $(V_\Theta/V_t) = 3$, one can see that the tornado path is almost a

straight line in Figure 6.12, because of the flat terrain (no topography effects).

Table 6.1 Grid details (all grid spacing in X&Y directions uniform equal 0.1H).

	Min spacing Z	Max spacing Z	Total point	CPU time Parallel MPI, 24P	Vortex Dissipation
Grid A	0.085H	0.085H	290x290x90 (7.569M)	14 hrs	30%
Grid B	0.025H	0.25H	290x290x90 (7.569M)	24 hrs	24%
Grid C	0.0025H	0.25H	290x290x90 (7.569M)	35 hrs	35%
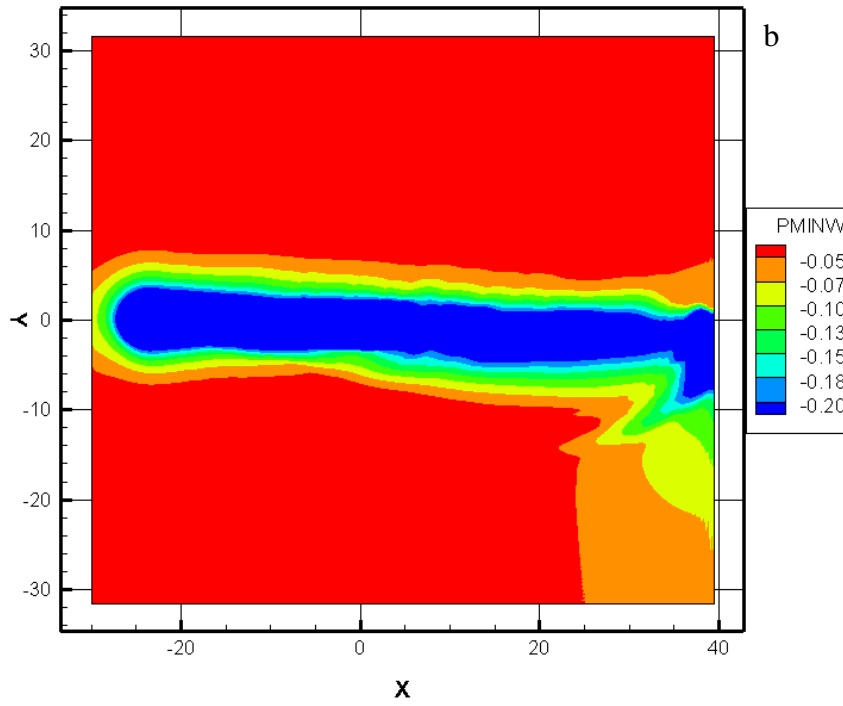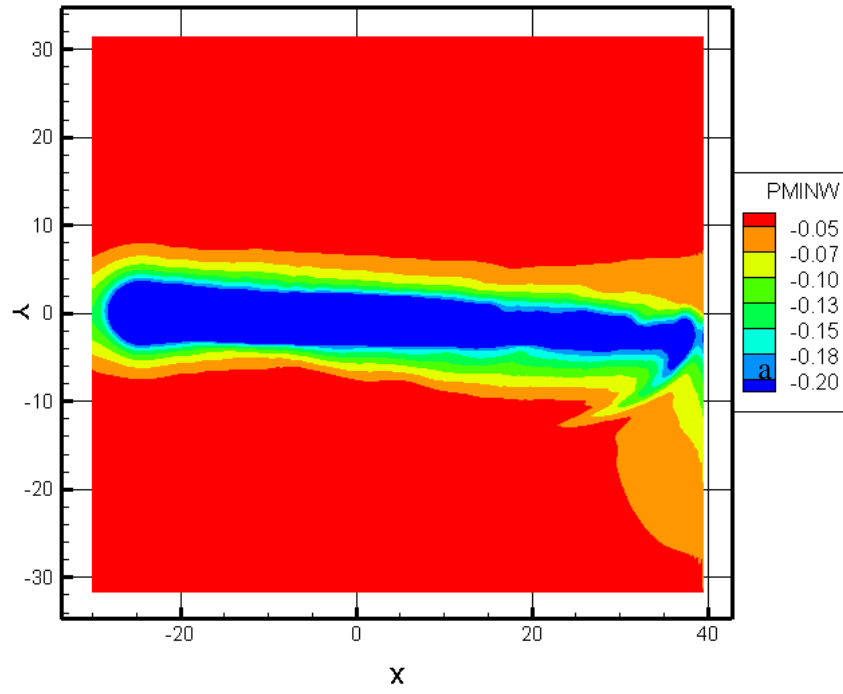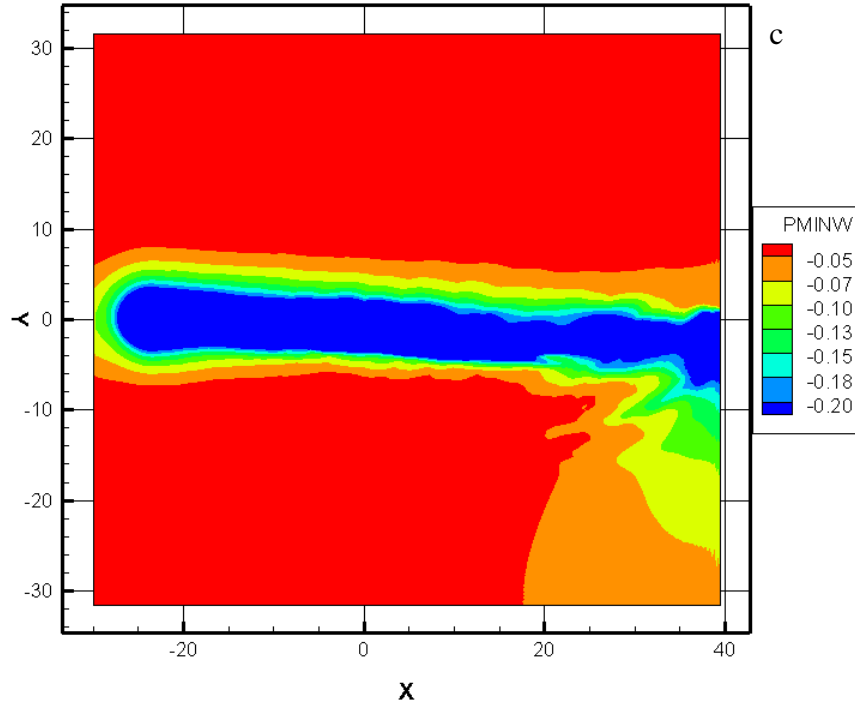
Figure 6.12 Minimum pressure on the domain ground (flat domain) a) grid A b) grid B c) grid C, $(V_\Theta/V_t) =3$.

6.6. Simulation Parameters

The tornado radius and ridge parameters used in this work are taken from Karstens (2012) for a better comparison between experimental and numerical simulations. However, details for angular to translation velocities ratio are not reported in Karstens works, so a range of values are considered in the model. The tornado radius is equal to ridge height, and the ridge profile is represented by the below Gaussian equation adopted from Karstens.

$$Z_i = H.e^{(-0.5x_i^2/500^2)}$$

(6.1)

Where Z_i is the height at distance x_i from the center, H is the height of the ridge.

There are several factors control and affect the tornado-terrain interaction. Some of these factors are; obstacle shape profile, slope of the obstacle, obstacle height, obstacle length, ratio of obstacle height to tornado radius, ratio of obstacle length to tornado radius and ratio of tornado angular velocity to translational velocity. In real life, there could be more factors involved. In this work, a ridge shape is used with height equal to tornado radius (r_{max}), width equal 30 r_{max} and slope equal 20% as illustrated in Figures 6.13 and 6.14. The shape profile of the ridge, the ratios of the tornado radius to both height and length of the ridge are all fixed and used similar to those reported in Karstens (2012). The ratio of (V_Θ/V_t) observed from real tornado is in the range (3-6). In this work, the ratio of angular velocity to translational velocity is varied within the range (1-8) to compare the results to experimental and field data as well as to verify its effects on tornado's path deviation. Simulation of (V_Θ/V_t) greater than (8) is not considered in this work because it is associated with very high error in capturing the boundary layer. Tornado radius (r_{max}) equal to 2 units and a ridge height of 2 units are used in this work. Table 6.1 illustrates parameters used in the wind tunnel experiment by Karestens (2102), University of Arkansas (UA) numerical simulations and that estimated for field data. In Table 6.1, values of velocities and tornado radius for numerical and experimental simulations are normalized with respect to ridge height (H). Numerical domain and pressure Iso-surface of tornado approaching the ridge is shown in Figure 6.13. Figure 6.14a shows the grid in XZ plane but the coarseness of the grid is increased for vitalization purposes. Figure 6.14b is a close-up view for the grid close to the ridge surface with all grid points drawn.
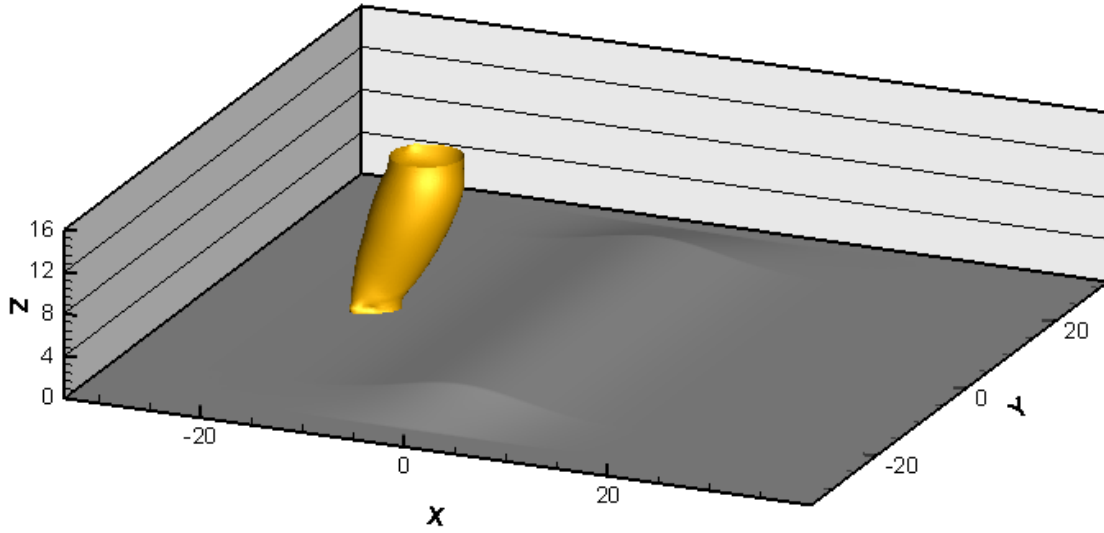
Figure 6.13 Numerical domain with pressure Iso-surface approaching the ridge.
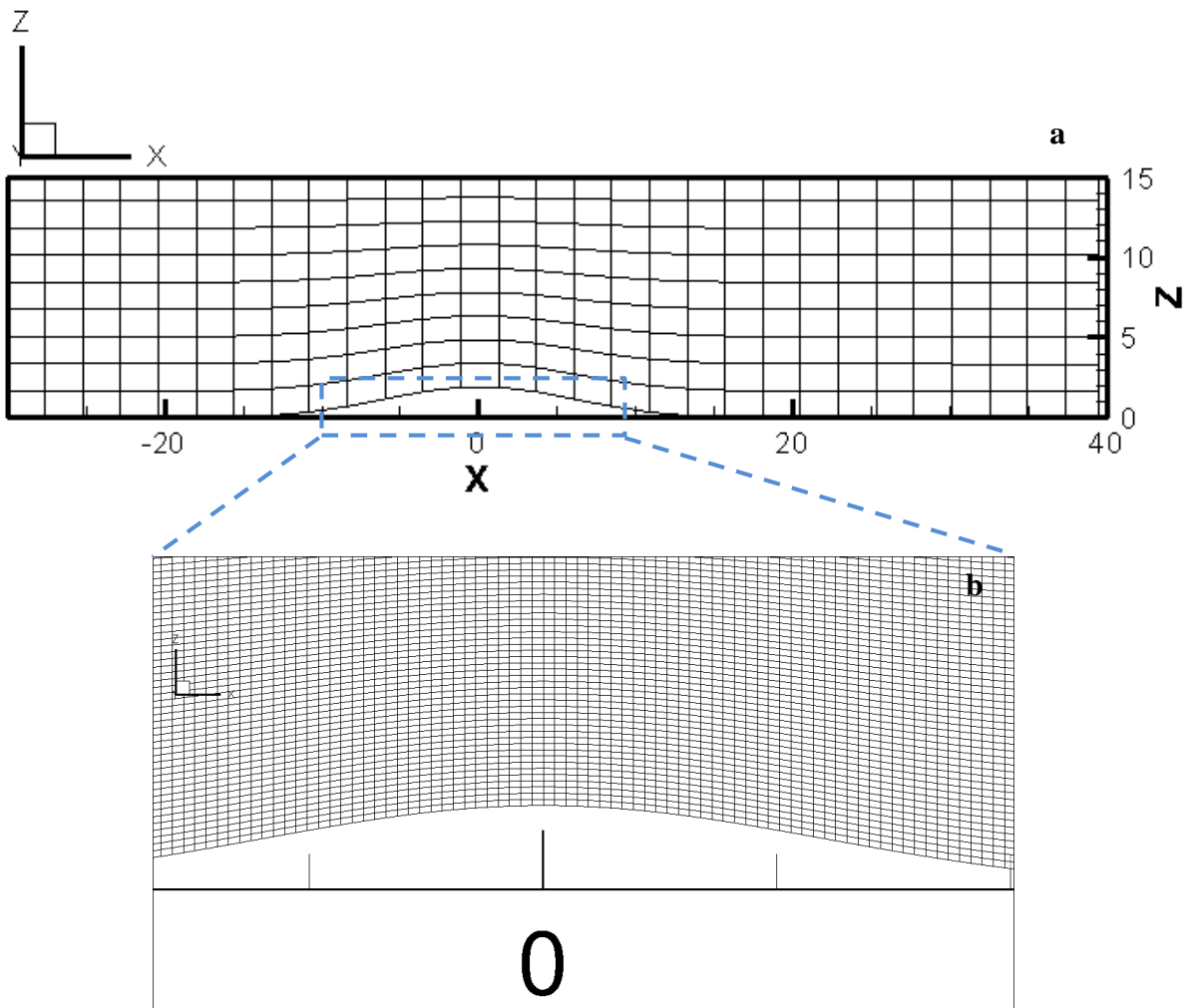
Figure 6.14 a) Grid configuration in XZ plane (10 points skipped). b) A close-up view close to the ridge surface (all the points drawn). (Total grid point is 290x290x90)

6.7. Results Discussion of the Computer Model

The effect of changing the ratio (V_Θ/V_t) on tornado path deviation is investigated. Six different ratios (i.e.1, 2, 3, 4, 6, 8) are considered. These six parameters are mentioned in Table 6.2 as UA1 to UA6. The coordinates, in both X and Y axis, are normalized with respect to the ridge height. The outcome is striking, and it shows that there is a significant effect of changing the ratio (V_Θ/V_t) on tornado path deviation. For ratio equal to one, the path is almost straight (no deviation) as shown in Figure 6.15. For ratios (2 &3), the path has tiny little bend to the left close to the center of the hill, then it deviates sharply to the right. This can be defined as single curvature as shown in Figures 6.16 & 6.17. When the ratio is greater than 4, one can see that the path has double curvature as shown in Figures 6.18 to 6.20. The ratio 6 is considered for discussion for better clarity. From Figure 6.19, one can see that tornado starts to deviate left from the center line while climbing up the ridge. The maximum devotion is about 0.75H when tornado reaches the top of the ridge. Then, it turns about 0.75H off the center line to the right as it goes down the ridge. After it is off the ridge, it starts to move back to the center. (V_Θ/V_t) ratio greater than (8) is not considered in this work due to high error in capturing the boundary layer flow.

6.8. Comparison of Computer Model with Field and Wind Tunnel Data

From the aforementioned results, one can see that as the ratio (V_Θ/V_t) increases, the tornado path changes from straight line (no deviation) to single curvature then to double curvature. This gives better understanding for the mechanism responsible for this behavior as discussed later.

These results explain why tornadoes have different path shapes in different situations in real life tornadoes. For ratio equal to one, the result is in very good agreement with tornado path over H1

and H2 in Tuscaloosa-2011 tornado as illustrated in Figures 6.6 & 6.7. Also, at location H3 in

Mayflower-2014 tornado shown in Figure 6.11, the estimated average value for (V_Θ/V_t) is about

four. Therefore, it is expected to see double curvature for the path deviation if the ratio is greater

than or equal four. It does show single curvature which means that the actual (V_Θ/V_t) ratio in that

specific location is less than four.

Table 6.2 (V_θ/V_t) for experimental, numerical and real life tornado.

	H	r_{max}	slope	V_θ	V_t	(V_θ/V_t)
Experimental Karstens (2012)	1	1	20%	31.6 unit/s	0.7 unit/s	45
Numerical UA1	1	1	20%	1.5 unit/s	1.5 unit/s	1
Numerical UA2	1	1	20%	1.5 unit/s	0.75 unit/s	2
Numerical UA3	1	1	20%	1.5 unit/s	0.5 unit/s	3
Numerical UA4	1	1	20%	1.5 unit/s	0.375 unit/s	4
Numerical UA5	1	1	20%	1.5 unit/s	0.25 unit/s	6
Numerical UA6	1	1	20%	1.5 unit/s	0.185 unit/s	8
Mayflower tornado	~100ft	~200ft	~32%	190 mph	40 mph	4.75
Tuscaloosa tornado	~60ft	~246ft	~26%	190 mph	59 mph	3.2
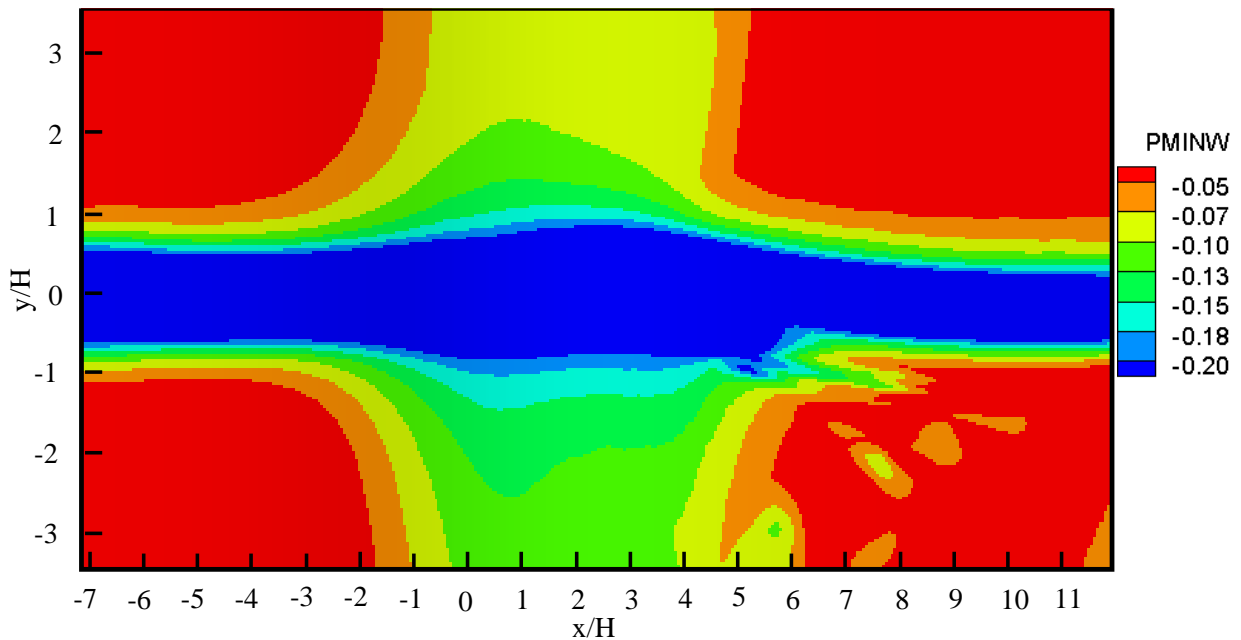
Figure 6.15 Minimum pressure on 2D ridge surface for $(V_\Theta/V_t=1)$.
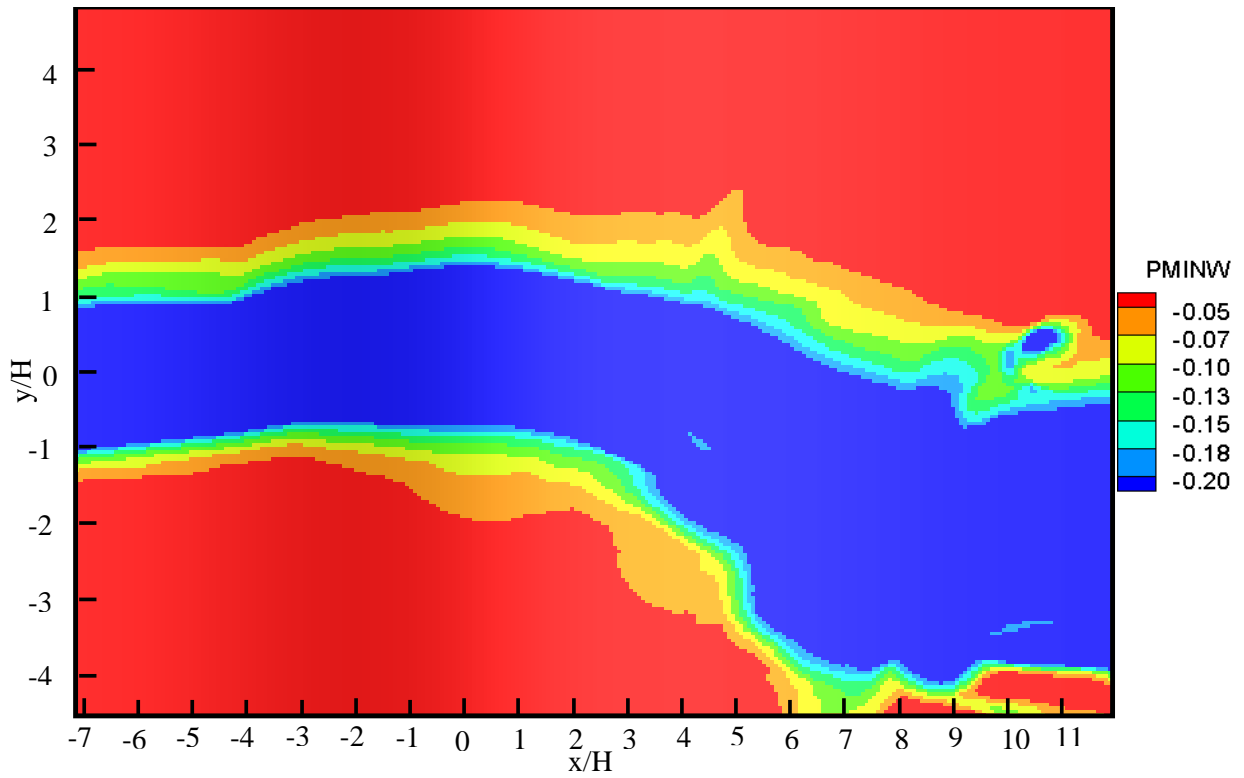
Figure 6.16 Minimum pressure on 2D ridge surface for ($V_\Theta/V_t=2$).
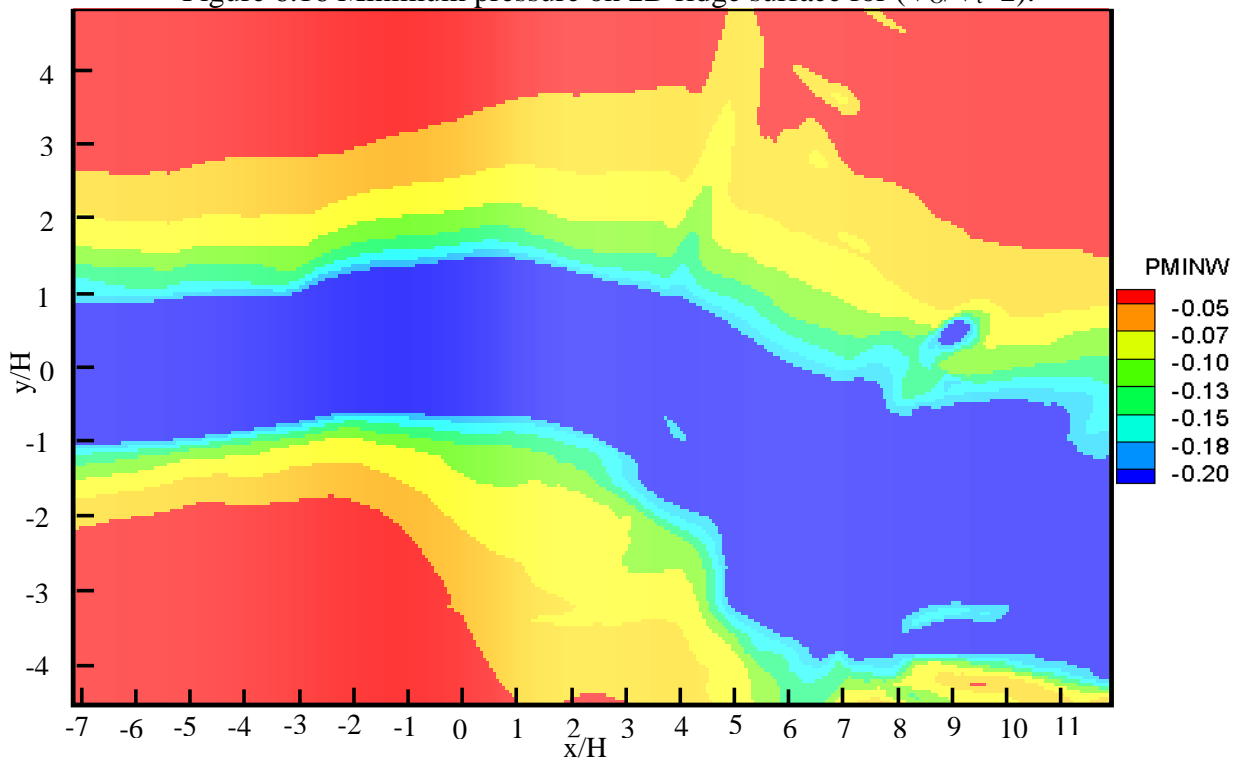
Figure 6.17 Minimum pressure on 2D ridge surface for ($V_\Theta/V_t=3$).
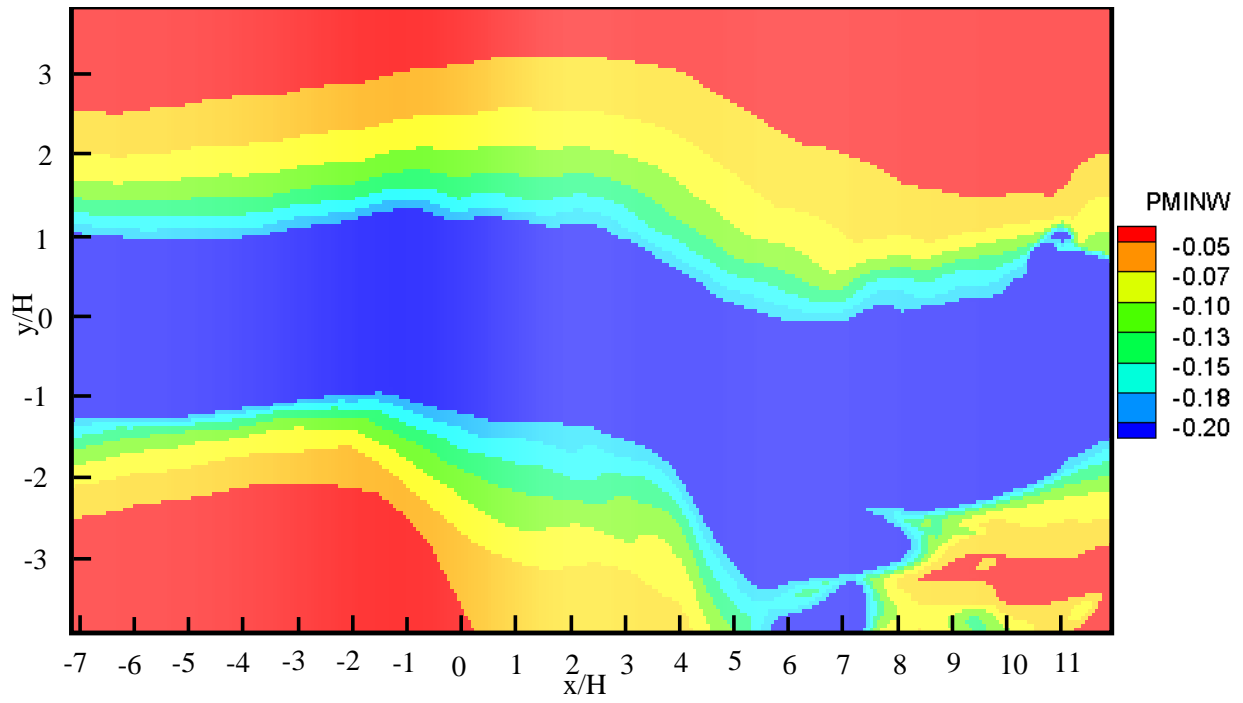
Figure 6.18 Minimum pressure on 2D ridge surface for ($V_\Theta/V_t=4$).
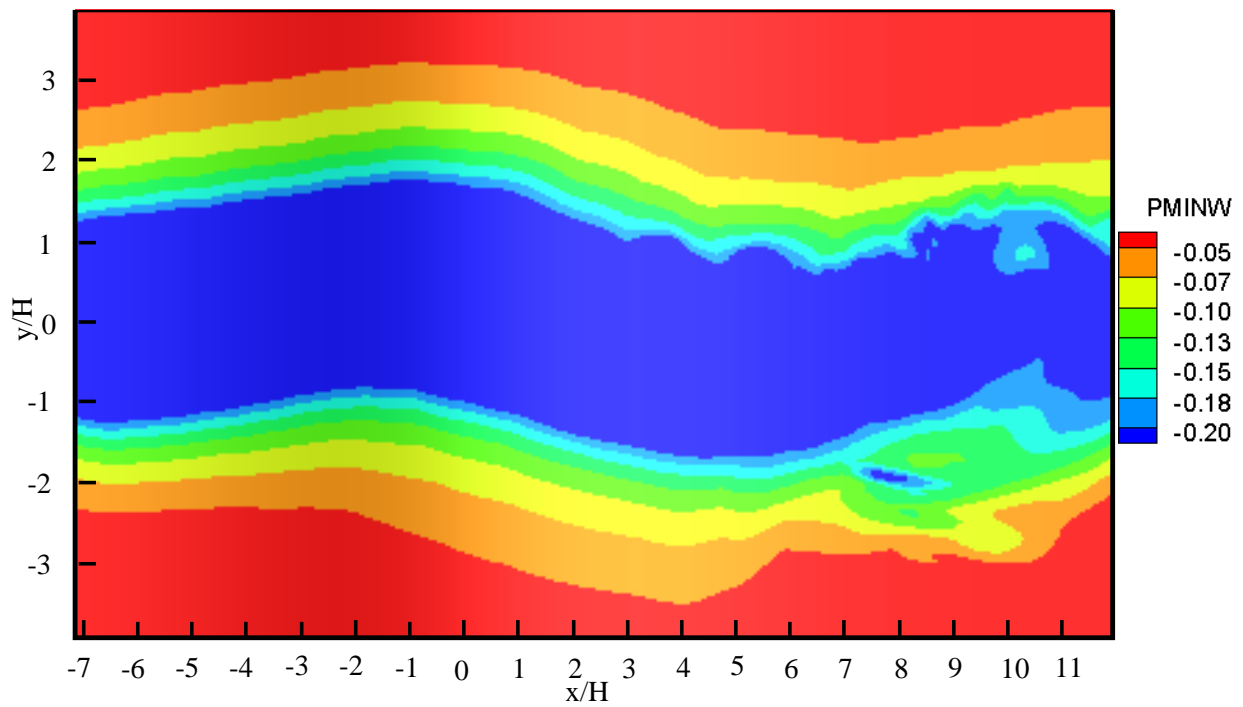
Figure 6.19 Minimum pressure on 2D ridge surface for ($V_\Theta/V_t=6$).
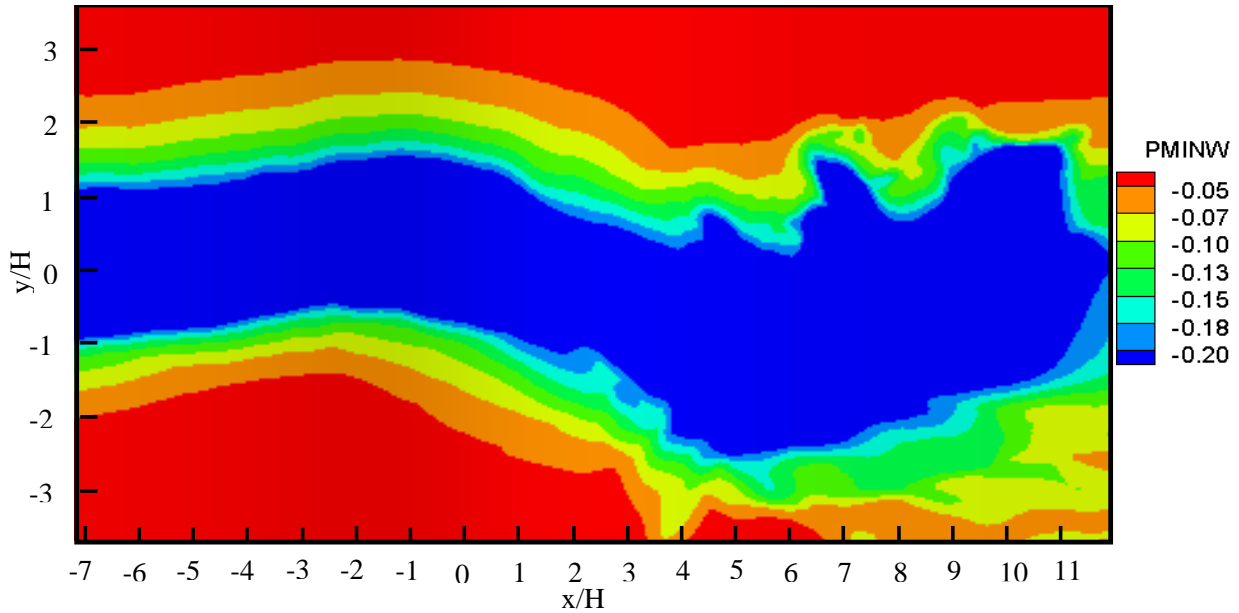
Figure 6.20 Minimum pressure on 2D ridge surface for (V_Θ/V_t=8).

6.9. Deviation Analysis

In this section an explanation of why tornado deviates while interacting with topography is sought. First, it is important to make the terminology used here clear and easy to follow. The tornado is transported along the X-axis in the numerical domain as mentioned early. Therefore, any deviation in the tornado path is going to be either on the positive side (left) or the negative side (right) along Y-axis. Different 2D and 3D views are used to interpret the tornado deviation, and in all these views the term (left) is used whenever the tornado deviates toward the positive Y, and the term (right) is used whenever the tornado deviates toward the negative Y. The ratio (V_Θ/V_t =6) is considered in this section. The pressure contours for two slices in the YZ plane are drawn in 2D and 3D to make our terminology clear and show the tornado deviation. Figure 6.21 a shows 3D view for the pressure contours for a slice in YZ plane at position (X=-5) while the

tornado is climbing up the ridge. From Figure 21 a, one can see the tornado tilts toward the left

(+Y). The 2D view of the same slice is shown in Figure 21 b and it shows that there is clear

deviation to the left. Similarly Figure 22 a and b show the tornado deviates toward the right (-Y)

while the tornado is moving down the ridge. The pressure iso-surface for the tornado while

climbing up the ridge and going down the ridge is illustrated in Figure 23 a and b. From Figure

23, one can see that the tornado base is not level as long as the tornado on the ridge surface. This

creates channeling effects and makes the tornado deviates. The velocity vectors are drawn at the

two locations shown in Figure 23 a and b for better explanations. The velocity vectors are plotted

in the horizontal plane (XY) as shown in Figure 24 a to visualize the guiding velocities direction

while the tornado moving up the ridge. From Figure 24 b, one can see that velocity vectors

toward (+Y) left (red vectors) are much more than that in the opposite direction (blue vectors),

and that finally makes the velocity magnitude leads the tornado toward the left as shown in

Figure24 c. On the leeward side of the ridge (Figure 25 a), one can see that the channeling effect

is governing the flow to the right (-Y). Velocity vectors in the XY plane on the way down ridge

are shown in Figure 25 a where the velocity vectors (red vectors) toward the left (+Y) are very

less comparing to the ones pushing towards the right (blue vectors) as shown in Figure 25 b.

Therefore, the tornado is guided toward the right by the resultant velocity vectors as shown in

Figure 25 c. For low (V_Θ/V_t) ratio, the translational velocity is high, and it controls the tornado

toward forward direction. The results for ratios greater than four are comparable to wind tunnel

results presented by Karstens (2012). However, there is little difference in the location of the

maximum deviation and the magnitude of these deviations due huge difference in the simulated

ratios. Due to limitations in numerical model the simulated (V_Θ/V_t) ratio in experimental work

could not be consider exactly. As the ratio increase, the results are more comparable to the wind

tunnel results. This means that the computer model is capable of generating reasonable tornado

and can be considered for further applications and studies.
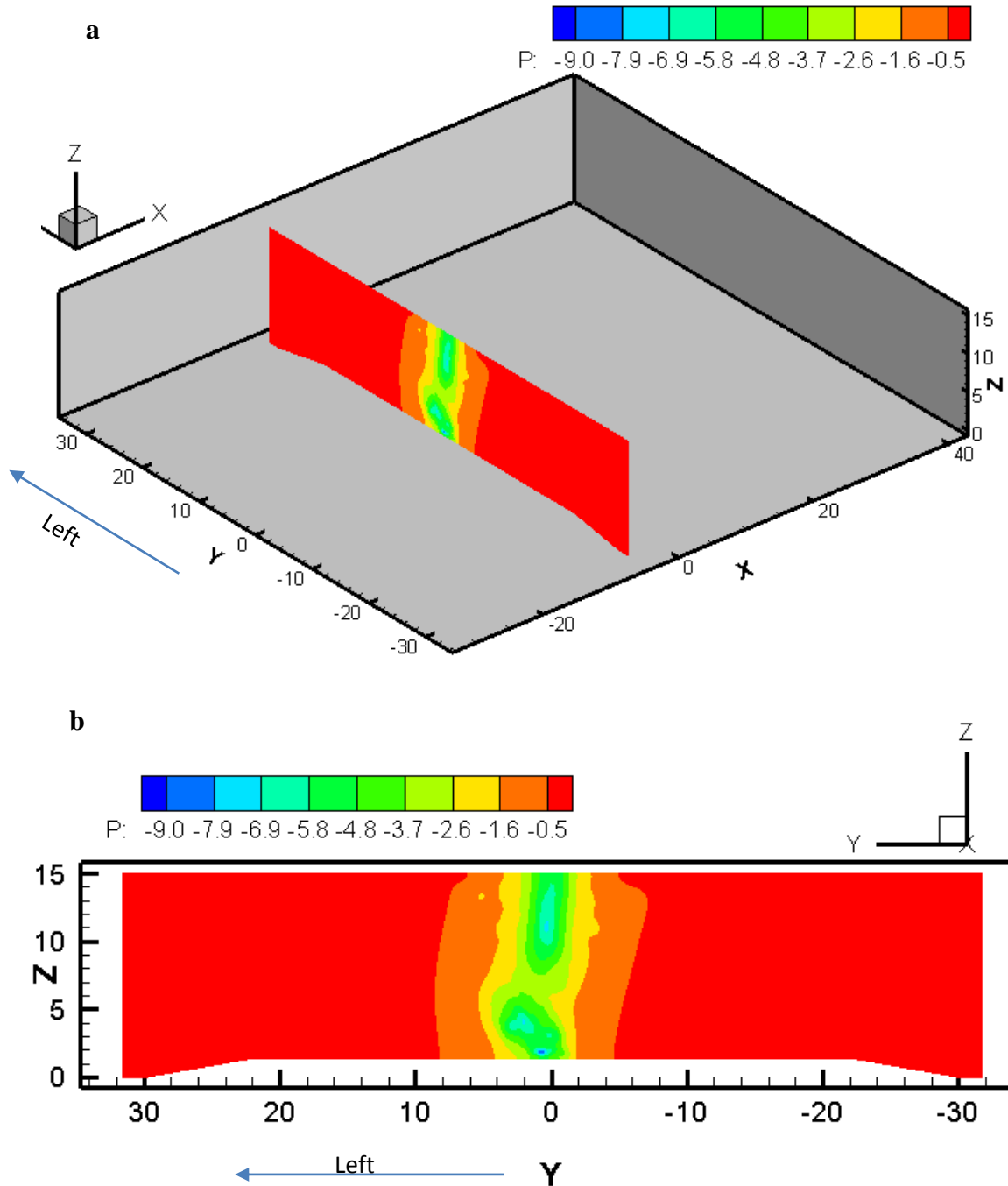
Figure 6.21 tornado deviation toward the left (+Y) while climbing up the ridge a) a 3D view for the pressure contours of a slice in YZ plane b) a 2D view of the same slice.
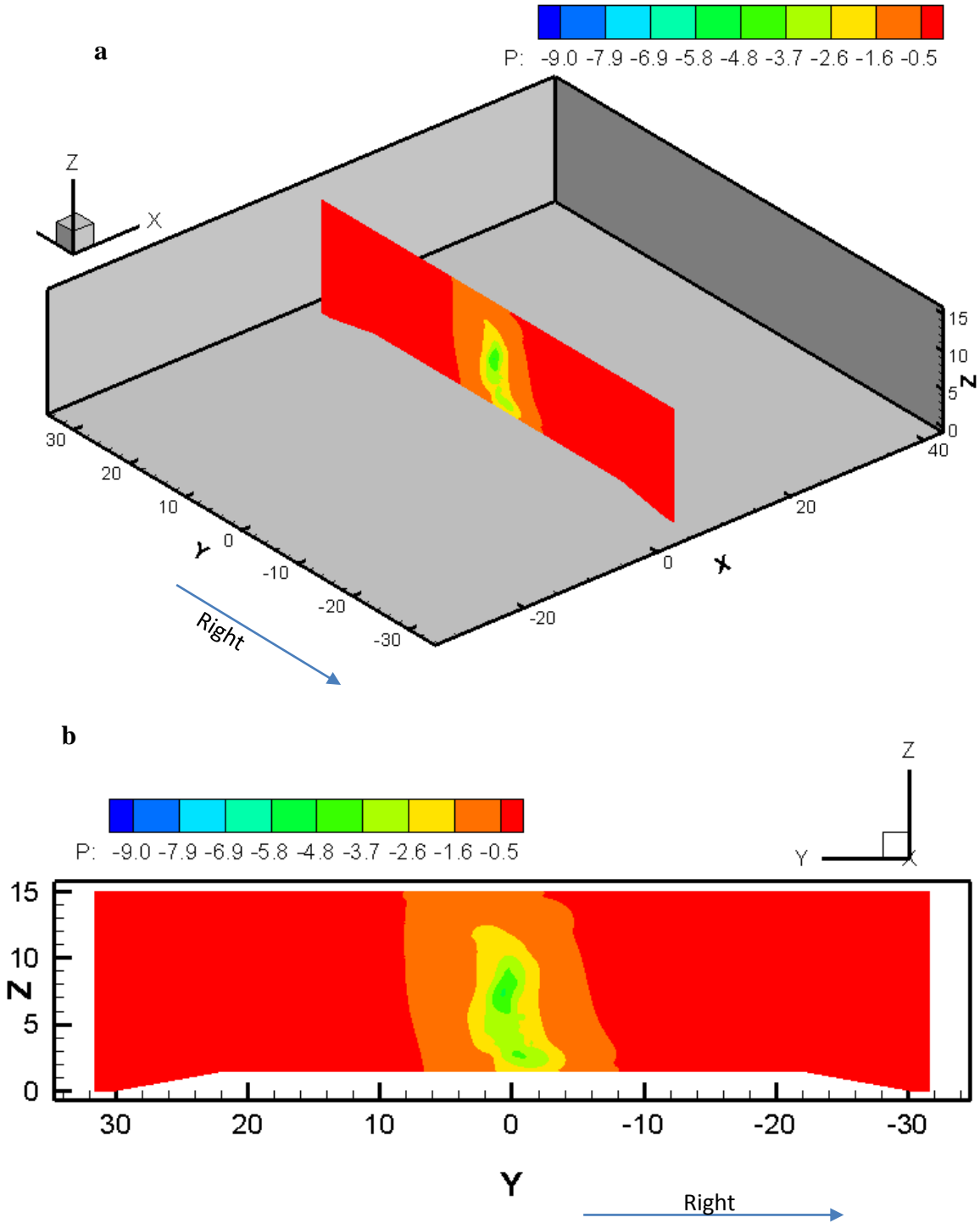
Figure 6.22 tornado deviation toward the right (-Y) while moving down the ridge a)3D view for the pressure contours of a slice in YZ plane b)2D view of the same slice.
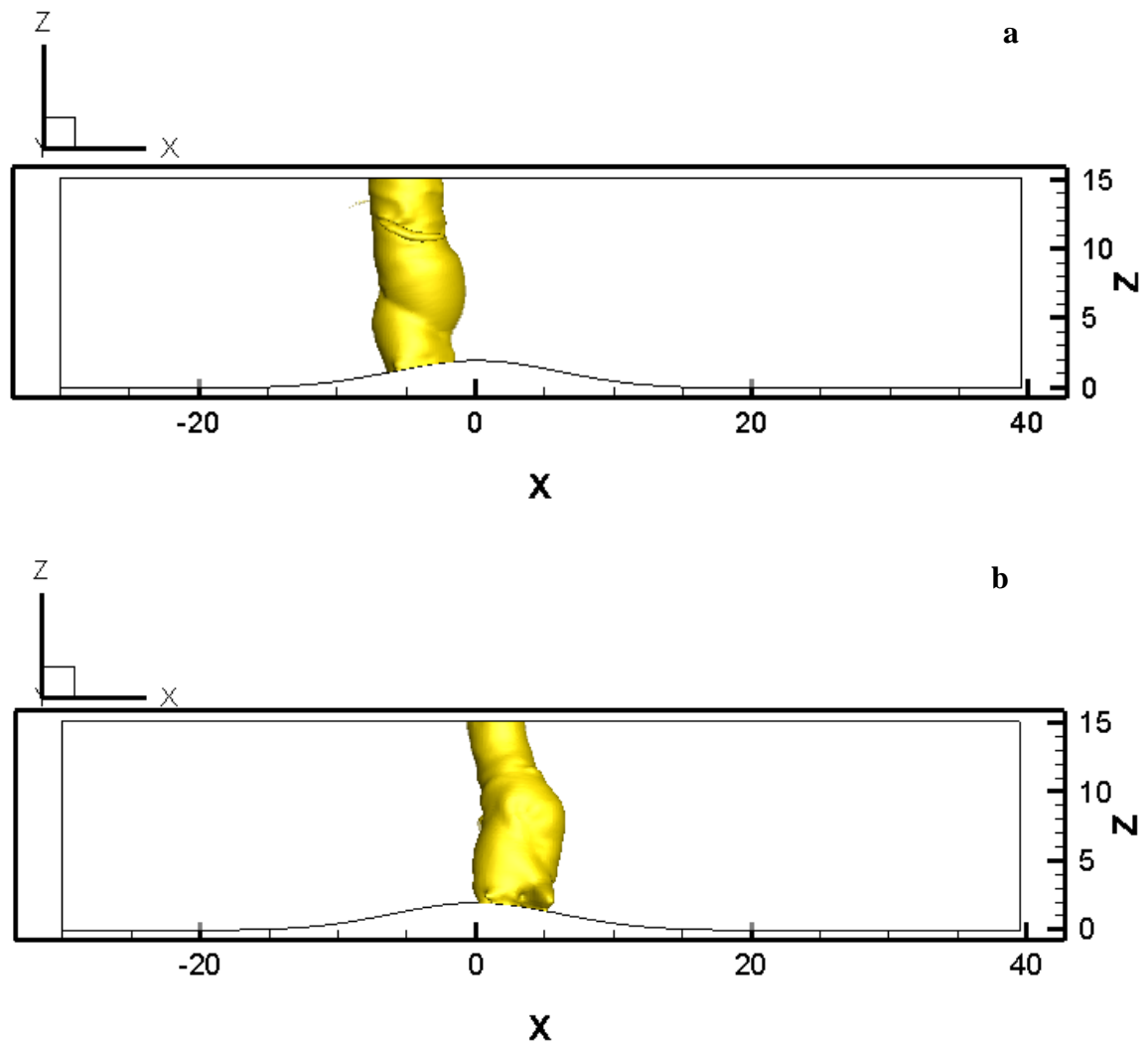
Figure 6.23 Pressure Iso-Surface of the tornado a) climbing up the ridge b) moving down the ridge.
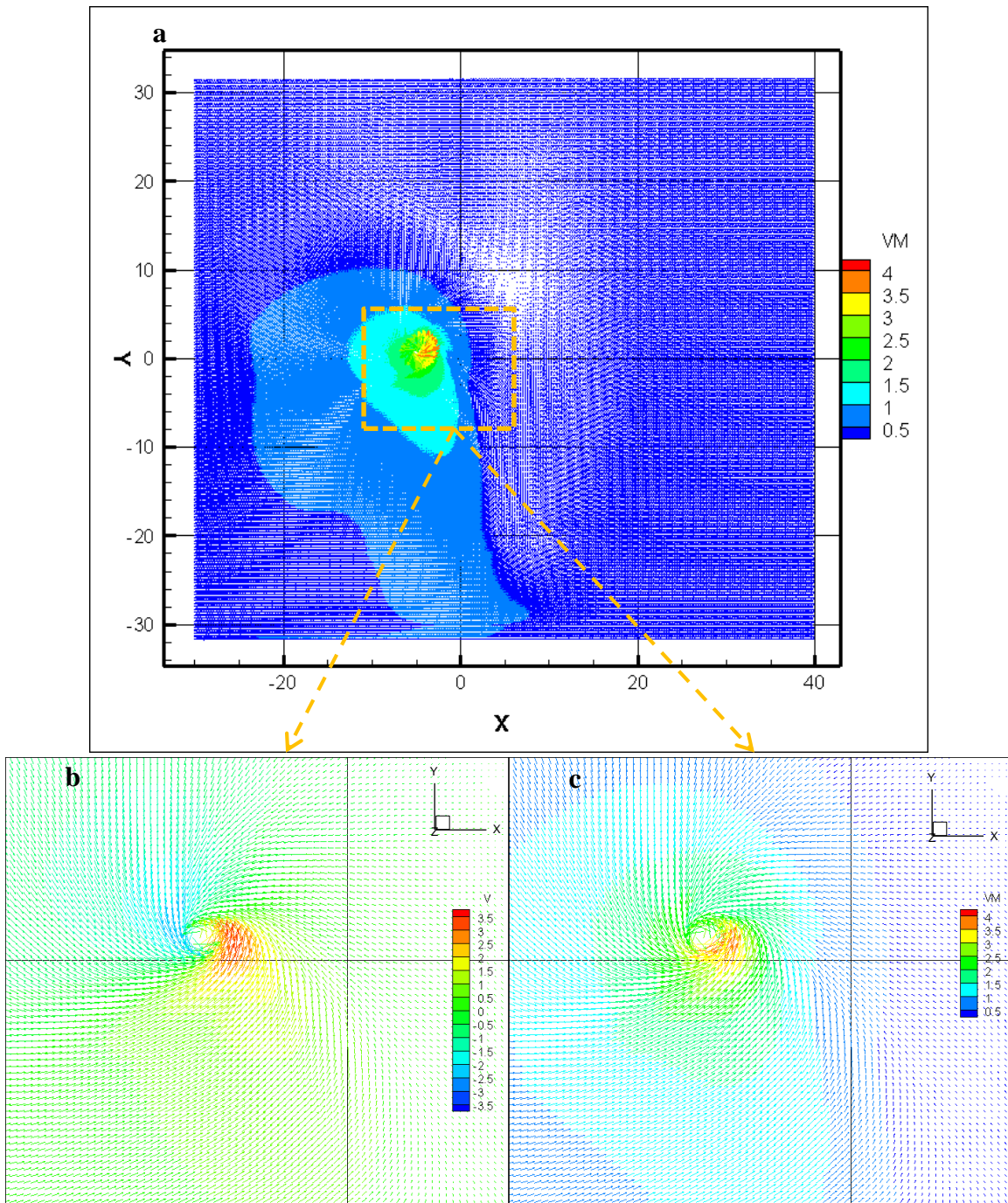
Figure 6.24 Velocity vectors while climbing up the ridge a) Velocity magnitude vector for the whole domain b) close up view for velocity vectors in y direction c) close up view for velocity magnitude vectors $(V_\Theta/V_t=6)$.
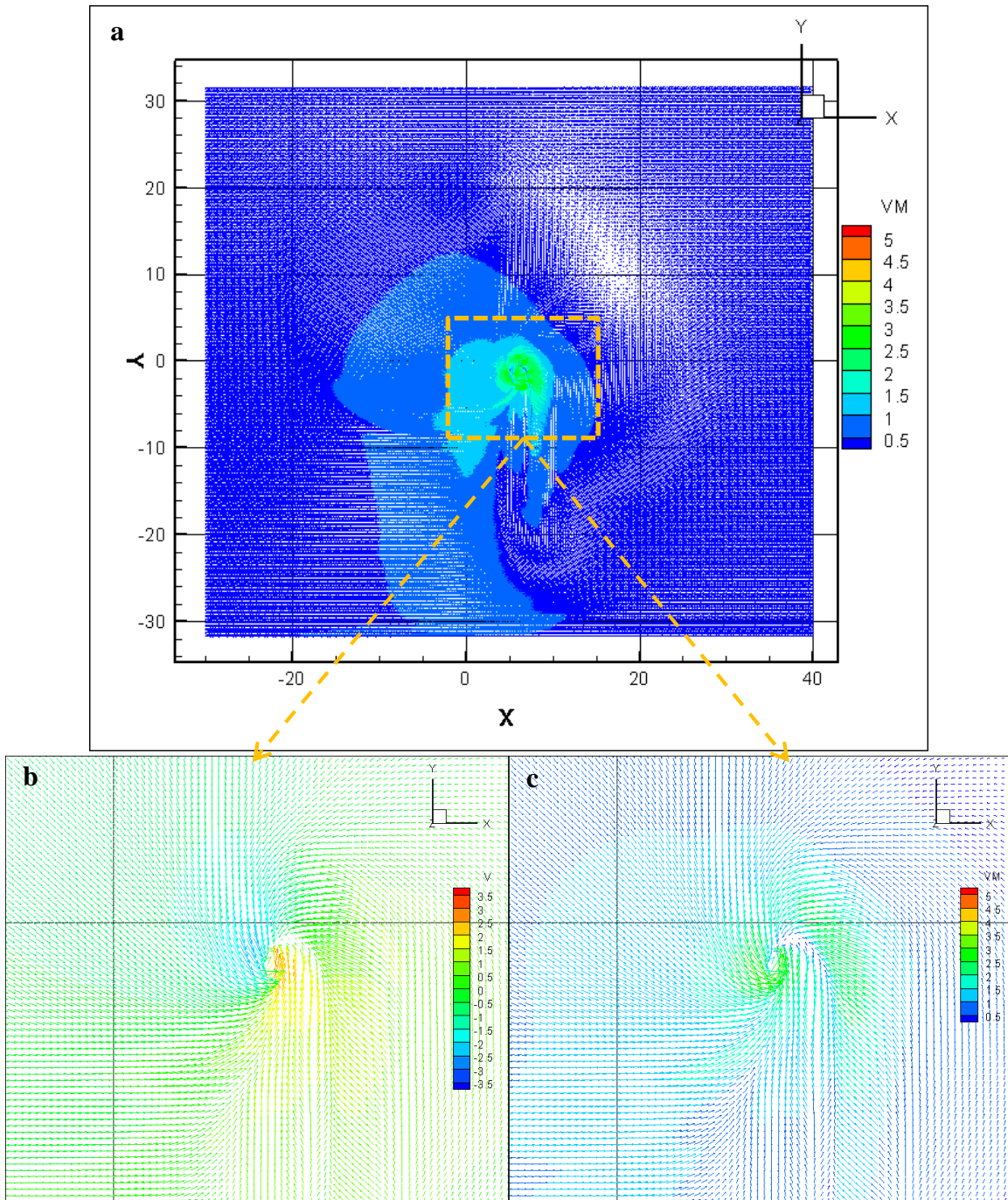
Figure 6.25 Velocity vectors while climbing down the ridge a) Velocity magnitude vector for the whole domain b) close up view for velocity vectors in y direction c) close up view for velocity magnitude vectors $(V_\Theta/V_t=6)$.

6.10. Results Summary

With the existing three different sources of data, it is shown that there is a connection between (V_Θ/V_t) ratio and tornado path deviation. First, from wind tunnel and field data (H3 on Mayflower-2014), it is shown that for higher velocity ratios, there is more deviation (single and double curvature) for similar hills. Then, from field data (H1& H2 on Tuscaloosa-2011) using Google Earth data, it is shown that there is not much deviation (no deviation almost a straight line) for low ratios for similar hills. By using the computer model, the influence of various ratios are predicted and compared. The comparison shows that as the ratio (V_Θ/V_t) increases, the path deviation shape changes from straight line to double curvature. Figure 6.26 shows different tornado paths associated with its traveling speed as reported by Fujita (1989). It shows that slow tornado, high (V_Θ/V_t) ratio, experiences path deviations while traveling. Also, it shows that fast tornadoes, low (V_Θ/V_t) ratio, move in straight lines (no deviation). However, in Fujita (1989), no attention was paid to topography effects. In all the aforementioned results, the effect of topography whose height is equal to tornado radius is considered on tornado path deviation for various (V_Θ/V_t) ratios. However, the field data show that topography height has an effect on tornado path deviation. After crossing the Arkansas River 3.5 miles south west Mayflower, the tornado travels over almost flat terrain until it hits the interstate I40 as illustrated by Figure 6.27 taken from Civil Air Patrol (CAP, 2014). The interstate I40 location and elevation is illustrated by using Google Earth as shown in Figure 6.28. As aforementioned, tornado gains energy as it travels over relatively flat terrain or water surface. Therefore, we hypothesize that tornado has high intensity before it coincides I40. However, due to low height for I40, just few meters (2 m) above the surrounding ground, it does not affect tornado path. The same behavior also noticed when the tornado with ratio (V_Θ/V_t) equal to (3) is transported over flat terrain as illustrated in

Figure 6.12. Further understanding of the influence of ridge height, ridge length along the

tornado path or the influence of the slope needs to be investigated.
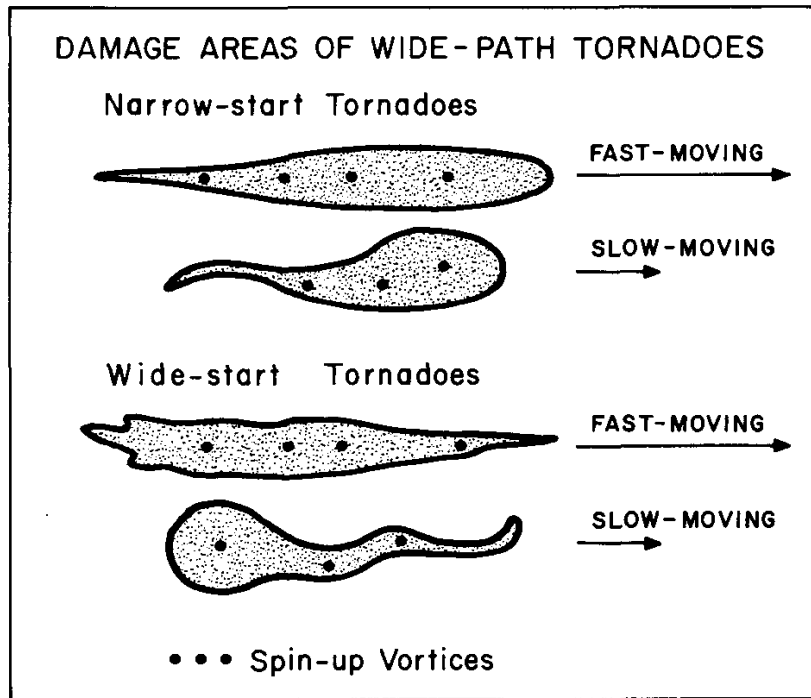
Figure 6.26 Tornado path configuration associated with its traveling speed taken from Fujita (1989).
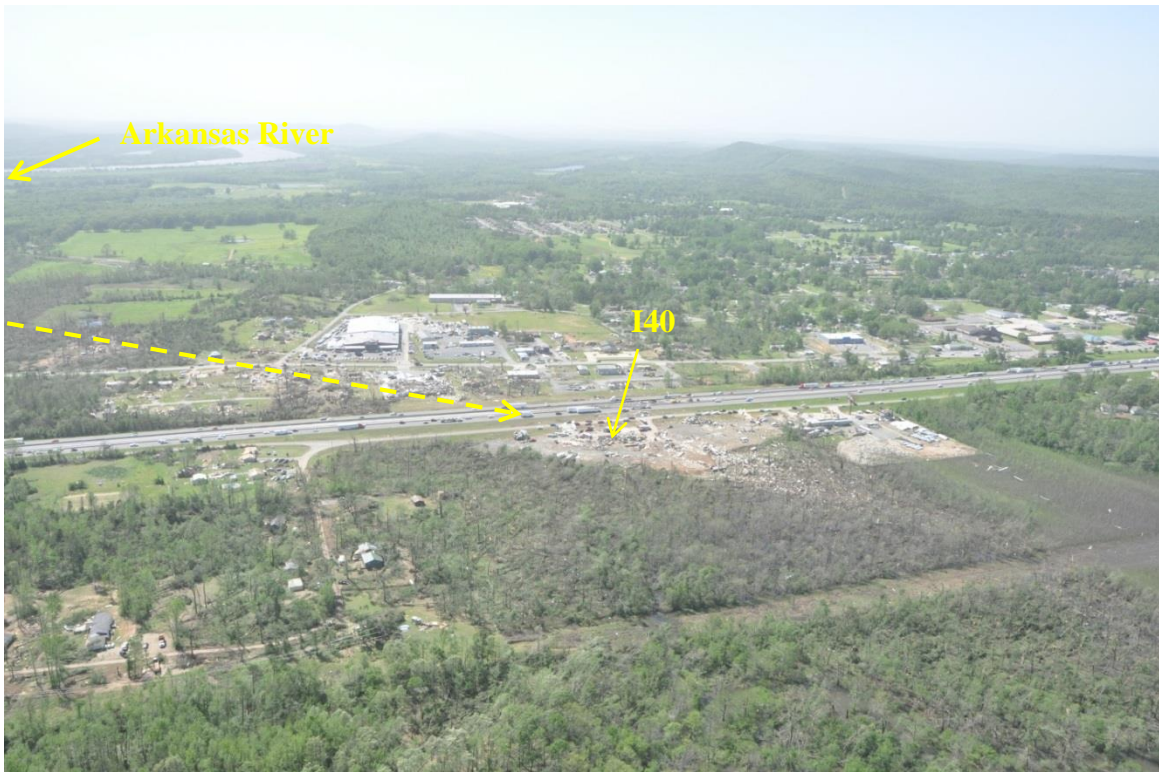
Figure 6.27 Tornado path at I40 showing no path deviation, ($V_\Theta/V_t \geq 4$, but low hill height) adopted from CAP (2014).
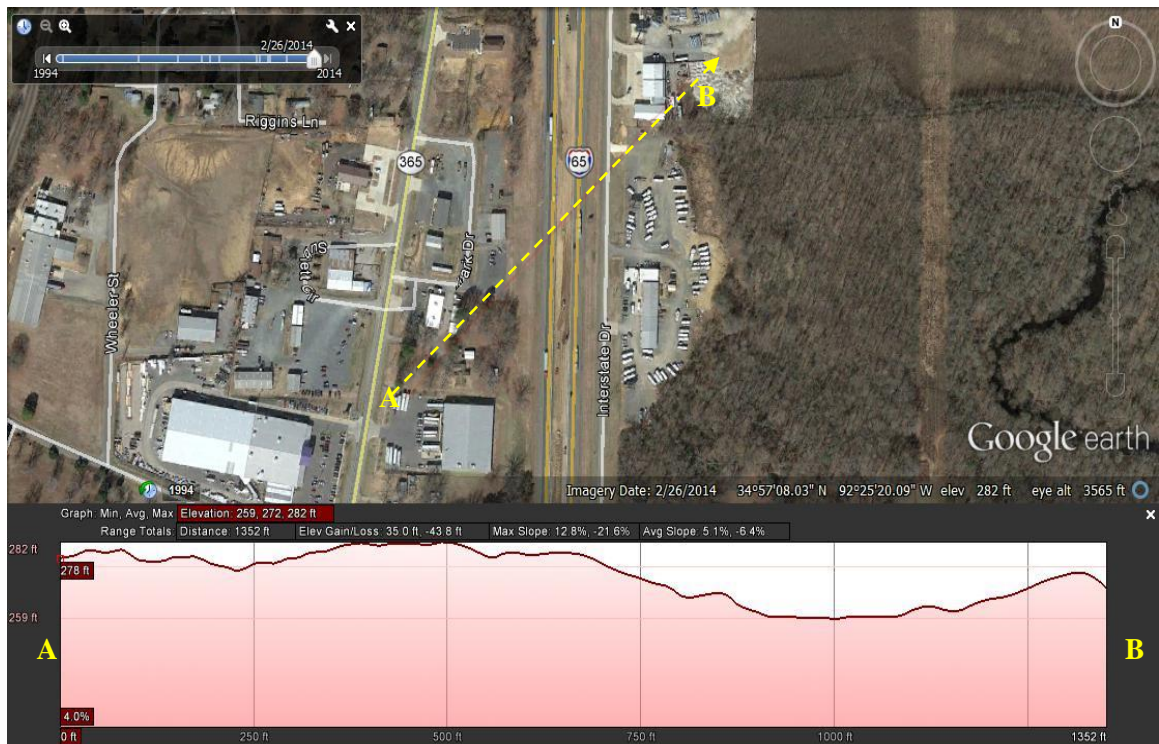
Figure 6.28 Elevation profile for line AB at interstate I40 where it is hit by the tornado.

6.11. Conclusions

The topography effect on tornado path deviation is studied using three data sources (i.e. Field Data, Wind tunnel data and Numerical simulations). The following conclusions are drawn.

- The ratio (V_θ/V_t) significantly affects the tornado deviation shape and magnitude when interacts with 2D ridge.

- The curvature changes from straight line to double curvature shape as the ratio (V_Θ/V_t) increases.

- For ratio (V_Θ/V_t) =1, the deviation shape is almost a straight line. For $2 \le$ (V_Θ/V_t) <4, the deviation shape becomes a single curvature shape. When the ratio (V_Θ/V_t) $\ge$4, the deviation shape changes to double curvature.

- For (V_Θ/V_t) <4, The UA numerical results for tornado path deviation shape are comparable to field data (single and no curvature).

- The UA Numerical results for (V_Θ/V_t) >4 are comparable to wind tunnel data (double curvature). Therefore the computer model can be considered for further investigation.

Only one topography configuration is considered in this study which is a ridge of height equal to the tornado radius. The ridge slope is 20%, and maximum considered (V_Θ/V_t) ratio is 8. More investigation for different ridge height and slopes need to be examined for better understanding of this complicated phenomenon.

134

7. Tornado Forces on a Sheltered Building

7.1. Introduction

Tornadoes are one of the major threats for life losses and economy crises in the United States. Therefore, much research has been going on in the last five decades to develop a better understanding for this complex wind. One of a great interest for researchers is tornado-structure interaction due to its impact on human's lives and economy disasters. Selvam and Millett (2003) simulated the first translating tornado interaction with a cubical building utilizing a computer model and showed that tornado forces are different than straight boundary layer wind forces of the same velocity. Since then, several developments for understanding this complex phenomenon have been achieved by Selvam group. Recently, field investigation by Selvam et al (2014 and 2015) has reported that terrain has significant effects on tornado damage (forces) and path. They reported that tornado damage ratings are less over hilly terrain, and the damage ratings are much higher over the flat regions. Gorecki and Selvam (2014 and 2015) have conducted tornado-prism interaction using CFD, and they presented that there is about 40% reduction in tornado velocities on the leeward side of the prism. From field investigation using Google Earth, Ahmed and Selvam (2015a) showed that hills provided sheltered zone on their leeward side when interacting with tornadoes. Also, they showed that houses on the leeward side of a hill close to Lake Conway experienced less damage than that on the windward side.

Tornado forces on different structures have been measured and reported by wind tunnel (Haan et al 2008 and Yang et al 2011) and by computer model (Selvam and Millet 2003 and 2005). However, terrain effects on tornado forces have never been investigated, and tornado forces on a structure sheltered by terrain have never been measured neither by wind tunnel nor by computer

models. Evaluating terrain influence on tornado forces helps to understand how terrain affects tornado destructive ability, and it also helps to determine how much the structure factor of safety against tornado forces might increase if the structure is built on the leeward side of a hill or any other terrain profiles.

In this chapter, tornado forces on a sheltered dome building are measured and compared with forces on a building directly exposed to tornado. Two terrain profiles (a rounded hill and a triangular hill) are considered to demonstrate terrain effects on tornado forces applied on a sheltered building. The objective of this chapter is to determine the terrain effects on tornado forces applied on a sheltered dome building. First, tornado forces on a dome building located on the leeward side of the terrain (a rounded hill or a triangular hill) are measured. Then, hills sheltering ability are evaluated by comparing the measured forces on the sheltered building with those on a non-sheltered building. Next, the sheltering ability for two different terrain profiles with four different heights is determined. Finally, the sheltered zone length and the influence of the building location far away from the hill on its leeward side are evaluated.

7.2. Computer Model

The computer model utilized by Ahmed and Selvam (2015b) is modified to account for tornado interaction with multi-structures. Using terrain following grid system gives a great advancement to our computer model to introduce several structures in the numerical domain. A grid generation program is developed to generate different terrain profiles as shown in Figure 7.1 a and b. Tornado-like vortex wind profile is modeled by implementing Rankine Combined Vortex Model (RCVM) which satisfies the Navier Stokes equations (NSEs) as reported by Lewellen (1976). As represented by the RCVM, the tangential velocity of a tornado-like vortex

(V_θ) increases linearly up to the vortex radius R_{max}, where R is the distance from the vortex center. When R is larger than R_{max}, the tangential velocity decreases exponentially. RCVM represents two regions: the forced vortex region ($R<R_{max}$) and the free vortex region ($R>R_{max}$). Selvam (1985) was the first one who introduced RCVM for the tornado-structure interaction problems. The turbulence is modeled using Large Eddy Simulation (LES). Finite Elements Method (FEM) is used to approximate the NSEs. Then the approximated equations are solved using a semi-implicit method as explained in Selvam (1997). The computer model was validated by comparing tornado path deviation due to interaction with terrain with both wind tunnel and field observation results as presented by Ahmed and Selvam (2015b).
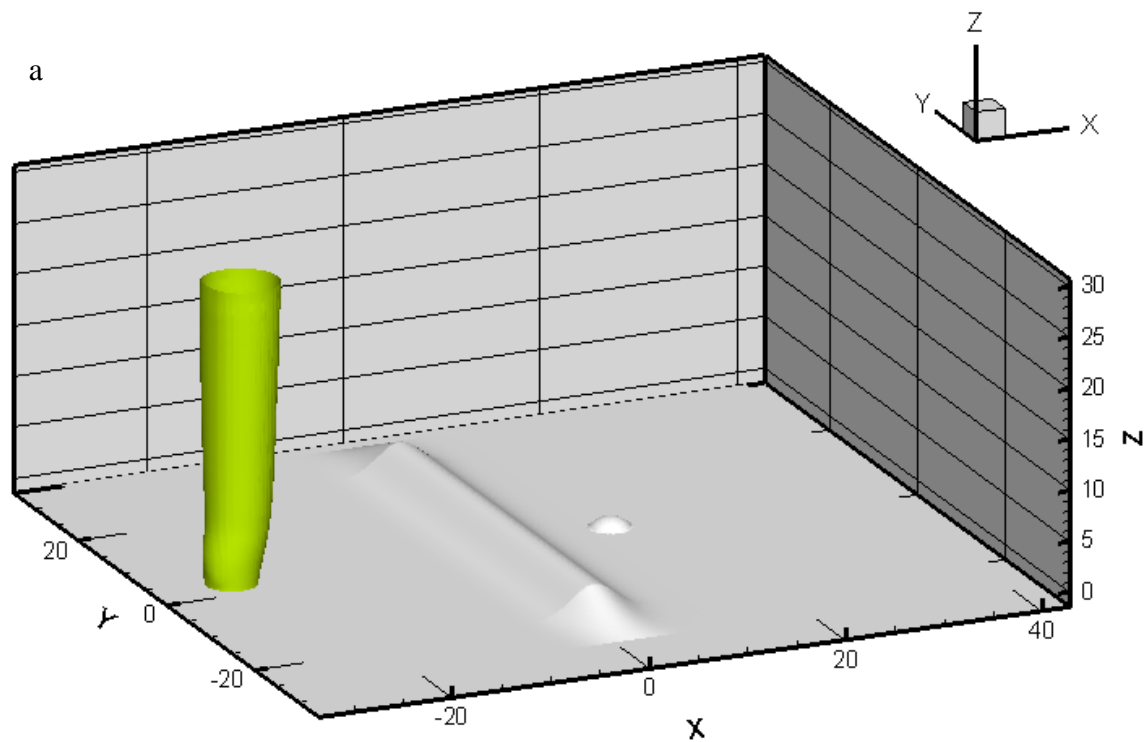
b
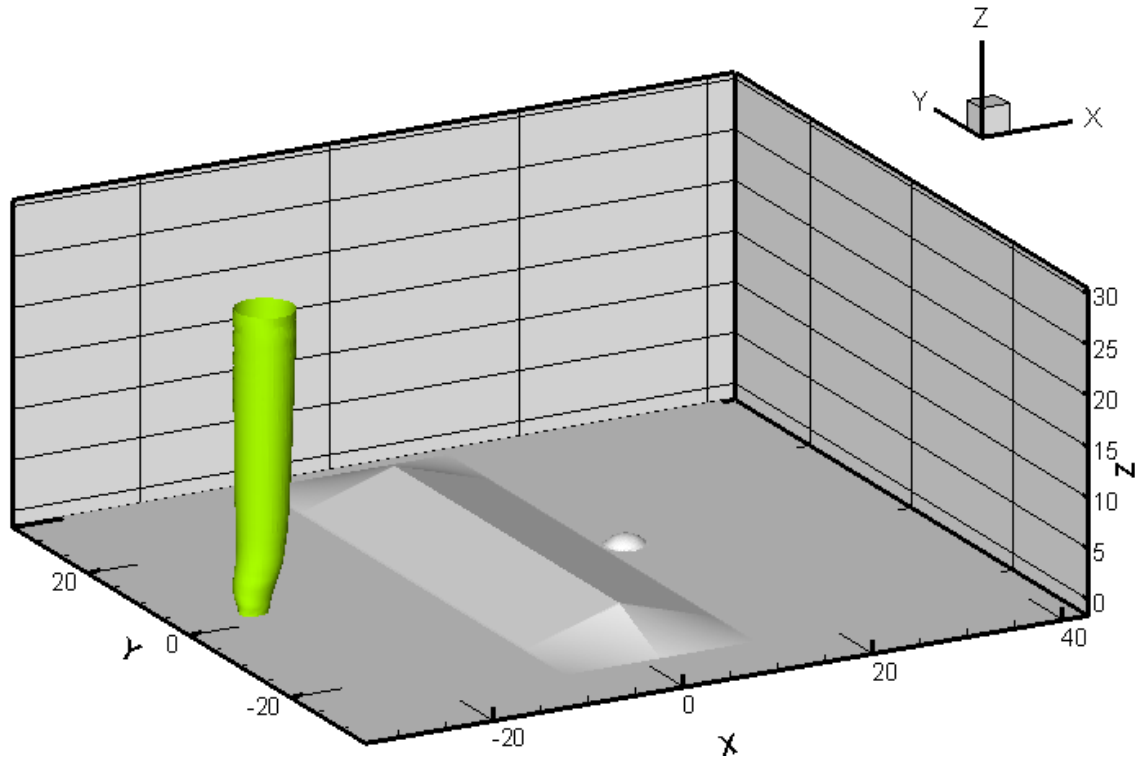
Figure 7.1 a) A building on the leeward side of a rounded hill b) A building on the leeward side of a triangular hill.

7.3. Problem Geometry

The tornado-like vortex wind velocity field is considered by implementing Rankine Combined Vortex Model (RCVM). Three main parameters are used to specify the characteristics of the tornado. These parameters are: α is a rotational constant (the vortex strength), R_{max} is the tornado radius where the maximum tangential velocity occurs and V_{trans} is the tornado translational velocity. The tornado-like vortex is advanced, along x-axis, with the free stream flow. The translational velocity of the tornado is equal to the free stream velocity. Tornado-like vortex dimensional and non-dimensional parameters are demonstrated in Table 7.1. Where V_θ is the tornado-like vortex tangential velocity, and $V_{\theta max}=\alpha \cdot R_{max}$ and $V_{max} = V_{\theta max}+V_{trans}$.

Table 7.1 Dimensional and non-dimensional parameters.

UNITS	α	R_{max}	U_{tran}	$U_{\theta,max}$	U_{max}
DIMENSIONLESS	1.5	2.0	1.0	3.0	4.0
SI	1.5 (s-1)	31.3m	15.65 ms-1	46.95 ms-1	62.6 ms-1
U.S.	1.5 (s-1)	102.65 ft.	35 mph	105 mph	140 mph

The simulated tornado-like vortex is translated along x-axis with a translational velocity, V_{trans}, of 1.0 unit (15.65 m s-1). When the simulation starts, the tornado-like vortex is introduced away from the computational domain and then it slowly enters into the computational domain. When the tornado-like vortex is far away from the terrain, only the free stream flow is present in the computational domain. The total computational time of the simulation is 90 time units. The schematic illustration for tornado-like vortex interaction with multi-structures is shown in Figure 7.2 a and b. The tornado-like vortex first interacts with the terrain then with the building on the leeward side of the terrain. In all the simulations, the tornado-like vortex radius is held fixed and equal twice the building height ($R_{max}=2xh$). Where h is the building height. The hill height and the building location are varied as explained in the results section. Forces on the sheltered dome building are measured and reported for different cases as discussed later.
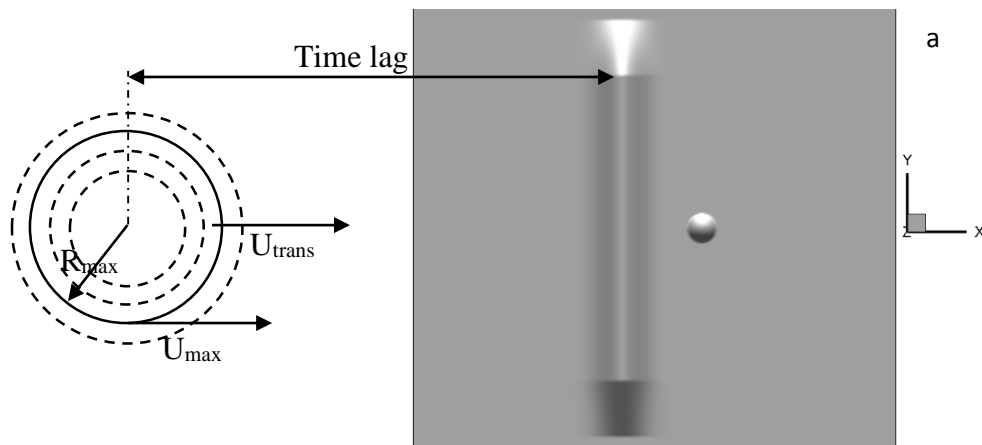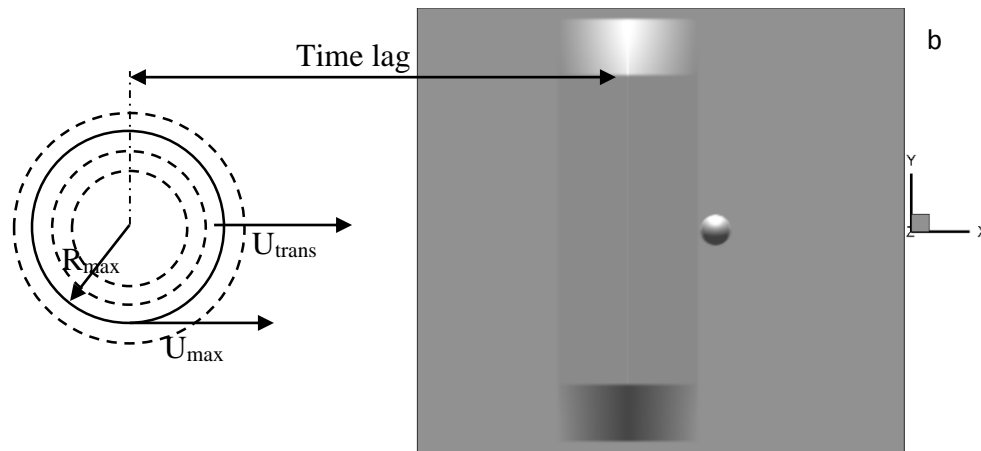
Figure 7.2 problem geometry for tornado-terrain interaction a) a dome building on a leeward side of a rounded hill b) a dome building on a leeward side of a triangular hill.

7.4. Results and Discussion

7.4.1. Forces on a dome building exposed directly to the tornado-like vortex wind (no sheltering)

For evaluating whether terrain provides sheltering on its leeward side, first tornado-like vortex forces on a reference building need to be measured. A dome building is selected since it suits the terrain following coordinate system. As aforementioned, the dome building dimensions are selected to have the building height equals half the tornado-like vortex radius and the width equals twice the tornado-like vortex radius as shown in Figure7.3. Recommendations from Gorecki and Selvam (2014 & 2015) for numerical domain size are considered here. For side boundaries, they recommended that side boundaries need to be placed at least about nine times the tornado-like vortex radius ($9R_{max}$). For top boundary, it is recommended to be at least about $15R_{mas}$ from the domain bottom to sustain the tornado-like vortex strength. The numerical domain used in the present study is shown in Figure 7.4. R_{max} is equal to two uints ($R_{max}=2$). Three different heights ($7.5R_{max}$, $15R_{max}$, $22.5R_{max}$) are explored to verify the recommended numerical domain height. The same grid B explained in chapter six is used here. Figure 7.5 (a, b

and c) illustrates tornado-like vortex forces on the dome building in X, Y and Z directions

respectively. From Figure 7.5 (a, b and c), it is shown that the influence of the upper boundary on

the tornado-like vortex strength is negligible when height of the upper boundary is greater than

15R_{max}. Therefore, the upper boundary height is kept 15R_{max} for the rest of the simulations. The

forces calculation is done by assuming the tornado maximum velocity as a reference velocity.

Table 7.2 presents the maximum measured forces on the dome building due to direct exposure to

tornado-like vortex wind (not-sheltered).
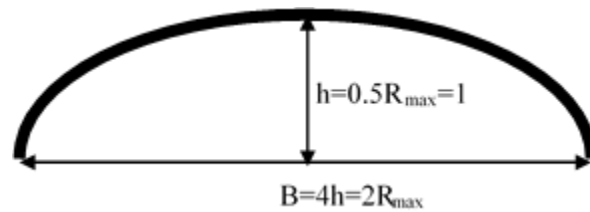
Figure 7.3 Shape of the structure on the leeward side of the
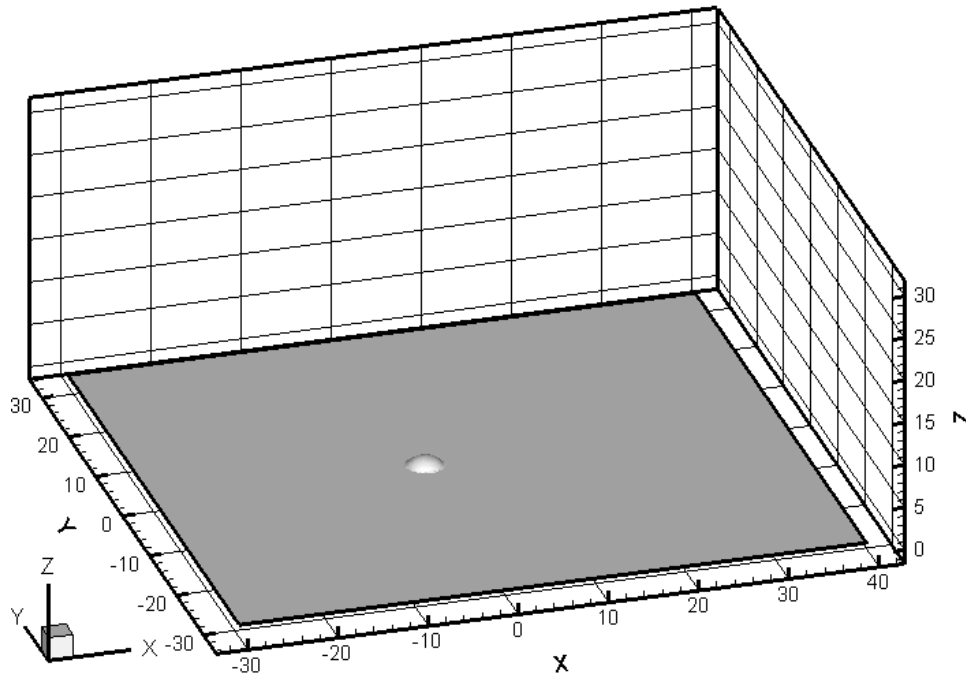
Figure 7.4 Numerical domain size used in the present study.

141
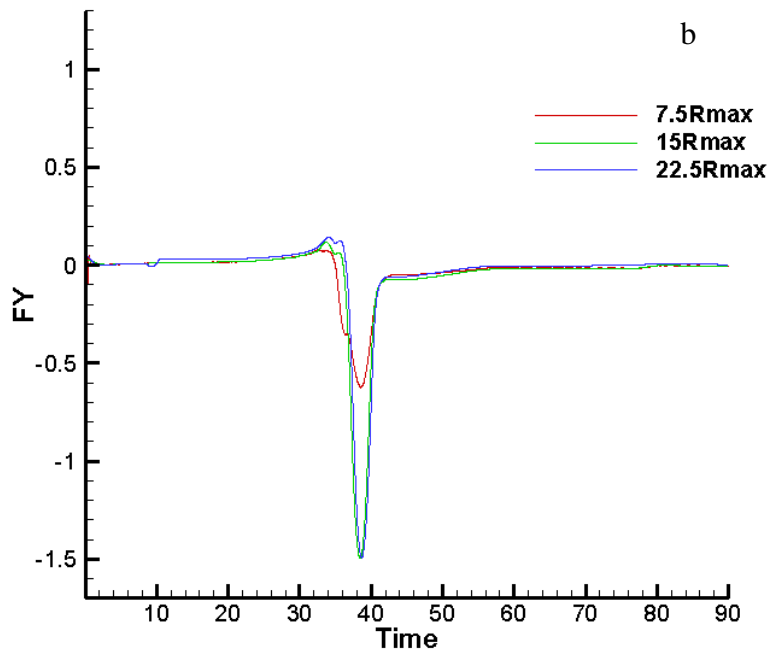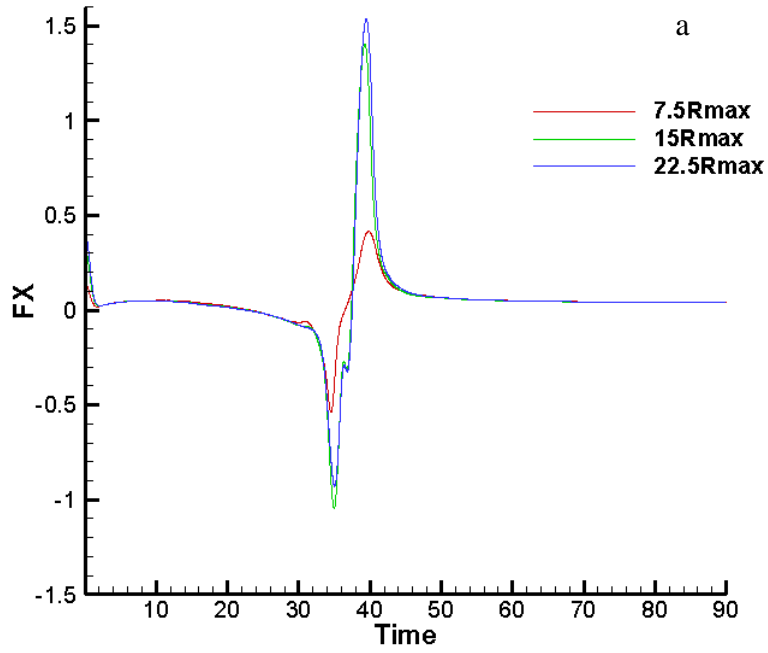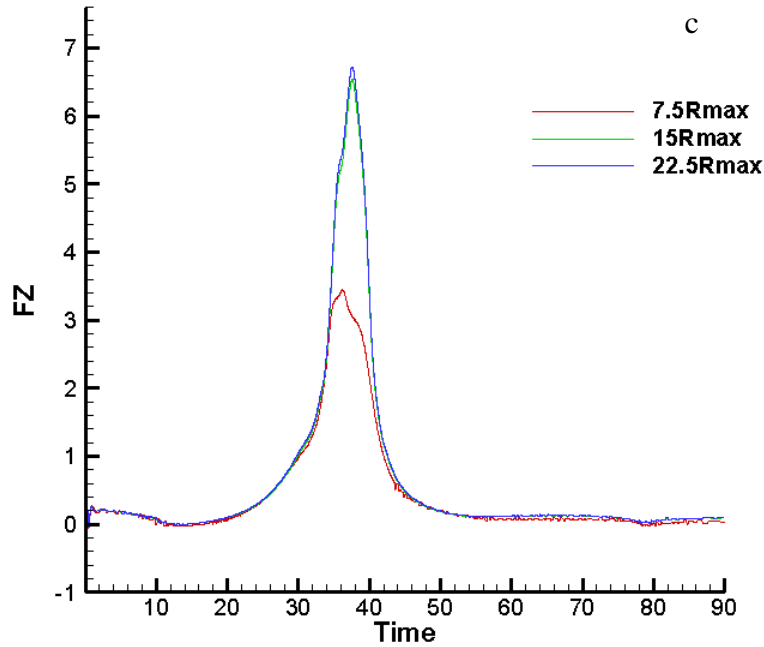
Figure 7.5 Tornado forces on a non-sheltered dome building a) X direction b) Y direction c) Z direction.

Table 7.2 Tornado-like vortex forces on a non-sheltered dome building.

Structure Type	FX+	FX-	FY+	FY-	FZ+
A dome building (non-sheltered)	1.42	1.1	0.12	1.52	6.53

7.4.2. Tornado-like vortex forces on a dome building sheltered by a rounded hill

Tornado-like vortex forces on a dome building sheltered by a rounded hill (see Figure 7.6 a) are measured and compared with those of the non-sheltered building. The same reference building shown in Figure 7.3 is considered. Tornado-like vortex parameters and numerical domain size are kept the same as aforementioned. The hill width is held fixed and equal 30Rmax. The hill length along tornado-like vortex traveling path (X-axis) is also kept unchanged and equal 10Rmax (see Figure 7.6 b). The hill height is varied from twice the building height up to

five times the building height. For the different hill heights, sheltering ability for the rounded hill is evaluated by measuring tornado-like vortex forces on the reference building and comparing it with the non-sheltered case. The building is kept at distance equals six times tornado-like vortex radius (6Rmax) on the leeward side of the rounded hill as shown in Figure 7.6 b. The height of the rounded hill is ranged from two times the building height (H2) to five times the building height (H5). Results of tornado-like vortex forces exerted on the dome building when sheltered and non-sheltered are summarized in Table 7.3 and Figure 7.7 (a, b and c). Figure 7.7 (a, b and c) presents tornado-like vortex forces on the reference building when sheltered and non-sheltered in X-axis, Y-axis and Z-axis respectively. Reduction in these forces is calculated as shown in Table 7.3. As observed from field investigation by Ahmed and Selvam (2015a), there is huge reduction in tornado-like vortex forces on the leeward side of the hill. The reduction ranges from almost 50% to 99%. These results show that terrain has a great influence on tornado-like vortex wind velocities as shown in Figure 7.8 and then on tornado-like vortex forces. The same method used and explained by Gorecki and Selvam (2014) to create the compacted slice for maximum velocity reduction is considered here.
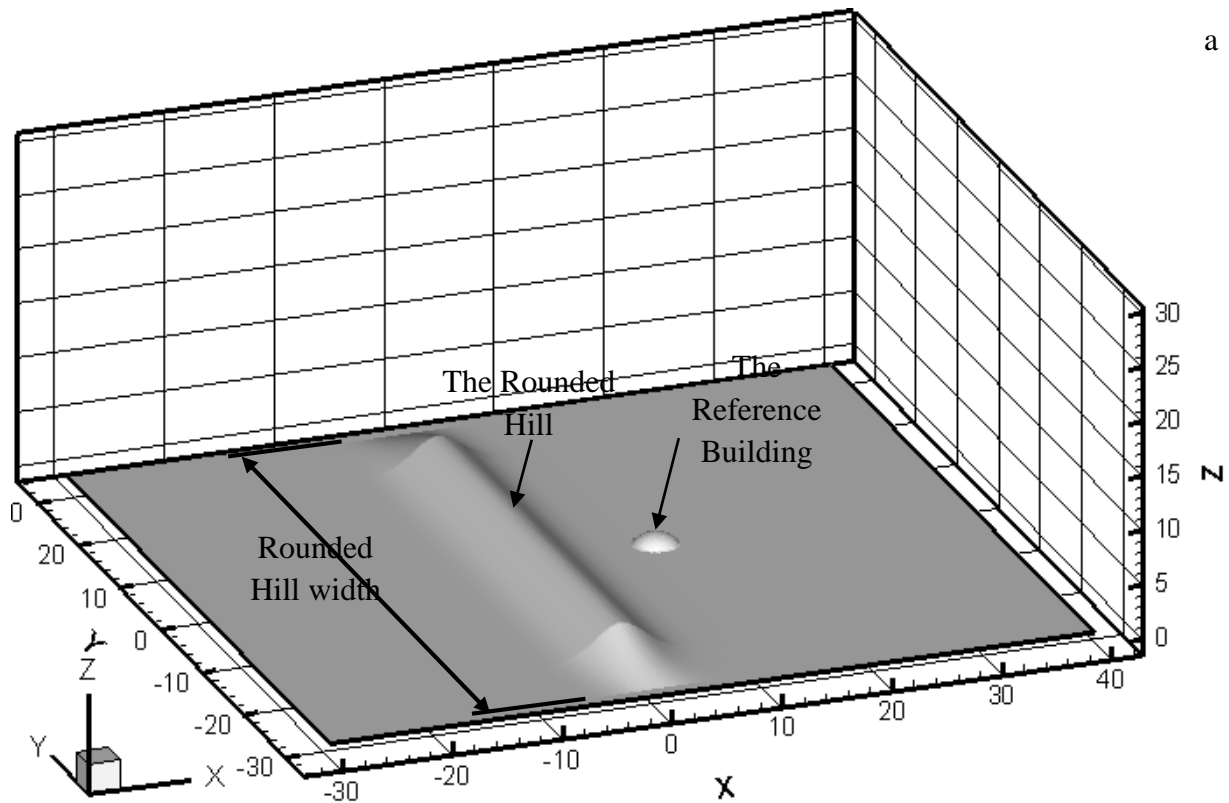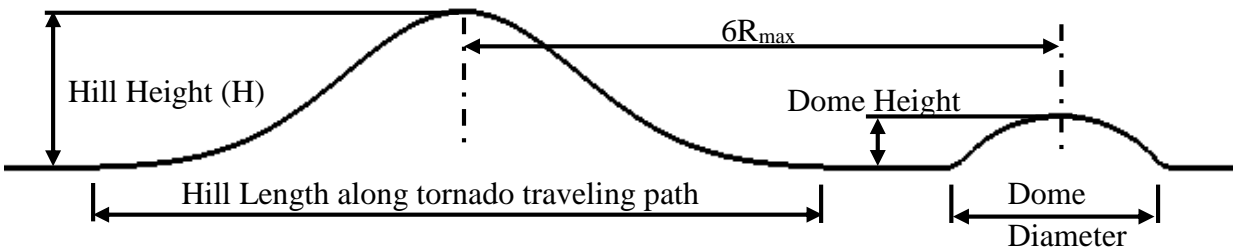
Figure 7.6 Terrain and building parameters a) 3D view b) 2D schematic view.

Table 7.3 Tornado-like vortex forces on a sheltered dome building by a rounded hill.

Structure Type	FX+	FX-	FY+	FY-	FZ+
A dome building (non-sheltered)	1.42	1.1	0.12	1.52	6.53
H2	0.13	0.30	0.06	0.14	1.88
H3	0.10	0.32	0.06	0.15	1.66
H4	0.08	0.32	0.06	0.18	1.60
H5	0.01	0.32	0.06	0.12	1.48
Max reduction	99%	72%	50%	92%	77%
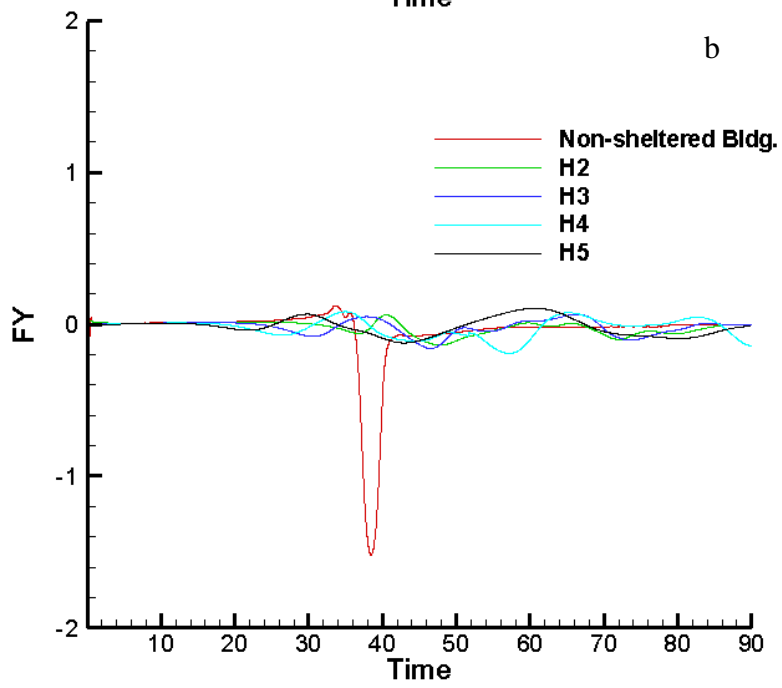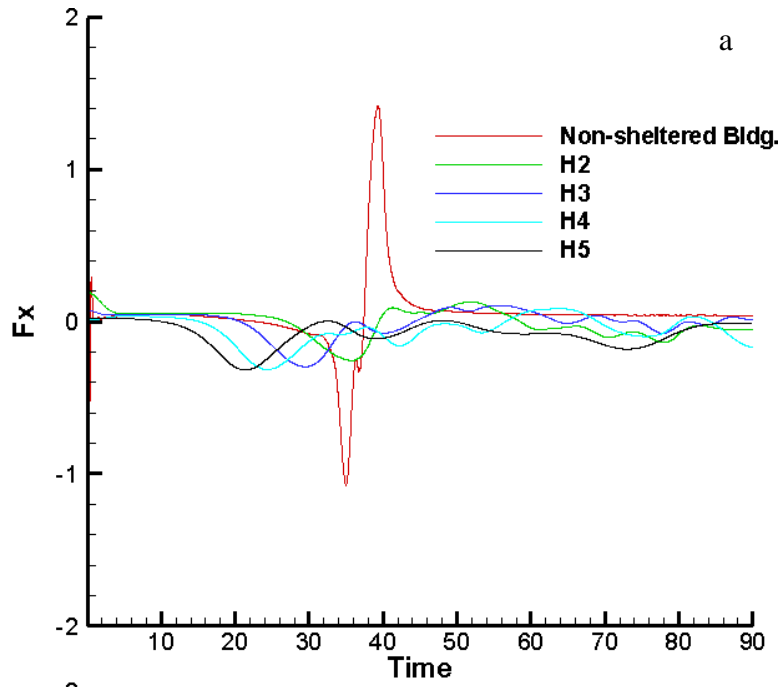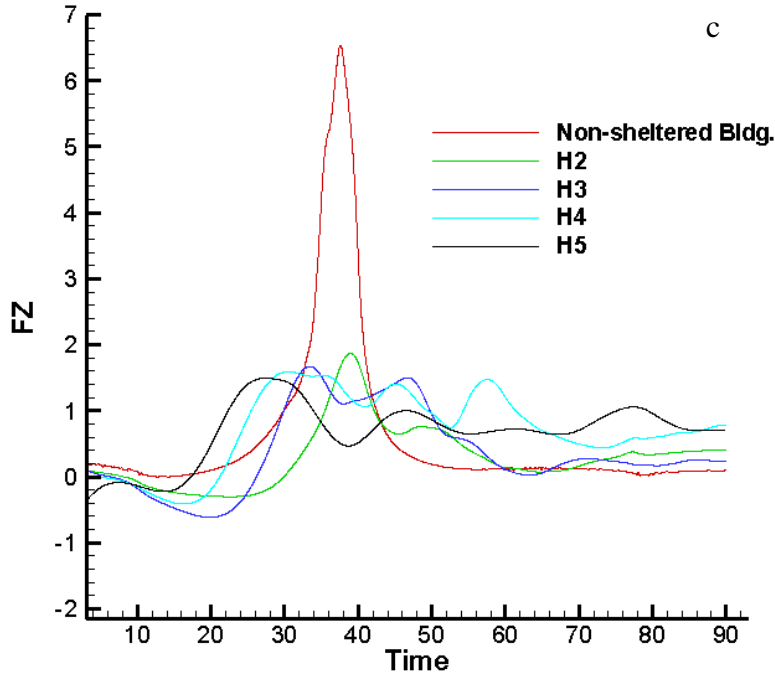
Figure 7.7 Tornado-like vortex forces on a sheltered dome building by a rounded hill a) X direction b) Y direction c) Z direction.
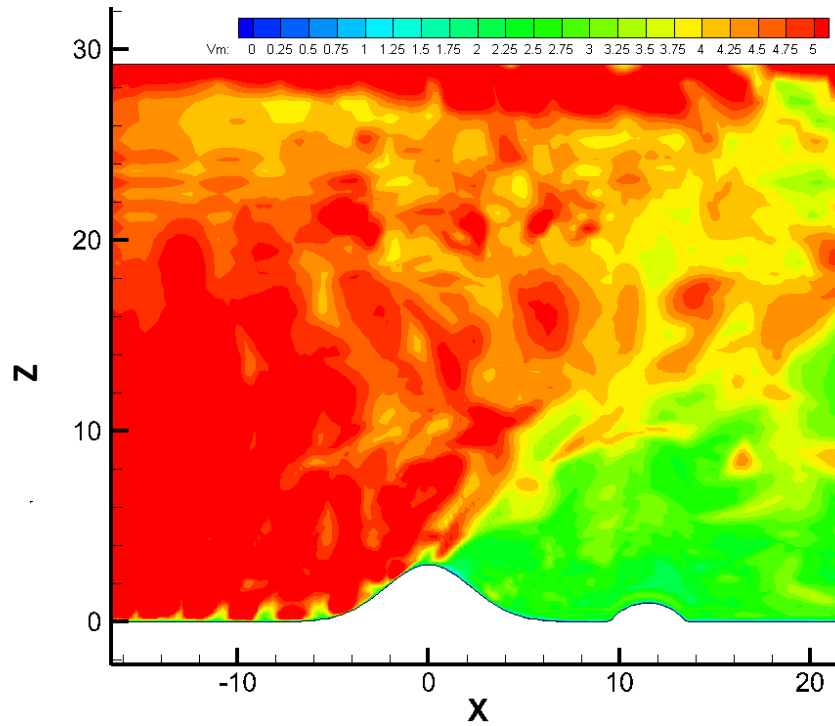
Figure 7.8 Reduction in tornado-like vortex maximum velocity when interacting with a rounded hill.

7.4.3. Tornado-like vortex forces on a dome building sheltered by a Triangular Hill

In this section, the sheltering hill profile is selected to be a triangular hill as shown in Figure 7.9 (a and b). Tornado-like vortex forces are measured on a dome building sheltered by the triangular hill. Then, the measured forces are compared with those excreted on the non-sheltered reference building. Tornado-like vortex parameters and numerical domain size are kept the same as that used in the previous simulations for the rounded hill. The hill width is held fixed and equal 30Rmax. The hill length along tornado-like vortex traveling path (X-axis) is also kept unchanged and equal 10Rmax (see Figure 7.9 b). The hill height is varied from twice the building height up to five times the building height. For the different hill heights, sheltering ability for the hill is evaluated by the same procedure utilized for the rounded hill. The building is kept at distance equals six times tornado-like vortex radius (6Rmax) on the leeward side of the hill as shown in Figure 7.9 b. The height of the hill is ranged from two times the building height (H2) to five times the building height (H5). Tornado-like vortex forces exerted on the dome building when sheltered and non-sheltered are illustrated in Figure 7.10 (a, b and c) and summarized in Table 7.4. Figure 7.10 (a, b and c) show tornado-like vortex forces on the building in X, Y and Z directions respectively. Reduction in these forces is calculated as shown in Table 7.4. The reduction ranges from almost 70% to 100%. These results show that terrain has significant influence on tornado-like vortex wind velocities as shown in Figure 7.11 and then on tornado-like vortex forces. When comparing results for both the rounded hill and the triangular hill sheltering abilities as presented in Tables 7.3 and 7.4, the comparison shows that both the rounded hill and the triangular hill provide great sheltering. However, there are slight differences: the rounded hill provides better sheltering for positive forces in X direction, and less sheltering for the negative ones. In the Y direction, the triangular is in the lead for the positive

forces, while both the rounded hill and the triangular hill have provided almost the same sheltering for the negative forces. Also, both of them have provided the same level of sheltering against the forces in Z direction.
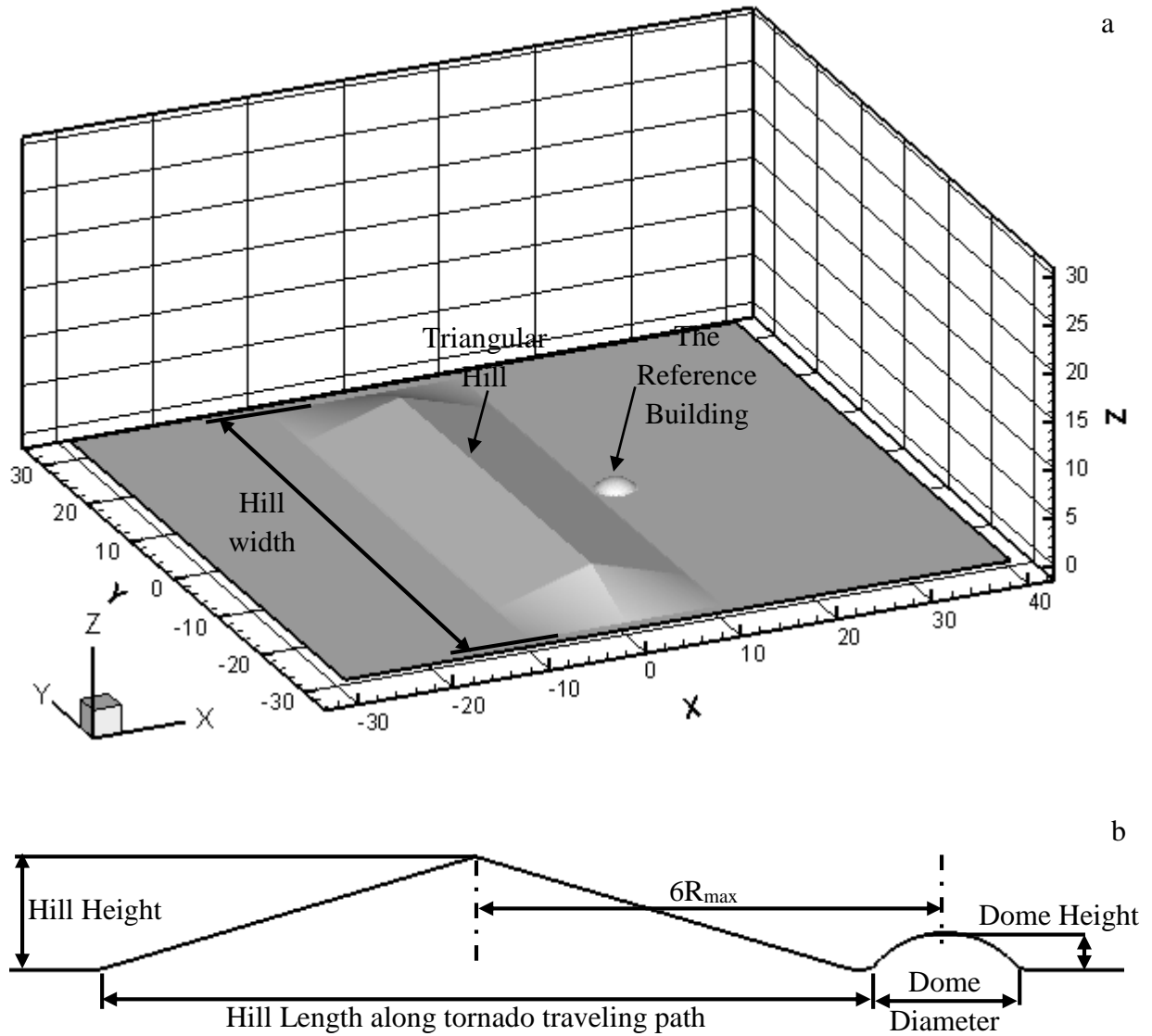
Figure 7.9 Triangular hill and building parameters a) 3D view b) 2D schematic view.

Table 7.4 Tornado-like vortex forces on a sheltered dome building by a hill.

Structure Type	FX+	FX-	FY+	FY-	FZ+
A dome building (non sheltered)	1.42	1.1	0.12	1.52	6.53
H2	0.18	0.23	0.05	0.32	2.44
H3	0.13	0.18	0.05	0.20	1.5
H4	0.09	0.18	0.05	0.19	1.3
H5	0.01	0.18	0.04	0.17	1.4
Max reduction	99%	84%	67%	89%	79%
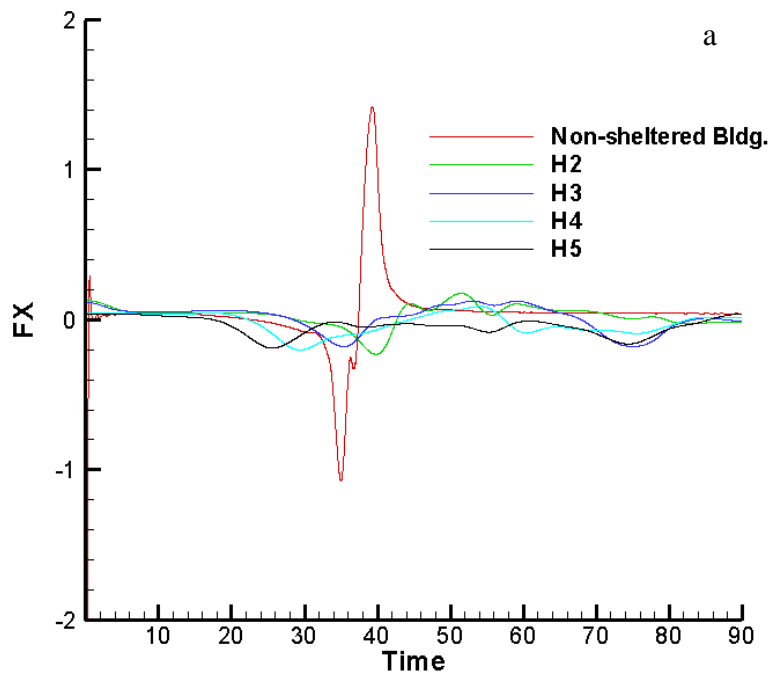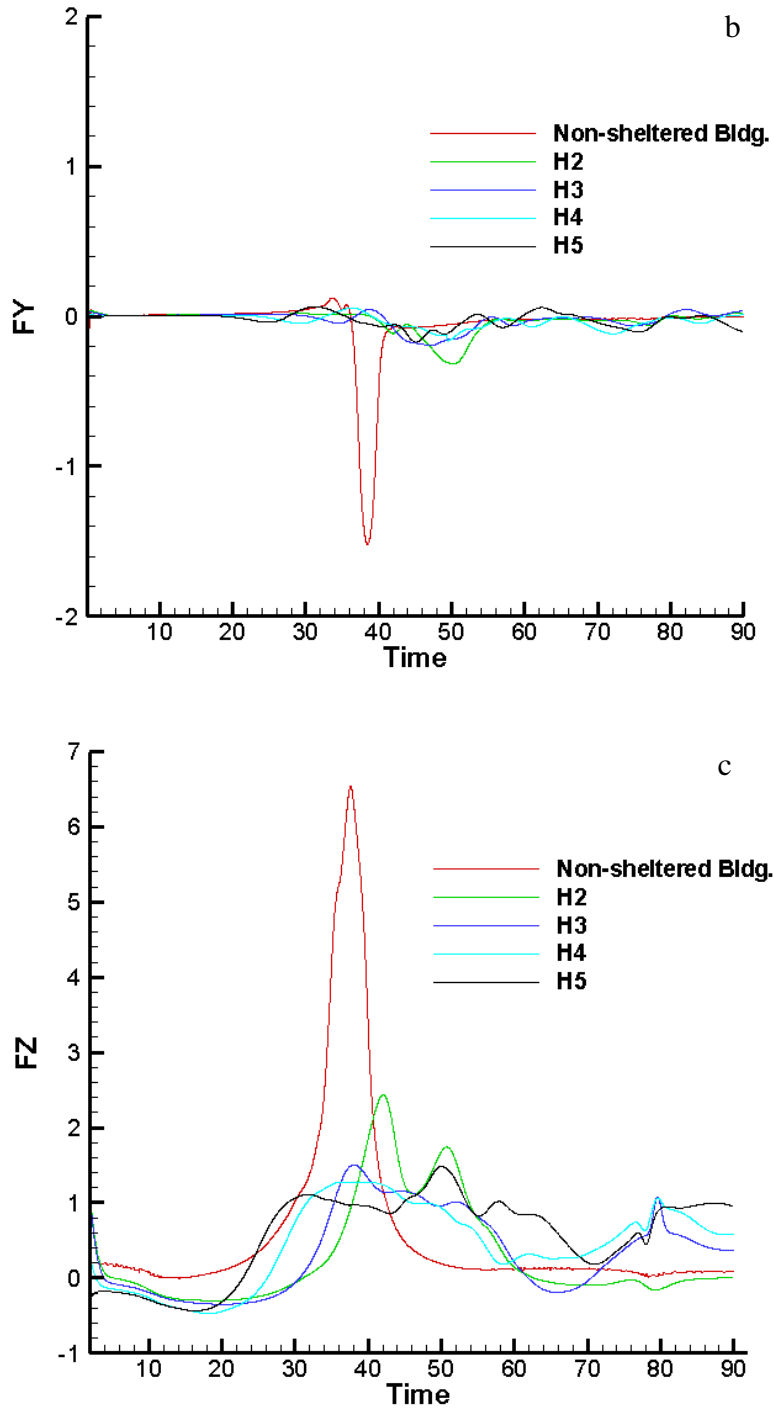
Figure 7.10 Tornado-like vortex forces on a sheltered dome building by a triangular hill a) X direction b) Y direction c) Z direction.
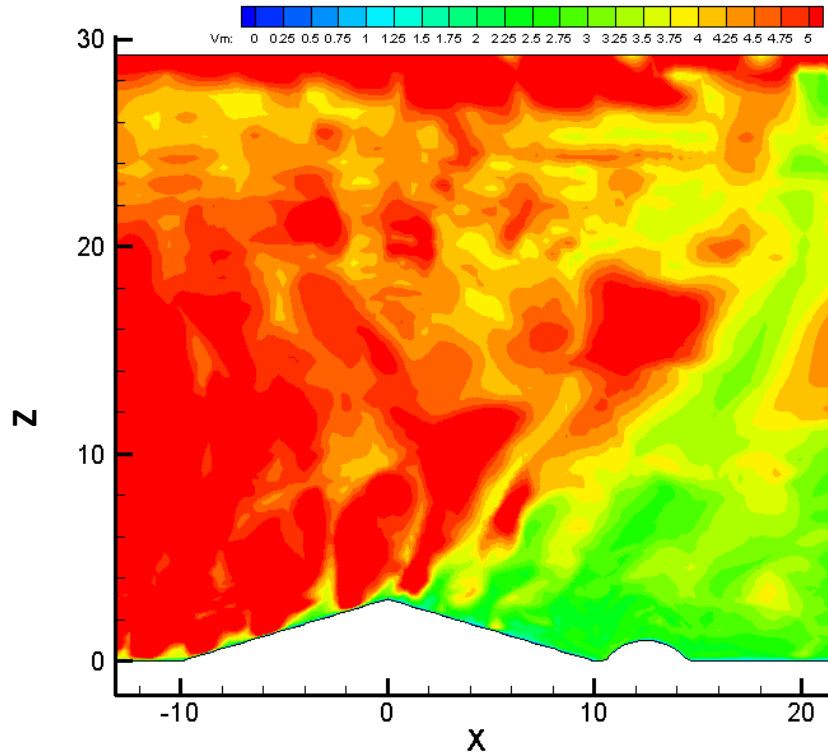
Figure 7.11Reduction in tornado-like vortex maximum velocity when interacting with a rectangular hill.

7.4.4. Effects of building location on the tornado-like vortex forces.

Both the rounded hill and the triangular hill are examined to evaluate sheltering abilities at different locations on the leeward side. The building is placed at three different distances (six times the hill height (6H, 8H and 10H). Height of the terrain profiles (H) is considered to be two times the building height, and forces are measured on the dome building sheltered by the terrain. Figure 7.12-14 (a and b) Show tornado-like vortex forces on a building sheltered by a rounded hill (a) and a triangular hill (b) in X, Y and Z directions respectively . Also, these forces are summarized in Table 7.5 for the building sheltered by a rounded hill and in Table 7.6 for the building sheltered by a triangular hill. One can see from these results in both the Figures and the tables that the rounded hill provided longer sheltered zone on its leeward side than that provided

by the triangular hill. In the x direction, the building has experienced forces (FX+) increment by

70% when it is moved from 6H to 10H on the leeward side of a rounded hill, whereas these

forces increment is 320% when the building is moved from 6H to 10H on the leeward side of the

triangular hill (see Figure 7.12 a and b). In the Y direction, when the building is moved far away

from the rounded hill (6H to 10H), the forces (FY-) has increased by 79%, while it has magnified

by 150% for the triangular hill sheltering. There is no forces increasing in the Z direction when

the building place is shifted from 6H to 10H on the leeward side of the rounded hill as shown in

Figure 7.14 a. For the triangular hill case, the forces increment in Z direction is about 45% as

shown in Figure 7.14 b. Results of maximum velocity reduction are of great agreement with the

measured forces on the building as shown in Figures 7.15 (a and b) and Figure 7.16 (a and b).

Also, the Figures show that the rounded hill provides better sheltering and longer sheltered zone

than the triangular hill of the same height. From Figure 7.15 b, one can see that the sheltered

zone on the leeward side of the rounded hill extends to 10H in the X direction and 2H (the

rounded hill height) in the Z direction with reduction in maximum velocity ranges from 40% to

80%. For the triangular hill (see Figure 7.16 b), the sheltered zone is up to 6H in X direction and

1H in the Z direction. It is anticipated that the sharp change in the rounded hill slope has great

effects on providing better sheltering.

Table 7.5 Tornado-like vortex forces on a building at different locations on the leeward side of a rounded hill.

Bldg. location	FX+	FX-	FY+	FY-	FZ+
6H	0.13	0.3	0.06	0.14	1.88
8H	0.17	0.3	0.04	0.18	1.88
10H	0.22	0.3	0.03	0.25	1.88
Maximum force increment	70%	0%	-50%	79%	0%

Table 7.6 Tornado-like vortex forces on a building at different locations on the leeward side of a triangular hill.

Bldg. location	FX+	FX-	FY+	FY-	FZ+
6H	0.18	0.23	0.05	0.32	2.44
8H	0.41	0.25	0.05	0.56	2.4
10H	0.75	0.20	0.05	0.80	3.5
Maximum force increment	316%	-15%	0%	150%	43%
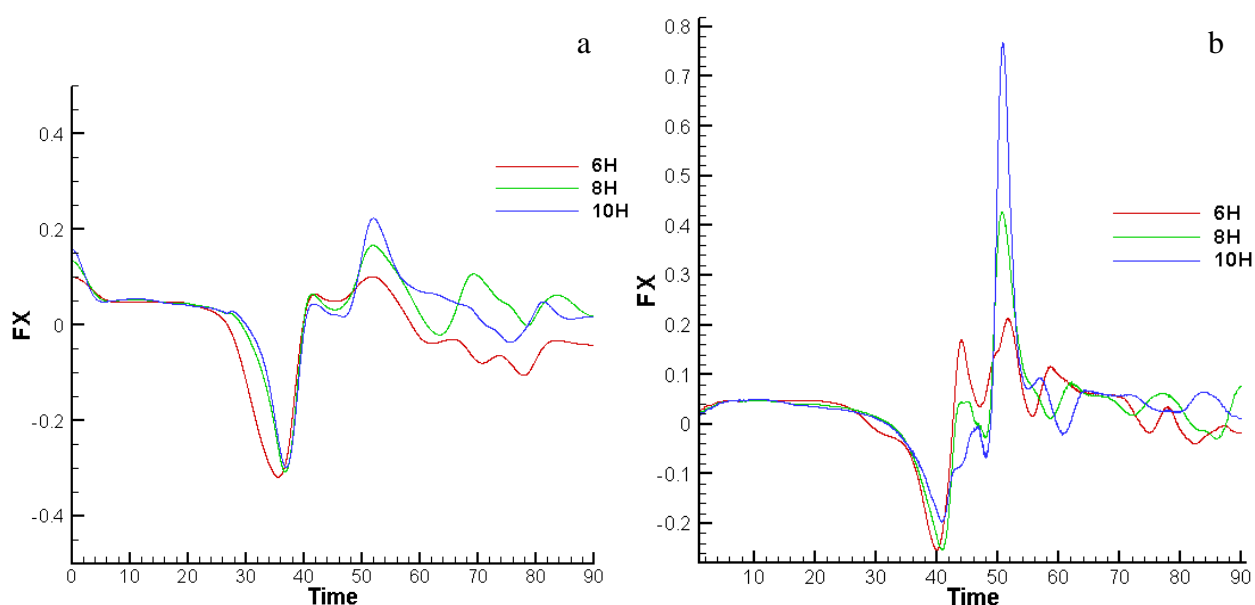
Figure 7.12 Tornado-like vortex forces in the X direction a) a rounded hill b) a triangular hill

a   b
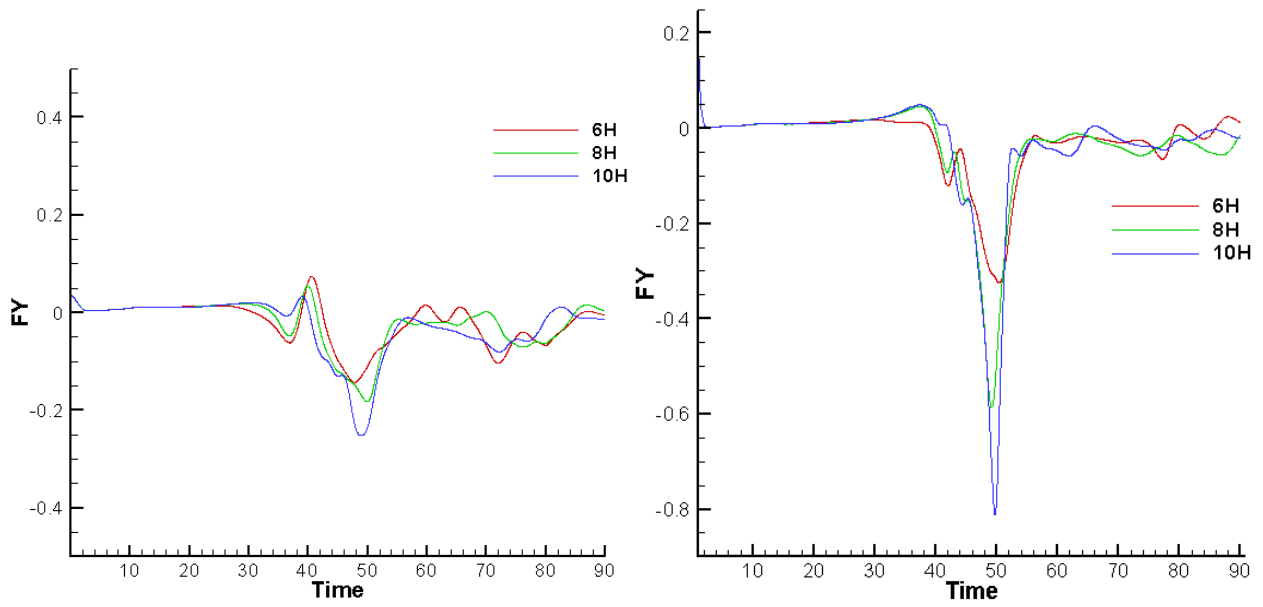
Figure 7.13 Tornado-like vortex forces in the Y direction a) a rounded hill b) a triangular hill
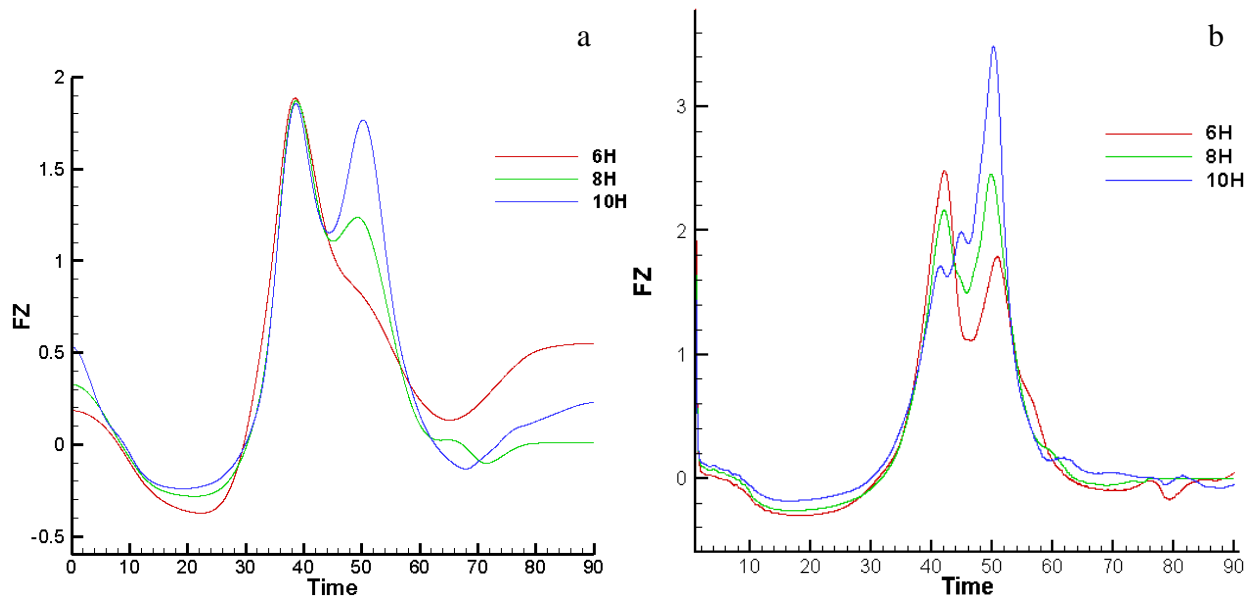
Figure 7.14 Tornado-like vortex forces in the Z direction a) a rounded hill b) a triangular hill
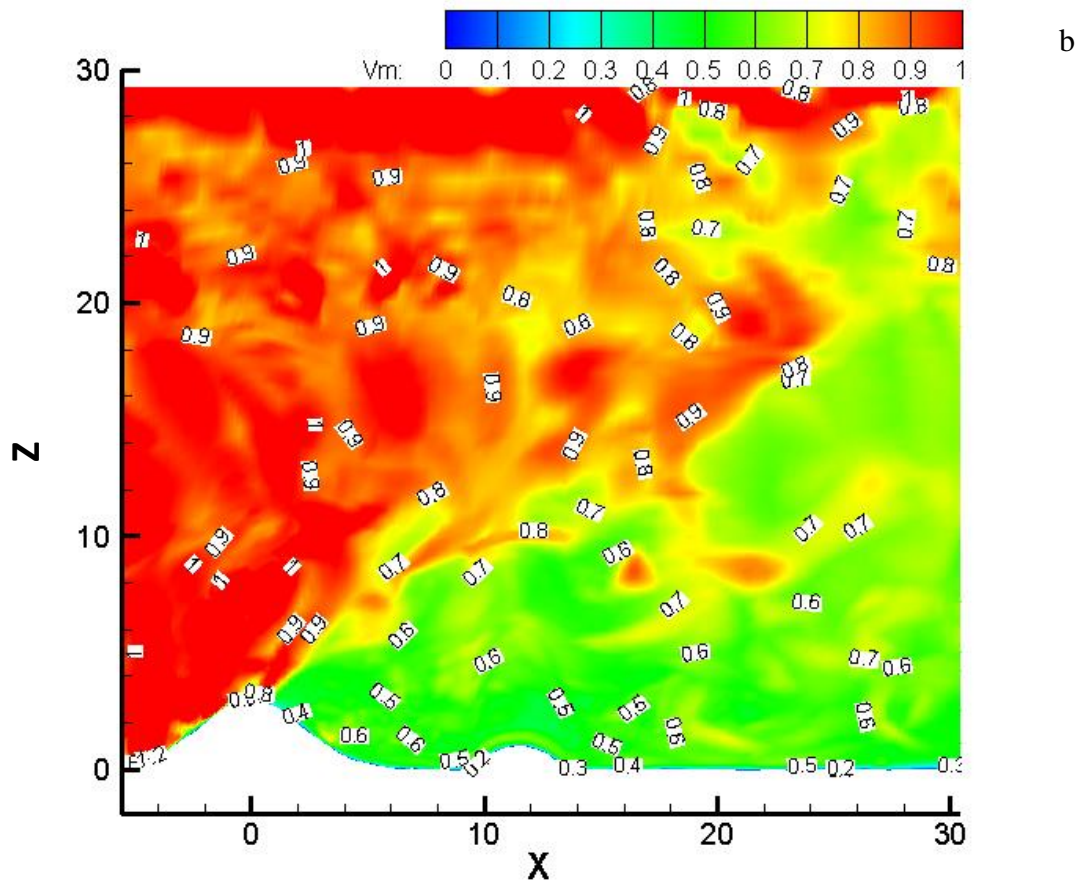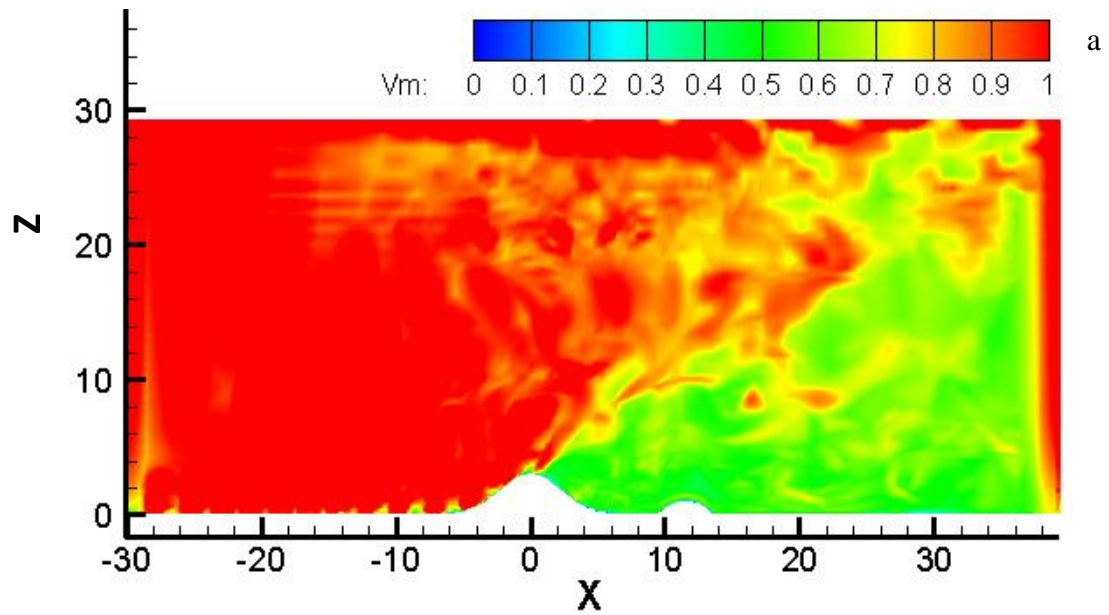
Figure 7.15 Reduction in tornado-like vortex maximum normalized velocity when interacting with a rounded hill a) consolidated 2D view b) close-up view.
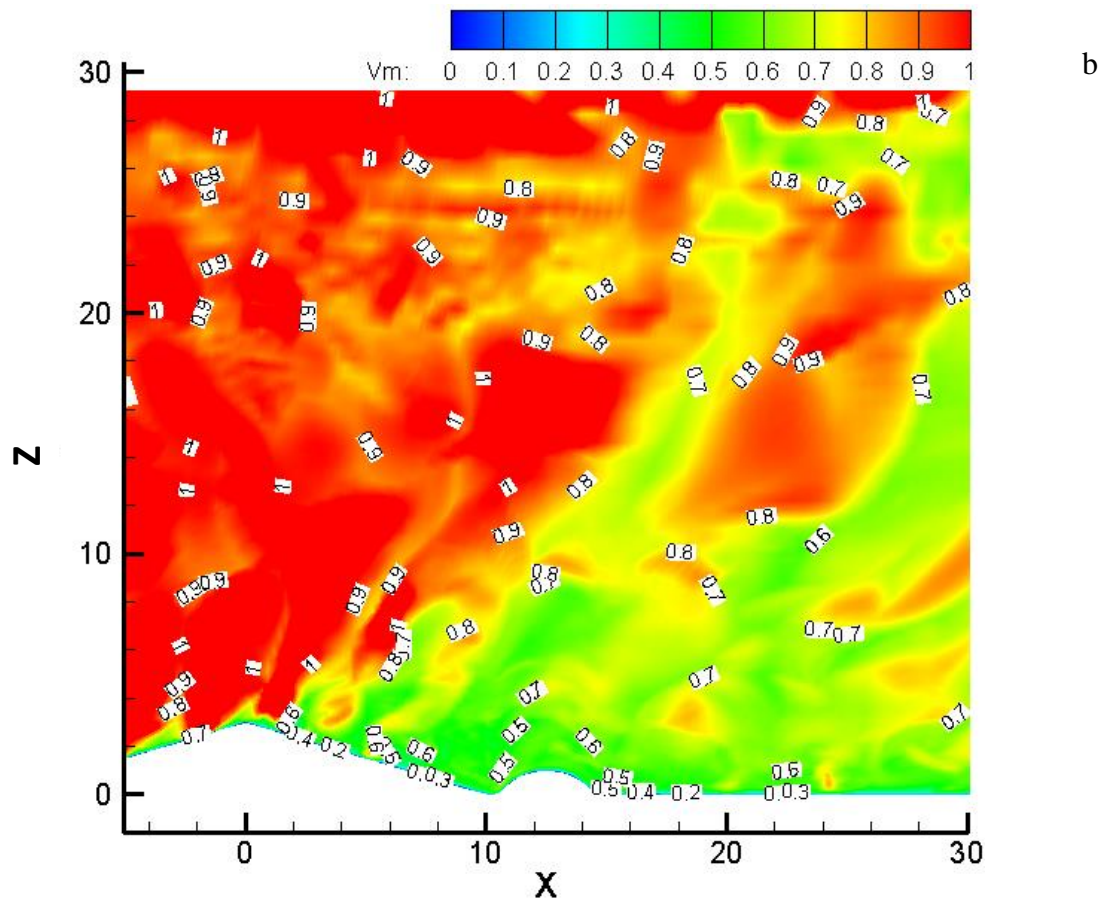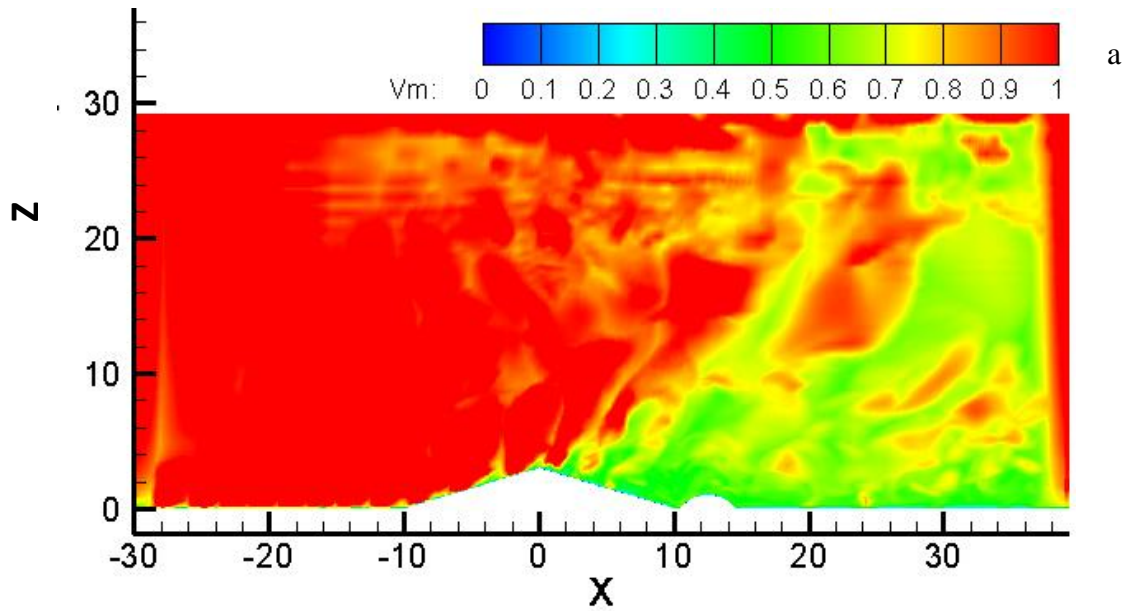
Figure 7.16 Reduction in tornado-like vortex maximum normalized velocity when interacting with a triangular hill a) consolidated 2D view b) close-up view.

7.5. Conclusion

Tornado-like vortex-terrain interaction is simulated using a computer model. Two different terrain profiles are considered with varied heights. Tornado-like vortex forces are measured on a dome building placed at different distances on the leeward side of the terrain. From results comparison and analysis, the following conclusions are arrived.

- The Terrain obstacles reduce tornado-like vortex forces and velocities on the leeward side of the terrain.

- Both the rounded hill and the triangular hill can be considered as good shelters for structures on their leeward side.

- Tornado-like vortex forces applied on a structure are reduced by more than 70% when the structure is located within six times the hill height on the leeward side of a rounded hill or a triangular hill.

- The sheltering ability for both the rounded hill and the triangular hill is increased by 25% when their heights is increased from H2 (twice the building height) to H5 (five time the building height).

- The rounded hill provide better sheltering and longer sheltered zone than the triangular hill.

- The sheltered zone on the leeward side of the rounded hill extends to 10H in the X direction and 1H (the hill height) in the Z direction with reduction in maximum velocity ranges from 40% to 80%.

- For the triangular hill, the sheltered zone is up to 6H in X direction and 1H in the Z direction with reduction in maximum velocity ranges from 40% to 60%.

8. Summary and Conclusions

8.1. Summary of the Conducted Work

In this work, a field investigation through field survey and utilizing the software Google Earth is conducted to evaluate terrain influence on tornado damage and path. Also, a CFD computer model is used to simulate tornado-like vortex over a real-terrain data. Tornado-like vortex path deviation due to interaction with terrain is investigated and validated in a qualitative sense with wind tunnel results. Also, tornado-like vortex forces on a sheltered dome building are computed. The conclusions arrived from the conducted work are listed next.

8.2. Conclusions

Google Earth is employed to investigate hills effects on tornado damage. The difference in damage between hill's sides (windward and leeward) is evaluated for several hills at the location of Parish-2011 tornado. It is observed that there is significant effects of hills on tornado damage. Much damage is observed on windward side of a hill comparing to its leeward side. When the tornado crosses the investigated hills, the hills provide sheltered zone on their leeward side. The measurements for the sheltered zone on the leeward side of the investigated hills show that the sheltered zone length is about five times the hill height (5H). Another tornado (Tuscaloosa-2011) is investigated for hills effects on tornado damage. It is observed that when a tornado hit a place surrounded by hills and the distance between the hills along the tornado path is less than or equals the tornado radius, the damage is noticed only on the top of the surrounding hills and the region surrounded by the hills is completely protected. Also, from site investigation for Mayflower-2014 tornado it has been shown that the tornado damage observed uphill on the

windward side is higher than the damage observed downhill on the leeward side for the same hill hit by the tornado.

Terrain effects on tornado damage intensity are investigated at Mayflower-2014 tornado location. Site investigation, Google Terrain Maps and Google Earth are employed to explore terrain influence on tornado damage intensity. It is quantified that the presence of hilly terrain influences tornado damage intensity, and Damage intensity is observed to be less when the tornado travels over a hilly terrain. Also, Damage intensity increases when tornado travels over a flat terrain. In additions, Topography influences the path of the tornado. The tornado finds the least resistance path (gap in a ridgeline) as for as possible in passing a hill.

CFD is utilized to develop a computer model for tornado-terrain interaction. The tornado-like vortex is translated along X-axis of the numerical domain, and the tornado-like vortex pressure on the ground of the numerical domain is monitored. Different ratios of rotational to translational velocities (V_θ/V_t) are studied. It is concluded that the ratio (V_θ/V_t) significantly affects the tornado-like vortex path deviation shape and magnitude when interacts with 2D ridge (rounded hill). The deviation shape changes as the ratio value increases. The deviation curvature shape changes from straight line to double curvature shape as the ratio (V_Θ/V_t) increases. For ratio (V_Θ/V_t) =1, the deviation shape is almost a straight line (no deviation). For $2 \leq (V_\theta/V_t) < 4$, the deviation shape becomes a single curvature shape. When the ratio (V_Θ/V_t) ≥ 4, the deviation shape changes to double curvature. The results show qualitative agreement with both field investigation data and wind tunnel data. For (V_Θ/V_t) <4, the UA numerical results for tornado-like vortex path deviation shape are comparable to field data (single and no curvature). The UA Numerical results for (V_Θ/V_t) >4 are comparable to wind tunnel data (double curvature). Therefore the computer model can be considered for further investigation.

160

Finally, tornado-terrain interaction is simulated using a computer model to measure tornado-like vortex forces on a sheltered structure on the leeward side of the terrain profile. Two different hill profiles are considered with varied heights, and it is concluded that the terrain obstacles reduce tornado-like vortex forces and velocities on the leeward side of the hills. Also, both rounded hill and triangular hill can be considered as good shelters for structures on their leeward side. A fascinating outcome is that tornado-like vortex forces applied on a structure are reduced by more than 70% when the structure is located within six times the hill height on the leeward side of a rounded hill or a triangular hill. If the hill height is increased from H2 (two times the building height) to H5 (five times the building height), the tornado forces on the sheltered building are reduced by 25% or more for both investigated hills. The rounded hill provides better sheltering and longer sheltered zone than the triangular hill because of the steep slope of the rounded hill. The sheltered zone on the leeward side of the rounded hill extends to 10H (ten times the hill height) in the X direction and 1H (the hill height) in the Z direction with more than 70% reduction in tornado forces. For the triangular hill, the sheltered zone is up to 6H in X direction and 1H in the Z direction with more than 70% reduction in tornado forces.

8.3. Recommendations for Future Study

There are still many interesting and important ideas that are developed during the conduction of the study but did not explored due to time limit. Therefore, this section addresses most of the recommended research areas by the author based on this study and its conclusions.

- There are still many uninvestigated tornadoes need to be explored utilizing the great features of Google Earth and looking for tornado-terrain integration hidden facts.

- Tornado deviation due interaction with terrain is explored in this study considering a ridge (rounded hill) profile with a fixed height, so different terrain heights as well as terrain profiles effects on tornado deviation need to be explored in details.

- Tornado forces are measured on a sheltered dome building with a fixed tornado parameters. First, the ratio of tornado tangential velocity to translational velocity (V_Θ/V_t) influence on tornado forces applied on the sheltered structure need to be investigated. Also, the influence of the ratio of tornado radius to the dome building height has not explored. Similarly, the ratio of tornado radius to hill height is another important factor needs to have its effects determined.

- Tornado forces are only measured when tornado approach the hill with zero angle of attack. The angle of attack influence on hills sheltering needs to be investigated.

- Tornado forces on a building completely surrounded by hills as shown in the Figure 8.1 is not measured and need to be done. Then, the results can be compared with field data for Tuscaloosa-2011 tornado.

- Tornado forces on building right in the center of a ridgeline gap on the leeward side as shown in Figure 8.2 is one of the most interesting ideas and need to be explored and determined.
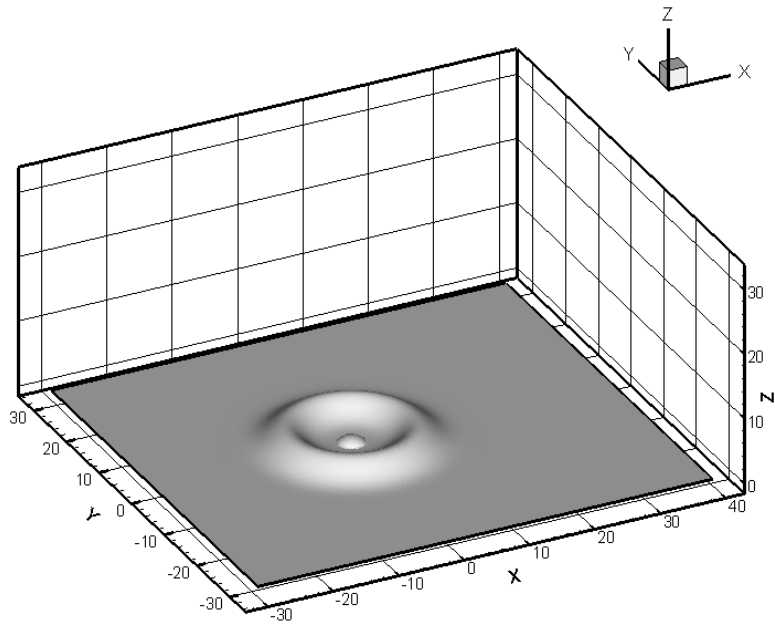
Figure 8.1 A dome building completely surrounded by hills
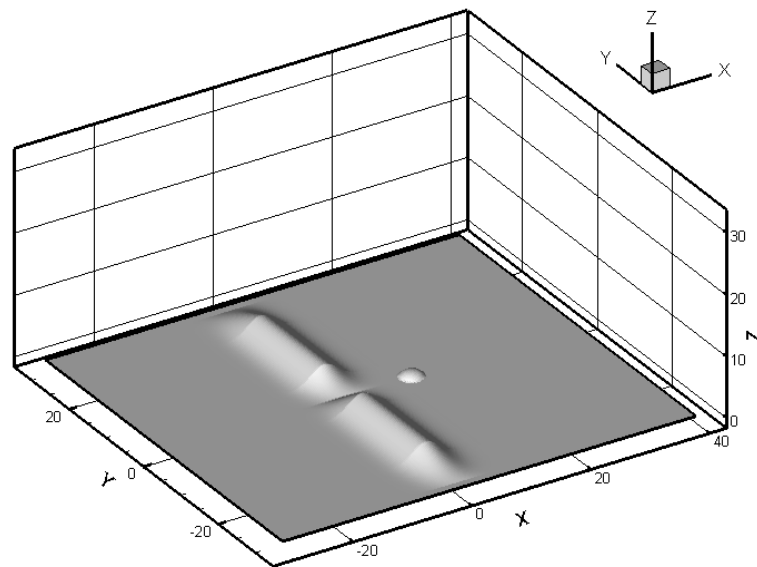
Figure 8.2 A dome building on the leeward side of ridge line with a gap.

References

Ahmed, N., & Selvam, R. (2015a). Tornado-Hill Interaction: Damage and Sheltering Observations. *International Journal of Applied Earth Observation and Geoinformation strucs.* (Pair review)

Ahmed, N., & Selvam, R. (2015b). Ridge effects on tornado path deviation. *International Journal of Civil and Structural Engineering Research*, *3(1), 273-294.*

Alrasheedi N. H., & Selvam R. P. (2011). Computing Tornado Forces on Different Building Sizes. In Proceedings of the 13th International Conference on Wind Engineering (ICWE13), Amsterdam, Netherlands.

Alrasheedi, N. H. (2012). Computer Modeling of the Influence of Structure Plan Areas on Tornado Forces. PhD dissertation, University of Arkansas, Fayetteville, USA.

ARCgis (2014). Damage Track and Timeline: https://disastermapping.maps.arcgis.com/apps/MapTour/index.html?appid=78c5a5ed38204aac92e0ef2a2b8f1288&webmap=d9bdb352021147e3b5256d0ab42c33bf.

ArkansasOnline (2014). Death Locations: http://www.arkansasonline.com/news/2014/apr/28/names-arkansas-tornado-victims-released/.

Brooks, H. E., & Dotzek, N. (2008). The spatial distribution of severe convective storms and an analysis of their secular changes. Climate Extremes and Society, 340, 35-53.

CAP (2014). Civil Air Patrol Images. (2014, September 25). *ArcGIS*. Retrieved October 7, 2014, from http://www.arcgis.com/home/webmap/viewer.html?useExisting=1.

Catastrophes: U.S. (2014). Retrieved December 21, 2014, from http://www.iii.org/fact-statistic/catastrophes-us.

Church, C. R., Snow, J. T., & Agee, E. M. (1977). Tornado vortex simulation at Purdue University. Bulletin of the American Meteorological Society, 58(9), 900-908.

Davies-Jones, R. P. (1973). The dependence of core radius on swirl ratio in a tornado simulator. Journal of the Atmospheric Sciences, 30(7), 1427-1430.

de Sampio, P.A.B, Lyra, P.R.M., Morgan, K. & Weatherill, N.P., (1993). Petro-Galerkin solutions of the incompressible Navier-Stokes equations in primitive variables with adaptive remeshing, Computer Methods in Applied Mechanics and Engineering, 106, 143-178

DOE-US. (2002). Natural phenomena hazards design and evaluation criteria for Department of Energy facilities. *Department of Energy standard DOE-STD-1020.*

Doswell III, C. (2011). On the Role of Deep Columnar Convective Vortices within the Atmosphere. Retrieved November 23, 2014, from http://www.flame.org/~cdoswell/SuptorRoles/SuptorRoles.html

Doswell, C. A., Brooks, H. E., & Dotzek, N. (2009). On the implementation of the enhanced Fujita scale in the USA. *Atmospheric Research*, *93*(1), 554-563.

Fujita, T. T. (1981). Tornadoes and downbursts in the context of generalized planetary scales. J. Atmos.Sci., 38, 1511-1534.

Fujita, T. T. (1989). The Teton-Yellowstone tornado of 21 July 1987. Monthly Weather Review, 117(9), 1913-1940.

Fujita, T. T., Bradbury, D. L., & Black, P. G. (1967). Estimation of tornado wind speed from characteristic ground marks. University of Chicago.

Fujita, T. T., Bradbury, D. L., & THULLENAR, C. V. (1970). Palm Sunday tornadoes of April 11, 1965. Monthly Weather Review, 98(1), 29-69.

Fujita, T. T., Forbes, G. S., & Umenhofer, T. A. (1976). Close-up view of 20 March 1976 tornadoes: Sinking cloud tops to suction vortices. Weatherwise, 29(3), 116-145.

Gorecki, P. & R.P. Selvam (2013), Three-dimensional simulation of tornado over complex terrain, Proceedings: The 12th Americas Conference on Wind Engineering (12ACWE), Seattle, Washington, USA, June 16-20, 2013.

Gorecki, P. (2015). Three Dimensional Simulations of Tornado Sheltering Effect of Man-made Structures. PhD dissertation, University of Arkansas.

Gorecki, P. M., & Selvam, R. P. (2014). Visualization of tornado-like vortex interacting with wide tornado-break wall. *Journal of Visualization*, 1-14.

Gorecki, P., & Selvam, R. P. (2015). Rankine combined vortex interaction with a rectangular prism. *International Journal of Computational Fluid Dynamics*, *29*(1), 120-132.

Gropp, W., Lusk, E., & Skjellum, A. portable parallel programming with the message-passing interface, 1994.

Haan, F. L., Sarkar, P.P., & Gallus, W.A. (2008). Design, Construction and Performance of a Large Tornado Simulator for Wind Engineering Applications, Engineering Structures, Vol.30, pp. 1146–1159.

Jischke, M. C., & Light, B. D. (1983). Laboratory simulation of tornadic wind loads on a rectangular model structure. Journal of Wind Engineering and Industrial Aerodynamics, 13(1), 371-382.

Jischke, M. C., & Parang, M. (1974). Properties of simulated tornado-like vortices. Journal of the Atmospheric Sciences, 31(2), 506-512.

Karstens, C. D., (2012). Observations and Laboratory Simulations of Tornadoes in Complex Topographical Regions. PhD Dissertation, Department of Meteorology, Iowa State University.

Karstens, C. D., Gallus Jr, W. A., Lee, B. D., & Finley, C. A. (2013). Analysis of Tornado-Induced Tree Fall Using Aerial Photography from the Joplin, Missouri, and Tuscaloosa–Birmingham, Alabama, Tornadoes of 2011*. Journal of Applied Meteorology and Climatology, 52(5), 1049-1068.

Karstens, C. D., Gallus, W.A, Jr., Sarkar, P.P, Lee, B.D., & Finley, C, A., (2012). "Understanding terrain impacts on tornado flow through tree-fall analysis of the joplin and tuscaloosa-birmingham tornadoes of 2011 and through numerical and laboratory vortex simulations". 26th Conference on Severe Local Storms (5 - 8 November 2012) Nashville, TN, American Meteorological society https://ams.confex.com/ams/26SLS/webprogram/Paper211978.html.

Lewellen, D. C. (2012) 4B. 1 "Effects of topography on tornado dynamics: a simulation study". 26th Conference on Severe Local Storms (5 - 8 November 2012) Nashville, TN, American Meteorological society https://ams.confex.com/ams/26SLS/webprogram/Paper211460.html.

Lewellen, D. C., Gong, B., & Lewellen, W. S. (2008). Effects of finescale debris on near-surface tornado dynamics. Journal of the Atmospheric Sciences, 65(10), 3247-3262.

Lewellen, W. S. (1976). Theoretical models of the tornado vortex", Proceedings of the Symposium on Tornadoes, Edited by: R.E. Peterson, Texas Tech University, Lubbock, June 22-24, pp. 107-143.

McDonald, J. R., & Mehta, K. C. (2006). *A recommendation for an Enhanced Fujita scale (EF-Scale).* Wind Science and Engineering Center, Texas Tech University.

McDonald, J. R., & Selvam, R. P. (1985). Tornado Forces on Buildings Using the Boundary Element Method. In Proceedings: Fifth US National Conference on Wind Engineering, Texas Tech University, Lubbock, TX.

Mehta, K., Womble, J., & Liang, D. (2008). Use of Satellite Images to Document Windstorm Damage: A Future Trend. *Journal of Wind and Engineering, 5*(1), 1-7.

Millett, P. C. (2003). Computer Modeling of the Tornado-Structure Interaction: Investigation of Structural Loading on a Cubic Building. *Unpublished Master's Thesis. University of Arkansas, Fayetteville, AR*.

Mishra, A. R., James, D. L., & Letchford, C. W. (2008a). Physical simulation of a single-celled tornado-like vortex, part A: flow field characterization. Journal of Wind Engineering and Industrial Aerodynamics, 96(8), 1243-1257.

Mishra, A. R., James, D. L., & Letchford, C. W. (2008b). Physical simulation of a single-celled tornado-like vortex, Part B: Wind loading on a cubical model. Journal of Wind Engineering and Industrial Aerodynamics, 96(8), 1258-1273.

Mitsuta, Y., & Monji, N. (1984). Development of a laboratory simulator for small scale atmospheric vortices. Natural disaster science, 6(1), 43-54.

NASA (2014). National Aeronautics and Space Administration. Tornado Damage in Mayflower, Arkansas : Image of the Day. Retrieved October 7, 2014, from http://earthobservatory.nasa.gov/IOTD/view.php?id=83612.

NOAA (2011). Tornado Information,' accessed 10 January2013, http://www.noaanews.noaa.gov/2011_tornado_information.html

NOAA (2010a). NOAA National Severe Storms Laboratory. (2010, July 1). Retrieved November 23, 2014, from http://www.nssl.noaa.gov/education/svrwx101/tornadoes/

NOAA (2010b). Thunderstorms and Severe Weather Spotting. [2010]. Retrieved November 23, 2014, from http://www.erh.noaa.gov/lwx/swep/Spotting.html

NWS (2010). Thunderstorms, Tornadoes, Lightning. Nature's Most Violent Storms. (2010, May 1). Retrieved November 23, 2014, from http://www.nws.noaa.gov/os/severeweather/resources/ttl6-10.pdf

NWS (2011a). National Weather Service Weather Forecast Office. (2011, August 19). Retrieved November 23, 2014, from http://www.srh.noaa.gov/ama/?n=supercell

NWS (2011b).National Weather Service Weather Forecast Office. [2011]. Parrish/Cordova Tornado. Retrieved October 20, 2014, from http://www.srh.noaa.gov/bmx/?n=event_04272011parrish

NWS (2011c).National Weather Service Weather Forecast Office. [2011]. *Tuscaloosa-Birmingham Tornado*. Retrieved October 7, 2014, from http://www.srh.noaa.gov/bmx/?n=event_04272011tuscbirm

NWS (2014a).National Weather Service Weather Forecast Office. [2014]. *NWS Little Rock, AR*. Retrieved October 7, 2014, from http://www.srh.noaa.gov/lzk/?n=pns043014txt.htm

NWS (2014b), Damage Track (Google Earth): http://www.srh.noaa.gov/lzk/?n=svr0414c.htm.

Pielke, RA. (1984). Mesoscale Meteorological Modeling. Academic Press, 612 pp.

Ragan, Q.S., Selvam, R.P. & Gorecki, P. (2012) Tornado-Induced Wind-Forces for Cylindrical Structures, Proceedings of the 12th Americas Conference on Wind Engineering (12th ACWE), Seattle, Washington, USA, June 16-20, 2013.

Rankine, W. J. M. (1882). A Manual of Applied Mechanics. Charles Griffin and Company, London.

Safeguard (2009). Safeguard Storm Shelters - Fujita Scale. [2009]. Safeguard Storm Shelters - Fujita Scale. Retrieved October 21, 2014, from http://www.safeguardshelters.com/fujitascale.php.

Sarkar, P. P., Haan, F. L., Balaramudu, V., & Sengupta, A. (2006). Laboratory simulation of tornado and microburst to assess wind loads on buildings. In ASCE Structures Congress, May 17th–19th, St. Louis, MO, USA.

Sarkar, S., & Selvam, R. P. (2009). Direct Numerical Simulation of Heat Transfer in Spray Cooling Through 3D Multiphase Flow Modeling Using Parallel Computing. *Journal of Heat Transfer*, *131*(12), 121007.

Selvam R.P., & Millett, P.C. (2002). Computer Modeling of the Tornado-Structure Interaction: Investigation of Structural Loading on Cubic Building", Second International Conference on Fluid Mechanics and Fluid Power, Indian Institute of Technology-Roorkee, Dec.12-14.

Selvam R.P., & Millett, P.C. (2005). Large Eddy Simulation of the Tornado-Structure Interaction to Determine Structural Loadings", Journal of Wind Engineering and Structures, Vol. 8,pp. 49-60.

Selvam RP, & Gorecki P. (2012b). CFD for infrastructure, thermal management and energy. In: Proceedings of international conference on application of fluid dynamics. Gaborone, Botswana

Selvam, R. P. & Ahmed, N. S. (2013). The Effect of Terrain Elevation on Tornado Path. Proceedings of 12th Americas Conference on Wind Engineering. Seattle, WA, USA, June 16-20, 2013.

Selvam, R. P. (1985). Application of the Boundary Element Method for Tornado Forces on Building. *PhD Dissertation*. Texas Tech University, Lubbock, TX, USA.

Selvam, R. P. (1993) .Computer Modeling of Tornado Forces on Buildings. Proceedings: The 7th US National Conference on Wind Engineering, Edited by: Gary C. Hart, Los Angeles, June 27-30, pp.605-613.

Selvam, R. P., & Gorecki, P. (2012a). Effect of tornado size on forces on thin 2d cylinder . 3 rdamerican association for wind engineering workshop, Hyannis, Massachusetts, USA

Selvam, R. P., & Millett P. C. (2003). Computer modeling of tornado forces on buildings. Wind and Structures, 6, 209-220.

Selvam, R. P., & Rao, K. S. (1996). *WINDFCT: A mass consistent wind field model for complex terrain* (No. CONF-960127--). American Meteorological Society, Boston, MA (United States).

Selvam, R. P., Ahmed, N. S., Yousof ,M.A, Strasser, M, & Ragan, Q. (2014).Study of Tornado-Terrain Interaction from Damage Documentation of April 27, 2014 Mayflower, AR Tornado. Department of Civil Engineering, University of Arkansas, Fayetteville,AR 72701.

Selvam, R. P., M.A, Strasser, Ahmed, N. S., Yousof , M, & Ragan, Q. (2015).Study of Tornado-Terrain Interaction from Damage Documentation of April 27, 2014 Mayflower, AR Tornado. Proceeding of the Structures Congress 2015. Portland, Oregon, USA, 2711-2721.

Selvam, R.P. & Peng, Y., (1998). Issues in computing pressure around buildings, in Structural Engineering World Wide 1998, N.K. Srivastava (eds), Elsevier, New York, pp: 941, Paper reference T171-3.

Selvam, R.P. (1997). Computation of Pressures on Texas Tech Building Using Large Eddy Simulation, J. Wind Engineering and Industrial Aerodynamics, 67 & 68, 647-657.

Selvam, R.P. and Paterson, D.A., (1993). Computation of Conductor Drag Coefficients, J. Wind Engineering and Industrial Aerodynamics, 50, 1-8.

Selvam, R.P., (1998). Computational procedures in grid based computational bridge aerodynamics, in Bridge Aerodynamics, Larsen, A. and Esdahl (eds), Balkema, Rotterdam, pp. 327-336.

Selvam, R.P., 2002. Computer modeling of tornado forces on buildings, in Proceedings of the Second Interna-tional Symposium on Advances in Wind & Structures, C.K. Choi et. al. (Ed.), Techno-Press, Korea, 2002, pp. 105-114.

Selvam, R.P., Roy, U.K., & Jung, Y. (2002). Investigation of Tornado Forces on 2D Cylinder Using Computer Modeling. In Wind Engineering, Proceedings of NCWE 2002, Edited by: K. Kumar, Phoenix Publishing House, New Delhi, pp. 342-353.

Sengupta, A., Haan, F.L., Sarkar, P.P., Balaramudu, V. (2008). Transient Loads on Buildings in Microbursts and Tornado Winds. Journal of Wind Engineering and Industrial and Aerodynamics,Vol. 96,pp.2173-2187.

Snow, J. (2014). Tornado. Retrieved November 23, 2014, from http://www.britannica.com/EBchecked/topic/599941/tornado.

Strasser, M. N., & Selvam, R. P. (2015). The variation in the maximum loading of a circular cylinder impacted by a 2D vortex with time of impact. Journal of Fluids and Structures, 58, 66-78.

Tamura, T. (1999). Reliability on CFD estimation for wind-structure interaction problems. Journal of Wind Engineering and Industrial Aerodynamics, 81(1), 117-143.

Tamura, T. E. T. S. U. R. O., Itoh, Y., Wada, A., & Kuwahara, K. (1995). Numerical study of pressure fluctuations on a rectangular cylinder in aerodynamic oscillation. Journal of wind engineering and industrial aerodynamics, 54, 239-250.

Tornadoes (2011). Tornadoes - Annual 2011. [2011]. Retrieved December 21, 2014, from http://www.ncdc.noaa.gov/sotc/tornadoes/2011/13.

Tornadoes. (2012). Retrieved December 21, 2014, from http://severe-wx.pbworks.com/w/page/15957991/Tornadoes.

U.S. Demographic History (2011).U.S. Demographic History | U.S. Immigration Policy - Environmental Impact Statement |. [2011]. Retrieved December 21, 2014, from http://www.immigrationeis.org/eis-documents/us-demographic-history#_ftnref1.

Ward, N. B., (1972). The Exploration of Certain Features of Tornado Dynamics Using a Laboratory model, Journal of the Atmospheric Sciences, Vol. 29,pp. 1194-1204.

Wen, Y. K. (1975). Dynamic tornadic wind loads on tall buildings. Journal of the Structural Division, 101(1), 169-185.

Yang, Z., Sarkar, P., & Hu, H. (2011). An experimental study of a high-rise building model in tornado-like winds. *Journal of Fluids and Structures*, *27*(4), 471-486.

Ying, S.J., & Chang, C.C. (1970). Exploratory Model Study of Tornado-Like Vortex Dynamics. Journal of Atmospheric Science, Vol. 27, No.1, pp. 3-14.

APPENDIX A: TORNADO POST DAMAGE INVESTIGATION TOOLS

1. Introduction

Tornado post damage investigation represents the best way to have clear vision for tornado behavior while interacting with the terrain. Tornado could occur over flat terrain, city, mountain or hilly terrain, most of these places are very difficult to access by cars. For thorough investigation, it usually requires both ground and aerial investigations. The man-hour involved in this process is very high as well as it is time overwhelming, and finally it is very difficult to ingrate and interpret the collected data due to mapping and scaling issues. Therefore, alternates are required to develop the current state for tornado-terrain interaction. Due to the advancement in computer technology and images processing, several software are utilized here for tornadoes damage locating, visualizing, coordinating and interpreting with regards to specific terrain features. Mainly, these software are Google Earth, Google Picasa and Global Mapper. Also, the new I phone technology provides great features that the photo taken by an I-phone camera is associated with a GPS coordinates that can be identified by the aforementioned software. In this appendix, detailed description for each of the software used in this dissertation is illustrated.

2. Google Earth

Google Earth is a free software which allows the user to navigate the world through a virtual globe and view satellite imagery, maps, terrain, 3D buildings, and much more. Google Earth is rich with detailed geographical content that allows the user to experience a more realistic view of the world, fly to his/her favorite places, search for businesses and even navigate through

directions. However, the focus in this section is to give general description for the software

interface and to explain how the Google Earth is utilized for tornado post damage investigation.

The main interface for the software is illustrated in Figure A.1. A definition and description for

each tool bar and button are provided next.
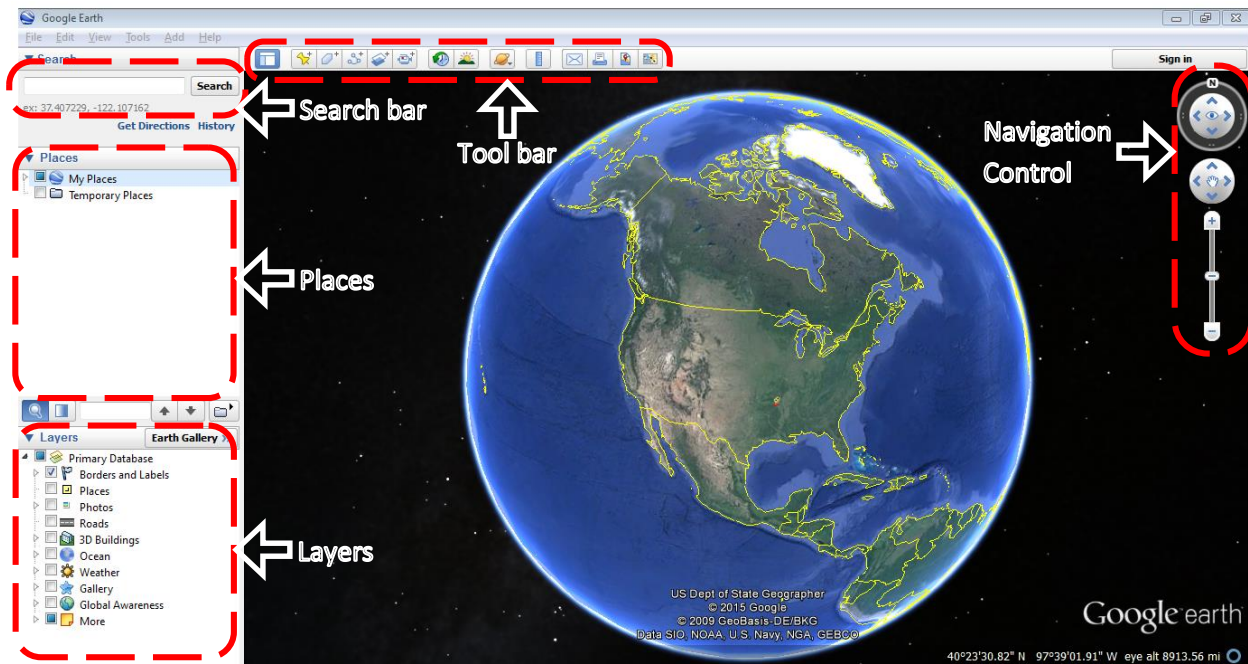
Figure A.1 Google Earth main interface and main control panels.

- **Search Bar**

  The search panel is the first tool needs to be used to create the investigated paths or

places. In this search bar name of places or locations wanted to be fly to can be typed. Different

formats can be inserted as shown in the table below.

Format	Example
City, State	Fayetteville, AR
City Country	Baghdad Iraq
Number Street City State	2100 N Leverett Ave Fayetteville, AR 72703

| Zip code or Postal code | 72704 |
| Latitude, Longitude | 36° 4'57.72"N, 94°12'44.86"W |

- **Tool Bar**

Google Earth tool bar showing in Figure A.2 has several of the important features which

serve tornado post damage investigation.

Figure A.2 tool bar description. 1- Show/hide sidebar   2- Placemark   3-Polygon   4- Path   5- Image overlay   6-Tour recorder   7- Historical imagery   8- Day/Night   9- Switch between Earth, Sky and other plants   10- Ruler   11- Email info   12- Print   13- Save image   14- Switch to Google maps.

Some of the tool bar buttons relevant to the investigation work are explained in more details next.

- **Place a Mark (2)**

By clinking on the place mark button , the new sub-window and a yellow place mark

pin will appear as shown below. Then, the place name and the pin shape and color can be

modified as need by the user from the new sub-window shown in Figure A.3.

The place can be identified by typing a name in the **Name** box. There are wide range selctions

for the place mark icons color and shapes which can be accessed by clicking on the yellow pin

on the top right hand corner.

The longitude and latitude boxes give the exact longitude and latitude coordinates of that

location.

The **Description** tab can be used to describe the specific location. The description will appear when the pointer is moved over that place mark. The color of the place mark and the text can be modified from **Style, Color** tab.
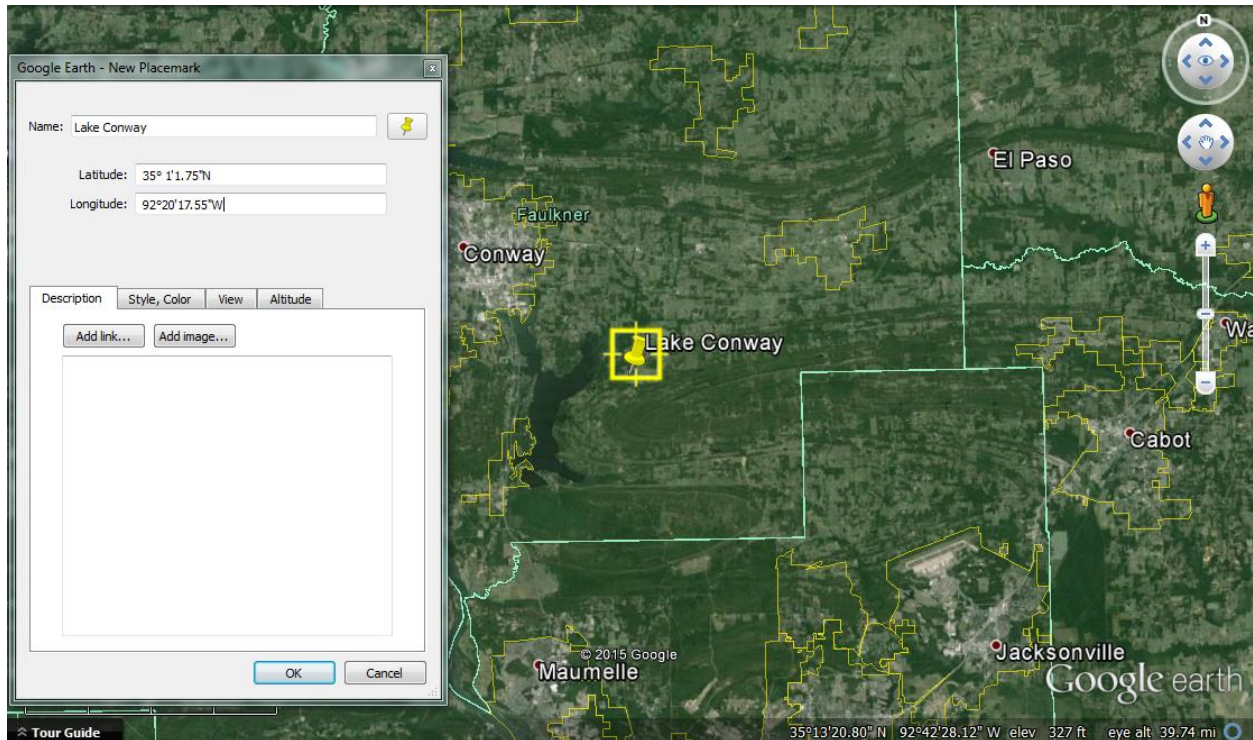
Figure A.3 Place a mark and modify its name and properties

▪ **Path, Ruler and Line (4)&(10)**

Basically the steps to create a path or a line are same. However, a line is only two points, whereas a path can have unlimited number of points. Also, the path can be access by clicking the path button [icon] or by clicking the ruler button [icon] as shown in the sub-window (See Figure A.4). The path can be created by placing a first marker at the start point and then several points can be added as required to create an accurate path. After that, the last marker should be at the

end point. For both a line and a path, name, color and thickness as well as other properties can be modified from the properties window as explained above for a place mark. Also, both a line and a path provide a length measurements in several units (e.g. miles, kilometers, feet, inches, etc.). One very important sub feature for a line and a path is the elevation profile which is described with some details in the next subsection.
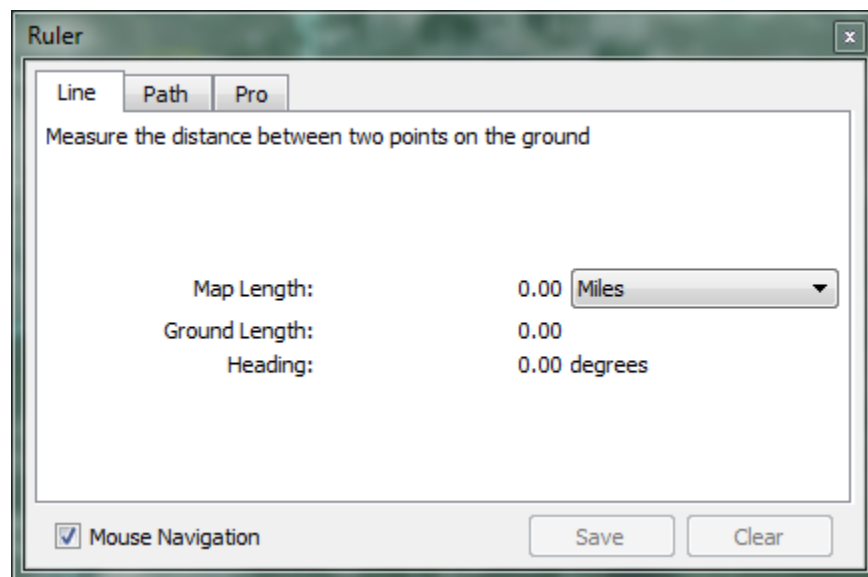
Figure A.4 a line or path creation using the ruler button.

▪ **Elevation Profile**

After a line or a path is drawn, the elevation profile for that line or path can be drawn next. Once a line or a path has been chosen from the Places panel, there are two ways to see its Elevation profile. First, click on **Edit** > **Show Elevation Profile** to have the elevation profile presented. The second way is by right-clicking on the desired path from the Places panel and also select **Show Elevation Profile**. An Elevation Profile for the selected line or path is going to show in the lower part of the Google Earth window as shown below (see Figure A.5). The

vertical-axis of the chart displays the elevation, and the horizontal-axis of the chart displays the distance.
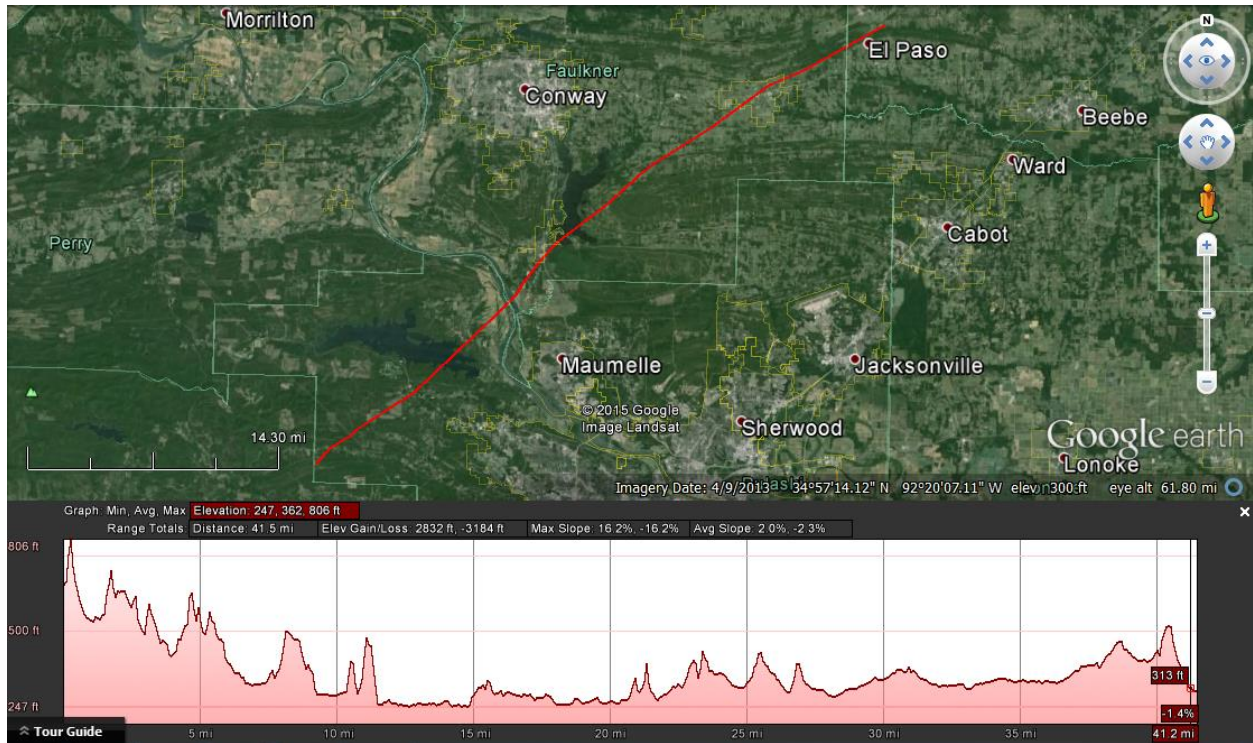
Figure A.5 elevation profile for a selected path.

▪ **Historical Imagery (7)**

This feature is the most important one for tornado post damage investigation, and it can be accessed by clicking this button [image] in the tool bar. Using this feature a tornado damage path can be investigated by moving the date bar [image] to a date after and before the tornado occurrence time. Figure A.6 a shows a selected area right next to Arkansas River close to Mayflower, AR prior to the Mayflower-Tornado on April-27 2014. Figure A.6 b shows the same area after the tornado occurrence, and one can see the damaged region.

Figure A.6 A selected area right next to Arkansas River close to Mayflower, AR a) before the tornado occurrence on April-27 2014 b) after the tornado occurrence.

- **Navigation Control**

    To navigate through the Google Earth viewer, use the navigation tools on the right-hand side of the screen.

    A. The **Look joystick** allows to adjust the view in the **3D viewer** from a single fixed point as if a person is turning his/her head.

    B. The **Move joystick** allows to move from location to location.

    C. **Street viewer** allows to switch to the street view.

    D. The **Zoom slider** allows to zoom in and out of the viewer to get a closer or more remote view.
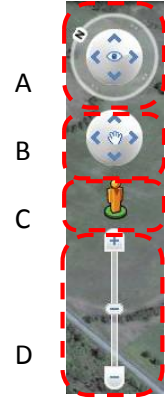
3. **Photo Geotag (Google Picasa and IPhone)**

    During tornado post damage ground investigation, a high quality camera is very important to provide good detailed photo as well as it is so crucial to have a camera supports photo geotagging. The geotag is adding GPS identification for the photo. Recently, several companies have developed and added this feature in their products, cameras. The IPhones 5 and later have a good quality camera of eight megapixel as well as they support the photo geotag. However, using the IPhone screen does not provide good visualization and details. Therefore, it is essential to synchronize the photos with a computer keeping their geotag feature. Google Picasa is one of the best photo viewer which allows to do geotagging on Google maps as well as on Google Earth. The basic details for turning the photo geotag in the IPhone and how to use Google Picasa is illustrated next.

- **IPhone Geotag**

    To have the geotag feature activated in any IPhone, the following steps need to be followed.

o   Go to **Setting**.

o   Then **Privacy**.

o   Then to **Location Services** and make sure it is on.

o   Under location services, go to **Camera** to set the configuration either **always** or **while using**.

▪   **Google Picasa**

Google Picasa is a free photo viewer and manager. Its interface is shown in Figure A.7.
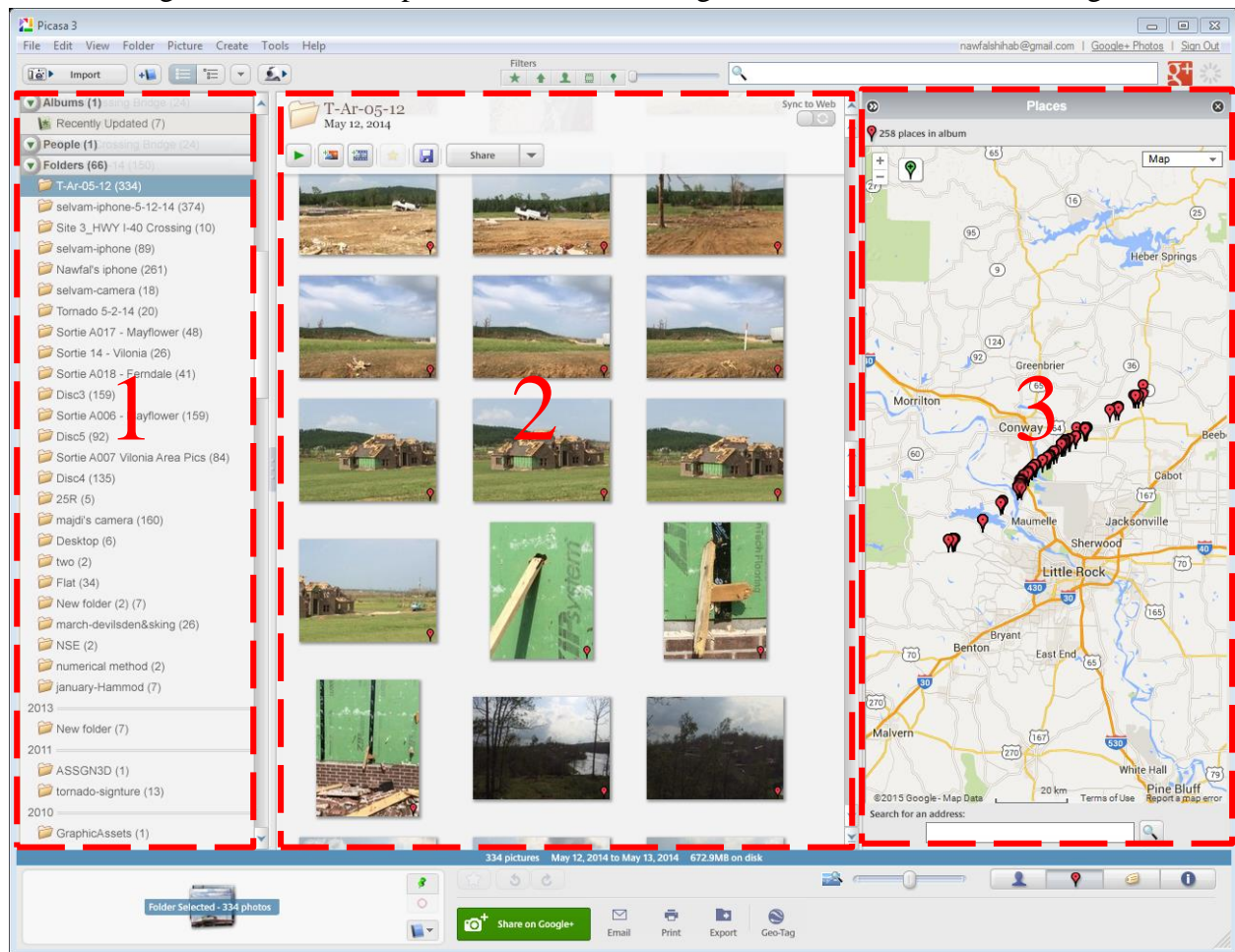
Figure A.7 Google Picasa main interface window.

1- Folder Panel: Shows the storage folders which contain photos.

2- Photo panel: views the selected folder photos.

3- Geotag Panel: Shows the locations for the selected folder's photos. Then, these photo can be synchronized and viewed by using either Google Earth or Google Maps. Also, It allows extract the location for each photo manually and then impose on the terrain map to study the terrain effects on the damaged location. Also, by connecting the photos locations on Google Earth or Google Maps, Tornado traveling path or the damage path can be accurately drawn and compared with available radar data.

APPENDIX B: TORNADO-TERRAIN INTERACTION CFD CODE INPUT FILE USER MANUAL AND RUN DETAILS FOR HPC MACHINE.

1. Input File User Manual

The CFD code PCTT442.OUT is utilized to simulate tornado interaction with huge variety of terrain including but limited the followings: a ridge, a knoll, a hill, a valley, and multi-topographical configurations. The PCTT442.OUT program is a parallelized program which in the present study utilizes up to 24 processers. The benefit achieved by this process is a speed up of ten times the serial computation using one processer. The grid points in X, Y and Z directions as well as the terrain elevations are generated using a FORTRAN code which is presented in this appendix. Then, the basic vortex variables are combined with the generated grid in the input file, ctt-i.txt. The input file user manual is illustrated next.

- **Input File: ctt-i.txt**

OPEN (5, FILE='ctt-i.txt')

First line: READ (5,*) IM, JM, KM, DTT, TTIME, TMIN, TMAX

IM   Total number of the grid points in the X-axis.

JM   Total number of the grid points in the Y-axis.

KM   Total number of the grid points in the Z-axis.

DTT   Time step.

TTIME   Total time of the computer simulation.

TMIN   The start time to calculate the minimum pressure in the computational domain.

TMAX   The finale time to calculate the maximum pressure in the computational domain.

Second line: READ (5,*) C11, C2, RAMAX, VTRAN, TLAG, ROTC, ANG, IFL2

C11   Calculated as C11= u*/k ln((z+z0)/z0)

C2   The roughness length of the ground (usually z0=0.00375 for building)

RAMAX   Maximum inner core radius of the tornado

VTRAN   Translating velocity

TLAG   Time lag (the time at which the center of tornado coincides with grid origin)

ROTC   Alpha rotational constant (RAMAX*ROTC =Max tangential velocity)

ANG   Attack Angle

IFL2   Time step interval to write a movie file (max no. of movies 999)

Where:

z is the height from the ground which sets to be equal to the obstacle height (h_{hill})

u* is the frictional velocity

After the second line, the input file introduces the grid points in X, Y and Z directions.

READ(5,*)(X(I), I=1,IM)

READ(5,*)(Y(J), J=1,JM)

READ(5,*)(Z(K), K=1,KM)

Then it introduces the terrain elevations.

DO J=1,JM

READ(5,*)(HI(I,J), I=1,IM)

END DO

- Input file example for very coarse grid.

This data is just presented for explanation purposes. This grid is 20x20x10.

20, 20, 11, 0.01, 90.0, 10.0, 80.0						Line 1&2
0.159, 0.00375, 2.0, 1.0, 40.0, 1.5, 0.0, 200						
-4.7500	-4.2500	-3.7500	-3.2500	-2.7500		
-2.2500	-1.7500	-1.2500	-0.7500	-0.2500		
0.2500	0.7500	1.2500	1.7500	2.2500		Grid points in X axis
2.7500	3.2500	3.7500	4.2500	4.7500		
-4.7500	-4.2500	-3.7500	-3.2500	-2.7500		
-2.2500	-1.7500	-1.2500	-0.7500	-0.2500		
0.2500	0.7500	1.2500	1.7500	2.2500		Grid points in Y axis
2.7500	3.2500	3.7500	4.2500	4.7500		
0.0000	0.0500	0.1000	0.1500	0.3000		Grid points in Z axis
0.5000	0.7500	1.0000	1.4500	1.9000		

Terrain elevations

0.0000	0.0000	0.0000	0.0791	0.2093
0.3077	0.3786	0.4245	0.4472	0.4472
0.4245	0.3786	0.3077	0.2093	0.0791
0.0000	0.0000	0.0000		
0.0000	0.0000	0.0000	0.0967	0.2558
0.3761	0.4627	0.5189	0.5466	0.5466
0.5189	0.4627	0.3761	0.2558	0.0967
0.0000	0.0000	0.0000		
0.0000	0.0000	0.0000	0.1143	0.3023
0.4444	0.5468	0.6132	0.6459	0.6459
0.6132	0.5468	0.4444	0.3023	0.1143
0.0000	0.0000	0.0000		
0.0000	0.0000	0.0000	0.1319	0.3489
0.5128	0.6309	0.7076	0.7453	0.7453
0.7076	0.6309	0.5128	0.3489	0.1319
0.0000	0.0000	0.0000		
0.0000	0.0000	0.0000	0.1494	0.3954
0.5812	0.7150	0.8019	0.8447	0.8447
0.8019	0.7150	0.5812	0.3954	0.1494
0.0000	0.0000	0.0000		
0.0000	0.0000	0.0000	0.1670	0.4419
0.6496	0.7992	0.8963	0.9441	0.9441
0.8963	0.7992	0.6496	0.4419	0.1670
0.0000	0.0000	0.0000		
0.0000	0.0000	0.0000	0.1758	0.4651
0.6837	0.8412	0.9434	0.9937	0.9937
0.9434	0.8412	0.6837	0.4651	0.1758
0.0000	0.0000	0.0000		
0.0000	0.0000	0.0000	0.1758	0.4651
0.6837	0.8412	0.9434	0.9937	0.9937
0.9434	0.8412	0.6837	0.4651	0.1758

0.0000	0.0000	0.0000		
0.0000	0.0000	0.0000	0.1758	0.4651
0.6837	0.8412	0.9434	0.9937	0.9937
0.9434	0.8412	0.6837	0.4651	0.1758
0.0000	0.0000	0.0000		
0.0000	0.0000	0.0000	0.1758	0.4651
0.6837	0.8412	0.9434	0.9937	0.9937
0.9434	0.8412	0.6837	0.4651	0.1758
0.0000	0.0000	0.0000		
0.0000	0.0000	0.0000	0.1758	0.4651
0.6837	0.8412	0.9434	0.9937	0.9937
0.9434	0.8412	0.6837	0.4651	0.1758
0.0000	0.0000	0.0000		
0.0000	0.0000	0.0000	0.1758	0.4651
0.6837	0.8412	0.9434	0.9937	0.9937
0.9434	0.8412	0.6837	0.4651	0.1758
0.0000	0.0000	0.0000		
0.0000	0.0000	0.0000	0.1758	0.4651
0.6837	0.8412	0.9434	0.9937	0.9937
0.9434	0.8412	0.6837	0.4651	0.1758
0.0000	0.0000	0.0000		
0.0000	0.0000	0.0000	0.1758	0.4651
0.6837	0.8412	0.9434	0.9937	0.9937
0.9434	0.8412	0.6837	0.4651	0.1758
0.0000	0.0000	0.0000		
0.0000	0.0000	0.0000	0.1670	0.4419
0.6496	0.7992	0.8963	0.9441	0.9441
0.8963	0.7992	0.6496	0.4419	0.1670
0.0000	0.0000	0.0000		
0.0000	0.0000	0.0000	0.1494	0.3954
0.5812	0.7150	0.8019	0.8447	0.8447
0.8019	0.7150	0.5812	0.3954	0.1494
0.0000	0.0000	0.0000		
0.0000	0.0000	0.0000	0.1319	0.3489
0.5128	0.6309	0.7076	0.7453	0.7453
0.7076	0.6309	0.5128	0.3489	0.1319
0.0000	0.0000	0.0000		
0.0000	0.0000	0.0000	0.1143	0.3023
0.4444	0.5468	0.6132	0.6459	0.6459
0.6132	0.5468	0.4444	0.3023	0.1143
0.0000	0.0000	0.0000		
0.0000	0.0000	0.0000	0.0967	0.2558
0.3761	0.4627	0.5189	0.5466	0.5466
0.5189	0.4627	0.3761	0.2558	0.0967
0.0000	0.0000	0.0000		
0.0000	0.0000	0.0000	0.0791	0.2093

```
0.3077    0.3786    0.4245    0.4472    0.4472
0.4245    0.3786    0.3077    0.2093    0.0791
0.0000    0.0000    0.0000
```

- **Input File: ctt-i.txt for code pctt45.out (interaction of tornado with multiple structures)**

OPEN (5, FILE='ctt-i.txt')
First line: READ (5,*) IM, JM, KM, DTT, TTIME, TMIN, TMAX
IM   Total number of the grid points in the X-axis.
JM   Total number of the grid points in the Y-axis.
KM   Total number of the grid points in the Z-axis.
DTT   Time step.
TTIME   Total time of the computer simulation.
TMIN   The start time to calculate the minimum pressure in the computational domain.
TMAX   The finale time to calculate the maximum pressure in the computational domain.

Second line: READ (5,*) C11, C2, RAMAX, VTRAN, TLAG, ROTC, ANG, IFL2
C11   Calculated as C11= u*/k ln((z+z0)/z0)
C2   The roughness length of the ground (usually z0=0.00375 for building)
RAMAX   Maximum inner core radius of the tornado
VTRAN   Translating velocity
TLAG   Time lag (the time at which the center of tornado coincides with grid origin)
ROTC   Alpha rotational constant (RAMAX*ROTC =Max tangential velocity)
ANG   Attack Angle
IFL2   Time step interval to write a movie file (max no. of movies 999)
Where:
z is the height from the ground which sets to be equal to the obstacle height (h_{hill})
u* is the frictional velocity, K is Von Karman constant (0.4)

Third line: READ (5,*) IHS1,IHE1,IHS2,IHE2
IHS1&IHE1   the boundary grids point between which the first structure (hill) is located
IHS2&IHE2   the boundary grids point between which the second structure (dome) is located

After the third line, the input file introduces the grid points in X, Y and Z directions.
READ(5,*)(X(I), I=1,IM)
READ(5,*)(Y(J), J=1,JM)
READ(5,*)(Z(K), K=1,KM)
Then it introduces the terrain elevations.
DO J=1,JM
READ(5,*)(HI(I,J), I=1,IM)
END DO

- Input file example for very coarse grid.

This data is just presented for explanation purposes. This grid is 20x20x10.

20, 20, 11, 0.01, 90.0, 10.0, 80.0				
0.159, 0.00375, 2.0, 1.0, 40.0, 1.5, 0.0, 200				
5,10,11,14				
-4.7500	-4.2500	-3.7500	-3.2500	-2.7500
-2.2500	-1.7500	-1.2500	-0.7500	-0.2500
0.2500	0.7500	1.2500	1.7500	2.2500
2.7500	3.2500	3.7500	4.2500	4.7500
-4.7500	-4.2500	-3.7500	-3.2500	-2.7500
-2.2500	-1.7500	-1.2500	-0.7500	-0.2500
0.2500	0.7500	1.2500	1.7500	2.2500
2.7500	3.2500	3.7500	4.2500	4.7500
0.0000	0.0500	0.1000	0.1500	0.3000
0.5000	0.7500	1.0000	1.4500	1.9000
0.0000	0.0000	0.0000	0.0791	0.2093
0.3077	0.3786	0.4245	0.4472	0.4472
0.4245	0.3786	0.3077	0.2093	0.0791
0.0000	0.0000	0.0000		
0.0000	0.0000	0.0000	0.0967	0.2558
0.3761	0.4627	0.5189	0.5466	0.5466
0.5189	0.4627	0.3761	0.2558	0.0967
0.0000	0.0000	0.0000		
0.0000	0.0000	0.0000	0.1143	0.3023
0.4444	0.5468	0.6132	0.6459	0.6459
0.6132	0.5468	0.4444	0.3023	0.1143
0.0000	0.0000	0.0000		
0.0000	0.0000	0.0000	0.1319	0.3489
0.5128	0.6309	0.7076	0.7453	0.7453
0.7076	0.6309	0.5128	0.3489	0.1319
0.0000	0.0000	0.0000		
0.0000	0.0000	0.0000	0.1494	0.3954
0.5812	0.7150	0.8019	0.8447	0.8447
0.8019	0.7150	0.5812	0.3954	0.1494
0.0000	0.0000	0.0000		
0.0000	0.0000	0.0000	0.1670	0.4419
0.6496	0.7992	0.8963	0.9441	0.9441
0.8963	0.7992	0.6496	0.4419	0.1670
0.0000	0.0000	0.0000		
0.0000	0.0000	0.0000	0.1758	0.4651
0.6837	0.8412	0.9434	0.9937	0.9937
0.9434	0.8412	0.6837	0.4651	0.1758
0.0000	0.0000	0.0000		
0.0000	0.0000	0.0000	0.1758	0.4651
0.6837	0.8412	0.9434	0.9937	0.9937

Line 1, 2&3

Grid points in X axis

Grid points in Y axis

Grid points in Z axis

Terrain elevations

0.9434	0.8412	0.6837	0.4651	0.1758
0.0000	0.0000	0.0000		
0.0000	0.0000	0.0000	0.1758	0.4651
0.6837	0.8412	0.9434	0.9937	0.9937
0.9434	0.8412	0.6837	0.4651	0.1758
0.0000	0.0000	0.0000		
0.0000	0.0000	0.0000	0.1758	0.4651
0.6837	0.8412	0.9434	0.9937	0.9937
0.9434	0.8412	0.6837	0.4651	0.1758
0.0000	0.0000	0.0000		
0.0000	0.0000	0.0000	0.1758	0.4651
0.6837	0.8412	0.9434	0.9937	0.9937
0.9434	0.8412	0.6837	0.4651	0.1758
0.0000	0.0000	0.0000		
0.0000	0.0000	0.0000	0.1758	0.4651
0.6837	0.8412	0.9434	0.9937	0.9937
0.9434	0.8412	0.6837	0.4651	0.1758
0.0000	0.0000	0.0000		
0.0000	0.0000	0.0000	0.1758	0.4651
0.6837	0.8412	0.9434	0.9937	0.9937
0.9434	0.8412	0.6837	0.4651	0.1758
0.0000	0.0000	0.0000		
0.0000	0.0000	0.0000	0.1758	0.4651
0.6837	0.8412	0.9434	0.9937	0.9937
0.9434	0.8412	0.6837	0.4651	0.1758
0.0000	0.0000	0.0000		
0.0000	0.0000	0.0000	0.1670	0.4419
0.6496	0.7992	0.8963	0.9441	0.9441
0.8963	0.7992	0.6496	0.4419	0.1670
0.0000	0.0000	0.0000		
0.0000	0.0000	0.0000	0.1494	0.3954
0.5812	0.7150	0.8019	0.8447	0.8447
0.8019	0.7150	0.5812	0.3954	0.1494
0.0000	0.0000	0.0000		
0.0000	0.0000	0.0000	0.1319	0.3489
0.5128	0.6309	0.7076	0.7453	0.7453
0.7076	0.6309	0.5128	0.3489	0.1319
0.0000	0.0000	0.0000		
0.0000	0.0000	0.0000	0.1143	0.3023
0.4444	0.5468	0.6132	0.6459	0.6459
0.6132	0.5468	0.4444	0.3023	0.1143
0.0000	0.0000	0.0000		
0.0000	0.0000	0.0000	0.0967	0.2558
0.3761	0.4627	0.5189	0.5466	0.5466
0.5189	0.4627	0.3761	0.2558	0.0967
0.0000	0.0000	0.0000		

```
  0.0000    0.0000    0.0000    0.0791    0.2093
  0.3077    0.3786    0.4245    0.4472    0.4472
  0.4245    0.3786    0.3077    0.2093    0.0791
  0.0000    0.0000    0.0000
```

2. FORTRAN Code For Grid Generation

```fortran
C    PROG. Terrain.F, Jan. 16, 2014
     PARAMETER(NX=300)
     DIMENSION RA(NX),X(NX),Y(NX),Z(NX),RB(NX),RZ(NX),HI(NX,NX)
     OPEN(2,FILE='bu2d-3D.txt')
     OPEN(3,FILE='hillshape.plt')
C.....Generate grid points in X-axies before the hill
     HX=0.1    !grid spacing within the hill range
     NXB=1./0.1
     H=0.1
     RB(1)=0.0
     RB(2)=H      !specify the first grid spacing
     I1=2
     FAC=1.0     !identify the growth factor
     DO I=1,300
     I1=I1+1
     IF(I.GT.40)FAC=1.05
     IF(I.GT.60)FAC=1.1
     H=H*FAC
     IF(H.GT.1)H=1.   !specify maximum grid spacing
     RB(I1)=RB(I1-1)+H
     IF(RB(I1).GT.9)GO TO 100
     END DO
100  NP=I1
C.....Generate grid points in X-axies beyond the hill
     H=0.1
     RA(1)=0.0
     RA(2)=H
     I1=2
     FAC=1.0
     DO I=1,300
     I1=I1+1
     IF(I.GT.40)FAC=1.05
     IF(I.GT.60)FAC=1.1
     H=H*FAC
     IF(H.GT.1)H=1.
     RA(I1)=RA(I1-1)+H
     IF(RA(I1).GT.9)GO TO 200
     END DO
200  NP1=I1
C.....Set X- POINTS BEFORE BUILDING
     I3=0
     DO I=1,NP
```

```fortran
      X(I)=-RB(NP-I+1)-(NXB*HX*0.5)
      Y(I)=X(I)
      I3=I3+1
      END DO
C.....Set X-POINTS FOR BUILDING
      DO I=1,NXB
      X(NP+I)=X(NP)+I*HX
      Y(I)=X(I)
      I3=I3+1
      END DO
C.....Set X-POINTS BEYOND BUILDING
      DO I=2,NP1
      X(NP+NXB+I-1)=X(NP+NXB)+RA(I)
      Y(I)=X(I)
      I3=I3+1
      END DO
      IM=I3  ! total number of points in X-axies
      JM=IM  ! total number of points in Y-axies
C.....GNERATE POINTS IN Z-axies
      HZ=0.05
      RZ(1)=0.0
      RZ(2)=HZ
      I1=2
      FAC=1.0
      DO I=1,300
      I1=I1+1
      IF(I.GT.32)FAC=1.05
      IF(I.GT.60)FAC=1.1
      HZ=HZ*FAC
      IF(HZ.GT.1)HZ=1.
      RZ(I1)=RZ(I1-1)+HZ
      IF(RZ(I1).GT.10)GO TO 300
      END DO
300   NPZ=I1
      Z(1)=0.0
      Z(2)=0.005
      Z(3)=0.0112
      Z(4)=0.0191
      Z(5)=0.0288
      Z(6)=0.05
      I2=6
      NZB=I2
      DO I=2,NPZ
      Z(NZB+I-1)=Z(NZB)+RZ(I)
      I2=I2+1
      END DO
      KM=I2    ! total number of points in Z-axies
```

```fortran
      HH=2    ! Hill height
      LH=22    ! Hill width
      DO J=1,JM
      DO I=1,IM
      HI(I,J)=0.0
      YH=Y(J)
      XH=X(I)
      SF=1        ! identify the slope on both sides of the hill
      IF(ABS(YH).GE.LH)THEN
      SF=(LH+8-ABS(YH))*0.125
      END IF
      IF(SF.LT.0)THEN
      SF=0
      END IF
      IF(XH.LE.16.0.and.XH.GE.-16.0) then
      HI(I,J)=HH*exp(-0.1*XH**2)*SF        !hill profile
      END IF
      END DO
      END DO
C     WRITE(2,*)IM,JM,KM
      WRITE(2,*)IM,JM,KM
      WRITE(2,20)(X(I),I=1,IM)
      WRITE(2,20)(Y(I),I=1,JM)
      WRITE(2,20)(Z(K),K=1,KM)
      DO J=1,JM
      WRITE(2,20)(HI(I,J),I=1,IM)
      END DO
20    FORMAT(5(F10.4,2X))
      IFILE1=4
C    Write to TECPLOT for Visulization
      write(IFILE1,*)'VARIABLES = "X","Y","Z"'
      write(IFILE1,*)'ZONE I=',IM, ',J=',JM,',K=',KM, ',F=POINT'
      do k=1,km
      do j=1,jm
      do i=1,im
      Z1=HI(I,J)+Z(K)
      write(IFILE1,*)x(i),Y(j),Z1
      end do
      end do
      end do
      STOP
      END
```

3. TECPLOT- Converting ASCII to Binary

The following code is a Windows batch file (pre.dat). The first line is just a default command for

the batch file. The second line specifies the loop start (1), the loop increment (1) and the loop

end (100). The third line start the program preplot.exe to convert the files which start with

(mv**.plt) from ascii to binary as (m**.plt). the fourth line sets the time increment for the loop

in millisecond (W 5000).

```
@echo off
FOR /L %%G IN (1,1,100) DO (
start preplot.exe mv%%G.plt m%%G.plt
ping 192.0.2.2 -n 1 -w 5000 > nul
)
```

4. HPC Computers

1- Create a new account

All students, faculty and staff of the University of Arkansas, Fayetteville are eligible to create an

account on the AHPCC clusters. A new account request must be sponsored by a member of

faculty or staff (usually a major professor or adviser) if a student wants to apply for an account.

The link below can be followed to log in with a UofA credentials and complete the online

request form.

- Internal User Account Request

- https://hpc.uark.edu/account-request/

Accounts are usually activated within 24 hours of the sponsor approval.

2- Log in to your account
- Use SSH software

- Host name (razor.uark.edu) or (stargate.uark.edu)

- User name (your UARK email ID) e.g. nsa001@uark.edu the ID is nsa001

- Password is your UARK email Password

3- Rules

- *ALL* jobs must be submitted through the job scheduler. Execution of jobs from the command line is not allowed.

- Jobs should be run in your scratch directory (/fasttmp/<mark>nsa001</mark> on Star and /scratch/<mark>nsa001</mark> on Razor).

4- Environment Modules

Using "module" to set proper paths:

➢ Common Commands:

- "module list" - shows currently loaded apps

- "module avail" - apps available on system

- "module load" - loads a new app into your path

- "module unload" - removes an app from path

- "module switch" - exchanges one for another

5- Compiling and Executing a Basic Program

- ❖ <mark>C Various Compilers Available:</mark>

  - ● "gcc" and "icc" for C source

  - ● "g++" and "icpc" for C++ source

  - ● "gfortran" and "ifort" for Fortran source

- ❖ <mark>Compilers "wrapped" for MPI parallel apps</mark>

  - ● "mpicc" for C source

  - ● "mpicxx" for C++ source

  - ● "mpif90" for Fortran source

- ❖ <mark>OpenMP Directives Available</mark>

●Gnu (gcc, g++, and gfortran) use "-fopenmp"

● Intel (icc, icpc, and ifort) use "-openmp"

6- Compilation of program pctt44.out and pctt45.out

To compile the parallel code, the <u>mpif77</u> compiler is used. In the computational mechanics lab computer, the compiler <u>mpif77</u> can be used directly with three levels of optimization. Example:

mpif77 –o1 pctt45.f

The optimization level (o1) can be (o2) or (o3) to provide shorter computation time depends on the compiled problem.

In the HPC computers, the same exact compiler is utilized, but two models need to be loaded to the system before compilation as shown below.

- module load intel/14.0.3

- module load impi/5.0.0

Then, the compiler can be used: mpif77 –o3 pctt45.f

7- File Transfer between Users

The available way to transfer files and data between users is by using the SORAGE directory as shown below.

User1:rps

Move the required file (tor.txt) to his STORAGE directory (e.g. cp tor.txt /storage/rps)

User2:nsa001

Copy the required file from user1 storage to his own home or scratch directory (e.g. cp /storage/rps/tor.txt /home/nsa001)

8- Creating a job script

   To create a job script you have to save the below lines (1-15) in a file with an extension

   of (.pbs) (e.g. , RUN.pbs). The description for each line is given below.

   1. #PBS -N MPI-test.job

   2. #PBS -q mem96GB12core

   3. #PBS -o MPI-test.output.$PBS_JOBID

   4. #PBS -j oe

   5. #PBS -l nodes=2:ppn=12

   6. #PBS -l walltime=40:00

   7.

   8. module load intel/14.0.3

   9. module load impi/5.0.0

   10.

   11.

   12. cd /home/nsa001/Hill2

   13. NP=$(wc -l < $PBS_NODEFILE)

   14.

   15. mpirun -np $NP -machinefile $PBS_NODEFILE ./pctt44.out

❖ Explanation for each line

   1. Names the job MPI-test.job in scheduler output such as showq and qstat

   2. Puts the job into the short12core queue. (See the queues

      http://hpc.uark.edu/hpc/support/queues.html page for information on other job queues)

3. Puts all output into the file MPI-test.output.$PBS_JOBID. **Note:** This file contains output that in an interactive job would be printed to the screen.

4. Puts stderr, error output, and stdout, standard output, into the same file (MPI-test.output.$PBS_JOBID)

5. Requests 1 compute nodes with 12 cores per node for a total of 12 cores

6. Sets the maximum runtime of the job to 10 minutes. If the job runs more than 10 minutes, it will be killed. (The format is walltime=DD:HH:MM:SS)

7. Blank line

8. Loud a module

9. Loud a module

10. Blank line

11. Blank line

12. On beginning execution, cd to the directory that the script was submitted from

13. Calculate how many MPI threads will be used by multiplying nodes times cores per node.

14. Blank line

15. Executes the program MPI-test by calling mpirun with the calculated NP and using the machine file automatically set by PBS, the file $PBS_NODEFILE which contains a list of the hosts that the scheduler has allocated to the job.

9- Queue command summary

qsub - submit a job to the queue (e.g. , qsub RUN.pbs)

qdel - delete a job from the queue

showq - show the current state of the queue (-u <userid>

qstat - show the current state of a job (-f option <jobid>)

pbsnodes – check state of a compute node (<node>)

showstart – check the start time of a queued job

10- Some useful Linux commands used in a typical session:

- "pwd" - lists your current location on system

- "cd" - changes to a different directory

- "cp" - copies a file to another name or location

- "mv" - moves or renames a file

- "grep" - searches for specific words or strings

- "diff" - compares two files to show differences

- "tar" - archive and unarchive source files

- "man" - help/usage for all system commands

- "exit" - terminate ssh session

- who – list users logged on

- pwd – present working directory

- ls – list files (-l, -a, -t, -r, -h; * . [ ]) shows content of current directory

- df – disk free

- mount – what file systems are mounted and how

- date

- wc – word count (-l to count lines)

- cat – show contents of a file

- touch – create a file/change modification time

- nano – simple file editor vi – more powerful editor

General Startup

To use vi: vi filename

To exit vi and save changes: ZZ   or :wq

To exit vi without saving changes: :q!

To enter vi command mode: *[esc]*

Counts: A number preceding any vi command tells vi to repeat that command that many times.

Cursor Movement

h   move left (backspace)

j   move down

k   move up

l   move right (spacebar)

[return]   move to the beginning of the next line

$ last column on the current line

0   move cursor to the first column on the current line

^   move cursor to first nonblank column on the current line

w   move to the beginning of the next word or punctuation mark

W move past the next space

b move to the beginning of the previous word or punctuation mark

B move to the beginning of the previous word,ignores punctuation

e end of next word or punctuation mark

E end of next word, ignoring punctuation

H move cursor to the top of the screen

M move cursor to the middle of the screen

L move cursor to the bottom of the screen

Screen Movement

G move to the last line in the file

xG move to line x

z+ move current line to top of screen

z move current line to the middle of screen

z- move current line to the bottom of screen

^F move forward one screen

^B move backward one line

^D move forward one half screen

^U move backward one half screen

^R redraw screen   (Does not work with VT100 type terminals)

^L redraw screen   (Does not work with Televideo terminals)

Inserting

r replace character under cursor with next character typed

R keep replacing character until *[esc]* is hit

i insert before cursor

a append after cursor

A append at end of line

O open line above cursor and enter append mode

12- Recourses

For more information it's recommended to visit the following websites.

- http://hpc.uark.edu/hpc/support.html
- Cluster documentation is available here:
  http://hpc.uark.edu/hpc/support.html
- Especially helpful to new users is the Quick start Cluster Tutorial:
  http://hpc.uark.edu/hpc/support/razor_cluster_tutorial.html
- Another useful link is the CI-TRAIN Lecture Series page:
  http://www.ci-train.org/training/lectureseries.html

APPENDIX C : HEXAHEDRAL ELEMENT JACOBEAN MATRIX

1. Hexahedral Element Jacobean Matrix

Finite elements method (FEM) is used to approximate the flow governing equations. Different element shapes are resulted in the terrain following grid system. For the region over flat terrain (no hill), the elements have orthogonal cubic shape as shown in Figure C.1 a, whereas the elements shape is non-orthogonal over the terrain region. The derivation of the Jacobean matrix for both orthogonal and non-orthogonal elements is presented in the following sections. Also, the FORTRAN code for calculating the Jacobean determinant and inverse is presented. Form the derivation steps for calculating the Jacobean matrix determinate, one can see that there are about thirty mathematical operations when the element is in the terrain region while these operations are reduced in an elegant way to three operations when there is no terrain. The percentage of the elements over no terrain region is about 70%. Therefore, using this reduced calculations for this huge percent of the elements reduce the computational time enormously.
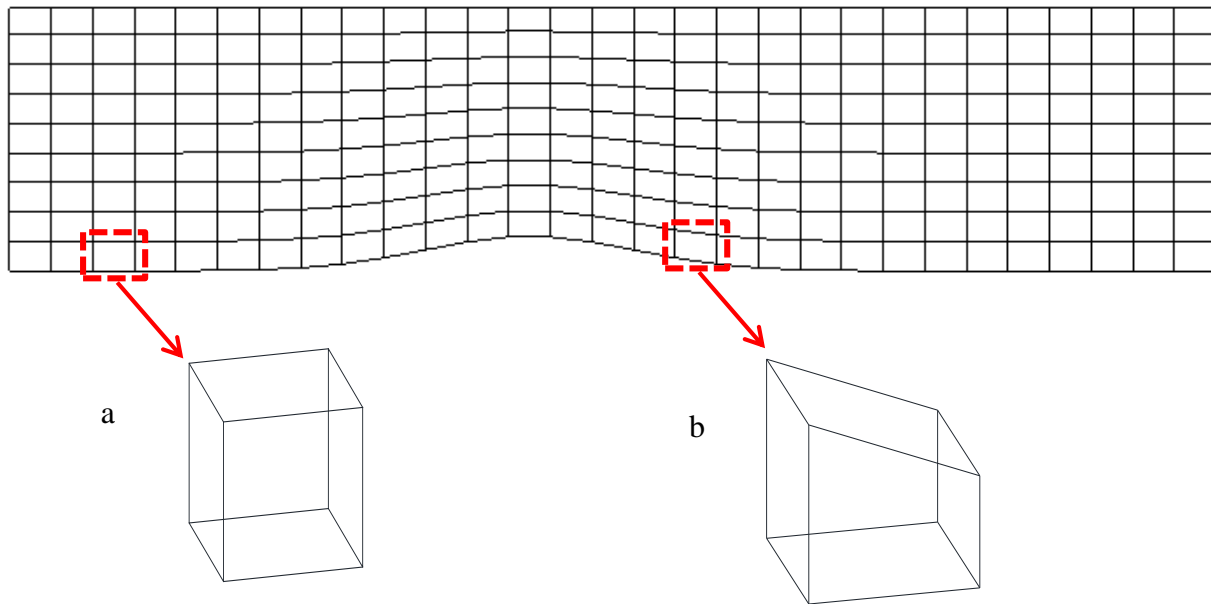
Figure C.1 Elements shapes over different regions of the numerical domain a) orthogonal hexahedral element (no terrain) b) non-orthogonal hexahedral element over the hill region.

Hexahedral Element Shape Functions

$$N_1 = \frac{1}{8}(1-\xi)(1-\eta)(1-\mu)$$

$$N_2 = \frac{1}{8}(1+\xi)(1-\eta)(1-\mu),$$

$$N_3 = \frac{1}{8}(1+\xi)(1+\eta)(1-\mu)$$

$$N_4 = \frac{1}{8}(1-\xi)(1+\eta)(1-\mu)$$

$$N_5 = \frac{1}{8}(1-\xi)(1-\eta)(1+\mu)$$

$$N_6 = \frac{1}{8}(1+\xi)(1-\eta)(1+\mu)$$

$$N_7 = \frac{1}{8}(1+\xi)(1+\eta)(1+\mu)$$

$$N_8 = \frac{1}{8}(1-\xi)(1+\eta)(1+\mu)$$
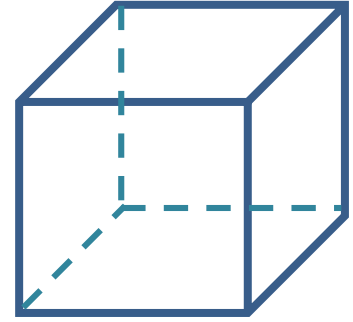
Hexahedral Element

Coordinates

$$X = X_1N_1 + X_2N_2 + X_3N_3 + X_4N_4 + X_5N_5 + X_6N_6 + X_7N_7 + X_8N_8$$

$$Y = Y_1N_1 + Y_2N_2 + Y_3N_3 + Y_4N_4 + Y_5N_5 + Y_6N_6 + Y_7N_7 + Y_8N_8$$

$$Z = Z_1N_1 + Z_2N_2 + Z_3N_3 + Z_4N_4 + Z_5N_5 + Z_6N_6 + Z_7N_7 + Z_8N_8$$

Jacobean Matrix

$$J = \begin{bmatrix} \frac{\partial X}{\partial \xi} & \frac{\partial Y}{\partial \xi} & \frac{\partial Z}{\partial \xi} \\ \frac{\partial X}{\partial \eta} & \frac{\partial Y}{\partial \eta} & \frac{\partial Z}{\partial \eta} \\ \frac{\partial X}{\partial \mu} & \frac{\partial Y}{\partial \mu} & \frac{\partial Z}{\partial \mu} \end{bmatrix} = \begin{bmatrix} J_{11} & J_{12} & J_{13} \\ J_{21} & J_{22} & J_{23} \\ J_{31} & J_{32} & J_{33} \end{bmatrix}$$

$$J = \begin{bmatrix} \frac{\partial N_1}{\partial \xi} & \frac{\partial N_2}{\partial \xi} & \frac{\partial N_3}{\partial \xi} & \frac{\partial N_4}{\partial \xi} & \frac{\partial N_5}{\partial \xi} & \frac{\partial N_6}{\partial \xi} & \frac{\partial N_7}{\partial \xi} & \frac{\partial N_8}{\partial \xi} \\ \frac{\partial N_1}{\partial \eta} & \frac{\partial N_2}{\partial \eta} & \frac{\partial N_3}{\partial \eta} & \frac{\partial N_4}{\partial \eta} & \frac{\partial N_5}{\partial \eta} & \frac{\partial N_6}{\partial \eta} & \frac{\partial N_7}{\partial \eta} & \frac{\partial N_8}{\partial \eta} \\ \frac{\partial N_1}{\partial \mu} & \frac{\partial N_2}{\partial \mu} & \frac{\partial N_3}{\partial \mu} & \frac{\partial N_4}{\partial \mu} & \frac{\partial N_5}{\partial \mu} & \frac{\partial N_6}{\partial \mu} & \frac{\partial N_7}{\partial \mu} & \frac{\partial N_8}{\partial \mu} \end{bmatrix} \begin{bmatrix} X_1 & Y_1 & Z_1 \\ X_2 & Y_2 & Z_2 \\ X_3 & Y_3 & Z_3 \\ X_4 & Y_4 & Z_4 \\ X_5 & Y_5 & Z_5 \\ X_6 & Y_6 & Z_6 \\ X_7 & Y_7 & Z_7 \\ X_8 & Y_8 & Z_8 \end{bmatrix}$$

$$\frac{\partial N_{i=1-8}}{\partial \xi} = \frac{-1}{8}(1-\eta)(1-\mu), \frac{1}{8}(1-\eta)(1-\mu), \frac{1}{8}(1+\eta)(1-\mu), \frac{-1}{8}(1+\eta)(1-\mu), \frac{-1}{8}(1-\eta)(1$$

$$+\mu), \frac{1}{8}(1-\eta)(1+\mu), \frac{1}{8}(1+\eta)(1+\mu), \frac{-1}{8}(1+\eta)(1+\mu)$$

$$\frac{\partial N_{i=1-8}}{\partial \eta} = \frac{-1}{8}(1-\xi)(1-\mu), \frac{-1}{8}(1+\xi)(1-\mu), \frac{1}{8}(1+\xi)(1-\mu), \frac{1}{8}(1-\xi)(1-\mu), \frac{-1}{8}(1-\xi)(1$$

$$+\mu), \frac{-1}{8}(1+\xi)(1+\mu), \frac{1}{8}(1+\xi)(1+\mu), \frac{1}{8}(1-\xi)(1+\mu)$$

$$\frac{\partial N_{i=1-8}}{\partial \mu} = \frac{-1}{8}(1-\xi)(1-\eta), \frac{-1}{8}(1+\xi)(1-\eta), \frac{-1}{8}(1+\xi)(1+\eta), \frac{-1}{8}(1-\xi)(1+\eta), \frac{1}{8}(1-\xi)(1$$

$$-\eta), \frac{1}{8}(1+\xi)(1-\eta), \frac{1}{8}(1+\xi)(1+\eta), \frac{1}{8}(1-\xi)(1+\eta)$$

For the Element shown

$$\begin{bmatrix} X_1 & Y_1 & Z_1 \\ X_2 & Y_2 & Z_2 \\ X_3 & Y_3 & Z_3 \\ X_4 & Y_4 & Z_4 \\ X_5 & Y_5 & Z_5 \\ X_6 & Y_6 & Z_6 \\ X_7 & Y_7 & Z_7 \\ X_8 & Y_8 & Z_8 \end{bmatrix} = \begin{bmatrix} 0 & 0 & 0 \\ a & 0 & 0 \\ a & b & 0 \\ 0 & b & 0 \\ 0 & 0 & c \\ a & 0 & c \\ a & b & c \\ 0 & b & c \end{bmatrix}$$

$$J_{11} = \frac{a}{8}[(1-\eta)(1-\mu) + (1+\eta)(1-\mu) + (1-\eta)(1+\mu) + (1+\eta)(1+\mu)]$$

$$J_{11} = \frac{a}{8}[1-\mu-\eta+\eta\mu+1-\mu+\eta-\eta\mu+1+\mu-\eta-\eta\mu+1+\mu+\eta+\eta\mu] = \frac{a}{8}[4]$$

$$J_{12} = \frac{b}{8}[(1+\eta)(1-\mu) - (1+\eta)(1-\mu) + (1+\eta)(1+\mu) - (1+\eta)(1+\mu)]$$

$$J_{12} = \frac{b}{8}[1-\mu+\eta-\eta\mu-1+\mu-\eta+\eta\mu] = 0$$

$$J_{13} = \frac{c}{8}[-1(1-\eta)(1+\mu) + (1-\eta)(1+\mu) + (1+\eta)(1+\mu) - (1+\eta)(1+\mu)]$$

$$J_{13} = 0$$

$$J_{21} = \frac{a}{8}[-1(1+\xi)(1-\mu) + (1+\xi)(1-\mu) - (1+\xi)(1+\mu) + (1+\xi)(1+\mu)]$$

$$J_{21} = 0$$

$$J_{22} = \frac{b}{8}[(1+\xi)(1-\mu) + (1-\xi)(1-\mu) + (1+\xi)(1+\mu) + (1-\xi)(1+\mu)]$$

$$J_{22} = \frac{b}{8}[1 - \mu + \xi - \xi\mu + 1 - \mu - \xi + \xi\mu + 1 + \mu + \xi + \xi\mu + 1 + \mu - \xi - \xi\mu] = \frac{b}{8}[4]$$

$$J_{23} = \frac{c}{8}[-1(1 - \xi)(1 + \mu) - (1 + \xi)(1 + \mu) + (1 + \xi)(1 + \mu) + (1 - \xi)(1 + \mu)]$$

$$J_{23} = 0$$

$$J_{31} = \frac{a}{8}[-1(1 + \xi)(1 - \eta) - (1 + \xi)(1 + \eta) + (1 + \xi)(1 - \eta) + (1 + \xi)(1 + \eta)]$$

$$J_{31} = 0$$

$$J_{32} = \frac{b}{8}[-1(1 + \xi)(1 + \eta) - (1 - \xi)(1 + \eta) + (1 + \xi)(1 + \eta) + (1 - \xi)(1 + \eta)]$$

$$J_{32} = 0$$

$$J_{33} = \frac{c}{8}[(1 - \xi)(1 - \eta) + (1 + \xi)(1 - \eta) + (1 + \xi)(1 + \eta) + (1 - \xi)(1 + \eta)]$$

$$J_{33} = \frac{c}{8}[1 - \eta - \xi + \xi\eta + 1 - \eta + \xi - \xi\eta + 1 + \eta + \xi + \xi\eta + 1 + \eta - \xi - \xi\eta]$$

$$J_{33} = \frac{c}{8}[4]$$

$$\therefore J = \begin{bmatrix} \frac{1}{2}a & 0 & 0 \\ 0 & \frac{1}{2}b & 0 \\ 0 & 0 & \frac{1}{2}c \end{bmatrix}$$

$$\therefore \det(J) = \frac{abc}{8}$$

For non-orthogonal Hexahedral Element (in the middle of the hill)

$$J = \begin{bmatrix} \frac{\partial N_1}{\partial \xi} & \frac{\partial N_2}{\partial \xi} & \frac{\partial N_3}{\partial \xi} & \frac{\partial N_4}{\partial \xi} & \frac{\partial N_5}{\partial \xi} & \frac{\partial N_6}{\partial \xi} & \frac{\partial N_7}{\partial \xi} & \frac{\partial N_8}{\partial \xi} \\ \frac{\partial N_1}{\partial \eta} & \frac{\partial N_2}{\partial \eta} & \frac{\partial N_3}{\partial \eta} & \frac{\partial N_4}{\partial \eta} & \frac{\partial N_5}{\partial \eta} & \frac{\partial N_6}{\partial \eta} & \frac{\partial N_7}{\partial \eta} & \frac{\partial N_8}{\partial \eta} \\ \frac{\partial N_1}{\partial \mu} & \frac{\partial N_2}{\partial \mu} & \frac{\partial N_3}{\partial \mu} & \frac{\partial N_4}{\partial \mu} & \frac{\partial N_5}{\partial \mu} & \frac{\partial N_6}{\partial \mu} & \frac{\partial N_7}{\partial \mu} & \frac{\partial N_8}{\partial \mu} \end{bmatrix} \begin{bmatrix} X_1 & Y_1 & Z_1 \\ X_2 & Y_2 & Z_2 \\ X_3 & Y_3 & Z_3 \\ X_4 & Y_4 & Z_4 \\ X_5 & Y_5 & Z_5 \\ X_6 & Y_6 & Z_6 \\ X_7 & Y_7 & Z_7 \\ X_8 & Y_8 & Z_8 \end{bmatrix}$$
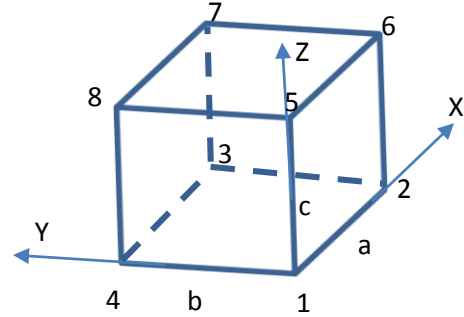
$$\begin{bmatrix} X_1 & Y_1 & Z_1 \\ X_2 & Y_2 & Z_2 \\ X_3 & Y_3 & Z_3 \\ X_4 & Y_4 & Z_4 \\ X_5 & Y_5 & Z_5 \\ X_6 & Y_6 & Z_6 \\ X_7 & Y_7 & Z_7 \\ X_8 & Y_8 & Z_8 \end{bmatrix} = \begin{bmatrix} 0 & 0 & 0 \\ a & 0 & 0 \\ a & b & 0 \\ 0 & b & 0 \\ 0 & 0 & c_1 \\ a & 0 & c_2 \\ a & b & c_2 \\ 0 & b & c_1 \end{bmatrix}$$

$$J_{11} = \frac{a}{8}[(1-\eta)(1-\mu) + (1+\eta)(1-\mu) + (1-\eta)(1+\mu) + (1+\eta)(1+\mu)]$$

$$J_{11} = \frac{a}{8}[1 - \mu - \eta + \eta\mu + 1 - \mu + \eta - \eta\mu + 1 + \mu - \eta - \eta\mu + 1 + \mu + \eta + \eta\mu] = \frac{a}{8}[4]$$

$$J_{12} = \frac{b}{8}[(1+\eta)(1-\mu) - (1+\eta)(1-\mu) + (1+\eta)(1+\mu) - (1+\eta)(1+\mu)]$$

$$J_{12} = \frac{b}{8}[1 - \mu + \eta - \eta\mu - 1 + \mu - \eta + \eta\mu] = 0$$

$$J_{13} = \frac{1}{8}[-C_1(1-\eta)(1+\mu) + C_2(1-\eta)(1+\mu) + C_2(1+\eta)(1+\mu) - C_1(1+\eta)(1+\mu)]$$

$$J_{13} = \frac{(C_2 - C_1)}{8}[(1 + \mu - \eta - \eta\mu) + (1 + \mu + \eta + \eta\mu)] = \frac{(C_2 - C_1)}{8}[(2 + 2\mu)]$$

$$J_{21} = \frac{a}{8}[-1(1+\xi)(1-\mu) + (1+\xi)(1-\mu) - (1+\xi)(1+\mu) + (1+\xi)(1+\mu)]$$

$$J_{21} = 0$$

$$J_{22} = \frac{b}{8}[(1+\xi)(1-\mu) + (1-\xi)(1-\mu) + (1+\xi)(1+\mu) + (1-\xi)(1+\mu)]$$

$$J_{22} = \frac{b}{8}[1 - \mu + \xi - \xi\mu + 1 - \mu - \xi + \xi\mu + 1 + \mu + \xi + \xi\mu + 1 + \mu - \xi - \xi\mu] = \frac{b}{8}[4]$$

$$J_{23} = \frac{c}{8}[-C_1(1-\xi)(1+\mu) - C_2(1+\xi)(1+\mu) + C_2(1+\xi)(1+\mu) + C_1(1-\xi)(1+\mu)]$$

$$J_{23} = 0$$

$$J_{31} = \frac{a}{8}[-1(1+\xi)(1-\eta) - (1+\xi)(1+\eta) + (1+\xi)(1-\eta) + (1+\xi)(1+\eta)]$$

$$J_{31} = 0$$

$$J_{32} = \frac{b}{8}[-1(1+\xi)(1+\eta) - (1-\xi)(1+\eta) + (1+\xi)(1+\eta) + (1-\xi)(1+\eta)]$$

$$J_{32} = 0$$

$$J_{33} = \frac{1}{8}[C_1(1-\xi)(1-\eta) + C_2(1+\xi)(1-\eta) + C_2(1+\xi)(1+\eta) + C_1(1-\xi)(1+\eta)]$$

$$J_{33} = \frac{1}{8}[C_1(2-2\xi) + C_2(2+2\xi)]$$

$$\therefore J = \begin{bmatrix} \frac{1}{2}a & 0 & \frac{(C_2-C_1)}{8}[(2+2\mu)] \\ 0 & \frac{1}{2}b & 0 \\ 0 & 0 & \frac{1}{8}[C_1(2-2\xi) + C_2(2+2\xi)] \end{bmatrix}$$

$$\therefore \det(J) = \frac{1}{16}ab[C_1(1-\xi) + C_2(1+\xi)]$$

For non-orthogonal Hexahedral Element (on the side of the hill)

$$J = \begin{bmatrix} \frac{\partial N_1}{\partial \xi} & \frac{\partial N_2}{\partial \xi} & \frac{\partial N_3}{\partial \xi} & \frac{\partial N_4}{\partial \xi} & \frac{\partial N_5}{\partial \xi} & \frac{\partial N_6}{\partial \xi} & \frac{\partial N_7}{\partial \xi} & \frac{\partial N_8}{\partial \xi} \\ \frac{\partial N_1}{\partial \eta} & \frac{\partial N_2}{\partial \eta} & \frac{\partial N_3}{\partial \eta} & \frac{\partial N_4}{\partial \eta} & \frac{\partial N_5}{\partial \eta} & \frac{\partial N_6}{\partial \eta} & \frac{\partial N_7}{\partial \eta} & \frac{\partial N_8}{\partial \eta} \\ \frac{\partial N_1}{\partial \mu} & \frac{\partial N_2}{\partial \mu} & \frac{\partial N_3}{\partial \mu} & \frac{\partial N_4}{\partial \mu} & \frac{\partial N_5}{\partial \mu} & \frac{\partial N_6}{\partial \mu} & \frac{\partial N_7}{\partial \mu} & \frac{\partial N_8}{\partial \mu} \end{bmatrix} \begin{bmatrix} X_1 & Y_1 & Z_1 \\ X_2 & Y_2 & Z_2 \\ X_3 & Y_3 & Z_3 \\ X_4 & Y_4 & Z_4 \\ X_5 & Y_5 & Z_5 \\ X_6 & Y_6 & Z_6 \\ X_7 & Y_7 & Z_7 \\ X_8 & Y_8 & Z_8 \end{bmatrix}$$

$$\begin{bmatrix} X_1 & Y_1 & Z_1 \\ X_2 & Y_2 & Z_2 \\ X_3 & Y_3 & Z_3 \\ X_4 & Y_4 & Z_4 \\ X_5 & Y_5 & Z_5 \\ X_6 & Y_6 & Z_6 \\ X_7 & Y_7 & Z_7 \\ X_8 & Y_8 & Z_8 \end{bmatrix} = \begin{bmatrix} 0 & 0 & 0 \\ a & 0 & 0 \\ a & b & 0 \\ 0 & b & 0 \\ 0 & 0 & c_1 \\ a & 0 & c_2 \\ a & b & c_3 \\ 0 & b & c_4 \end{bmatrix}$$

$$J_{11} = \frac{a}{8}[(1-\eta)(1-\mu) + (1+\eta)(1-\mu) + (1-\eta)(1+\mu) + (1+\eta)(1+\mu)]$$

$$J_{11} = \frac{a}{8}[1 - \mu - \eta + \eta\mu + 1 - \mu + \eta - \eta\mu + 1 + \mu - \eta - \eta\mu + 1 + \mu + \eta + \eta\mu] = \frac{a}{8}[4]$$

$$J_{12} = \frac{b}{8}[(1+\eta)(1-\mu) - (1+\eta)(1-\mu) + (1+\eta)(1+\mu) - (1+\eta)(1+\mu)]$$

$$J_{12} = \frac{b}{8}[1 - \mu + \eta - \eta\mu - 1 + \mu - \eta + \eta\mu] = 0$$

$$J_{13} = \frac{1}{8}[-C_1(1 - \eta)(1 + \mu) + C_2(1 - \eta)(1 + \mu) + C_3(1 + \eta)(1 + \mu) - C_4(1 + \eta)(1 + \mu)]$$

$$J_{13} = \left[\frac{(C_2 - C_1)}{8}(1 + \mu - \eta - \eta\mu) + \frac{(C_3 - C_4)}{8}(1 + \mu + \eta + \eta\mu)\right]$$

$$J_{21} = \frac{a}{8}[-1(1 + \xi)(1 - \mu) + (1 + \xi)(1 - \mu) - (1 + \xi)(1 + \mu) + (1 + \xi)(1 + \mu)]$$

$$J_{21} = 0$$

$$J_{22} = \frac{b}{8}[(1 + \xi)(1 - \mu) + (1 - \xi)(1 - \mu) + (1 + \xi)(1 + \mu) + (1 - \xi)(1 + \mu)]$$

$$J_{22} = \frac{b}{8}[1 - \mu + \xi - \xi\mu + 1 - \mu - \xi + \xi\mu + 1 + \mu + \xi + \xi\mu + 1 + \mu - \xi - \xi\mu] = \frac{b}{8}[4]$$

$$J_{23} = \frac{1}{8}[-C_1(1 - \xi)(1 + \mu) - C_2(1 + \xi)(1 + \mu) + C_3(1 + \xi)(1 + \mu) + C_4(1 - \xi)(1 + \mu)]$$

$$J_{23} = \left[\frac{(C_4 - C_1)}{8}(1 + \mu - \xi - \xi\mu) + \frac{(C_3 - C_2)}{8}(1 + \mu + \xi + \xi\mu)\right]$$

$$J_{31} = \frac{a}{8}[-1(1 + \xi)(1 - \eta) - (1 + \xi)(1 + \eta) + (1 + \xi)(1 - \eta) + (1 + \xi)(1 + \eta)]$$

$$J_{31} = 0$$

$$J_{32} = \frac{b}{8}[-1(1 + \xi)(1 + \eta) - (1 - \xi)(1 + \eta) + (1 + \xi)(1 + \eta) + (1 - \xi)(1 + \eta)]$$

$$J_{32} = 0$$

$$J_{33} = \frac{1}{8}[C_1(1 - \xi)(1 - \eta) + C_2(1 + \xi)(1 - \eta) + C_3(1 + \xi)(1 + \eta) + C_4(1 - \xi)(1 + \eta)]$$

$$\therefore J = \begin{vmatrix} \frac{1}{2}a & 0 & \left[\frac{(C_2 - C_1)}{8}(1 + \mu - \eta - \eta\mu) + \frac{(C_3 - C_4)}{8}(1 + \mu + \eta + \eta\mu)\right] \\ 0 & \frac{1}{2}b & \left[\frac{(C_4 - C_1)}{8}(1 + \mu - \xi - \xi\mu) + \frac{(C_3 - C_2)}{8}(1 + \mu + \xi + \xi\mu)\right] \\ 0 & 0 & \frac{1}{8}[C_1(1 - \xi)(1 - \eta) + C_2(1 + \xi)(1 - \eta) + C_3(1 + \xi)(1 + \eta) + C_4(1 - \xi)(1 + \eta)] \end{vmatrix}$$

$$\therefore \det(J) = \frac{a \times b}{32} \times [C_1(1 - \xi)(1 - \eta) + C_2(1 + \xi)(1 - \eta) + C_3(1 + \xi)(1 + \eta) + C_4(1 - \xi)(1 + \eta)]$$

- FORTRAN code for calculating the Jacobean determinant and inverse

```
SUBROUTINE STDM(XX,H,B,DET,R,S,T,NEL)
    INTEGER NEL,I,J,K
    DOUBLE PRECISION B(3,8),XX(3,8),H(8),P(3,8),XJ(3,3),XJI(3,3)
   &,R,S,T,RP,SP,TP,RM,SM,TM,DUM,DET
C    PROGRAM TO EVALUVATE THE STRAIN-DISPLACEMENT TRANSFORMATION
C    MATRIX B AT POINT (R,S,T) FOR A BRICK8 ELEMENT
C
    RP=1.0+R
    SP=1.0+S
    TP=1.0+T
    RM=1.0-R
    SM=1.0-S
    TM=1.0-T
C.....INTERPOLATION FUNCTIONS
C.....AT THIS STAGE NO NEED FOR H?
    H(1)=0.125*RM*SM*TM
    H(2)=0.125*RP*SM*TM
    H(3)=0.125*RP*SP*TM
   H(4)=0.125*RM*SP*TM
    H(5)=0.125*RM*SM*TP
    H(6)=0.125*RP*SM*TP
    H(7)=0.125*RP*SP*TP
    H(8)=0.125*RM*SP*TP
C.....NATURAL COORDINATE DERIVATIVES OF THE INTERPOLATION FUNCTIONS
C..... 1. WITH RESPECT TO R
    P(1,1)=-0.125*SM*TM
    P(1,2)=-P(1,1)
    P(1,3)=0.125*SP*TM
    P(1,4)=-P(1,3)
    P(1,5)=-0.125*SM*TP
    P(1,6)=-P(1,5)
    P(1,7)=0.125*SP*TP
    P(1,8)=-P(1,7)
C..... 2. WITH RESPECT TO S
    P(2,1)=-0.125*RM*TM
    P(2,2)=-0.125*RP*TM
    P(2,3)=-P(2,2)
    P(2,4)=-P(2,1)
    P(2,5)=-0.125*RM*TP
    P(2,6)=-0.125*RP*TP
    P(2,7)=-P(2,6)
    P(2,8)=-P(2,5)
```

```
C..... 3. WITH RESPECT TO T
    P(3,1)=-0.125*RM*SM
    P(3,2)=-0.125*RP*SM
    P(3,3)=-0.125*RP*SP
    P(3,4)=-0.125*RM*SP
    P(3,5)=-P(3,1)
    P(3,6)=-P(3,2)
    P(3,7)=-P(3,3)
    P(3,8)=-P(3,4)
c....EVALUATE THE JACOBIAN MATRIX AT POINT (R,S)
    DO 30 I=1,3
    DO 30 J=1,3
    DUM=0.0
    DO 20 K=1,8
  20 DUM=DUM+P(I,K)*XX(J,K)
  30 XJ(I,J)=DUM
c     write(6,*)nel,r,s,t
c     write(6,3)((xx(i,j),j=1,3),i=1,3)
c     write(6,3)((xj(i,j),j=1,3),i=1,3)
3     format(9(1x,f5.3))
C.....COMPUTE THE DETERMINANT OF THE JACOBIAN MATRIX AT POINT (R,S,T)
C.....COMPUTE THE ADJOINT MATRIX OF XJ
    XJI(1,1)=XJ(2,2)*XJ(3,3)-XJ(3,2)*XJ(2,3)
    XJI(2,1)=-XJ(2,1)*XJ(3,3)+XJ(3,1)*XJ(2,3)
    XJI(3,1)=XJ(2,1)*XJ(3,2)-XJ(3,1)*XJ(2,2)
    XJI(1,2)=-XJ(1,2)*XJ(3,3)+XJ(3,2)*XJ(1,3)
    XJI(2,2)=XJ(1,1)*XJ(3,3)-XJ(3,1)*XJ(1,3)
    XJI(3,2)=-XJ(1,1)*XJ(3,2)+XJ(3,1)*XJ(1,2)
    XJI(1,3)=XJ(1,2)*XJ(2,3)-XJ(2,2)*XJ(1,3)
    XJI(2,3)=-XJ(1,1)*XJ(2,3)+XJ(2,1)*XJ(1,3)
    XJI(3,3)=XJ(1,1)*XJ(2,2)-XJ(2,1)*XJ(1,2)
    DET=0.0
    DO 31 I=1,3
31    DET=DET+XJ(1,I)*XJI(I,1)
    IF(DET.GT.0.00000001) GO TO 40
    WRITE(*,2000)NEL
2000  FORMAT('ERROR, ZERO OR NEGETIVE JACOBIAN DET. FOR ELEMENT=',I6)
    PRINT *,DET
    STOP
C.... COMPUTE INVERSE OF THE JACOBIAN MATRIX
  40 DUM=1./DET
    DO 41 J=1,3
    DO 41 I=1,3
41    XJI(I,J)=XJI(I,J)*DUM
```

```fortran
C.....EVALUATE GLOBAL DERIVATIVE OPERATOR B
      DO 50 I=1,3
      DO 50 J=1,8
50    B(I,J)=XJI(I,1)*P(1,J)+XJI(I,2)*P(2,J)+XJI(I,3)*P(3,J)
c     DUM=0.0
c     DO 55 K=1,3
c55   DUM=DUM+XJI(I,K)*P(K,J)
c50   B(I,J)=DUM
      RETURN
      END
      SUBROUTINE STDM2(H,P,R,S,T)
      DOUBLE PRECISION H(8),P(3,8),R,S,T,RP,SP,TP,RM,SM,TM
C     PROGRAM TO EVALUVATE THE STRAIN-DISPLACEMENT TRANSFORMATION
C     MATRIX B AT POINT (R,S,T) FOR A BRICK8 ELEMENT
c     get H & P matrix for storage
C
      RP=1.0+R
      SP=1.0+S
      TP=1.0+T
      RM=1.0-R
      SM=1.0-S
      TM=1.0-T
C.....INTERPOLATION FUNCTIONS
C.....AT THIS STAGE NO NEED FOR H?
      H(1)=0.125*RM*SM*TM
      H(2)=0.125*RP*SM*TM
      H(3)=0.125*RP*SP*TM
      H(4)=0.125*RM*SP*TM
      H(5)=0.125*RM*SM*TP
      H(6)=0.125*RP*SM*TP
      H(7)=0.125*RP*SP*TP
      H(8)=0.125*RM*SP*TP
C.....NATURAL COORDINATE DERIVATIVES OF THE INTERPOLATION FUNCTIONS
C..... 1. WITH RESPECT TO R
      P(1,1)=-0.125*SM*TM
      P(1,2)=-P(1,1)
      P(1,3)=0.125*SP*TM
      P(1,4)=-P(1,3)
      P(1,5)=-0.125*SM*TP
      P(1,6)=-P(1,5)
      P(1,7)=0.125*SP*TP
      P(1,8)=-P(1,7)
C..... 2. WITH RESPECT TO S
      P(2,1)=-0.125*RM*TM
```

```fortran
      P(2,2)=-0.125*RP*TM
      P(2,3)=-P(2,2)
      P(2,4)=-P(2,1)
      P(2,5)=-0.125*RM*TP
      P(2,6)=-0.125*RP*TP
      P(2,7)=-P(2,6)
      P(2,8)=-P(2,5)
C..... 3. WITH RESPECT TO T
      P(3,1)=-0.125*RM*SM
      P(3,2)=-0.125*RP*SM
      P(3,3)=-0.125*RP*SP
      P(3,4)=-0.125*RM*SP
      P(3,5)=-P(3,1)
      P(3,6)=-P(3,2)
      P(3,7)=-P(3,3)
      P(3,8)=-P(3,4)
      RETURN
      END
      SUBROUTINE STDM3(XX,H,B,H8,P8,DET,N1)
      INTEGER N1,NDF,I,J
      DOUBLE PRECISION B(3,8),XX(3,8),H(8),H8(8,8),P8(3,8,8),RJ(3)
     &,DET,DX,DY,DZ
c     GET H & B FOR HEXAHEDRAL ELEMENT -RECTANGULAR SYSTEM-AXIS CONCIDES
      NDF=8
      DX=XX(1,2)-XX(1,1)
      DY=XX(2,4)-XX(2,1)
      DZ=XX(3,5)-XX(3,1)
      DET=DX*DY*DZ/8.
      RJ(1)=2./DX
      RJ(2)=2./DY
      RJ(3)=2./DZ
c
      DO I=1,NDF
      H(I)=H8(I,N1)
      END DO
      DO J=1,NDF
      DO I=1,3
      B(I,J)=RJ(I)*P8(I,J,N1)
      END DO
      END DO
      RETURN
      END
```

2. Finite Element Numbering and Assembling

Solving a large system of type Ax=b is computationally expensive. A numbering system depending on the geometric connection between the elements is established to reduce the computational cost. Only the upper triangle is stored. The location of the adjacent points is the main function for the numbering system. For example, each point on the east side is numbered two and the west is numbered three. Table 1 illustrates the location and number for each point in geometric and IJK systems. Then the north and south side is numbered accordingly. However, because only the upper triangle is considered, some shifting is done in the middle layer as shown in Figure C.2. The joints numbers for the 3-D element's faces are shown in Figure C.3. In Figure C.2, T,B and M represent the top layer, middle layer and bottom layer respectively as the color is corresponded to each layer in the 3-D shape in Figure C.4.

The assembling of global matrix from the element matrix and the matrix multiplication are done for the fourteen points in the upper triangle as shown the code below. The lower triangle elements are not stored but connected to the upper triangle elements as shown in table2. Table 3 shows the upper triangle of the stiffness matrix.
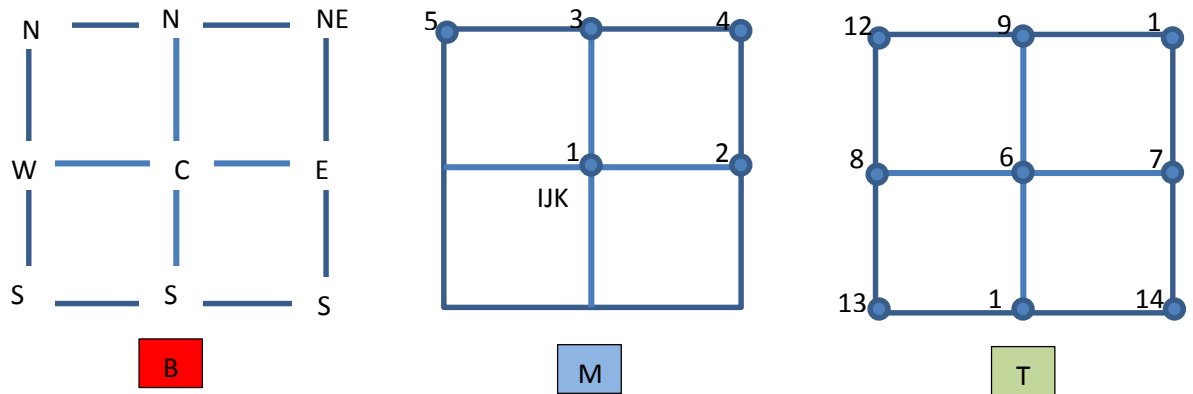
Figure C.2 Elements assembly.
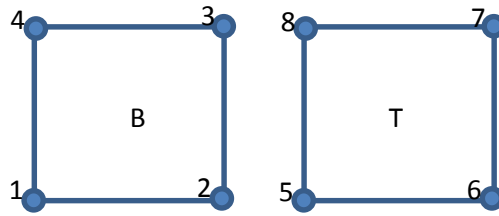
Figure C.3 Element faces.
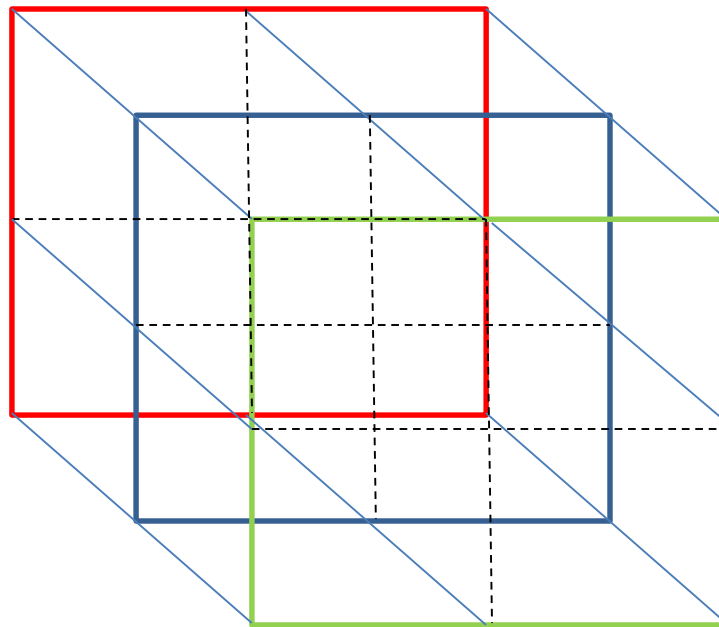
Figure C.4 ELEMENTS 3-D SHAPE.

Table C.1 numbering system according to the center point location.

ijk	(i+1)jk	I(j+1)k	(i+1) (j+1)k	(i-1) (j+1)k
MC	ME	MN	MNE	MNW
1	2	3	4	5
ij(k+1)	(i+1)j(k+1)	(i-1)j(k+1)	i(j+1)(k+1)	i(j-1)(k+1)
TC	TE	TW	TN	TS
6	7	8	9	10
(i+1) (j-1)(k+1)	(i-1)(j+1)(k+1)	(i-1)(j-1)(k+1)	(i+1)(j-1)(k+1)	
TNE	TNW	TSW	TSE	
11	12	13	14	

$$SM = \begin{bmatrix} 11 & 12 & 13 & 14 & 15 & 16 & 17 & 18 \\ & 22 & 23 & 24 & 25 & 26 & 27 & 28 \\ & & 33 & 34 & 35 & 36 & 37 & 38 \\ & & & 44 & 45 & 46 & 47 & 48 \\ & & & & 55 & 56 & 57 & 58 \\ & & & & & 66 & 67 & 68 \\ & & & & & & 77 & 78 \\ & & & & & & & 88 \end{bmatrix}$$

Element Stiffness Matrix

Table C.2 relation between the lower and upper triangle elements.

12	9	11
8	6	7
13	10	14

5	3	4
A(IW,j,k,2)	1	2
A(IW,,JS,k,4)	A(i,JS,k,3)	A(IE,,JS,k,5)

A(IW,JN,KB,14)	A(i,JN,KB,10)	A(IE,JN,KB,13)
A(IW,j,KB,7)	A(i,j,KB,6)	A(IE,j,KB,8)
A(IW,JS,KB,11)	A(i,JS,KB,9)	A(IE,JS,KB,12)

Table C.3 The upper triangle of the stiffness matrix.

	1	2	3	4	5	6	7	8	9	10	11	12	13	14	15	16	17	18	19	20	21	22	23	24	25	26	27
1	1	2		3	4					6	7			9	11												
2		1	2	5	3	4				8	6	7	12	9	11												
3			1		5	3					8	6		12	9												
4				1	2		3	4		10	14		6	7		9	11										
5					1	2	5	3	4	13	10	14	8	6	7	12	9	11									
6						1		5	3		13	10		8	6		12	9									
7							1	2					10	14		6	7										
8								1	2				13	10	14	8	6	7									
9									1					13	10		8	6									
10										1	2		3	4					6	7		12	9				
11											1	2	5	3	4				8	6	7	12	9	11			
12												1		5	3				8	6		12	9				
13													1	2		3	4		10	14		6	7		9	11	
14														1	2	5	3	4	13	10	14	8	6	7	12	9	11
15															1		5	3		13	10		8	6		12	9
16																1	2					10	14		6	7	
17																	1	2				13	10	14	8	6	7
18																		1					13	10		8	6
19																			1	2		3	4				
20																				1	2	5	3	4			
21																					1		5	3			
22																						1	2		3	4	
23																							1	2	5	3	4
24																								1		5	3
25																									1	2	
26																										1	2
27																											1

```
C.....ASSEMBLE THE RHS-HERE F IS FORMULATED AS A*D=F TERM

IE=I+1, JN=J+1, IE=I-1, JS=J-1, KT=K+1, KB=K-1
C.....FOR POINT 1
      A(I,J,K,1)= A(I,J,K,1)+SM(1,1)

      A(I,J,K,2)= A(I,J,K,2)+SM(1,2)

      A(I,J,K,4)= A(I,J,K,4)+SM(1,3)

      A(I,J,K,3)= A(I,J,K,3)+SM(1,4)
```

```
      A(I,J,K,6)= A(I,J,K,6)+SM(1,5)

      A(I,J,K,7)= A(I,J,K,7)+SM(1,6)

      A(I,J,K,11)= A(I,J,K,11)+SM(1,7)

      A(I,J,K,9)= A(I,J,K,9)+SM(1,8)

C.....FOR POINT 2
      A(IE,J,K,1)= A(IE,J,K,1)+SM(2,2)

      A(IE,J,K,3)= A(IE,J,K,3)+SM(2,3)

      A(IE,J,K,5)= A(IE,J,K,5)+SM(2,4)

      A(IE,J,K,8)= A(IE,J,K,8)+SM(2,5)

      A(IE,J,K,6)= A(IE,J,K,6)+SM(2,6)

      A(IE,J,K,9)= A(IE,J,K,9)+SM(2,7)

      A(IE,J,K,12)= A(IE,J,K,12)+SM(2,8)

      C.....FOR POINT 3
      A(I,JN,K,1)= A(I,JN,K,1)+SM(3,3)

      A(I,JN,K,13)= A(I,JN,K,13)+SM(3,5)

      A(I,JN,K,10)= A(I,JN,K,10)+SM(3,6)

      A(I,JN,K,6)= A(I,JN,K,6)+SM(3,7)

      A(I,JN,K,8)= A(I,JN,K,8)+SM(3,8)

C.....FOR POINT 4
      A(IE,JN,K,2)= A(IE,JN,K,2)+SM(4,3)

      A(IE,JN,K,1)= A(IE,JN,K,1)+SM(4,4)

      A(IE,JN,K,10)= A(IE,JN,K,10)+SM(4,5)

      A(IE,JN,K,14)= A(IE,JN,K,14)+SM(4,6)

      A(IE,JN,K,7)= A(IE,JN,K,7)+SM(4,7)

      A(IE,JN,K,6)= A(IE,JN,K,6)+SM(4,8)

C.....FOR POINT 5
      A(IW,JN,K,1)= A(IW,JN,K,1)+SM(5,5)

      A(IW,JN,K,2)= A(IW,JN,K,2)+SM(5,6)
```

```
      A(IW,JN,K,4)= A(IW,JN,K,4)+SM(5,7)

      A(IW,JN,K,3)= A(IW,JN,K,3)+SM(5,8)

C.....FOR POINT 6
      A(I,J,KT,1)= A(I,J,KT,1)+SM(6,6)

      A(I,J,KT,3)= A(I,J,KT,3)+SM(6,7)

      A(I,J,KT,5)= A(I,J,KT,5)+SM(6,8)

C.....FOR POINT 7
      A(I,J,KT,1)= A(I,J,KT,1)+SM(7,7)

C.....FOR POINT 8
      A(I,J,KT,2)= A(I,J,KT,2)+SM(8,7)

      A(I,J,KT,1)= A(I,J,KT,1)+SM(8,8)


      RHS=A(I,J,K,1)*X(I,J,K)+A(I,J,K,2)*X(IE,J,K)+

     &A(I,J,K,3)*X(I,JN,K)+A(I,J,K,4)*X(IE,JN,K)+

     &A(I,J,K,5)*X(IW,JN,K)+A(I,J,K,6)*X(I,J,KT)+

     &A(I,J,K,7)*X(IE,J,KT)+A(I,J,K,8)*X(IW,J,KT)+

     &A(I,J,K,9)*X(I,JN,KT)+A(I,J,K,10)*X(I,JS,KT)+

     &A(I,J,K,11)*X(IE,JN,KT)+A(I,J,K,12)*X(IW,JN,KT)+

     &A(I,J,K,13)*X(IW,JS,KT)+A(I,J,K,14)*X(IE,JS,KT)+

C

     &A(IW,J,K,2)*X(IW,J,K)+ A(I,JS,K,3)*X(I,JS,K)+

     &A(IW,JS,K,4)*X(IW,JS,K)+ A(IE,JS,K,5)*X(IE,JS,K)+

     &A(I,J,KB,6)*X(I,J,KB)+A(IE,J,KB,8)*X(IE,J,KB)+

     &A(IW,J,KB,7)*X(IW,J,KB)+A(I,JN,KB,10)*X(I,JN,KB)+

     &A(I,JS,KB,9)*X(I,JS,KB)+A(IE,JN,KB,13)*X(IE,JN,KB)+

     &A(IW,JN,KB,14)*X(IW,JN,KB)+ A(IW,JS,KB,11)*X(IW,JS,KB)

     &+A(IE,JS,KB,12)*X(IE,JS,KB)
```

3. Area Calculation Check

Area calculation is an important factor in computing wind or tornado forces on the structure. After the pressure is calculated by solving the Navier Stokes equations, it is multiplied by the calculated area to determine the forces. In this section, a simplified geometry as shown in Figure C.5 is utilized to show the area and area component calculation.
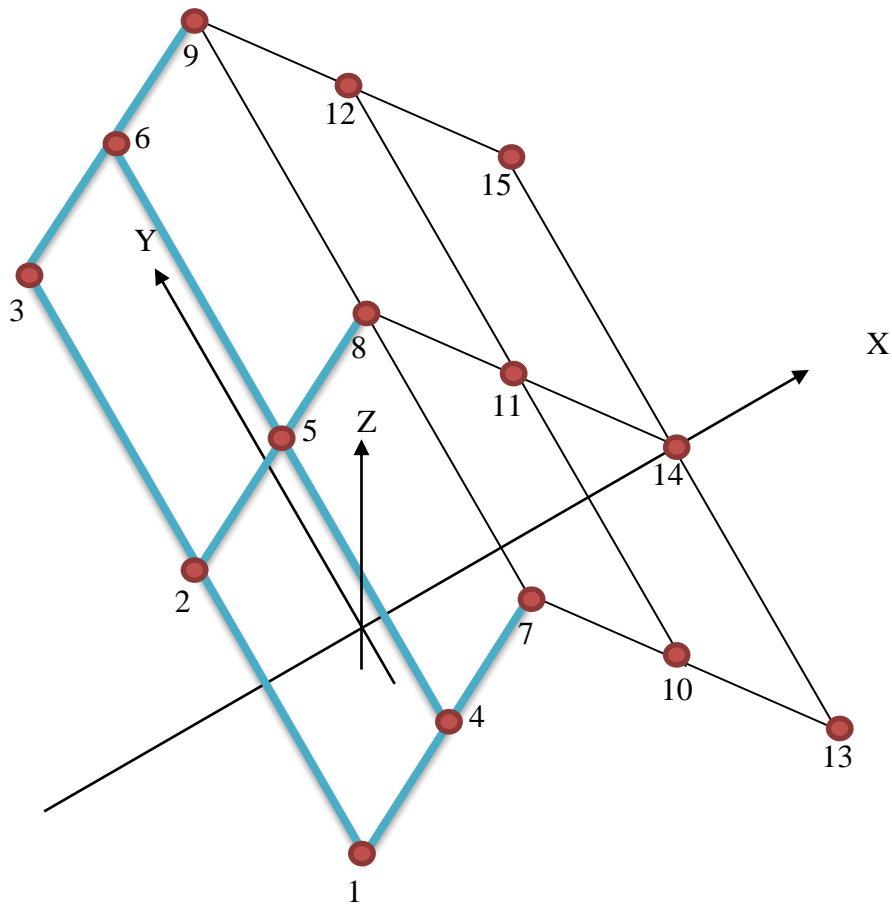

Figure C.5 Simple geometry utilized for area calculation check.

Table C.4 points' indices and coordinates.

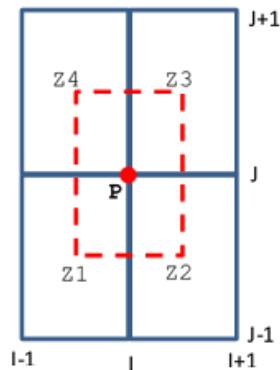| point	Index			Coordinates		
	I	J	K	X	Y	Z
1	1	1	1	-2	-1	1
2	1	2	1	-2	0	1
3	1	3	1	-2	1	1
4	2	1	2	-1	-1	1.5
5	2	2	2	-1	0	1.5
6	2	3	2	-1	1	1.5
7	3	1	3	0	-1	2
8	3	2	3	0	0	2
9	3	3	3	0	1	2
10	4	1	2	1	-1	1.5
11	4	2	2	1	0	1.5
12	4	3	2	1	1	1.5
13	5	1	1	2	-1	1
14	5	2	1	2	0	1
15	5	3	1	2	1	1

For point 5:

DX=(X(I+1)-X(I-1))/2. (Calculate the surface length along the X axis)

  = (0-(-2))/2=1

DY=(Y(J+1)-Y(J-1))/2. (Calculate the surface length along the Y axis)

  = (1-(-1))/2= 1

Projected view for selected area

(Calculate the average elevation for the corner Z1)

```
Z1=(HI(I-1,J-1)+HI(I,J-1)+HI(I,J)+HI(I-1,J))/4.

  = (1+1.5+1.5+1)/4=1.25

Z2=(HI(I,J-1)+HI(I+1,J-1)+HI(I+1,J)+HI(I,J))/4.

  = (1.5+2+2+1.5)/4=1.75

Z3=(HI(I,J)+HI(I+1,J)+HI(I+1,J+1)+HI(I,J+1))/4.

  = (1.5+2+2+1.5)/4=1.75

Z4=(HI(I-1,J)+HI(I,J)+HI(I,J+1)+HI(I-1,J+1))/4.

  = (1+1.5+1.5+1)/4=1.25
```

```
Z31=Z3-Z1   (Calculate the elevation difference for vector 13)

    =0.5

Z24=Z2-Z4   (Calculate the elevation difference for vector 24)

    =0.5

DX2=DX*DX

    =1*1=1

DY2=DY*DY

    =1*1=1

Z1=(Z24+Z31)*(Z24+Z31)
```

  = (0.5+0.5)*(0.5+0.5)=1

```
Z2=(Z31-Z24)*(Z31-Z24)

   =0
```

`AZ(I,J)=SQRT(DY2*Z1+DX2*Z2+4.*DX2*DY2)/2.`(Total Area)
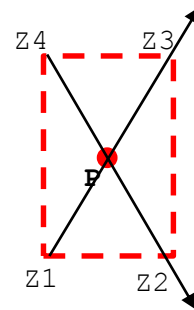
$$=(1*1+1*0+4*1*1)^{0.5}/2=1.118$$

AX=DY*(Z24+Z31)/2. (Area component in X direction)

=1*(0.5+0.5)/2=0.5

AY=DX*(Z31-Z24)/2. (Area component in Y direction)

=0.5*(0.5-0.5)/2=0

AZ=DX*DY (Area component in Z direction)

=1*1=1

For point 11:

DX=(X(I+1)-X(I-1))/2.

= (2-(0))/2=1

DY=(Y(J+1)-Y(J-1))/2.

= (1-(-1))/2= 1

Z1=(HI(I-1,J-1)+HI(I,J-1)+HI(I,J)+HI(I-1,J))/4.

= (2+1.5+1.5+2)/4=1.75

Z2=(HI(I,J-1)+HI(I+1,J-1)+HI(I+1,J)+HI(I,J))/4.

= (1.5+1+1+1.5)/4=1.25

Z3=(HI(I,J)+HI(I+1,J)+HI(I+1,J+1)+HI(I,J+1))/4.

= (1.5+1+1+1.5)/4=1.25

Z4=(HI(I-1,J)+HI(I,J)+HI(I,J+1)+HI(I-1,J+1))/4.

= (2+1.5+1.5+2)/4=1.75

Z31=Z3-Z1

=-0.5

Z24=Z2-Z4

```
   =-0.5
DX2=DX*DX
   =1*1=1
DY2=DY*DY
   =1*1=1
Z1=(Z24+Z31)*(Z24+Z31)
```

$= (-0.5+-0.5)*(-0.5+-0.5)=1$

```
Z2=(Z31-Z24)*(Z31-Z24)
   =0
AZ(I,J)=SQRT(DY2*Z1+DX2*Z2+4.*DX2*DY2)/2.
```

$= (1*1+1*0+4*1*1)^{0.5}/2=1.118$

```
AX=DY*(Z24+Z31)/2.
   =1*(-0.5+-0.5)/2=-0.5
AY=DX*(Z31-Z24)/2.
   =0.5*(-0.5--0.5)/2=0
AZ=DX*DY
   =1*1=1
```

- **Vector Cross product for Area Calculation**

$$Area = \frac{1}{2}(13 \times 42) = \frac{1}{2}\left(\overrightarrow{13} \times \overrightarrow{42}\right)$$

1(X1,Y1,Z1), 2(X2,Y2,Z2), 3(X3,Y3,Z3), 4(X4,Y4,Z4)

$Z31 = Z3 - Z1$

$Z24 = Z2 - Z4$

$$Area = \begin{bmatrix} i & j & k \\ Dx & Dy & Z31 \\ Dx & -Dy & Z24 \end{bmatrix}$$

$$= (DyZ24 + DyZ31)i + (DxZ31 - DxZ24)j - (DxDy + DxDY)k$$

$$= \frac{1}{2}\sqrt{Dy^2(Z24 + Z31)^2 + Dx^2(Z31 - Z24)^2 - 4(DxDy)^2}$$